ELUCIDATING THE ROLES OF WNT/BETA-CATENIN SIGNALING IN LIVER DISEASE, CANCER, AND REGENERATION

by

Morgan Elizabeth Preziosi

B.S. in Biochemistry, B.A. in Psychology, University of Rochester, 2013

Submitted to the Graduate Faculty of

University of Pittsburgh School of Medicine in partial fulfillment

of the requirements for the degree of

Doctor of Philosophy

University of Pittsburgh

2018

UNIVERSITY OF PITTSBURGH

SCHOOL OF MEDICINE

This thesis was presented

by

Morgan Elizabeth Preziosi

It was defended on

April 12, 2018

and approved by

Chairperson: Dr. Wendy M. Mars, PhD, Associate Professor, Department of Pathology

Dr. Youhua Liu, PhD, Professor, Department of Pathology

Dr. George Michalopoulos, MD, PhD, Professor and Chair, Department of Pathology

Dr. Prithu Sundd, PhD, Assistant Professor, Division of Pulmonary, Allergy, and Critical Care Medicine

Thesis Advisor: Dr. Satdarshan P.S. Monga, MD, Professor and Vice Chair, Division of Experimental Pathology, Department of Pathology

ELUCIDATING THE ROLES OF WNT/BETA-CATENIN SIGNALING IN LIVER DISEASE, CANCER, AND REGENERATION

Morgan Preziosi, PhD

University of Pittsburgh, 2018

Owing to its strategic location in the body along with performing over 500 daily functions, liver health is indispensable to survival. Following any form of acute or chronic hepatic injury, a repair process is induced which, if successful, restores histology and function. However, continuous insult can lead to unremitting immune response, hepatocyte death, proliferation, wound healing, and sets the stage for DNA damage and errors, eventually leading to dysplasia and neoplasia. Wnt/β-catenin signaling is implicated in a variety of processes to maintain liver homeostasis and promote regeneration, but its dysregulation is often evident in chronic liver diseases and cancer. To further understand the role and regulation of the Wnt/β-catenin pathway in hepatic pathophysiology, we focused on studying this pathway in a model of chronic iron overload replicating hereditary hemochromatosis (HH), hepatocellular carcinoma (HCC), a primary liver tumor with rising incidence, and in metabolic zonation and liver regeneration (LR) after partial hepatectomy (PH), two fundamental attributes innate to the liver. The underlying goal of our studies was to address the role of β-catenin in hepatocyte biology, and identify the cell source and identity of Wnt ligands that regulate β-catenin signaling in hepatocytes, both in hepatic health and in disease. HH is a genetic iron overload disorder with no cure, invasive treatments, and no representative animal models that recapitulate human disease. β-Catenin knockout mice (bKO), when subjected to chronic iron overload led to remarkable hepatic injury compared to control mice (bCON) and displayed inflammation, steatosis and fibrosis due to enhanced oxidative stress and lipid peroxidation. This led us to identify an

important role of β-catenin in regulating the redox state of hepatocytes as we alleviated the pathology by supplementing the antioxidant N-acetyl-L-cysteine to bKO while challenging them with iron overload. Additionally, bKO on high iron diet serve as a novel animal model that robustly mimic disease development and progression of an HH patient. Chronic injury like HH often progresses to HCC accompanied by ongoing hepatocyte death and proliferation, along with infiltration of immune cells including macrophages. We next assessed if hepatocytes and macrophages could be the source of Wnt ligands that may activate non-mutated β-catenin in hepatocytes to contribute to injury, inflammation and HCC. We generated hepatocyte-specific (HP-KO) and macrophage-specific (MP-KO) Wntless knockout mice, unable to secrete Wnts from respective cell types and subjected them to diethylnitrosamine/carbon tetrachloride (DEN/CCl_4). This model yields non-β-catenin mutated HCC with 100% penetrance by five months. HP-KO and respective controls (HP-CON) had comparable tumor burden albeit with some distinct signaling indicating overall that hepatocytes are not a major contributor of Wnts in HCC in this model. MP-KO displayed two distinct, litter-specific phenotypes. In one group, MP-KO had greater tumor burden than control mice (MP-CON), and in another group MP-KO had reduced tumor burden compared to MP-CON. We revealed different HCC phenotypes in MP-CON from both groups, suggesting MP Wnts will promote or suppress tumors depending on the underlying oncogenic and inflammatory milieu. Finally, we queried the role of cell-specific Wnts in metabolic zonation and LR. Using endothelial cell-specific Wntless knockout mice (EC-KO), we confirmed EC to be the source of Wnt ligands that directed β-catenin activation in pericentral hepatocytes. Also, EC lining sinusoids regulated Cyclin D1 expression and eventually hepatocyte proliferation during LR after PH. We next identified Wnt2 and Wnt9b as the Wnts chiefly from EC to be regulators of hepatic zonation and during LR after PH. Finally, we provide

in vitro evidence that shear stress produced after PH may initiate Wnt expression in EC and hence may initiate the process of LR. Overall, our data elucidates the role and regulation of Wnt/β-catenin signaling and begins to outline the complex paracrine cell-molecule circuitry of this intricate pathway in hepatic health and disease.

TABLE OF CONTENTS

LIST OF TABLES

LIST OF FIGURES

PREFACE

Pursuing a PhD has been the most challenging thing I have ever done, however I can look back at the past five years and be thankful for the help, friendships, memories, and progress. I entered the University of Pittsburgh Interdisciplinary Biomedical Graduate Program with wide eyes, passion for science and research, and a bit of imposter syndrome. Throughout all of the difficulties and hurdles faced in graduate school, I can say I am leaving the program the same way I entered; hopefully with a little less imposter syndrome and a little more scientific maturity.

I want to first thank my biggest supporters; my parents. Throughout my life they have supported all of my big and small goals with no question. From driving me to acting auditions when I thought I wanted to become an actress, to paying for guitar lessons that I stopped taking after six months, everything they have done has made me the person I am today and I thank them for everything. I'd like to thank the rest of my family, including my brother, sister, niece, aunts, uncles, and cousins, for supporting me in everything despite my "nerd" status.

I also have to thank the friends I have made along the way. Thanks to my high school and college friends who came to visit me every once in a while and help me remember where I came from. Thanks to the new friends I've made at Pitt. I couldn't have survived grad school without them all, and I am so proud of all of us. I will miss all of them but I know our friendships are life-long.

To the Monga lab, I thank them for putting up with my sass, messiness, and overall nonsense for four years. They are my family away from home and I will miss them terribly. I also want to thank my thesis committee for their unwavering help and input, and the mentors I have picked up along the way, including Dr. Cecelia Yates, Dr. Wendy Mars, and others that I have met through great organizations like the American Society for Investigative Pathology and the IBGP Admissions Committee right at Pitt.

Lastly I'd like to thank Dr. Monga for everything he has done throughout my graduate career. He has taught me a great deal about science, myself, and about life, and I think I have truly matured as a scientist and person because of him. I do not take for granted the freedom he gave me, allowing me to pursue my own questions and make my own path in his lab, and supporting my endeavors inside and outside the lab. While this door closes, another door is opening. I am excited to begin my post-doctoral research experience at the University of Pennsylvania under the guidance of Dr. Kirk Wangensteen researching hepatocellular carcinoma. Although I will never become a Philadelphia sports fan, I am excited to see what the future holds and I hope to make Pittsburgh proud.

1.0 INTRODUCTION

The liver is a vital organ unique in its ability to regenerate when up to 70% is removed or acute hepatic injury is sustained. However, during chronic liver diseases the ability to regenerate is impaired, and instead the hepatic injury progresses to fibrosis and hepatocellular carcinoma. Therapies for chronic liver diseases and liver cancer are limited and ineffective, so current studies aim to understand regeneration kinetics to eventually shift injured livers towards regeneration and away from fibrosis and cancer (Fig.1). A major signaling pathway in liver homeostasis and disease is the Wnt/β-catenin pathway. This dissertation focuses on the role of β-catenin in a specific chronic liver disease (Aim 1), namely hereditary hemochromatosis, hepatocellular carcinoma after chronic hepatic injury (Aim 2), and liver regeneration in the context of a healthy liver (Aim 3). We will show the importance of Wnt/β-catenin in each arm of the liver disease dogma and provide insights that will lead to further understanding of signaling in disease and health and to eventual therapeutic options. *For a list of all animal models used in this study, please refer to Appendix A.*

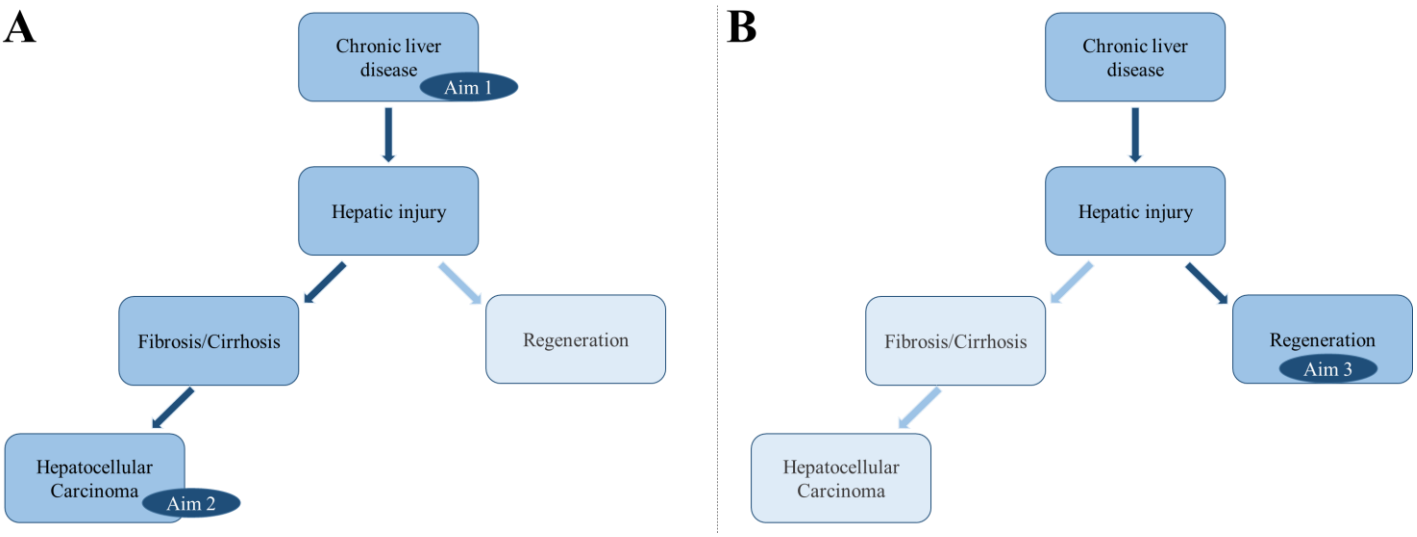

Figure 1: Central dogma of liver injury and regeneration.
(A) During chronic liver disease, the liver loses its ability to regenerate, and hepatic injury progresses to fibrosis and hepatocellular carcinoma. (B) Current studies to understand liver regeneration will lead to improved therapies for chronic liver diseases and induce hepatocyte repopulation while preventing fibrosis and hepatocellular carcinoma. This proposal focuses on the chronic liver disease hereditary hemochromatosis (Aim 1), hepatocellular carcinoma (Aim 2), and liver regeneration (Aim 3).

1.1 WNT/B-CATENIN SIGNALING OVERVIEW

1.1.1 Canonical Wnt signaling "on" and "off"

Canonical Wnt signaling is a highly regulated pathway functioning in processes ranging from development to cancer (Fig.2). Wnt ligands are insoluble secreted glycoproteins that require palmitoylation by Porcupine O Acyltransferase (PORC) in the endoplasmic reticulum, enabling Wnt interaction with Wntless (Wls) in the Golgi. Wls acts as a cargo receptor and modulates vesicular transport of Wnts outside the cell (1), making both Wls and PORC necessary for Wnt function and secretion. As Wnts are insoluble and hydrophobic, they likely travel short distances to target cells (2), although a complete understanding of the Wnt morphogen gradient is lacking.

Additional studies have suggested Wnts travel via exosomes, requiring Wls, and remain on exosomal membranes to interact with target cells (3, 4). It is also likely Wnts can remain tethered to their parent cell membrane.

In the absence of Wnt, β-catenin is bound by the "destruction complex" in the cytoplasm, composed primarily of Adenomatous Polyposis Coli (APC), Axin, Casein Kinase I alpha (CKIα), and Glycogen Synthase Kinase 3β (GSK3β) (5). This causes β-catenin phosphorylation at serine 45 by CKIα (6), which primes β-catenin phosphorylation by GSKβ3 at serines 33, 37, and threonine 41 (7). This results in β-catenin ubiquitination and subsequent proteasome-mediated degradation (8). When Wnt is present, it interacts with a Frizzled receptor (Fzd) and Low-Density Lipoprotein Receptor-Related Protein 5 or 6 (LRP) coreceptor. This complex recruits Dishevelled (Dsh) to the membrane, where it mediates Axin removal from the destruction complex and causes the complex to dissociate. β-Catenin stabilizes and levels increase in the cytoplasm, leading to translocation into the nucleus where it interacts with transcription factors to transcribe target genes (9) (Fig.2). There are 19 Wnts and 10 Fzds in the mammalian genome (10), with several of them being expressed in the different hepatic cell populations (11).

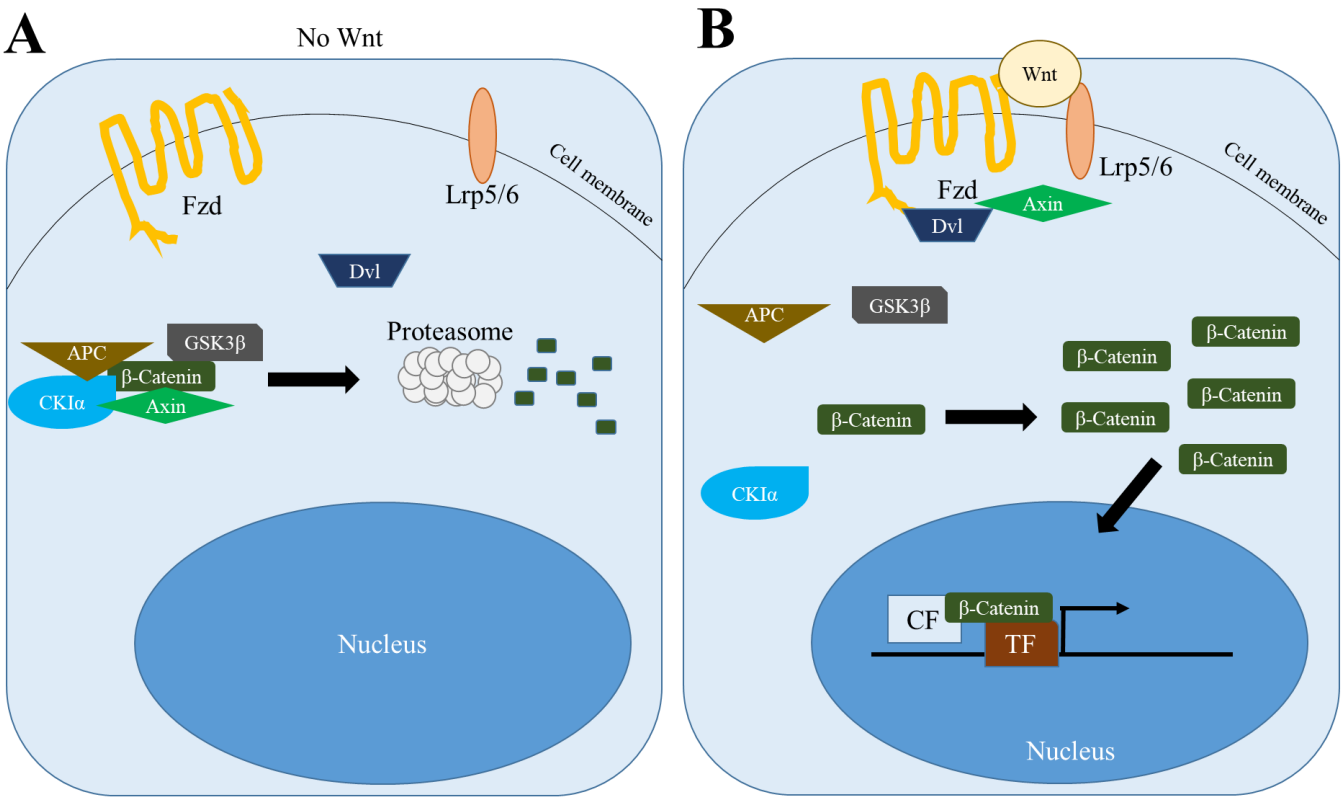

Figure 2: Schematic of canonical Wnt signaling pathway.
(A) In the absence of Wnts, the pathway is turned off. β-Catenin is bound by the destruction complex, leadings to subsequent phosphorylation and degradation via the proteasome. (B) When activated, a Wnt ligand binds an LRP5/6 and Frizzled coreceptor, recruiting Dishevelled to the membrane. Dishevelled recruits Axin and leads to dissociation of the destruction complex. β-Catenin then accumulates in the cytoplasm and translocates into the nucleus, where it interacts with various transcription factors and cofactors to transcribe target genes. Fzd, Frizzled; Lrp5/6, Low-density lipoprotein receptor-related protein 5/6; APC, Adenomatous polyposis coli; CKIα, Casein kinase I alpha; GSK3β, Glycogen synthase kinase beta; Dvl, Dishevelled; TF, transcription factor; CF, cofactor.

1.1.2 Wnts and accompanying agonists and antagonists

There is extensive questioning into whether the 19 Wnts have redundant or unique roles, considering Wnts and Wntless are evolutionarily conserved across mammals (12, 13). Developmental loss-of-function studies have revealed roles of specific Wnts, including Wnt1's role in midbrain development, Wnt2's and Wnt7b's roles in placental development, and

Wnt10b's and Wnt16's roles in bone development (14-18). However, the role of specific Wnts in liver pathobiology lacks characterization. Recent literature from us and others identify Wnt2 being important for liver regeneration (19), Wnt2 and Wnt9b important for hepatic zonation (20), Wnt5a important for termination of liver regeneration (21), and Wnt7b and Wnt10a to promote cholangiocyte proliferation (22). Challenges remain in studying liver-specific Wnts, including a lack of robust Wnt antibodies available, and the ability of hepatic cell populations to compensate for one another when Wnts are mutated or lost.

There are several known families of Wnt antagonists composed of secreted or transmembrane proteins, all being characterized to different extents. The Dickkopf proteins (Dkks) represent the most extensively studied group, and are composed of four secreted glycoproteins (Dkk1-4) that bind to Lrp6 and Wnt and inhibit their interaction (23, 24). The largest family of Wnt antagonists, secreted frizzled-related protein (sFrp), contains 5 members and binds to Wnts, sequestering them and preventing interaction with Fzd or Lrp5/6 receptors (24, 25). More recently identified, the E3 ubiquitin ligases Zinc Ring finger 3 (Znfr3a) and Ring finger 43 (Rnf43) promote internalization and endocytosis of Fzd and Lrp receptors (26, 27), although this is inhibited by the secreted Wnt agonist R-spondin (Rspo) (28). Intriguingly, Znfr3a and Rnf43 are Wnt targets, suggesting a negative feedback loop. Further, the enzyme Notum is able to remove palmitoleate groups from Wnts, inhibiting their interaction with Wls (29)

Additional lesser understood Wnt modulators include antagonists Wnt-inhibitory factor 1 (Wif1), Insulin-like growth factor binding protein 4 (IGFBP4), and transmembrane proteins Shisha, Adenomatosis polyposis coli down-regulated 1 (Apcdd1), and Waif1a, (24), and the agonist Norrin, which can bind and activate select Fzd receptors (1).

1.1.3 β-Catenin as a transcription cofactor

While β-catenin is not a bona fide transcription factor, it regulates transcription by serving as a scaffold for transcription factors and cofactors to bind (9, 30). Targets genes involved in several different cellular functions. The following is a partial list of known liver-specific β-catenin target genes:

Table 1: List of select beta-catenin target genes

Function	Target Genes	Citations
Cell cycle/proliferation	cMyc, Cyclin D1, Egfr, Tgfα, S100A6, Smp30 (context dependent)	(31-38)
Metabolism & Zonation	GS, Slc1a2, Oat, Rhbg, Cyp1a2, Cyp2e1, S100A6, cMyc (context dependent), Smp30, Lect2	(38-45)
Transcription factor	Lef1, Tcf1	(46, 47)
Angiogenesis & fibrosis	Vegf, Vegfr2, MMP7, MMP14, uPAR, CD44, PAI1, fibronectin	(42, 48-53)
Adult stem cell marker	EpCAM, Lgr5	(54, 55)
Negative feedback	Axin2, sFrp2, Dickkopf	(56-58)
Antiapoptosis	Bcl2, Survivin	(48)

Below is a list of transcriptional cofactors β-catenin can interact with, emphasizing interactions in the liver. We do not fully understand the spatial and temporal regulation of these interactions, or their comprehensive target genes.

Table 2: partial list of transcriptional regulators β-catenin can interact with in the liver

Cofactor	Notes	Citations
Tcf4	Most common; Can differentially interact with Cbp or P300; Known target Cyclin D1	(40, 59, 60)
Lef1	Known target Cyclin D1; may serve mutually exclusive role with Tcf4	(32, 61)
Klf4	Transcription factor that inhibits Wnt signaling when interacting with β-catenin	(62)
Hnf4α	Can compete with β-catenin by binding to Tcf4	(63)
Cbp	Histone acetyl transferase; May promote growth genes (ex. Cyclin D1, Survivin)	(64-66)

P300	Histone acetyl transferase; may promote differentiation genes (ex. cMyc)	(65, 66)
Hif1α	During hypoxia, competes with Tcf4 for β-catenin interaction; promotes hepatocyte survival under hypoxia	(67, 68)
FoxO3	Competes with Tcf4; during oxidative stress, interacts with β-catenin to inhibit proliferation and resist oxidative damage	(69)

1.1.4 Noncanonical β-catenin and noncanonical Wnt

Although Wnt-mediated nuclear translocation of β-catenin is the most common activation method, β-catenin signaling can be propagated through other Wnt-independent mechanisms. β-Catenin complexes with the receptor tyrosine kinase c-Met on hepatocyte membranes. The c-Met ligand, Hepatocyte growth factor (HGF), can cause β-catenin/c-Met dissociation, β-catenin phosphorylation at tyrosines 654 and 670, and subsequent nuclear translocation (70-72). Alternatively, V-Akt Murine Thymoma Viral Oncogene (AKT) downstream of growth factor receptors (73) or tyrosine kinase receptors (74) can initiate β-catenin nuclear translocation through inhibition of GSK3β (74, 75) or through direct phosphorylation of β-catenin at serine 552 (73, 76). Furthermore, G-protein coupled receptors can activate Protein Kinase A (PKA) to phosphorylate β-catenin at serine 675, leading to its activation (77, 78).

Wnt acts independently of β-catenin in the noncanonical planar cell polarity (PCP) pathway and the Wnt-calcium pathway. PCP regulates cell polarity through Wnt interaction with Fzd and another receptor, likely ROR2, although this is not clearly defined (79, 80). This activates Dishevelled, leading to activation of small GTPases Rho and Rac, subsequently modulating the actin cytoskeleton through JNK (81, 82). The Wnt-calcium pathway plays roles in development including dorsal axis formation and ventral cell fate. Noncanonical ligands

including Wnt5a and Wnt11 can induce calcium release from the ER by activating PKC and CamKII (83, 84).

1.2 WNT/B-CATENIN SIGNALING IN LIVER PATHOBIOLOGY

1.2.1 Role in liver development

During prenatal development, the endoderm consists of the foregut, midgut, and hindgut. The liver is derived from the foregut endoderm during gastrulation. Wnts from the mesoderm signal to the posterior endoderm to promote hindgut fate thus inhibiting foregut development. Concurrently, the anterior endoderm secretes Wnt antagonists to suppress β-catenin signaling and maintain foregut identity and allow liver development (85, 86). Upon conclusion of foregut development, Wnt/β-catenin activation is required for liver specification around embryonic day 8.5 (E8.5). When β-catenin is removed from hepatoblasts using Foxa3-Cre recombinase, mice have suboptimal liver development by E12 and lethality is observed by E17 resulting from increased oxidative stress, hepatocyte apoptosis, and lack of hepatocyte growth (87). The switch from repressing foregut development to being required for embryonic liver specification highlights a necessary temporal regulation of Wnt signaling.

Postnatally, β-catenin activation correlates with increased hepatic cell proliferation of developing livers up to 20 postnatal days, while β-catenin-null mice have lower liver weight to body weight ratios throughout their lifespan. Concomitantly, mice with hyperactivated β-catenin develop larger livers before one month of age resulting from increased cell cycle entry and proliferation (31, 88, 89).

1.2.2 Role in liver regeneration after acute liver failure

The contributions of Wnt/β-catenin during liver regeneration (LR) after partial hepatectomy (PH) will be discussed extensively in section 6.0. β-Catenin is also required for liver regeneration after acute liver failure from acetaminophen (APAP) overdose. APAP is metabolized by cytochrome P450 enzymes Cyp2e1 and Cyp1a2, which create a toxic metabolite N-acetyl-*p*-benzoquinone imine, which causes hepatocyte death. Cyp2e1 and Cyp1a2 are β-catenin target genes. Furthermore, hepatocyte-specific β-catenin-null mice, lacking these two enzymes, are completely protected from APAP-induced liver injury. Despite this, β-catenin is activated within one hour after a sub-lethal APAP injection in mice, and is required for hepatocyte proliferation after APAP injury. Indeed, patients with increased β-catenin activation exhibit improved LR after APAP overdose (90).

1.2.3 Role in oxidative stress, inflammation, and hepatic fibrosis

β-Catenin regulates production of the antioxidant ascorbic acid through target genes including Regulcalcin, which negatively regulates oxidative stress (36, 91). Consequentially, mice lacking liver-specific β-catenin develop increased reactive oxygen species and DNA breaks after injuries including ionizing radiation, diethylnitrosamine-induced HCC, and 3,5-diethoxycarbonyl-1,4-dihydrocollidine (DDC) diet (92-94).

Oxidative stress leads to hepatic fibrosis through various mechanisms including macrophage and stellate cell activation (95). *In vitro* studies suggest Wnt/β-catenin is activated in and necessary for stellate cell activation and thus fibrosis (96-98). Whether hepatocyte-specific β-catenin is required for fibrosis is unclear. While Wnt5a contributes to fibrosis and is

upregulated in fibrotic livers, it can activate or repress β-catenin depending on the specific Fzd receptor involved (96, 99).

Furthermore, our lab has shown the p65 subunit of NFκB interacts with β-catenin which prevents NFκB activation (100). During lipopolysaccharide-induced hepatotoxicity, p65 dissociates from β-catenin to transcribe genes including various cytokines, antiapoptotic factors and growth factors (100, 101), overall suggesting β-catenin is a negative regulator of inflammation.

β-Catenin is also protective against ischemia/reperfusion injury and the development of hepatic steatosis (67, 102). However, aberrant activation such as during chronic liver disease and hepatocarcinogenesis, often contributes to disease progression. Further understanding of β-catenin during pathogenesis is required, and we attempt to elucidate its role during the chronic liver disease hereditary hemochromatosis, as discussed in detail in section 2.0.

1.2.4 Role in oval cell response and tumorigenesis

Oval cells, or hepatic progenitor cells, do not contribute to liver homeostasis or liver regeneration unless hepatocyte proliferation is blocked, such as during chronic liver disease. Models including the 3,5-diethoxycarbonyl-1, 4-dihydrocollidine (DDC) diet or the 2-acetylaminofluorine (2-AAF)/partial hepatectomy model, force the liver to regenerate but prevent hepatocyte proliferation, and hence force oval cells to activate and differentiate into hepatocytes. After both DDC and 2-AAF/PH, nuclear β-catenin accumulation and upregulation of several Wnts is observed (103, 104), and β-catenin is recruited to the promoter regions of genes including cMyc to a greater extent during DDC-induced oval cell induction (105). Blocking β-catenin, such as with β-catenin knockout mice, leads to a blunted oval cell response after DDC (106). After a

choline-deficient ethionine-supplemented diet (CDE), another injury model leading to increased oval cell response, macrophage-specific Wnts activate oval cell-specific β-catenin and lead to hepatocyte differentiation (107).

Hepatocellular carcinoma (HCC) expressing progenitor-like cells often lead to poorer prognosis. While one study suggested oval cells compose up to 5% of a tumor, there was a strong positive correlation between stem-cell marker OV6 and Wnt/β-catenin activation. *In vitro* analysis confirmed β-catenin activation increases the number of OV6+ cells in various HCC cell lines (105) suggesting β-catenin is important for oval cell expansion.

Further roles of β-catenin in tumorigenesis are discussed in sections 4.0 and 5.0.

2.0 MICE LACKING LIVER-SPECIFIC B-CATENIN DEVELOP STEATOHEPATITIS AND FIBROSIS AFTER IRON OVERLOAD

In this section we utilize liver specific β-catenin knockout mice (bKO) to elucidate the role of β-catenin in hepatic iron metabolism by subjecting bKO and littermate controls to iron overload diet for three months (Fig.3). We predict loss of β-catenin in bKO will lead to increased hepatic injury after iron overload, and will discuss our results, interpretations, and future directions in detail. This work was published in the Journal of Hepatology PMID: 28341391 (108). As first author, the publisher Elsevier has granted full permission to reuse the manuscript in this dissertation.

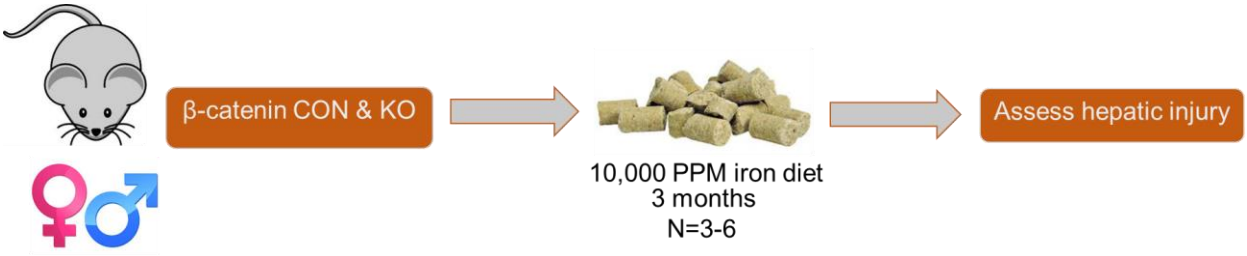

Figure 3: Schematic representation of iron overloading study.

2.1 ABSTRACT

Iron overload disorders such as hereditary hemochromatosis are a common cause of morbidity from liver diseases and increase risk of hepatic fibrosis and hepatocellular carcinoma (HCC). Once iron-induced damage occurs, treatment options are limited partly because of the lack of animal models recapitulating human disease, which do not exhibit relevant sequelae after chronic iron overload. Since liver-specific β-catenin knockout mice (bKO) are susceptible to injury, fibrosis and tumorigenesis following chemical carcinogen exposure, iron-overload diet was administered to KO and littermate control (bCON) mice for various times. To ameliorate an oxidant-mediated component of tissue injury, N-Acetyl-L-(+)-cysteine (NAC) was added to drinking water of mice on iron overload diet. bKO on iron diet (bKO+Fe) exhibited remarkable inflammation, followed by steatosis, oxidative stress, fibrosis, regenerating nodules and occurrence of occasional HCC. Increased injury in bKO+Fe was associated with activated AKT, ERK, and NFκB, along with reappearance of β-catenin and target gene Cyp2e1, which promoted lipid peroxidation and hepatic damage. Addition of NAC to drinking water protected bKO+Fe from hepatic steatosis, injury and fibrosis, and prevented activation of AKT, ERK, NFκB and re-appearance of β-catenin. In summary, we provide evidence that absence of hepatic β-catenin predisposes mice to hepatic injury and fibrosis following iron overload, which was reminiscent of hemochromatosis and associated with enhanced steatohepatitis and fibrosis. Disease progression was notably alleviated by antioxidant therapy, which supports its chemopreventive role in the management of chronic iron overload disorders.

2.2 BACKGROUND

2.2.1 Hereditary Hemochromatosis

The most common iron overload disorder is hereditary hemochromatosis (HH), occurring in approximately 1 in 200 Caucasians and 40% of healthy population in the US carries a mutation predisposing them to iron overload (109). This leads to an excess in hepatic iron stores, from 300mg-1g in adults to 25-30g in HH patients, with very limited methods of excreting iron which then accumulates in the parenchyma of organs including the liver, heart, and pancreas (110, 111). Early symptoms are nonspecific and include joint pain, fatigue, and palpitations, although this can progress into potentially fatal heart failure, diabetes, liver cirrhosis, or hepatocellular carcinoma (112). Because symptoms can be broad and generic, HH diagnosis requires assessing levels of iron content, which is performed by measuring serum ferritin levels. Generally, levels above 200-300 μg/L suggest elevated serum ferritin, and patients can have levels as high as 1000 μg/L, which likely indicates increased disease severity (111).

There are four main types of familial HH (113), characterized by various mutations in iron-regulatory genes (Table 3).

Table 3: Hemochromatosis types and corresponding mutations

Type	Mutation	Reference
Type 1	HFE gene (C282Y or H63D)	(113)
Type 2 (Juvenile)	Hepcidin (93delG or C166T) or hemojuvelin (G320V)	(113-115)
Type 3	Transferrin receptor 2 (Y250X)	(113, 116)
Type 4	Ferroportin (A77D)	(113, 117)

HFE gene, or the hemochromatosis protein, binds the transferrin receptor to inhibit cellular uptake of transferrin-bound iron. The mutated version loses binding affinity for

transferrin receptor and is unable to limit iron entrance, leading to cellular iron accumulation and overload (118, 119). Hepcidin promotes the internalization of ferroportin, which transports iron out of the cells including hepatocytes and macrophages (120). Hepcidin mutations are loss-of-function and lead to increased ferroportin-mediated iron export into circulation. Intriguingly, this leads to iron overload likely through excessive hepatocyte uptake of plasma non-transferrin bound iron that exceeds the rate of iron export (121). Hemojuvelin mutations similarly cause iron overload through downregulation of hepcidin expression (122). Transferrin receptor 2 is the liver-specific isoform, and mutations are predicted to be loss-of-function, again leading to decreased hepcidin expression (123, 124). Lastly, ferroportin mutants are unable to export iron (125).

Patients with type 1 or 3 experience a relatively minor phenotype, as HJV is able to compensate to an extent for loss of hepcidin activity. Type 2, the juvenile form, is the most severe and is associated with the most robust hepcidin inactivity leading to increased iron loading in the liver and in parenchymatous organs (126). Type 4 is milder than type 1 (127).

2.2.2 Impact on liver

Liver is one of the major organs affected by HH and around 75% of clinically affected hemochromatosis patients have evidence of liver disease at presentation. Iron localization is predominantly periportal in hepatocytes, as iron enters the liver through portal circulation (128). Kupffer cells also retain iron, often resulting from phagocytosing dead iron-rich hepatocytes. Intriguingly, in patients a strong positive correlation has been shown with iron overload in Kupffer cells, and ICAM-1 expression in hepatocytes, leading to increased fat deposition and fibrosis (129). The liver is the source of hepcidin production (126), and almost all HH types lead

to decreased hepcidin expression as described above, also explaining the increased hepatic insult compared to other organs.

Excess iron deposition in hepatocytes is also associated with hepatomegaly, elevated liver enzymes, oxidative stress, steatosis, inflammation, fibrosis, and cancer (130, 131). In fact, 50% of HH-related deaths result from hepatic cirrhosis or hepatocellular carcinoma, and HH patients are 200 times more likely to develop hepatocellular carcinoma (132, 133).

2.2.3 Current treatments for HH

Presently, recurrent phlebotomy is the only effective way to prevent chronic iron overload in patients with HH, baring absence of hepatic cirrhosis. In most cases, 400-500 mL of blood is removed weekly to reduce serum ferritin levels and hence, iron levels (111, 132, 134). Strikingly, phlebotomy has been the standard of care for HH patients since 1950 (111), highlight a lack of therapeutic advancement. Transplant is another therapeutic option for patients with liver complications, and five-year survival rates post liver transplant for HH patients are comparable to rates from non-HH liver recipients (135), although longitudinal studies did not control for HH type. Further, like any chronic liver disease, donor organs are severely lacking and liver transplant is an uncommon option for HH patients.

2.2.4 Animal models of hemochromatosis

One major obstacle in studying cellular and molecular mechanisms underlying hemochromatosis disease progression is the lack of relevant animal models. Rodents fed high iron diet do not display injury or disease progression like patients. Transgenic models, including an HFE-

deficient mouse, Trf2-mutated mouse, Trf1-mutated mouse, and hepcidin-knockout mouse inexplicably have no effect on iron loading, or exhibit increased iron stores with no associated injury (136-141).

Hepcidin knockouts fed 3% carbonyl iron diet displayed mild hepatic inflammation, apoptosis, and twelve-month old hepcidin knockouts developed liver fibrosis (but not six-month old) (136). Further, disrupting both HFE and Trf2 via double knockout lead to increased iron-induced hepatic injury in the form of inflammation and fibrosis compared to a single knockout or wildtype animal (142). However, further investigation identifies marginal inflammation and fibrosis, and steatosis is absent in this model. Thus there is a significant need for development of relevant animal models that can mimic human disease.

2.2.5 Role of Wnt/β-catenin in hemochromatosis

Studies assessing the role of Wnt and/or β-catenin in iron metabolism are limited, however one study identified a Wnt/β-catenin inhibitor *in vitro* that worked through chelating iron (143), suggesting iron can activate Wnt/β-catenin signaling. Another group demonstrated that increased cellular iron leads to elevated Wnt/β-catenin activity as measured by TOPFLASH reporter assay (144). This link has not been investigated further, or in the context of HH.

We hypothesize β-catenin is required for response to hepatic iron overload *in vivo*. Our lab has previously identified β-catenin to be a primary regulator of the antioxidant response through target gene regucalcin-dependent production of ascorbic acid (36). As mentioned, oxidative stress is present in HH patients (145) and likely an early symptom of disease onset (146). We have also identified β-catenin knockout mice (bKO) to have higher tumor burden and

fibrosis after diethylnitrosamine-induced oncogenesis due to increased inflammation and oxidative stress (94). We predict a similar phenotype in bKO mice after chronic iron overload.

2.3 METHODS

2.3.1 Animals

All animal work was performed in accordance with the University of Pittsburgh Institutional Animal Care and Use Committee. Liver-specific β-catenin knockout mice (bKO) were generated as previously described (89). Briefly, mice expressing Cre recombinase under the Albumin promoter were crossed with animals carrying LoxP sites flanking β-catenin.

One to three month old male and female bKO and littermate controls (bCON) were used in this study, n=3-5 for each condition. Mice were subjected to a 1% carbonyl 10,000ppm iron diet (Harlan Laboratories) (bCON+Fe, bKO+Fe) or basal diet (bCON–Fe, bKO–Fe) for three months. Male and female mice were also used for 4 week and 5 day timepoints, n=3-4. As no differences were observed in male versus female mice, and considering males are affected by iron overload more frequently than females (147), male mice were used for subsequent antioxidant studies (n=3-4). N-Acetyl-L-(+)-cysteine (NAC, 2g/kg, Fisher Chemical) was administered to mice on iron diet via drinking water for three months. For all studies, iron diet was replaced every two weeks, and NAC was replaced every week.

2.3.2 Immunohistochemistry

Four micron paraffin sections were dehydrated with xylene and graded ethanol, and rinsed in PBS. Heat-mediated antigen retrieval was performed and slides were inactivated for endogenous peroxidases. Unless mentioned, slides were blocked with Super Block (ScyTek Laboratores). The following antibodies used citrate buffer in microwave: β-Catenin, Cyclin D1, Glutamine Synthetase, Cyp2e1, 4-Hydroxynonenal, Malondialdehyde, α-Smooth Muscle Acin which required use of a Mouse On Mouse Kit (Vector). Ki67, used Tris EDTA in microwave. Sox9, used citrate buffer in pressure cooker. CD45 and CK19 required DAKO antigen retrieval in pressure cooker. F480 required proteinase K digestion for antigen retrieval. See Table 4 for antibody information. Secondary antibodies were purchased from Millipore and used at 1:400. Sections stained with antibodies were incubated with streptavidin-biotin and signal was detected with DAB.

Table 4: Antibodies used in Section 2.0

Name	Use and dilution	Supplier	Cat no.
β-catenin	IHC: 1:100	Santa Cruz	Sc-7199
Cyclin D1	IHC: 1:200	Neomarkers	RB-9041-P
Glutamine Synthetase (GS)	IHC: 1:50	Santa Cruz	Sc-9067
Cytochrome p450 2e1 (Cyp2e1)	IHC: 1:500	Sigma Aldrich	HPA009128
4-Hydroxynonenal (4HNE)	IHC: 1:2000	Millipore	393207
Malondialdehyde (MDA)	IHC: 1:200	Abcam	Ab6463
α-Smooth muscle actin (αSMA)	IHC: 1:200	Dako	M0851
Sox9	IHC: 1:10,000	Abcam	AB5535
CD45	IHC: 1:100	Santa Cruz	sc-53665
CK19	IHC: 1:10	DSHB	TROMA-III-S
β-catenin	WB: 1:1000	BD Biosciences	610154
Hypo-phosphorylated β-catenin at Ser33/Ser37/Thr41	WB: 1:1000	Cell Signaling	4270s
Regucalcin	WB: 1:1000	Santa Cruz	sc-130344
Cytochrome p450 1a2 (Cyp1a2)	WB: 1:200	Santa Cruz	sc-53241
Peroxisome proliferator-activated	WB: 1:200	Santa Cruz	sc7273

receptor γ (PPARγ)			
Phosphorylated Extracellular signal–regulated kinase (ERK) (T202/T204)	WB: 1:1000	Cell Signaling	4370
Extracellular signal–regulated kinase (ERK)	WB: 1:1000	Cell Signaling	4695
Phosphorylated Protein Kinase B (AKT) (T308)	WB: 1:1000	Cell Signaling	13038
Protein Kinase B (AKT)	WB: 1:1000	Cell Signaling	4685
Phosphorylated Nuclear factor kappa-light-chain-enhancer of activated B cells (NFκB) (Ser536)	WB: 1:1000	Cell Signaling	3033
Nuclear factor kappa-light-chain-enhancer of activated B cells (NFκB)	WB: 1:200	Santa Cruz	Sc-372
α-Smooth muscle actin (αSMA)	WB: 1:1000	Abcam	ab5694
Platelet Derived Growth Factor Receptor Beta (PDGFRB)	WB: 1:200	Santa Cruz	Sc-432
Interleukin 6 (IL6)	WB: 1:1000	Abcam	ab7737
C-C Motif Chemokine Ligand 2 (CCL2)	WB: 1:200	Santa Cruz	Sc-1785
Glyceraldehyde 3-phosphate dehydrogenase (GAPDH)	WB: 1:200	Santa Cruz	Sc-25778
Actin	WB: 1:1000	Millipore	MAB1501
Ki-67	IHC: 1:100	Thermo Fisher	RM-9106-S0
F480	IHC: 1:100	Serotec	MCA497A488

2.3.2.1 Special stains

For assessing collagen deposition, sections were deparaffinized and stained with picrosirius red (Biorad) for 1 hour, then dipped in acidified water (5ml acetic acid in 1L H_2O) and dehydrated. Prussian blue stain was performed by the Research Histology Services at the University of Pittsburgh. For terminal deoxynucleotidyl transferase dUTP nick end labeling (TUNEL), ApopTag peroxidase kit (Intergen) was used under the manufacturer's protocol.

2.3.3 Protein extraction and western blotting

Protein extraction from frozen liver tissue was performed using RIPA buffer with protease and phosphatase inhibitors (Sigma). Forty micrograms of protein were resolved by SDS-PAGE on a 7.5% precast gel (Biorad) and transferred to nitrocellulose membranes using semi-dry Trans-Blot Turbo Transfer System (Biorad). Antibodies used are available in Table 4. Horseradish peroxidase-conjugated secondary antibodies were purchased from Millipore.

2.3.4 Fatty acid and iron profiles

For triglyceride and cholesterol ester profiles, snap-frozen tissue was sent to the Hormone Assay and Analytical Services Core at Vanderbilt University for analysis.

For serum iron profiles, serum was collected through retro-orbital cavity and was analyzed according to manufacturer's instructions using the Iron-SL kit (Seikisui, Cat# 157-30, Lexington, MA). Briefly, 20µl serum samples or standard (provided in the kit) was added to 260µl R1 buffer and A595 measured with a 96 well plate reader [A1]. R2 buffer was added to bring the volume to 340µl, incubated at room temperature for 5 minutes then measured again at the same wavelength [A2]. The serum iron concentration (µM) was calculated with the following formula: (A2 –A1 Sample/A2-A1 Standard)*35

Liver tissue was weighed (mg) and homogenized in 1ml protein precipitation solution (0.53N HCl and 5.3% trichloroacetic acid in HPLC grade water using a Pro Gen PRO200 homogenizer (Pro-Scientific, Oxford, CT). Iron Standard (Ricca Chemical Company, Arlington, TX) was diluted in protein precipitation solution to generate a standard series from 5 – 0.08mM.

75µl of each standard was diluted to 1ml with protein precipitation solution in a microtube. Samples and standards were boiled for 60 minutes then centrifuged for 10 min at 14,000xg.

The Iron-SL iron kit was used as follows: 30µl sample and standards were placed in duplicate wells in a 96 well plate, 150µl R1 and then 40µl R2 buffers were added, mixed for 5 minutes at 330RPM then A595 measured and mM concentrations determined using the standard curve. Iron by weight was calculated using the following formula: µg/g Non-Heme Iron = [Iron mM/weight(mg)] x 75 x 55.5

2.3.5 RNA extraction and qPCR analysis

RNA was extracted from frozen liver using Trizol (Invitrogen) and 2µg of RNA was reverse-transcribed using Super Script III first strand kit (Invitrogen). Real-time PCR was ran using SYBR Green (Thermo) and all values were normalized to GAPDH. See Table 5 for primer information.

Table 5: Primer sequences for qPCR in Section 2.0

Name	Sequence	Supplier
GAPDH forward primer	AACTTTGGCATTGTGGAAGG	Integrated DNA Technologies
GAPDH reverse primer	ACACATTGGGGGTAGGAACA	Integrated DNA Technologies
Ceruloplasmin (CP) forward primer	TCCCTGGAACATACCAACC	Integrated DNA Technologies
Ceruloplasmin (CP) reverse primer	ATTTATTTCATTCAGCCAGACTTAG	Integrated DNA Technologies
Ferroportin (FP) forward primer	CTCTGTCAGCCTGCTGTTTG	Integrated DNA Technologies
Ferroportin (FP) reverse primer	TCAGGATTTGGGGCCAAGATG	Integrated DNA Technologies
Transferrin receptor 1 (TRF1) forward primer	ATAAGCTTTGGGTGGGAGGC	Integrated DNA Technologies
Transferrin receptor 1 (TRF1)	CTTGCCGAGCAAGGCTAAAC	Integrated DNA

reverse primer		Technologies
Transferrin receptor 2 (TRF2) forward primer	GTTGCTGAGCTGAACTTGGC	Integrated DNA Technologies
Transferrin receptor 2 (TRF2) reverse primer	TGAGTTCCATGGGGCAGAAC	Integrated DNA Technologies
Hepcidin (HAMP) forward primer	TGTCTCCTGCTTCTCCTCCT	Integrated DNA Technologies
Hepcidin (HAMP) reverse primer	CTCTGTAGTCTGTCTCATCTGTTG	Integrated DNA Technologies
Hemojuvelin (HJV) forward primer	GGGAGTCACGTGGAGATTCG	Integrated DNA Technologies
Hemojuvelin (HJV) reverse primer	ACGCAGGATTGGAAGTAGGC	Integrated DNA Technologies
Human hemochromatosis protein (HFE) forward primer	GCAATGGCTACAGGGTGACT	Integrated DNA Technologies
Human hemochromatosis protein (HFE) reverse primer	CTGGTCATCCACATAGCCCC	Integrated DNA Technologies

2.3.6 Proinflammatory cytokine analysis

To assess cytokine levels in 5 day iron-fed mice, the V-PLEX Proinflammatory Panel 1 Kit (MesoScale) was used per the manufacturer's instructions to assess TNFα, IL6, and KC/Gro. Duoset Kit (R&D) was used to assess CCL2/MCP1, CCL5, and CXCL10 per the manufacturer's instructions.

2.3.7 Statistics

Data presented as mean and individual data points. Graphs were generated using GraphPad Prism 7 and comparisons between two groups were performed using Student's T Test. Two-tailed P values of <0.05 (*) and <0.01 (**) or less were considered significant.

2.4 RESULTS

2.4.1 Mice lacking beta-catenin in liver epithelial cells develop steatohepatitis and fibrosis after iron overload

Iron overload diet was fed for 3 months to bKO (KO+Fe) and bCON (bCON+Fe). While both groups tolerated the treatment, bKO+Fe livers showed evidence of gross injury showing pale discoloration and rigidity (not shown). Serum ALT levels trended higher in bKO+Fe although the differences were not significant (Fig.4A). bKO-Fe had significantly lower basal liver weight to body weight ratio (LW/BW) when compared to the bCON-Fe group as reported previously (Fig.4B) (89). Intriguingly, both bCON+Fe and bKO+Fe showed comparable and significantly higher LW/BW ratio than their respective controls (Fig.4B).

Liver histology revealed notable macrovesicular steatosis and inflammation in bKO+Fe only (Fig.4C). To confirm hepatic steatosis, we examined levels of hepatic lipids. bCON+Fe and bKO+Fe had significantly greater hepatic triglycerides and cholesterol esters than respective controls although bKO+Fe showed highest and most significant increase (Fig.4D, E). PPARγ, a known adipogenic factor negatively regulated by β-catenin (148), was marginally increased in KO basally but was further induced in bKO+Fe (Fig.4F). KO-Fe livers show a small increase in CD45-positive inflammatory cells as reported previously (100).

Iron diet led to more pronounced inflammation in bKO along with F480-positive macrophage infiltration (Fig.5A, B). Enhanced inflammation in bKO+Fe was further verified by the presence of increased inflammatory markers IL-6 and CCL2 by Western blots (WB), both of which migrate slower likely due to glycosylation (149, 150) (Fig.5C). Presence of steatohepatitis was also associated with increased fibrosis as revealed by Sirius Red staining showing extensive

collagen accumulation in bKO+Fe only (Fig.5D and Fig.7A). This was further validated by the presence of activated myofibroblasts seen by increased α-smooth muscle actin (α-SMA) by both WB and IHC in KO+Fe only (Fig.5E, F). Presence of fibrosis was further supported by elevated PDGFRβ levels (Fig5E).

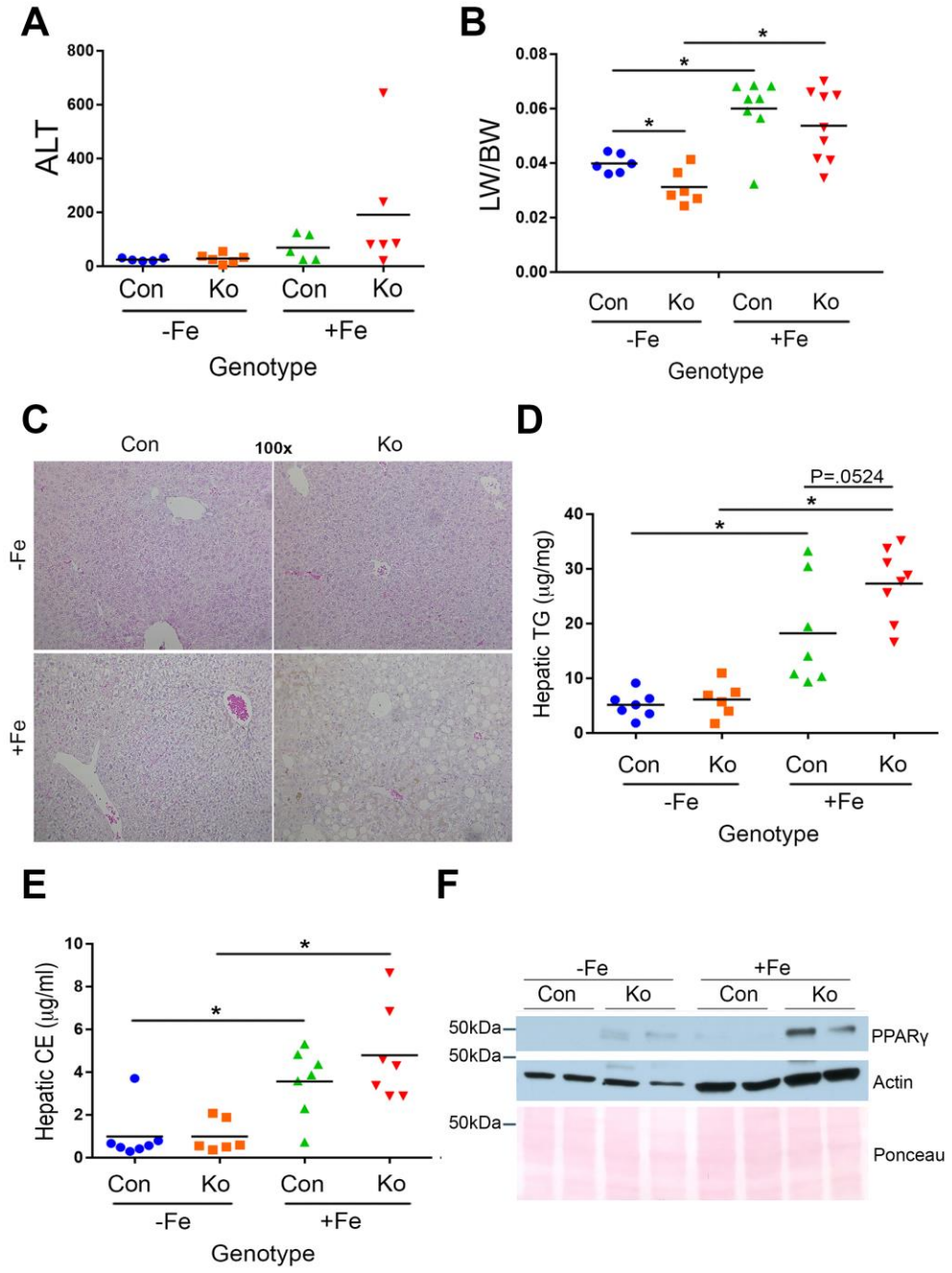

Figure 4: Chronic iron overload causes steatohepatitis in β-catenin knockout mice.

(A) Serum ALT levels reflect a modest but insignificant increase in bKO+Fe as compared to other groups. (B) Iron causes increased liver weight to body weight ratio (LW/BW) in bCON+Fe and bKO+Fe. At baseline, bKO show significantly lower LW/BW than bCON. (C) Representative H&E staining (100x) shows mild hepatic steatosis in bCON+Fe and more profound hepatic steatosis and inflammation in bKO+Fe. (D) Increased hepatic triglycerides (TG) (p=0.0524) in bKO+Fe as compared to bCON+Fe. (E) Cholesterol esters (CE) were

comparably increased after iron in bKO and bCON. (F) Representative WB showing increase in PPARγ in bKO+Fe as compared to other groups. *p<0.05 using Student's T test.

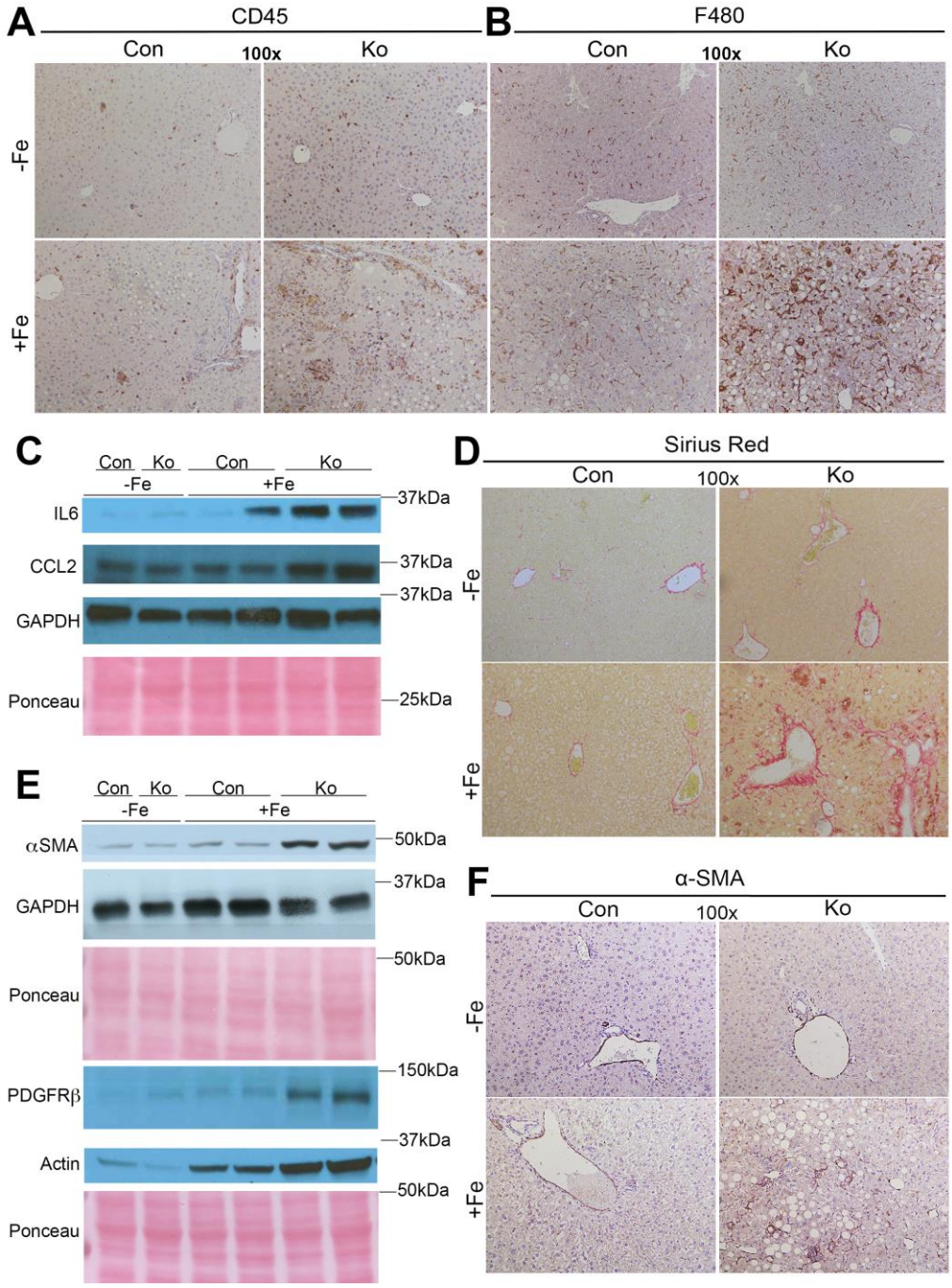

Figure 5: bKO+Fe have increased hepatic inflammation and fibrosis after chronic iron overload.
(A) Representative IHC images demonstrate increased CD45-positive inflammatory cells in bKO+Fe as compared to other groups. (B) Representative IHC images demonstrate increased F480-positive macrophages in bKO+Fe only. (C) Representative WB shows bKO+Fe have increased inflammatory markers including IL-6 and CCL2. IL-6 and CCL2 appear to be migrating slower due to glycosylation. (D) bKO+Fe have increased Sirius Red staining

suggesting increased collagen deposition. (E). WB show increased levels of α-SMA and PDGFRβ substantiating presence of fibrosis. (F) IHC for α-SMA also confirms presence of activated myofibroblasts in bKO+Fe only. (Image magnification: 100x)

2.4.2 bKO display enhanced ductular reaction in response to injury due to iron overload.

We next investigated cellular injury and repair in bKO+Fe. A marginal increase in cell death as seen by TUNEL staining was evident in bCON+Fe, which was exacerbated in bKO+Fe (Fig.6A). This was associated with modest but comparable increase in S-phase marker Ki-67, in hepatocytes in bCON+Fe and bKO+Fe (Fig.6B). Likewise, a mid-zonal increase in Cyclin D1 expression was evident in bCON+Fe, which was reduced in bKO+Fe and instead observed in periportal hepatocytes (Fig.6B). Chronic hepatic injury can lead to progenitor cell response in the form of ductular reaction, especially if hepatocyte proliferation is disproportionally lower than ongoing death (151). Indeed, bKO+Fe uniquely showed increased sox-9, EpCAM and CK19 positive ductular reaction (Fig.6D-F).

Continued injury in bKO+Fe led to development of bridging fibrosis outlining regenerating nodules (Fig.7A). We also observed occurrence of occasional HCC nodule in bKO+Fe (Fig.7B). Intriguingly, tumors were β-catenin and GS-positive (Fig.7B).

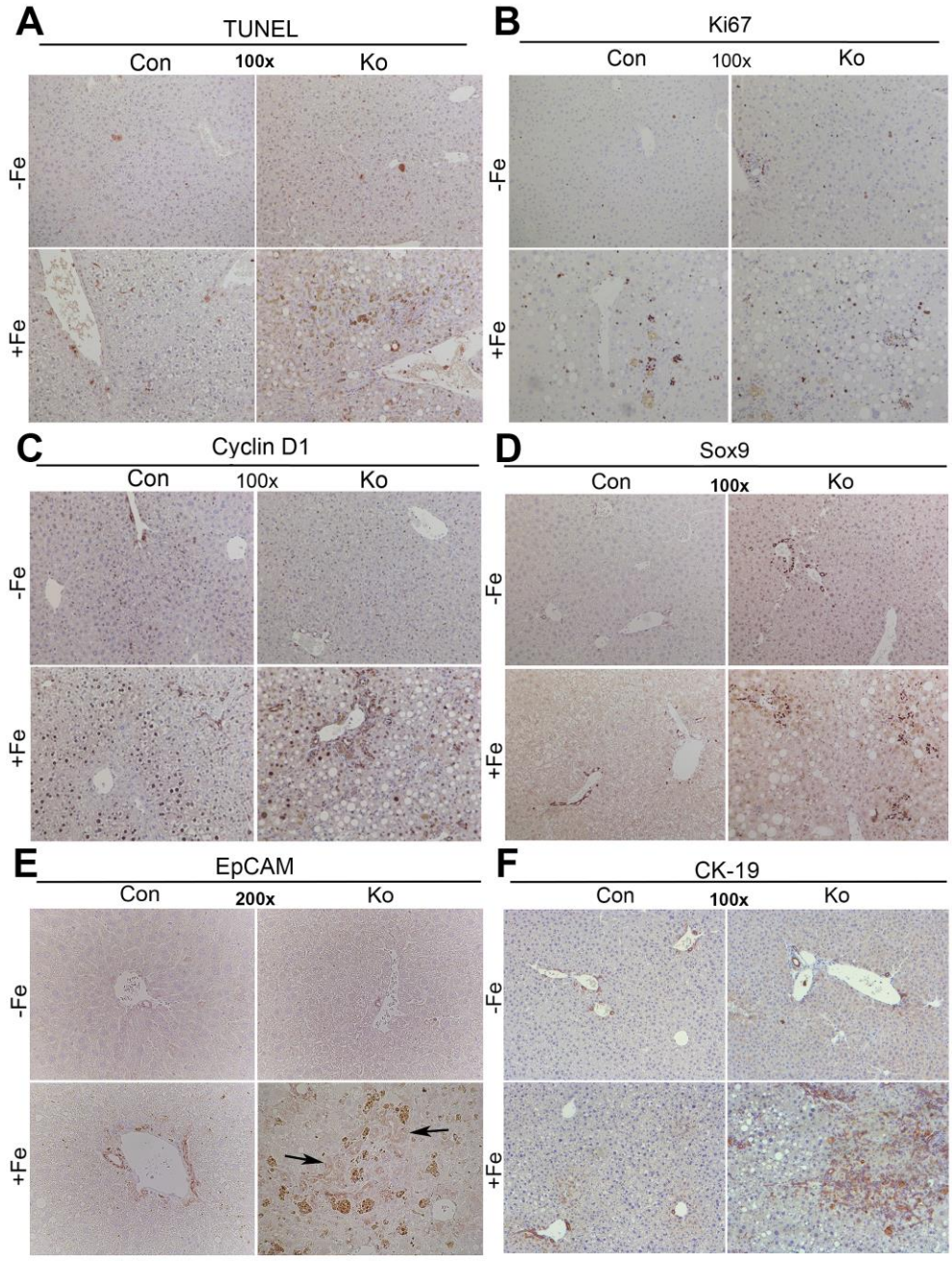

Figure 6: Analysis of cell death, proliferation and ductular reaction in bCON and bKO on normal and high iron diet.

(A) Representative images of TUNEL staining shows marginal increase in cell death in bCON+Fe, but a greater increase in bKO+Fe. (B) Ki-67 IHC demonstrates comparable and increased number of cells in S-phase after iron overload in both bCON+Fe and bKO+Fe. (C) Cyclin D1 staining is increased in midzonal hepatocytes in bCON+Fe compared tob CON-Fe. bKO+Fe exhibit less Cyclin D1 staining in periportal hepatocytes and in ductular cells. (D) bKO+Fe have increased ductular reaction as evident by IHC for Sox9. (E) Increased ductular reaction in bKO+Fe was confirmed by EpCAM staining. (F) Increased ductular reaction in

bKO+Fe was also confirmed by IHC for CK19. (Image magnification:100X, except EpCAM:200x).

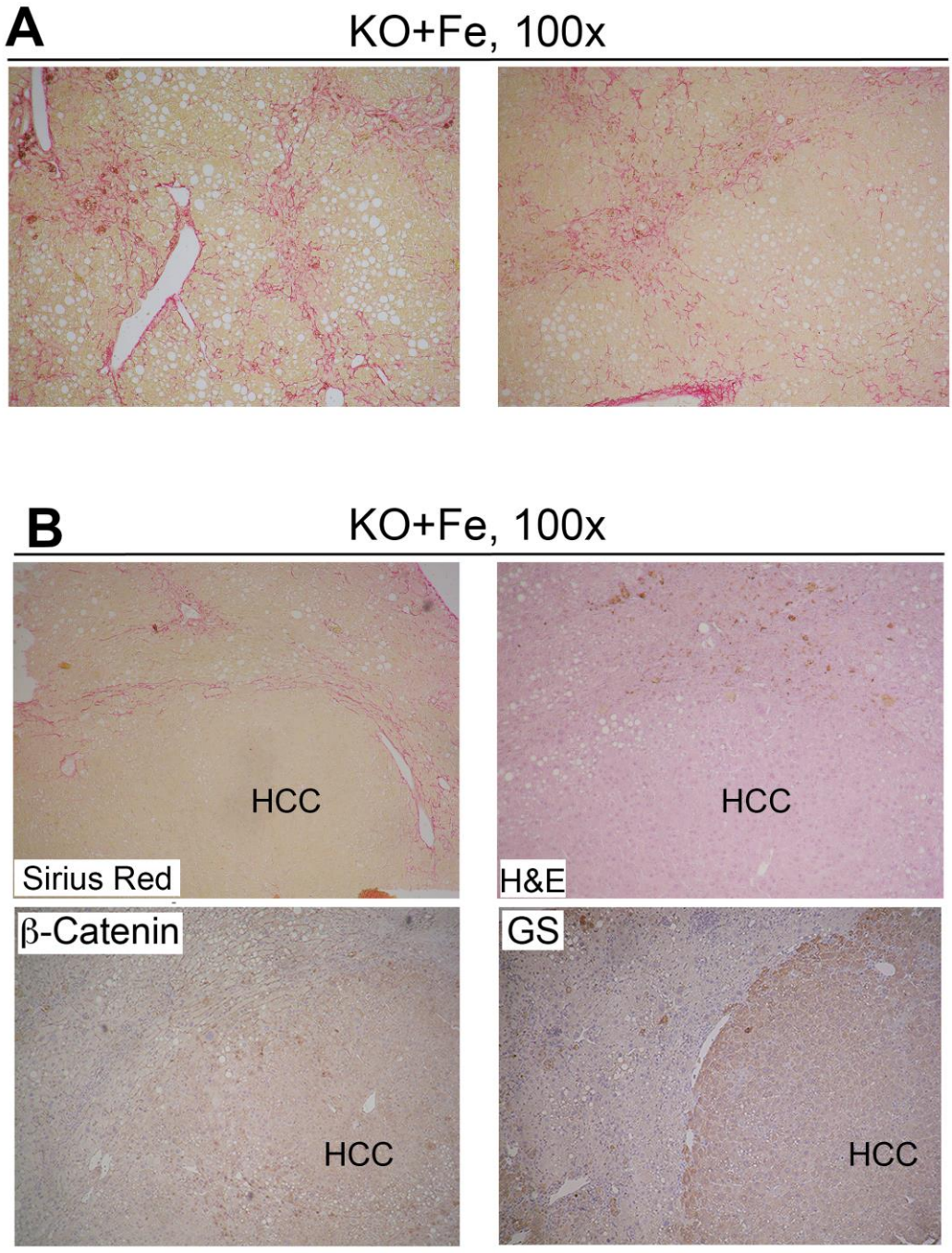

Figure 7: bKO+Fe display increased bridging fibrosis and development of HCC.
(A) Additional images of Sirius red staining showing bridging fibrosis in bKO+Fe. (100x). (B) Image of HCC observed in a subset of bKO+Fe mice. Sirius red staining shows tumor nodule lacking intratumoral fibrosis. H&E identifies HCC. IHC for β-catenin shows HCC to be composed of β-catenin-positive cells. IHC for Glutamine Synthetase (GS) also shows HCC to be positive for this β-catenin target. (100x).

2.4.3 Comparable hepatic iron accumulation in bKO and bCON following iron overload.

Next, we addressed if iron metabolism is altered in bKO+Fe. Prussian blue staining revealed iron accumulation in bCON+Fe predominantly in the periportal region (Fig.8A). Iron accumulation showed a more pan-zonal distribution in bKO+Fe (Fig.8B). An increase in aggregates of iron pigment in bKO+Fe reminiscent of iron-laden macrophages was also observed (Fig.8B). However, both bCON+Fe and bKO+Fe had an increase in total liver iron content compared to respective controls, and differences in the hepatic iron content between bCON+Fe and bKO+Fe were insignificant (Fig.8C). Interestingly, bKO+Fe showed increased serum iron when compared to bKO-Fe, whereas bCON+Fe and bCON-Fe showed no differences (Fig.8D).

Next, we determined expression levels of genes commonly mutated in hemochromatosis or otherwise involved in iron metabolism by RT-PCR. Hepcidin, a gene that inhibits iron export from a cell (152) was comparably induced in bCON and bKO after iron overload as reported previously (153) (Fig.9A). Human hemochromatosis protein and hemojuvelin, two genes frequently mutated in different hemochromatosis subtypes (142), demonstrated no significant differences in expression (Fig.9B,C). Expression of ceruloplasmin, which converts toxic ferrous form to a nontoxic ferric form (154), was increased in bKO+Fe as compared to bCON+Fe, with an insignificant increase compared to bKO-Fe (Fig.9D). Transferrin receptors 1 and 2 are cell surface receptors required for iron entry into cells (124, 155). Although TRF1 expression is low in the liver (124), we saw a further reduction in bCON+Fe and bKO+Fe compared to bCON-Fe and bKO-Fe (Fig.9E). TRF2 was not significantly altered in bCON+Fe compared to bCON-Fe, as also reported elsewhere (124). Interestingly, a modest but statistically significant decrease in TRF2 was observed in bKO+Fe when compared to bKO-Fe (Fig.9F). Ferroportin, the iron export protein negatively regulated by hepcidin (120), is increased in bCON and bKO after iron

although increase is significantly greater in bKO+Fe (Fig.9G). Overall, our data suggests that major iron regulatory genes are unaffected by β-catenin signaling basally, but bKO+Fe livers show altered expression of some iron regulatory genes, likely in an attempt to compensate for increased hepatic injury after high iron diet.

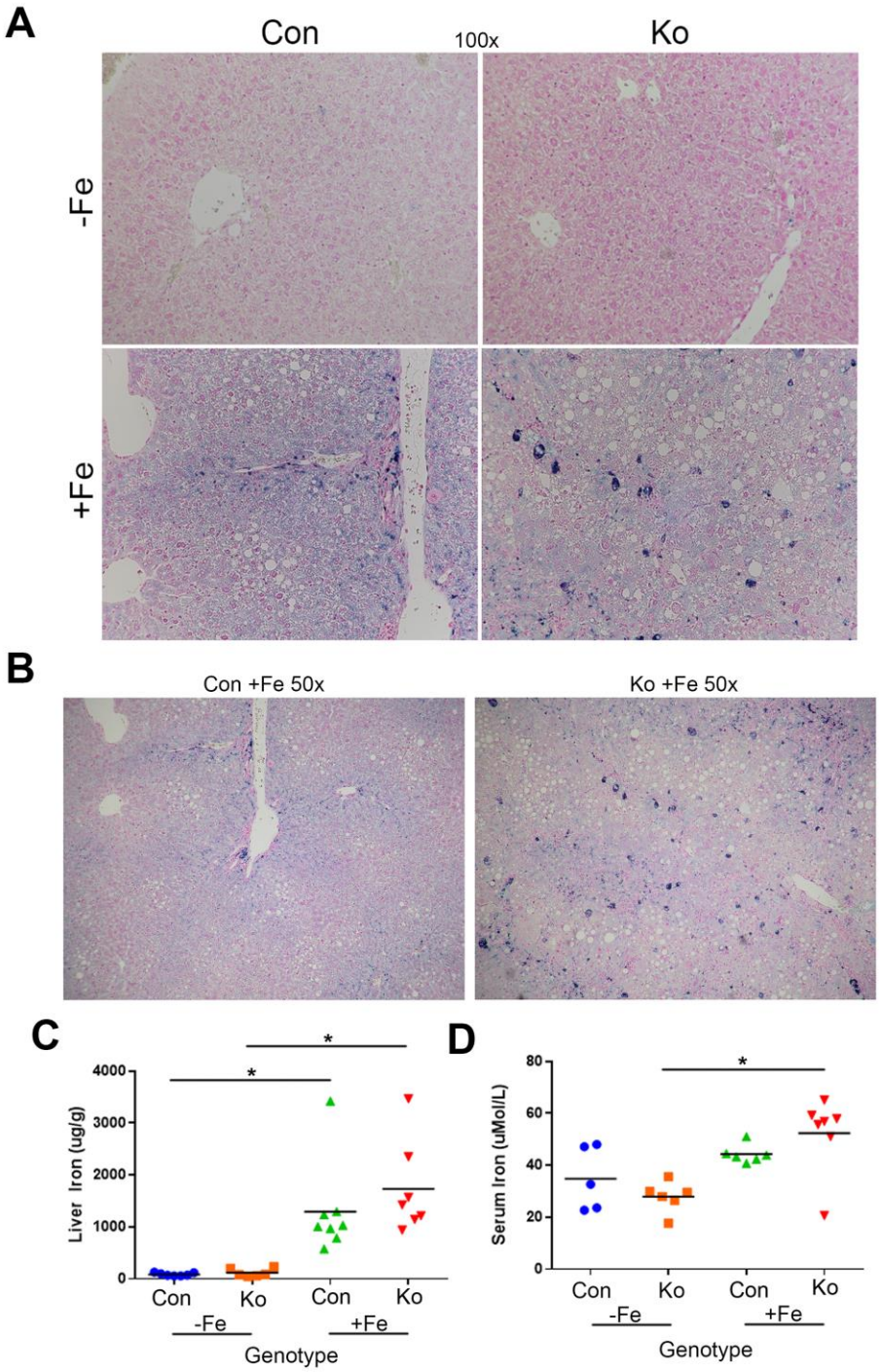

Figure 8: Comparable hepatic iron levels in bCON+Fe and bKO+Fe, despite increased serum iron and altered iron zonation in bKO+Fe.

(A) Prussian blue staining (100x) shows iron accumulation is periportal in bCON+Fe. In bKO+Fe, iron deposition is pan-zonal. Aggregates of iron pigment resembling iron-laden macrophages were observed in bKO+Fe (B) A Periportal Prussian blue staining in periportial region in bCON+Fe versus more pan-zonal staining in bKO+Fe can be appreciated in lower magnification (50x). (C) Liver iron levels increase comparably in bCON+Fe and bKO+Fe

compared to bCON-Fe and bKO-Fe. (D) Serum iron levels are increased in bKO+Fe compared to bKO-Fe, but there is no difference between bKO+Fe and bCON+Fe. *p<0.05 using Student's T test.

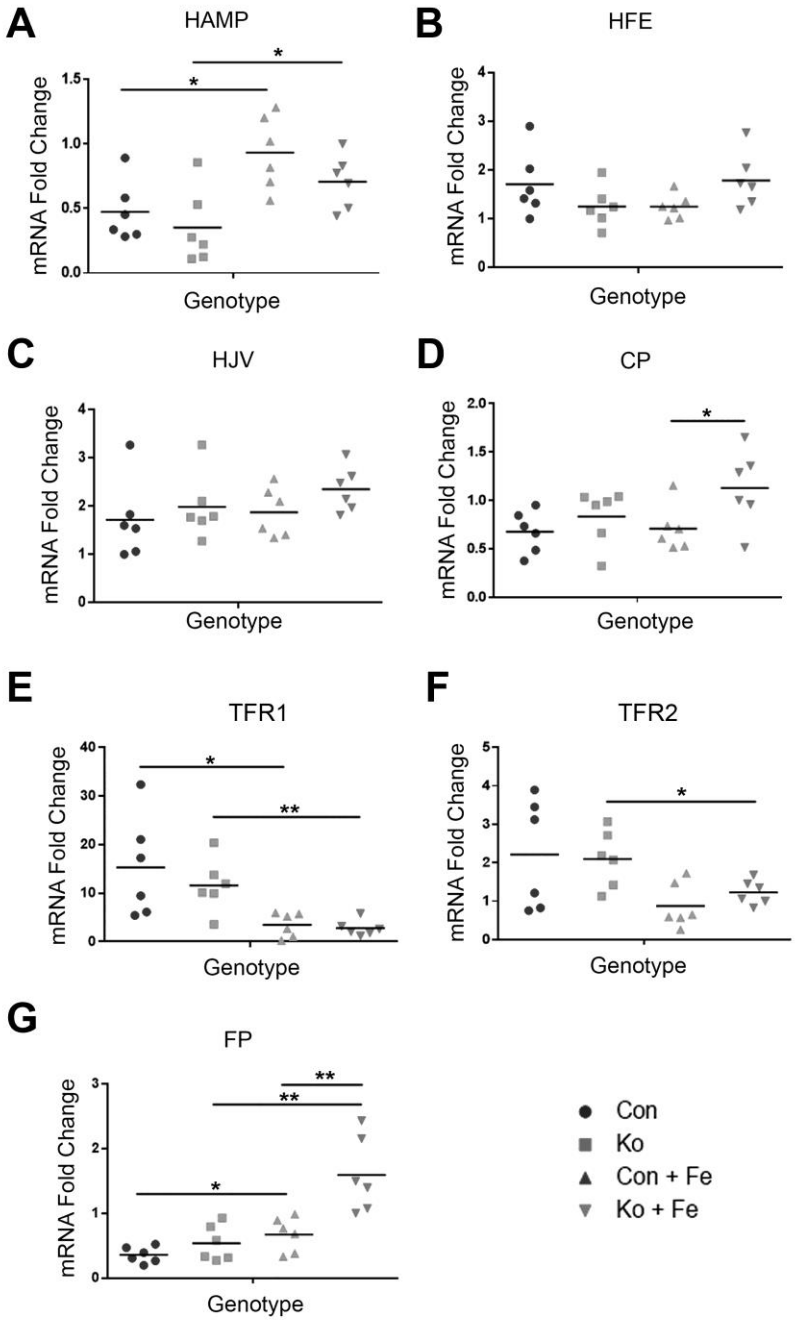

Figure 9: Changes in the expression of iron regulatory genes in bKO and bCON, on control or high iron diet.

RT-PCR displaying comparison of mRNA fold change of major iron regulatory genes in bCON-Fe, bKO-Fe, bCON+Fe, and bKO+Fe, including Hepcidin (HAMP) (A), Human

hemochromatosis protein (HFE) (B), Hemojuvelin (HJV) (C), Ceruloplasmin (CP) (D), Transferrin Receptor 1 (TRF1) (E), Transferrin Receptor 2 (TRF2) (F), and Ferroportin (FP) (G). Expression was normalized to bCon-Fe for each gene. *p<0.05, **p<0.01 using Student's T test.

2.4.4 Iron overload decreases β-catenin signaling in bCON but induces other cell survival and mitogenic signaling in bKO

Next, we asked if chronic iron overload impacts β-catenin signaling in the liver. Livers from mice fed high iron diet or basal diet were assessed for liver-specific β-catenin targets. Intriguingly, we observed a decrease in Glutamine synthetase (GS), Cyp1a2 and Cyp2e1 (Fig.10A.B). In the absence of any evidence of β-catenin activation by iron overload, the mechanism of worse injury in high iron-fed bKO mice required additional investigation.

We first assessed factors like Protein Kinase B (Akt), extracellular signal-regulated kinase 1/2 (Erk1/2), and nuclear factor kappa-light-chain-enhancer of activated B cells (NFκB). Akt, which is involved in cell survival, migration, and proliferation (156), showed increased phosphorylation in bKO+Fe compared to other groups (Fig.10C). Erk1 phosphorylation, which is associated with hepatic fibrosis (157), was increased at baseline in bKO-Fe, was induced by iron in both bCON and bKO, and was highest in bKO+Fe (Fig.10C). Erk2 phosphorylation showed only a modest increase in bKO-Fe with no notable differences between bCON+Fe or bKO+Fe (Fig.10C). NFκB, which regulates genes involved in inflammation (158), proliferation and survival (159), showed increased phosphorylation in bKO+Fe compared to other groups (Fig.10C). Taken together, these data suggest that iron overload leads to decreased β-catenin signaling but in its absence, leads to activation of Akt, Erk and NFκB, which may contribute to greater hepatic injury and repair response in bKO+Fe.

2.4.5 Evidence of increased hepatic oxidative stress and β-catenin activity in bKO after iron overload.

Since β-catenin has been shown to regulate redox homeostasis in hepatic tissue through multiple mechanisms (68, 87, 94), we next investigated if β-catenin-deficient livers are inept at counteracting oxidative stress generated normally by iron accumulation and inflammation, and known to contribute to chronic injury, fibrosis and cancer (160, 161). Indeed, increased oxidative stress in the form of lipid peroxidation was seen in bKO+Fe by IHC for both 4-hydroxynonenal (4HNE) and malondialdehyde (MDA) (Fig.10D). Predictably, lipid peroxidation products were visible in and around areas of steatosis in the bKO+Fe.

Since Cyp2e1 has been implicated in contributing to harmful reactive oxygen species (ROS) (162) and regulated by β-catenin signaling in liver (89, 163), we assessed its expression in bCON and bKO after iron. Decrease in Cyp2e1 staining and its localization to sparse areas of steatosis was observed in bCON+Fe as compared to bCON-Fe (Fig.11A). Intriguingly, while no Cyp2e1 was detected in bKO-Fe, iron overload led to an unexpected increase, which was localized to steatotic areas in bKO+Fe (Fig.11A). The reappearance of Cyp2e1 was also confirmed by WB (Fig.11B). Likewise, while total β-catenin levels decreased in bCON+Fe, its levels increased in bKO+Fe (Fig.11B-D). Similarly, GS staining decreased and was irregular in bCON+Fe as compared to uniform pericentral staining in hepatocytes in bCON-Fe (Fig. 11E), However, while GS was absent in bKO-Fe, we observed occasional areas of GS-positive hepatocytes especially in steatotic and even periportal areas in bKO+Fe (Fig.11E). Thus, presence of chronic injury in KO after iron overload led to some repopulation by β-catenin-positive hepatocytes, which led to reappearance of Cyp2e1.

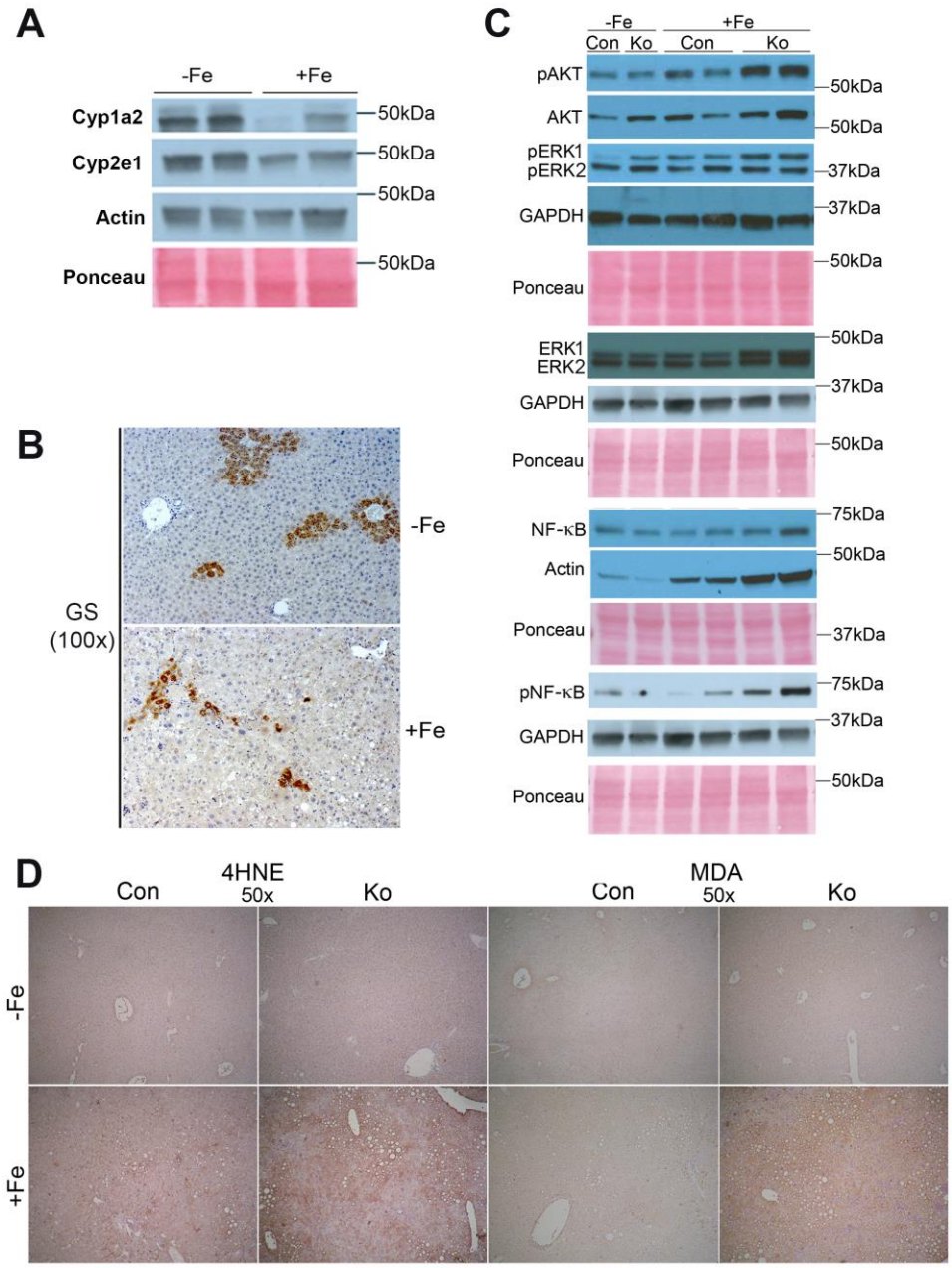

Figure 10: Chronic iron overload affects β-catenin signaling in bCON+Fe, but induces AKT, ERK, and NFκB signaling and lipid peroxidation in bKO+Fe.

(A) Representative WB show a decrease in hepatic levels of Cyp1a2 and Cyp2e1 levels after iron overload. (B) Representative IHC for GS shows decreased uniformity of GS staining in pericentral hepatocytes in bCON after iron overload (100x). (C) Representative WB show greater increases in pAKT (Thr308) and pERK1 (Thr202/Thr204) in KO+Fe as compared to bCON+Fe. pNFκB (Ser536) is induced only in bKO+Fe. (D) Representative IHC images show increased staining for lipid peroxidation markers 4-hydroxynonenal (4HNE) and malondialdehyde (MDA) in bKO+Fe. (50x).

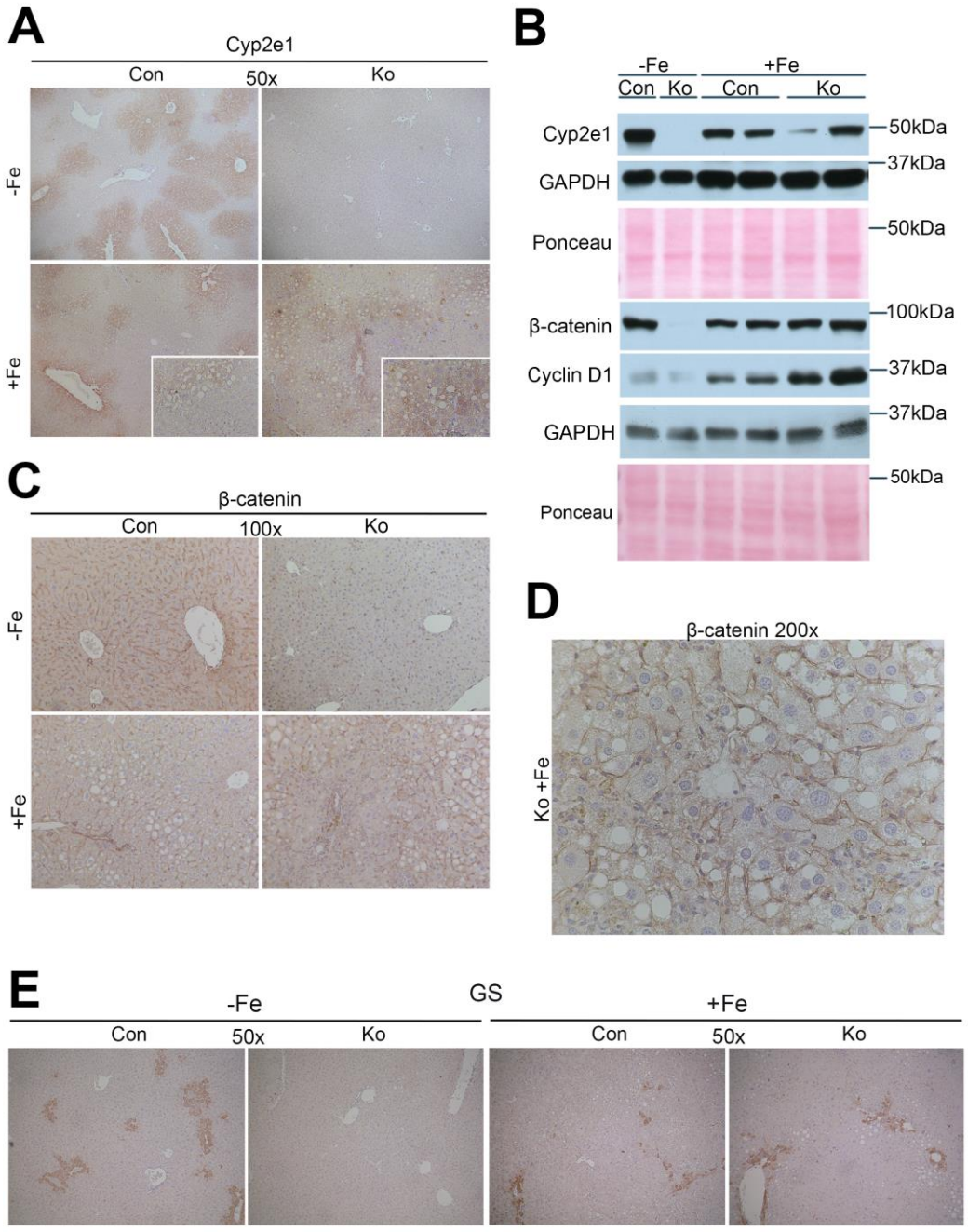

Figure 11: Reappearance of β-catenin and its targets following chronic iron overload in bKO.
(A) IHC for Cyp2e1 shows decrease in pericentral staining for Cyp2e1 in bCON after iron diet. bKO lack Cyp2e1 basally, however bKO+Fe show its re-appearance particularly in areas of steatosis. (B) WB confirm increases in levels of Cyp2e1, β-catenin, and Cyclin D1 in bKO+Fe compared to bKO-Fe. (C) Representative IHC images of β-catenin also confirm re-expression of β-catenin especially in steatotic areas in bKO+Fe (100x). (D) Higher magnification image of β-catenin IHC from bKO+Fe liver shows positive staining (200x). (E) Representative IHC of GS

shows decreased staining in bCON livers after iron diet, however in bKO which lack GS basally, show re-appearance of GS (50x).

2.4.6 N-Acetyl-L-(+)-cysteine (NAC) protects bKO after iron overload against injury and fibrosis.

Since increased lipid peroxidation appeared to be associated with steatohepatitis and fibrosis in bKO+Fe, we next administered NAC, an antioxidant, to bCON+Fe and bKO+Fe via drinking water for 3 months. NAC alleviated lipid peroxidation as observed by IHC for MDA and 4-HNE in KO+Fe (Fig.12). Simultaneously, we observed a modest decrease in steatosis, which was also reflected by a partial reduction in PPARγ levels (Fig.12,13A). NAC also led to a pronounced decrease in α-SMA IHC along with a dramatic decrease in fibrosis by Sirius Red staining (Fig.12). This was verified by decreased PDGFRβ and α-SMA protein levels (Fig.13A). Although numbers of CD45-positive cells remained unaffected by NAC in bKO, inflammation markers IL-6 and MCP1 lowered to match bCON+Fe+NAC levels (Fig.13A). Zonal iron distribution was also partially restored in bKO+Fe+NAC group (Fig.12).

Since we considered resurgence of β-catenin and its targets Cyp2e1 and GS as injury responses, we next posited that NAC may prevent such increase if injury is successfully alleviated. Indeed, levels of total β-catenin, Cyclin D1 and Cyp2e1 were diminished to non-existent levels as basal bKO, following NAC treatment as also verified by IHC (Fig.13B,C). NAC also prevented activation of AKT and NF-κB although pERK1 remained higher in bKO+Fe+NAC (Fig.13D). Intriguingly, pERK2 levels were markedly increased in both bCON and bKO after iron and NAC treatment (Fig.13E). Lastly, normalization of LW/BW ratio was evident in bKO+Fe+NAC group which was significantly lower than bCON+Fe+NAC (Fig.13F).

Thus, alleviating oxidative stress by NAC prevented several relevant complications of chronic iron overload in bKO.

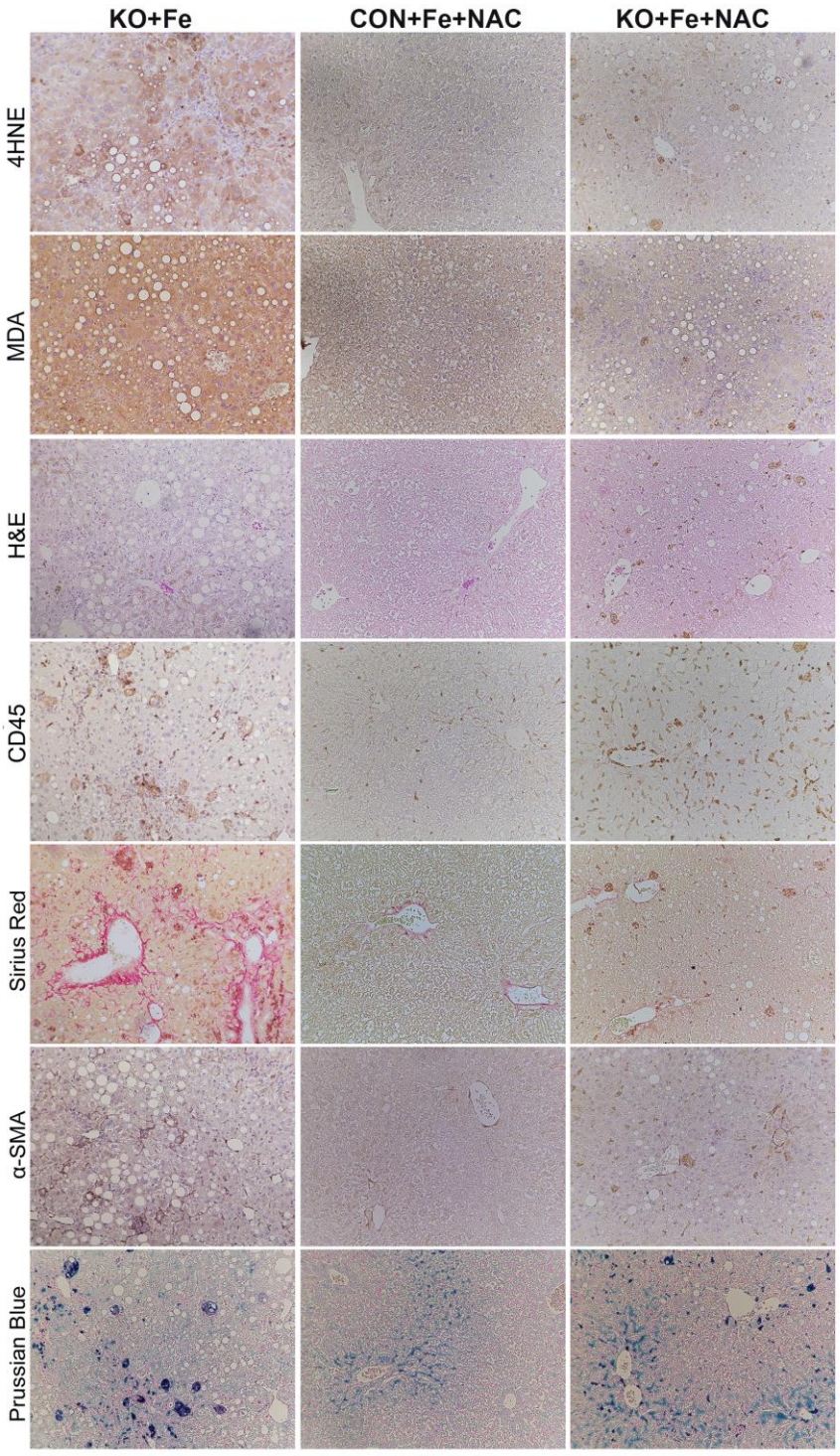

Figure 12: Inclusion of N-Acetyl-L-(+)-cysteine (NAC) in drinking water normalizes histology and affects oxidative stress, steatosis, fibrosis and iron staining in bKO+Fe, while inflammation remains unaltered.

Representative images from livers of bKO+Fe, bCON+Fe+NAC, and bKO+Fe+NAC mice showing a profound effect of NAC in reducing overall hepatic injury in bKO+Fe, which is depicted by decrease in staining for 4HNE, MDA, Sirius Red and αSMA. H&E shows

normalization of histology along with an overall decrease in steatosis. Prussian blue staining shows shift of pan-zonal staining to periportal staining after NAC treatment of bKO+Fe. No quantitative differences in the numbers of CD45 cells were seen. (100x).

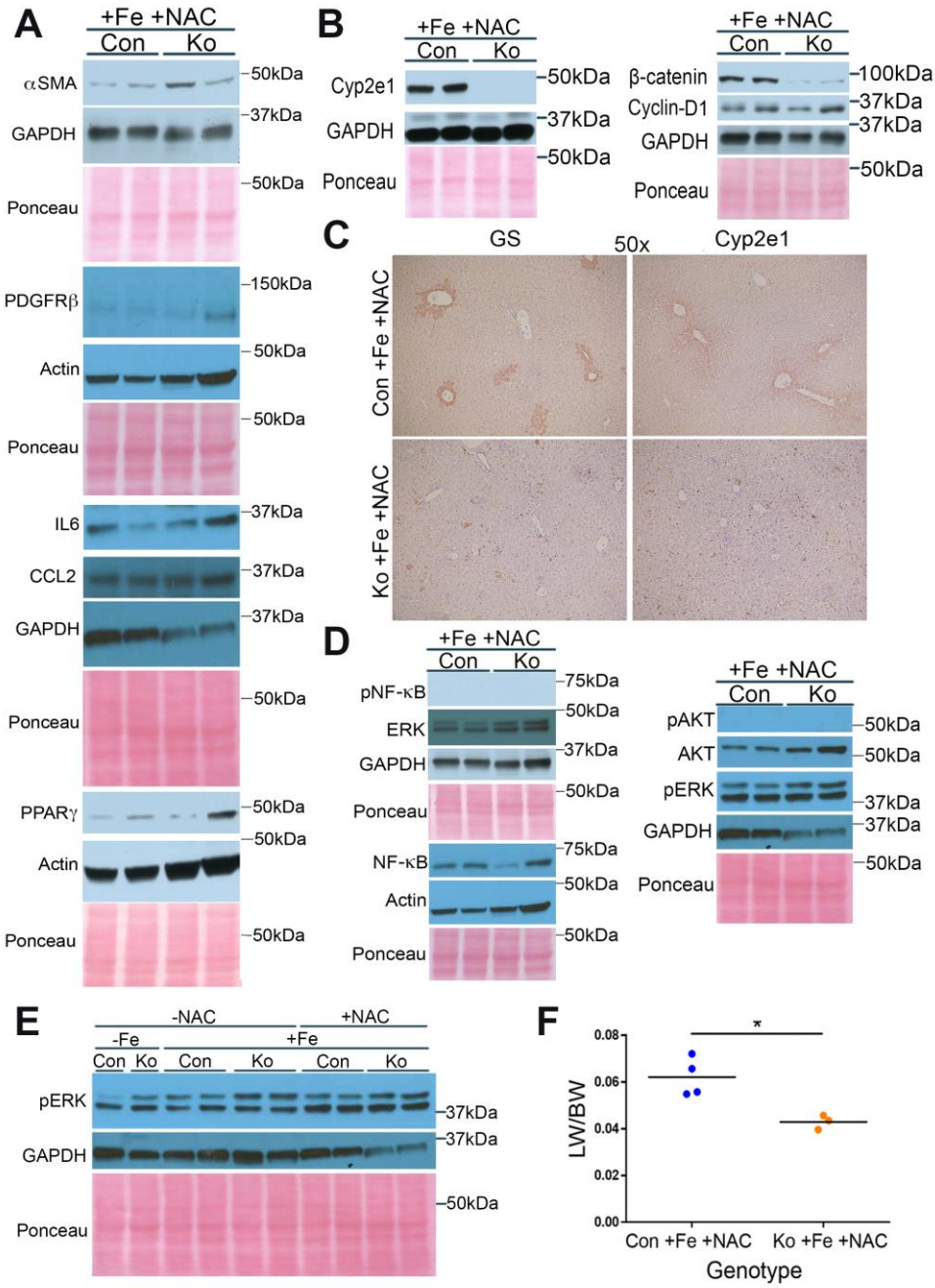

Figure 13: NAC rescues injury phenotype in bKO+Fe.

(A) WB confirms lack of increase in fibrosis markers α-SMA and PDGFR-β, and inflammation markers IL-6 and CCL2 in bKO+Fe+NAC. PPARγ levels are partially restored in bKO+Fe+NAC. (B) WB shows NAC treatment reduces levels of β-catenin, Cyp2e1, and Cyclin

D1 in bKO+Fe+NAC. (C) IHC shows absence of GS and Cyp2e1 in bKO+Fe+NAC (50x). (D) WB for total and activated ERK, AKT, and NFκB show lack of activation after NAC treatment. (E) WB shows pERK in bCON and bKO at baseline, with iron, and with iron and NAC. Same blot shown in Figure 13C and Figure 16D, shown here for direct comparison of pERK1 and pERK2 between NAC and non-NAC-treated groups. (F) LW/BW is decreased in bKO+Fe+NAC and is now similar to baseline bKO-Fe. *$p<0.05$ using Student's T test.

2.4.7 Inflammation precedes steatosis, which precedes fibrosis in bKO after iron overload.

To address the disease development in KO+Fe, we subjected bCON and bKO mice to 4-week iron-overload diet. Notable steatosis was evident in bKO+Fe, but not in bCON+Fe (Fig.14A). An associated increase in CD45- and F480-positive cells was also observed in bKO+Fe only along with mild fibrosis (Fig.14A). These observations suggest that fibrosis follows inflammation and steatosis in bKO+Fe.

We next challenged bKO and bCON with high iron diet for 5 days. No steatosis or fibrosis was evident in either group (Fig.14B). While no discernible differences in CD45-positive cells were evident, a small increase in F480-positive infiltrate was evident in bKO+Fe (Fig.14B). To more conclusively address differences, we assessed these livers for pro-inflammatory cytokines. A significant upregulation of CCL5, CXCL10, IL-6, and TNF-α was seen in bKO+Fe as compared to bCON+Fe (Fig.14C).

Thus, iron-overload in absence of β-catenin in liver leads to sequential increase in inflammation followed by steatosis and fibrosis.

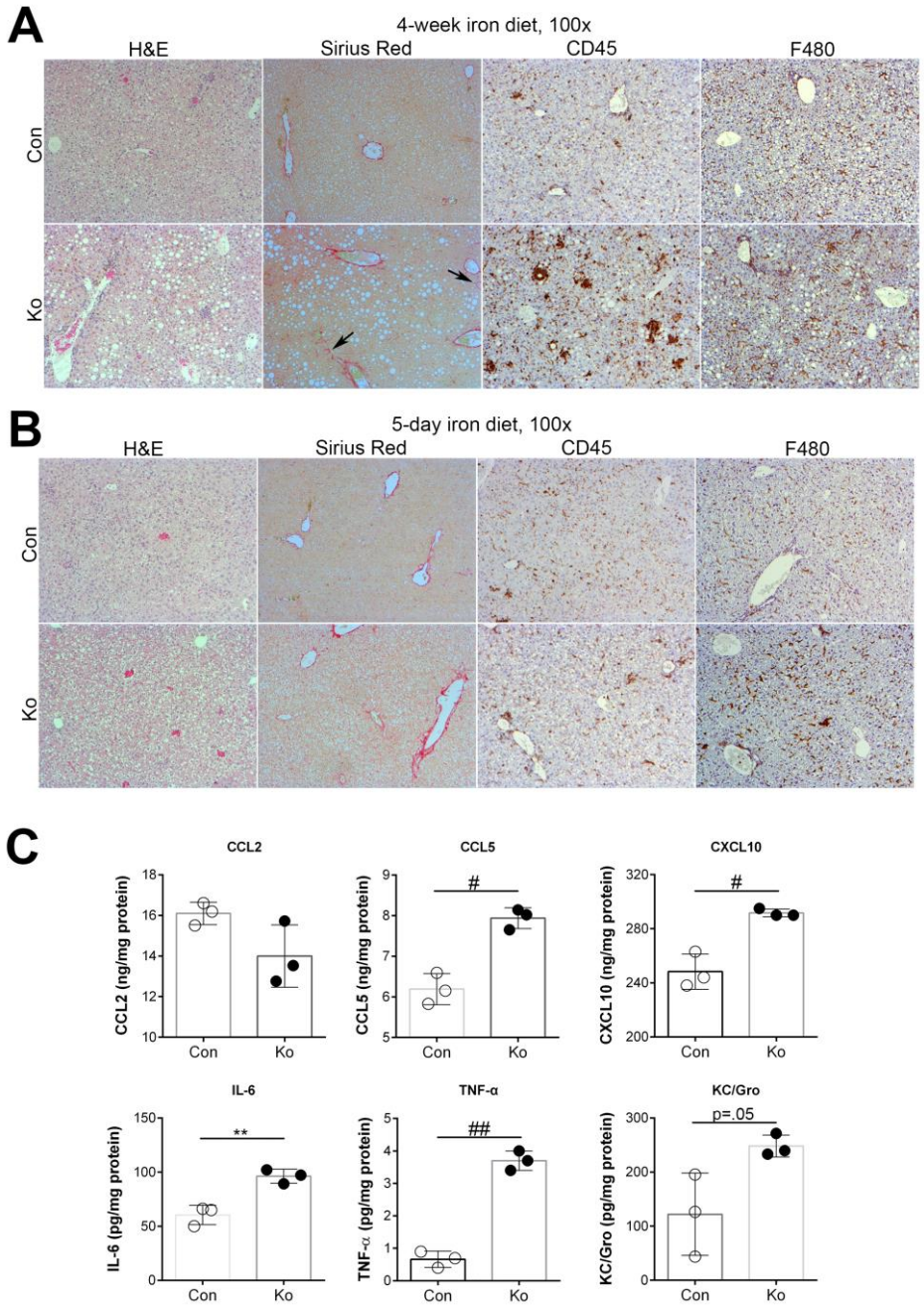

Figure 14: Increased levels of inflammatory cytokines precede steatohepatitis and fibrosis in bKO+Fe as shown by time course after iron-feeding.

(A) H&E, Sirius Red and IHC for CD45 and F480 in bCON and bKO livers after 4-week iron diet shows presence of steatohepatitis in bKO+Fe and initiation of fibrosis. (B) H&E, Sirius Red and IHC for CD45 and F480 in bCON and bKO livers after 5-day iron diet. bCon+FE and bKO+Fe lack steatosis and fibrosis while CD45-positive inflammatory cells and F480-macrophages appear to be comparably increased in both groups. (C) Cytokine assay using liver lysates from 5-day bCON+Fe and bKO+Fe reveals comparable increased protein levels of CCL5, CXCL10, IL-6, TNFα, and KC/Gro in BKO+Fe but no change in CCL2. *p<0.05, **p<0.01, #p<0.005, ##p<0.001 using Student's T test. (Image magnification: 100x)

2.5 DISCUSSION

Wnt/β-catenin signaling plays diverse roles in liver pathobiology (164), although its role in iron metabolism in the liver remains unknown. A previous study reported increased Wnt signaling after addition of cellular iron to APC-mutant cell lines (144). We used previously characterized liver-specific β-catenin KO (89, 163) to determine any changes in the expression of key iron-metabolism genes. None of the major genes were differentially expressed between bCON and bKO. To determine if iron had an impact on β-catenin signaling, control mice were fed a diet with excessive iron content. Two groups had individually identified iron chelators that inhibited Wnt signaling in different cancer models (143, 165). Interestingly, we observed decreased β-signaling after high iron diet as indicated by decreased expression of target genes Cyp2e1, Cyp1a2 and GS. Intriguingly, despite decreased signaling, a complete lack of β-catenin was a greater detriment to mice after hepatic iron overload, which exhibited activation of AKT, ERK, and NFκB, steatohepatitis, fibrosis, HCC and progenitor response, which led to re-appearance of β-catenin and its targets inadvertently making the injury worse. Thus overall, bKO on high iron diet recapitulated hemochromatosis-like disease. Addition of antioxidant NAC abrogated hepatic damage and normalized histology and cell signaling in bKO+Fe.

There was differential regulation of a few iron metabolism genes between bKO and bCON after high iron diet. We noted decreased transferrin receptor 2 mRNA levels while ferroportin and ceruloplasmin mRNA levels were increased in bKO+Fe. Since transferrin receptor 2 allows entry of iron into hepatocytes and ceruloplasmin converts toxic ferrous form to a nontoxic ferric form, the changes in bKO are likely compensatory to limit injury in bKO. This could also explain increased serum iron levels in bKO+Fe, which however could simply reflect

an increase in overall hepatic injury in bKO. Ferroportin mRNA is increased in bKO+Fe and bCON+Fe. Ferroportin is negatively regulated by hepcidin at a posttranslational level (120). Hepcidin binds to ferroportin to induce its internalization and degradation (152). Thus, we believe that increase in ferroportin mRNA in bKO+Fe and bCON+Fe is in response to its enhanced degradation by increased hepcidin. However, a significantly greater increase in ferroportin in bKO+Fe versus bCON+Fe may be due to additional mechanisms like inflammation and IL-6, which occur in bKO+Fe and have been shown to induce hepcidin expression (166).

Progression of injury in bKO after iron overload lends insights into pathogenesis of disease like hemochromatosis. Increase in inflammatory cytokines like CCL5, CXCL10, IL-6, and TNFα appear to be the first molecular event following iron overload in the absence of β-catenin in hepatocytes, which was evident at 5 days after iron diet. We believe that NFκB activation is responsible for inflammation in bKO+Fe (167). We have previously shown that β-catenin associates with NFκB to prevent its nuclear translocation, and β-catenin loss accelerates NFκB activation (100).

Steatosis follows inflammation as seen by the presence of steatohepatitis at 4 weeks. Steatosis in bKO is likely due to inflammation and also due to increased hepatic PPARγ, master regulator of adipogenesis (168). β-Catenin signaling suppress adipogenesis while its inhibition promotes pre-adipocyte differentiation to adipocyte through activation of lipogenic factors PPARγ and CEBPβ (169). How iron overload induces PPARγ uniquely in bKO remains under investigation. We also observe activation of AKT, ERK, and NFκB after long term iron diet administration to bKO. AKT activation impacts proteins involved in survival, cell cycle, autophagy, and protein synthesis (170, 171), including FoxO, which normally inhibits cell

growth and/or induces apoptosis (171). AKT phosphorylates and inhibits FoxO (172). Intriguingly, β-catenin can also act as a transcriptional cofactor for FoxO (67). While further studies are required to precisely address the role of AKT in bKO+Fe, we posit that excess iron enhances β-catenin and FoxO to induce apoptotic genes to clear damaged cells, thereby promoting proliferation of healthy cells. However, when β-catenin is absent, AKT phosphorylates and inactivates FoxO, allows persistence of damaged cells, eventually leading to HCC. We also observe increased ERK1 in bKO+Fe compared to bCON+Fe. Whether ERK1 and ERK2 have distinct roles is controversial (157). A rat study showed ERK1 upregulation augmented fibrosis and its suppression decreased fibrosis and increased hepatocyte proliferation (173). Therefore, it is likely that ERK1 activation in bKO+Fe contributes to fibrosis. Phospho-ERK2 levels increased in bCON and bKO after iron and NAC treatment. Since silencing ERK2, but not ERK1, affected hepatocyte proliferation (174), we believe that NAC-induced ERK2 activation contributes to hepatic regenerative response after iron overload. NFκB can also be activated by inflammation and lipid peroxidation (175). As a transcription factor, it regulates expression of a number of inflammatory cytokines and chemokines and also Cyclin D1 (176). This may explain in part the Cyclin D1 induction seen in bKO+Fe. Eventually steatohepatitis leads to cell death, stellate cell activation, fibrosis, and occasionally to development HCC.

The presence of increased oxidative stress appears to be chief perpetrator in disease progression in bKO+FE. We observe both increased MDA and 4HNE, especially in the areas of steatotic hepatocytes. Indeed, iron overload in genetically obese mice is associated with oxidative stress, injury and a NASH-like phenotype (177). Since mice are notoriously resistant to injury after high iron diet, we posit that lack of notable oxidative stress after iron feeding may explain the absence of a phenotype in control mice. Cyp2e1 is typically associated with

excessive lipid peroxidation and hepatic injury following iron overload, alcohol and high fat diet (162, 178-180). Cyp2e1 is a bona fide β-catenin target in pericentral hepatocytes (89, 163, 181). Our study shows that feeding high iron diet to control mice leads to decreased Wnt/β-catenin signaling and as a result, lowers Cyp2e1 levels. This may be the protective mechanism, which limits generation of oxidative stress to make mice resistant to iron overload injury.

Despite lack of Cyp2e1 in bKO, these mice showed worse injury to iron overload. This is likely a consequence of enhanced inflammation due to NFκB activation and dearth of β-catenin-dependent anti-oxidant mechanisms. Loss of β-catenin in liver is associated with enhanced oxidative stress following ischemia-reperfusion injury and chemical carcinogenesis (68, 94, 182). This is due to the lack of adequate glutathione content resulting from altered expression of several glutathione S-transferases, regucalcin (required for ascorbic acid biosynthesis) and interactions with HIF1α (36, 68, 87, 183). However, another unexpected and paradoxical event in bKO+Fe further underscores the importance of Cyp2e1 and oxidative stress as a mediator of iron-induced hepatic injury. Due to enhanced injury in bKO+Fe, we observed progenitor response characterized by Sox9, EpCAM, and CK19-positive ductular reaction (151). As a consequence, there is re-appearance of β-catenin-positive hepatocytes in bKO+Fe, along with targets like Cyp2e1 especially in the steatotic areas. A caveat is that as progenitor cells would differentiate into hepatocytes, they will re-express albumin which would lead to expression of cre-recombinase and β-catenin deletion. It is likely hepatocyte differentiation is suboptimal and hence these "hepatocyte-like" cells may not have optimum albumin-cre expression. Another possibility is repopulation by β-catenin-positive hepatocytes due to suboptimal deletion by 'leaky' albumin-cre, which has been reported during chronic injuries like 3,5-diethoxycarbonyl-1, 4-dihydrocollidine (DDC) diet (184). In the current study however, the survival advantage

attributed to the β-catenin deletion-escaped hepatocytes comes at an unexpected cost of reappearance of Cyp2e1, which is normally downregulated following iron overload in controls. This pivots the balance towards greater lipid peroxidation, injury and disease progression.

Alleviation of oxidative stress and lipid peroxidation in β-catenin KO with NAC following iron overload had a dramatic effect on the disease process. While inflammation was unaffected quantitatively, NAC treatment led to notable decreases in pro-inflammatory cytokines, steatosis, stellate cell activation and fibrosis, thus normalizing histology and phenotype and making bKO+Fe indistinguishable in phenotype from bCON+Fe. It may be beneficial to examine any role of antioxidants for chemopreventive use in iron overload disorders. A summary of our findings is presented in Figure 15.

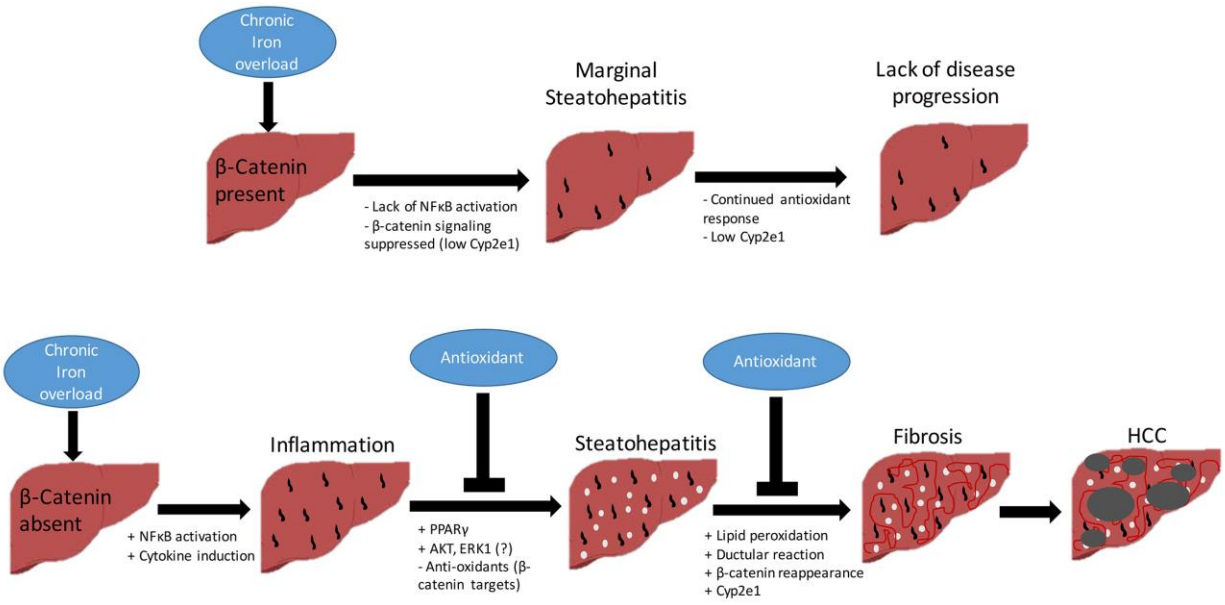

Figure 15: Schema of β-catenin's role in protection against hepatic iron overload.

3.0 HEPATOCYTE WNTS ARE DISPENSABLE DURING DIETHYLNITROSAMINE AND CARBON TETRACHLORIDE-INDUCED INJURY AND HEPATOCELLULAR CANCER

In section 3, we used a phenotypically relevant chemical carcinogenic model to induce hepatocellular carcinoma in the context of hepatic injury and fibrosis. We first confirm efficacy and relevance of the model, then apply it using hepatocyte-specific Wntless knockout mice to assess the role of hepatocyte Wnts in tumor progression. The work in this section was published in Gene Expression-The Journal of Liver Research, PMID: 29519268 (185). The publisher, Cognizant, has granted permission for reuse of the manuscript in this dissertation.

3.1 Abstract

Activation of the Wnt/β-catenin signaling is reported in large subsets of hepatocellular carcinoma (HCC). Upregulation of Wnt genes is one contributing mechanism. In the current study, we sought to address the role of hepatocyte-derived Wnts in a model of hepatic injury, fibrosis and carcinogenesis. We subjected hepatocyte-specific Wntless knockout mice (HP-KO), unable to secrete Wnts from hepatocytes, and littermate controls (HP-CON), to diethylnitrosamine and carbon tetrachloride (DEN/CCl_4) and harvested at 3, 5, and 6 months for

histological and molecular analysis. Analysis at 5 months displayed increased hepatic expression of several Wnts and upregulation of some but not all β-catenin targets, without mutations in Ctnnb1. At 5 months, HP-CON and HP-KO had comparable tumor burden and injury, however HP-KO uniquely showed small CK19-positive foci within tumors. At 6 months both groups were moribund with comparable tumor burden and CK19-positivity. While HCC histology was indistinguishable between the groups, HP-KO exhibited increased active-β-catenin, and decreased cMyc, Brd4, E-Cadherin, and others. Hepatic injury, inflammation and fibrosis were also indistinguishable at 3 months between both groups. Thus, lack of Wnt secretion from hepatocytes did not affect overall injury, fibrosis or HCC burden although there were protein expression differences in the tumors occurring in the two groups.

3.2 BACKGROUND

3.2.1 Introduction to liver cancer

HCC, the most common type of liver cancer, is the fourth most common cancer worldwide, with incidence rates ranging from 4.6 per 100,000 in North America to 80 per 100,000 in Asia (186-188). The frequency and cause of HCC clearly varies per region, with higher prevalence in developing countries (189), however incidence rates are rising in the US with increases in liver diseases including Hepatitis C and Non Alcoholic Fatty Liver Disease (190). It is the third most common global cancer death, and the ninth most common in the US (191). Additionally, fibrosis or cirrhosis is a prerequisite to HCC in 70-90% of cases (189, 192). Therefore, understanding what initiates and sustains tumorigenesis after fibrosis will not only have therapeutic potential

for HCC patients, but can aim to prevent HCC in patients with chronic liver diseases, which are both major concerns considering two thirds of patients are diagnosed at advanced stages of HCC (193).

3.2.2 Etiology of HCC

3.2.2.1 Fibrosis and Cirrhosis

Fibrosis is characterized by increased extracellular matrix collagen deposition after sustained hepatic injury (86, 87), leading to scar formation and gradual loss of functional hepatic tissue. Fibrosis may be reversible (88, 89), or it can progress to hepatocyte dysfunction, nodule development, and decreased blood flow, defined as cirrhosis (90). Fibrosis almost always accompanies chronic liver injury (91), and is the product of inflammation resulting from macrophages phagocytosing dead hepatocytes, which leads to increased reactive oxygen species (ROS) (92) and macrophage-specific TGFβ1 secretion (93). These responses activate hepatic stellate cells (HSC) to transdifferentiate into myofibroblasts and produce excess collagen (94, 95), leading to fibrosis. Macrophages also secrete profibrinogenic proteins including matrix metalloprotease inhibitors, which prevent extracellular matrix degradation (93).

Other potential mechanisms leading to fibrosis include increased growth factor signaling through extracellular matrix interactions or reduced natural killer T cell function (92). In this milieu of activated myofibroblasts, chronic inflammation, ongoing hepatocyte death and existence of ROS, hepatocytes may incur enough DNA damage and mutations which promote their survival and expansion and eventually lead to HCC development (91).

3.2.2.2 Hepatitis

Hepatitis B Virus (HBV) commonly leads to HCC, with 30-50% of HBV-related mortality resulting from HCC (100). HBV is a hepatotropic DNA-integrating virus encoding its own replication machinery (101) and contributes to HCC transformation by transcriptionally activating oncogenes (102) and inactivating tumor suppressors (103, 104). Additionally, viral-ER interactions can induce oxidative stress (105), leading to several responses such as activating HSCs (94, 95) leading to fibrosis.

Hepatitis C Virus (HCV), the most common cause of cirrhosis and chronic liver disease (106), also leads to HCC (107). As an RNA virus, it exhibits greater propensity than HBV to develop chronic infection and cirrhosis (108). Although less is known about the progression of HCV to HCC (109), the mechanism by which HCV contributes to HCC onset are similar to HBV (95) and include inducing ER-related oxidative stress and regulating cell proliferation (110, 111). HCV is accompanied by chronic inflammation, leading fibrosis through HSC activation (112-114).

3.2.2.3 Chronic alcohol consumption

In the US, over 18 million adults abuse alcohol, making it five times more common than HCV (115). The direct methods by which alcohol causes HCC are not well known, and given to rodents alone is not enough to induce carcinogenesis (115, 116). One theory is Cytochrome P450 2E1 (Cyp2E1), a β-catenin target gene, is induced during heavy alcohol use in order to metabolize ethanol (117, 118) and produces reactive oxygen species when activated (119), leading to HSC activation and DNA damage in hepatocytes (120).

3.2.2.4 Nonalcoholic Fatty Liver Disease/Nonalcoholic Steatohepatitis (NAFLD/NASH)

With obesity rates rising, NAFLD incidence is increasing with 25% of Americans currently suffering. Of this population, approximately 25% have NASH, a more severe form of hepatic steatosis, or fatty liver (121, 122). The number of HCC cases resulting from NAFLD ranges from 4 to 22% and is steadily rising in Western countries (123-125). Non-adipose tissues such as liver are unable to effectively store and metabolize increased triacylglyceride (TAG) content, and TAG overload leads to increased lipotoxicity, elevated ROS, and increased DNA damage (126-128).

A summary of HCC development is presented in Figure 16.

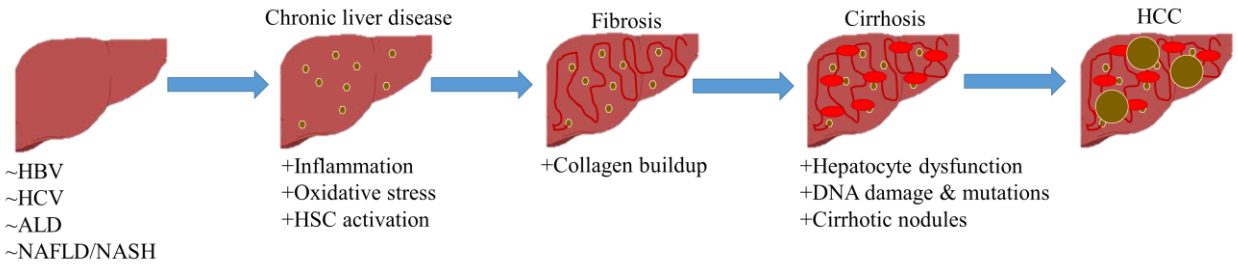

Figure 16: Progression from chronic liver injury to HCC.
Chronic liver diseases, including HBV, HCV, ALD, or NAFLD/NASH, lead to increased hepatic inflammation, oxidative stress, and hepatic stellate cell activation. This causes collagen deposition and fibrosis, which can progress into hepatocyte damage and dysfunction, leading to cirrhosis. Cirrhosis often leads to HCC. HBV, hepatitis B virus; HCV, hepatitis C virus; ALD, alcoholic liver disease; NAFLD/NASH, Nonalcoholic Fatty Liver Disease/Nonalcoholic Steatohepatitis; HSC, hepatic stellate cells; HCC, hepatocellular carcinoma.

3.2.3 Current treatments for hepatocellular carcinoma

The only curative treatment for HCC is liver transplant, which leads to a low recurrence rate and a high long-term survival rate (194). However, patients with several large tumor nodules, vascularized tumors, or metastatic HCC are ineligible for transplants (195). Surgical resection, where part of the liver is removed, is also promising for certain HCC patients although the

regenerative capacity of the remaining liver is usually unsatisfactory (196). If recurrence occurs after resection, the standard is to repeat resection, thereby requiring the injured liver to regenerate further (197).

To date, only three chemotherapeutic drugs are Food and Drug Administration (FDA) approved for unresectable HCC. Sorafenib, a multikinase inhibitor that inhibits tumor proliferation and angiogenesis, only extends patient survival by approximately three months (198). The multikinase inhibitor Lenvatinib has an FDA application pending for approval, but patient survival was comparable to Sorafenib in clinical trials (199). Recently Regorafenib, another multikinase inhibitor, was approved for patients who have tumor progression during Sorafenib treatment, however patient survival was only extended another three months during a phase 3 trial (200). Another second-line therapeutic, the Programmed Death-1 inhibitor Nivolumab, was also recently approved for patients experiencing recurrence after Sorafenib, but a response was observed in only 15-20% of patients during clinical trials (201, 202). Additional trials are continuously surfacing, including the second-line kinase inhibitor Cabozantinib with improved overall survival of 11.5 months (201, 203).

Transarterial chemoembolization may improve survival for patients in early disease stages by inducing tumor necrosis, although improvement is marginal (204). It is, therefore, of utmost importance to better understand underlying mechanisms of HCC initiation, progression, and advancement to provide better treatment options for patients with all liver diseases.

3.2.4 Mutated β-catenin in hepatocellular carcinoma

β-Catenin signaling is overactive in 20 to 90% of HCC patients (205). Approximately 8-44% of patients exhibit increased β-catenin signaling resulting from mutations (164). The most common

β-catenin mutations are found in exon 3 (corresponding exon 2 in mice) (206), which typically are single nucleotide substitutions that prevent β-catenin ubiquitination and degradation (207, 208), classically through alteration of the GSK3β phosphorylation sites (209). Furthermore, Axin and APC, parts of the β-catenin destruction complex, have been individually mutated in subsets of HCC patients rendering them defective and allowing constitutive β-catenin activity (209-211). Although mutated β-catenin alone is insufficient to induce HCC, it can cooperate with other signaling pathways including mutated Ha-ras (212), Met (213), P53 (214), or TERT (215), and is often associated with better prognosis and well-differentiated HCC (216).

3.2.5 Nonmutated β-catenin in hepatocellular carcinoma

Approximately 35 to 80% of HCC patients have increased β-catenin accumulation but do not display any related mutations. Studies show this aberrant accumulation is due in part to overexpression of Wnt and/or Fzd (217). In fact, overexpression of many Wnts and Fzds has been implicated in different cancers including HCC (192, 217, 218) as well as several HCC cell lines (219). These modifications result in increased nuclear accumulation of β-catenin (220), leading to transcriptional upregulation of target genes and promotion of tumorigenesis. When Wnt antagonist fusion proteins are injected into an orthotopic HCC model harboring wildtype β-catenin, animal survival and apoptosis increases, and tumor volume, β-catenin activity, and angiogenesis decreases (221), suggesting that Wnts may be a promising therapeutic target. Furthermore, patients with activated wild-type β-catenin resulting from upstream Wnt or Fzd activation have more aggressive, dedifferentiated tumors (218) and poorer prognosis than those with mutated β-catenin (222, 223), yet less is known about the mechanism of wild-type β-catenin

in tumor progression. Considering HCC arises from hepatocytes (224), we hypothesized they are a main cellular source of Wnts that contribute to tumor pathogenesis.

3.3 Methods

3.3.1 Animals

Animal work was performed in accordance with the Institutional Animal Care and Use Committee at the University of Pittsburgh. Albumin-Cre Wntless knockout mice were generated as described previously(40). Male pups (HP-KO, HP-CON) were injected with 25mg/kg diethylnitrosamine (Sigma) at 14-16 days prepared in sterile 0.9% saline. Animals were transferred to a BSL2+ facility and injected with 0.5ml/kg carbon tetrachloride (CCl_4) twice per week from week 8 to 22, prepared in corn oil. Three days after the last injection, animals were sacrificed (n=4) and livers were harvested. Livers were also harvested from a pre-cancer time-point of 3 months (n=3) and advanced-cancer time-point of 6 months (n=4). Animals were monitored daily for signs of morbidity. At time of sacrifice, liver weights (LW) and body weights (BW) were assessed for LW/BW and differences tested for significance by Student's T Test with $p<0.05$ to be considered significant. Blood was collected from the *inferior vena cava* and serum was sent to the University of Pittsburgh Medical Center Clinical Laboratory for ALT, AST, and ALP testing.

3.3.2 Immunohistochemistry

Paraffin sections were processed as described elsewhere (108). Sirius Red, Ki67, H&E, CD45, CK19 and GS staining was performed as also described in detail previously (108) in section 2.3.2.

3.3.3 Protein isolation and analysis

Protein was extracted in RIPA buffer, quantified, and 30µg was loaded onto a precast BioRad SDS gel. Gels were transferred using BioRad semi-dry transfer system. Antibody information can be found in Table 6. Horseradish peroxidase conjugated secondary antibodies (Invitrogen) were used. Ponceau or Gapdh was used as a loading control. Densitometric analysis was performed with ImageJ and normalized to housekeeping control. Statistics were calculated using One-way ANOVA with multiple comparisons and P values less than 0.05 were considered significant.

For reverse phase protein array (RPPA) analysis, samples were prepared via instructions from the MD Anderson Cancer Center RPPA Core Facility, and sent for analysis. Data was analyzed via Student's t-test, and select proteins with statistically significant differences were validated by western blot.

Table 6: List of antibodies used for western blot in section 3.0

Antibody	Company	Catalog number
GS	Santa Cruz	Sc74430
cMyc	Santa Cruz	Sc764
Hypo phosphorylated β-catenin	Cell Signaling	4270
PCNA	Santa Cruz	Sc56
Cyp2e1	Atlas Antibodies	HPA009128
β-catenin	BD Biosciences	610154

Gapdh	Proteintech	60004-1-Ig
Wee1	Cell Signaling	4936
Yap	Cell Signaling	4912
Erk1/2	Cell Signaling	4695
Bax	Cell Signaling	2772
Cdc25	Cell Signaling	4688
Brd4	Cell Signaling	13440
E cadherin	Cell Signaling	3195
PKAa	Cell Signaling	5675

3.3.4 RNA isolation and qPCR

RNA was extracted from DEN/CCl_4 treated control livers and untreated livers (n=3) using Trizol (Thermo Fisher), and after DNAse treatment (Thermo Fisher) 2µg of RNA was reverse transcribed using Superscript III (Thermo Fisher). Samples were pooled together and Sybr Green (Thermo Fisher) was used for qPCR. Ct values were normalized to GAPDH, and primer sequences are included in Table 7.

Table 7: qPCR primers used in Section 3.0

Primer (Mouse)	**Forward Sequence**	**Reverse Sequence**
Gapdh	AACTTTGGCATTGTGGAAGG	ACACATTGGGGGTAGGAACA
Wnt1	ATCCATCTCTCCCACCTCCTAC	GAATCTTTCTCTCACCCTCTGG
Wnt2	TCTGTCTATCTTGGGCATTCTG	TTCCTTCGCTATGTGATGTTTC
Wnt2b	ACCTTCCTCTACCCTCAATCCT	TCACTCAGCCTCCTAAATCCAT
Wnt3	GTCTGCTAATGCTGGCTTGAC	TAGGAAGGGATGGGAGGTGT
Wnt4	AGAACTGGAGAAGTGTGGCTGT	AAAGGACTGTGAGAAGGCTACG
Wnt6	TTTACACCAGCCCACGAAAG	ACTCACCCATCCATCCAAGTA
Wnt8b	GTTTGCTTGGGACCGTTG	TCCATTTCGGGAGTCATCA
Wnt9a	ATGGTGTGTCTGGCTCCTG	CAGTGGCTTCATTGGTAGTGCT
Wnt9b	GGGTGTGTGTGGTGACAATCT	GGTCCTTGCTTCCTCTCTTG
Wnt10a	TCCTGTTCTTCCTACTGCTGCT	ACGCACACACACCTCCATC
Wnt10b	CCACTACAGCCCAGAACCTC	GGAGAGACCCTTTCAACAACTG
Wnt11	CCCTGGAAACGAAGTGTAAATG	AGGTAGCGGGTCTTGAGGTC
Wnt16	GCTGTAACCTCCTCTGCTGTG	GTGGACATCGGTCATACTTTCA

3.3.5 DNA extraction and Ctnnb1 sequencing

gDNA was isolated from livers (XNAT, Sigma), and primers flanking intron-exon junctions of Ctnnb1 exon 2 (forward primer TACAGGTAGCATTTTCAGTTCAC, reverse primer TAGCTTCCAAACACAAATGC) (206) were used in PCR. Product was gel purified and sequenced by the Genomics Research Core at University of Pittsburgh. Sequences were validated using ApE Software. Tumors in HP-CON and HP-KO at 5 and 6 months (N=3) were sequenced.

3.4 Results

3.4.1 DEN/CCl4 leads to wildtype Ctnnb1 and upregulation of several Wnts

To develop an injury-based carcinogenesis model, we adapted the DEN/CCl_4 protocol used to induce inflammation, fibrosis, and tumors (225, 226). This model utilizes one injection of diethylnitrosamine at day 15, and biweekly injections of carbon tetrachloride from week 8 to week 22 (DEN/CCl_4) (Fig.17A). DEN/CCl_4 shows 100% penetrance at 5 months for HCC in conjunction with fibrosis and inflammation, thereby representing what is seen in patients (Fig.17B, 18F).

This model is known to cause HCC without β-catenin mutations as confirmed through sequencing and supported by lack of GS staining (227), which is a surrogate, *albeit* debated, for mutated β-catenin (216, 228). Via immunohistochemistry, all tumors were GS-negative (Fig.17C). Further, tumors were sequenced for mutations in exon 2 of Ctnnb1, analogous to exon

3 in humans. This is home to GSK3β phosphorylation sites and the most frequent activating mutations in HCC (206, 229). Wildtype Ctnnb1 was identified in all tumors (Fig.17D). This was also corroborated using microarray data obtained from Gene Expression Omnibus (http://www.ncbi.nlm.nih.gov/geo/), accession number GSE33446, comparing data from DEN/CCl_4 treated animals to untreated animals (225). We queried the data and noted no change in expression of Glul, gene encoding for GS, after DEN/CCl_4. However, several β-catenin targets were upregulated as listed in Table 8 suggesting that modest activation of the pathway does occur despite absent Ctnnb1 mutations.

Next, we assessed whether Wnts were overexpressed after DEN/CCl_4, and tested mRNA expression of select Wnts in livers after DEN/CCl_4 compared to untreated livers. Wnt1, Wnt6, Wnt10a, Wnt10b, Wnt11, and Wnt16 showed upregulation of at least two-fold in DEN/CCl_4 livers versus control livers (Fig.17E). We hypothesized that some of these may be originating from hepatocytes and hence interrogated tumorigenesis in mice lacking ability to secrete all Wnts from hepatocytes owing to Wntless loss.

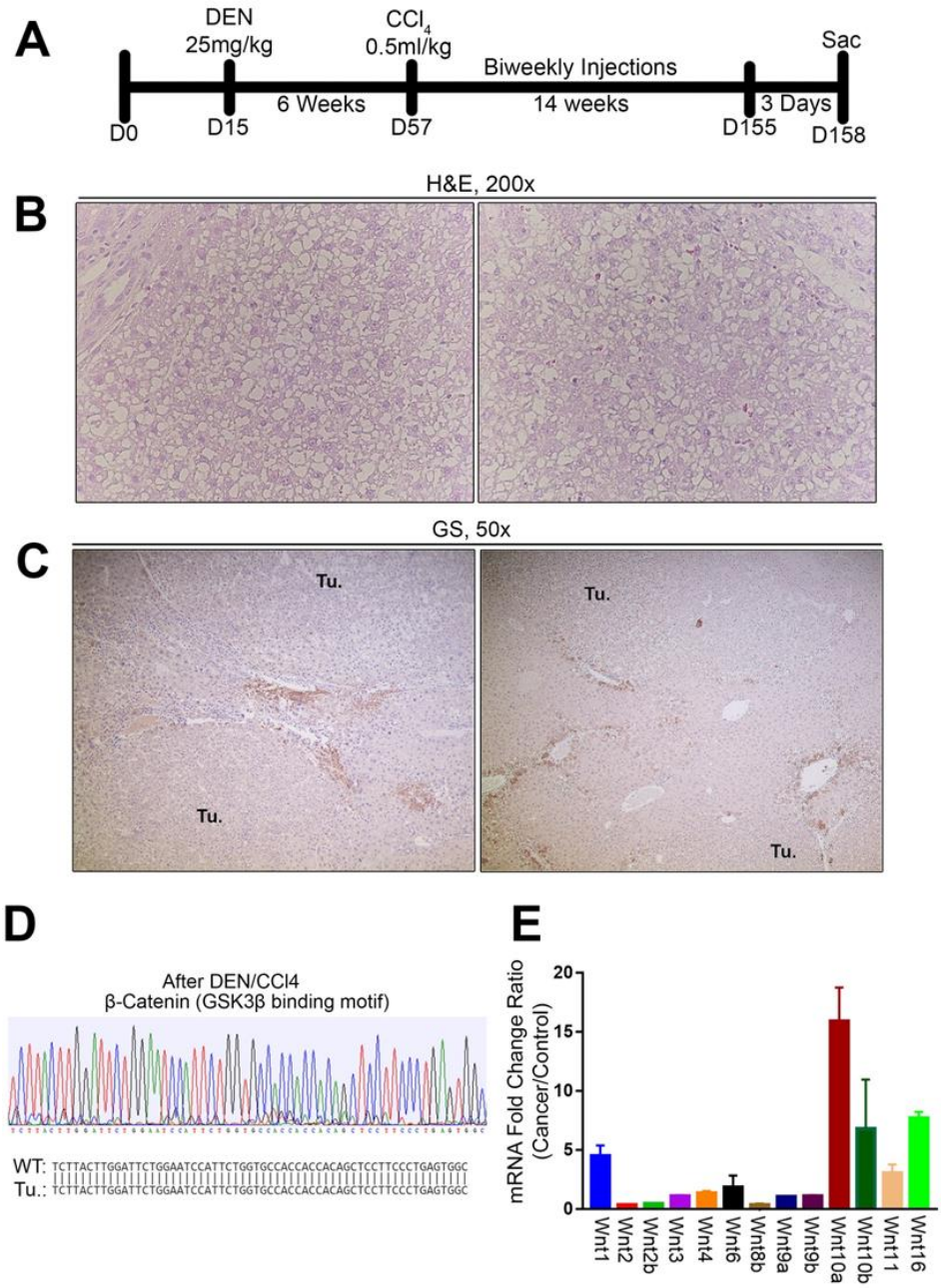

Figure 17: DEN/CCl4 model of HCC shows Wnt upregulation but non-mutated β-catenin.

(A) Schematic of DEN/CCl_4 injection protocol, beginning at day of birth and concluding at 5 months of age. (B) High magnification (200x) Hematoxylin and Eosin stain (H&E) highlighting intratumoral dysplastic hepatocytes. (C) Assessing GS staining in tumors in DEN/CCl_4 model of HCC. No GS-positive tumors were observed, suggesting wildtype β-catenin. (D) Representative sequencing of β-catenin exon 2, focusing on GSK3β phosphorylation motifs, displays non-mutated and identical sequence between tumors (Tu.) and wildtype (WT). (E) RT-PCR analysis showing upregulation in the transcript levels of several Wnts at 5 months of age after continued DEN/CCl_4 treatment in mice as compared to untreated controls.

Table 8: List of beta-catenin target genes altered in DEN/CCl4

Gene	Probe (from GSE33446)	Log2 Fold Change	Adjusted P value	Reference
CD44	1434376_at	3.55382771	8.71e-03	(230)
Survivin	1424278_a_at	3.36261188	6.73e-04	(231)
EGFR	1432647_at	2.58970608	3.94e-05	(31)
Ccnd1 (Cyclin D1)	1417419_at	2.46649404	4.01e-09	(89)
S100A6	1421375_a_at	2.40064056	8.99e-03	(232)
Ctnnb1 (β-catenin)	1430533_a_at	2.112623	5.53E-06	
MMP14	1448383_at	2.06551913	4.32e-06	(233)
Vegfa	1451959_a_at	0.7674417	2.87e-03	(234)
Tgfα	1450421_at	0.50142774	6.94e-04	(35)
Axin2	1436845_at	0.39369432	7.48e-01	(235)
Lef1	1421299_a_at	0.11541357	4.32e-01	(236)
Glul (GS)	1426236_a_at	-1.21199767	2.21e-01	(237)
Regucalcin	1448852_at	-1.28147025	7.64e-02	(36)
Lect2	1449492_a_at	-1.35084301	3.03e-01	(238)

3.4.2 HP-KO and HP-CON have comparable tumor burden at 5 months, although HP-KO have more CK19+ nodules after DEN/CCl4.

To assess the role of Wnts from hepatocytes, we subjected previously described hepatocyte-specific Wntless KO referred henceforth as HP-KO and littermate controls (HP-CON) to DEN/CCl_4 (40). Mice sacrificed at 5 months exhibited comparable tumor burden reflected by similar LW/BW between the two groups (Fig.18A,B). Serum analysis revealed comparable and modestly elevated ALT, AST, and ALP in HP-CON and HP-KO (Fig.18C-E). H&E staining verified these tumors to be similar HCCs as reflected by well-circumscribed lesions composed of hepatocytes with basophilic cytoplasm, some pleomorphic nuclei, and mitotic figures in HP-CON and HP-KO (Fig.18F). Further, we noted no differences in fibrosis via Sirius red or α-SMA (Fig.18F and data not shown), or inflammation, vascularization, or proliferation, via assessment

of CD45, CD31, and Ki67, respectively (Fig.18F and data not shown). We also validated wildtype Ctnnb1 in HP-CON and HP-KO (Fig.18G).

To further characterize the tumor phenotype, we queried the differentiation status and assessed the dedifferentiation marker CK19, as it positively correlates with poor prognosis, increased tumor size and invasiveness (239). Immunohistochemistry revealed small CK19-positive foci in all HP-KO mice, while expression was restricted to bile ducts in HP-CON mice (Fig.19A). Not all nodules in HP-KO were CK19-positive, however large tumors frequently contained smaller foci of heterogeneous CK-19-positive cells. These overall findings indicated that HCC occurring in absence of Wnts from hepatocytes were comparable to controls, other than the occurrence of small CK19-positive areas within tumors.

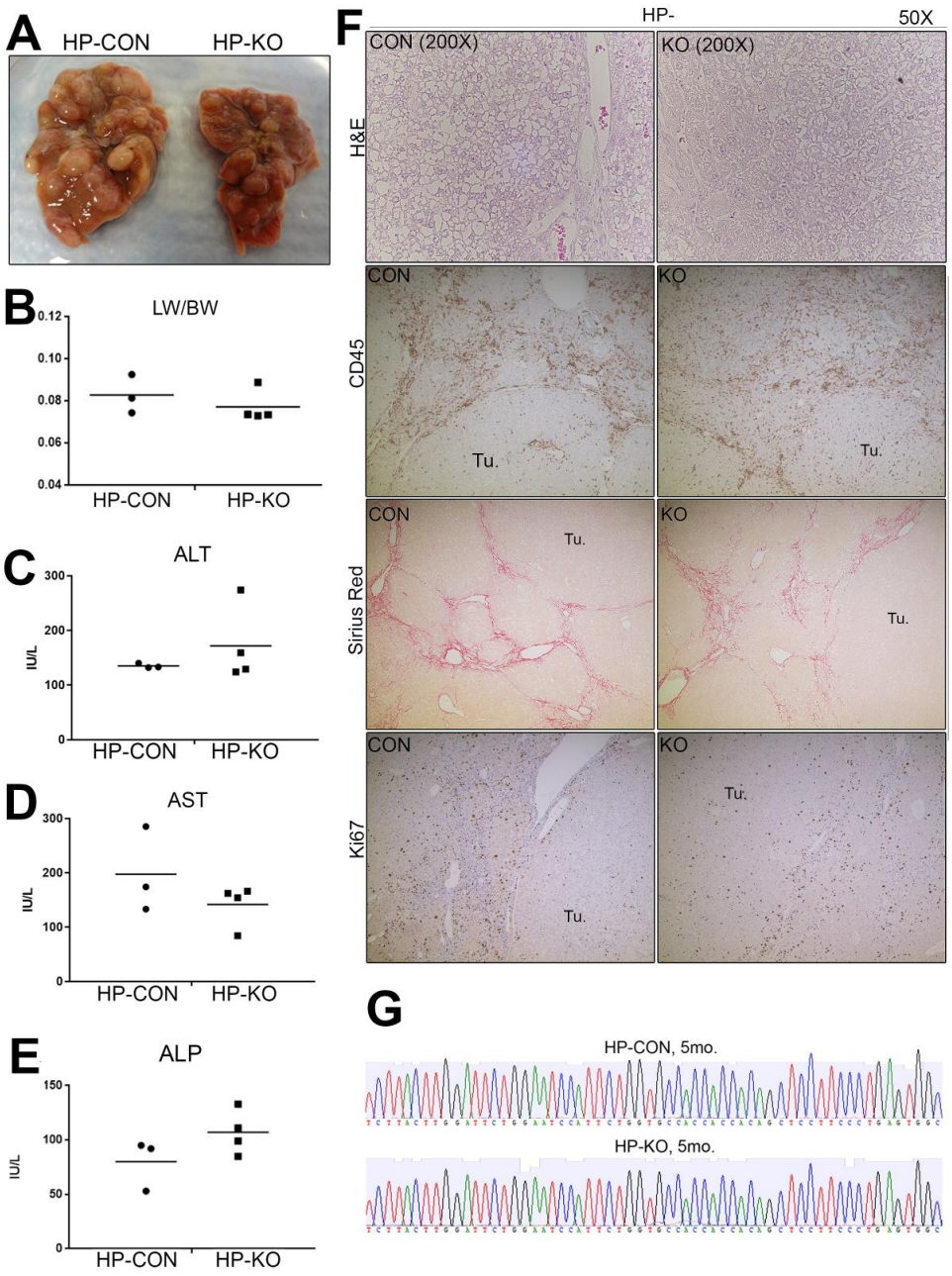

Figure 18: HP-CON and HP-KO have comparable tumor burden after 5 months of DEN/CCl4.
(A) Representative gross images of HP-CON and HP-KO at 5 months. (B) HP-CON and HP-KO have comparable liver weight to body weight ratios after DEN/CCl_4. (C-E) Serum analysis reveals comparable Alanine Aminotransferase (ALT), Aspartate Aminotransferase (AST), and Alkaline Phosphatase (ALP) in HP-CON and HP-KO. (F) Representative images of hematoxylin and eosin (200x), CD45, Sirius Red, and Ki67 (50x) reveal comparable tumors and injury burden in HP-CON and HP-KO. (G) Representative sequencing shown for HP-CON and HP-KO tumors, which are both CTNNB1 wildtype.

3.4.3 No difference in tumor burden in HP-KO versus HP-CON at advanced stages

We predicted CK19-positive foci in HP-KO to develop into more aggressive tumors than HP-CON. To test this, we followed an independent cohort for an additional timeframe. However, by 6 months, all mice became moribund and required euthanasia. Grossly, livers from both groups were excessively stiff and showed sizable tumor burden (Fig.19B). LW/BW at 6 months failed to show significant differences between the two groups and both groups showed increased ratios over the 5-month time-point (Fig.19C). Mutations in Ctnnb1 were still absent at 6 months (Fig.19D). Intriguingly, at 6 months, both HP-CON and HP-KO displayed comparable, diffuse, and broader staining for CK19 within tumors (Fig.19E). Similar to 5-month time-point, comparable fibrosis, inflammation and proliferation was observed as seen by Sirius red (Fig.19E), CD45, and Ki67 staining, respectively (data not shown). Thus, there were no phenotypic differences in HCC occurring in HP-CON and HP-KO at 6 months after DEN/CCl_4.

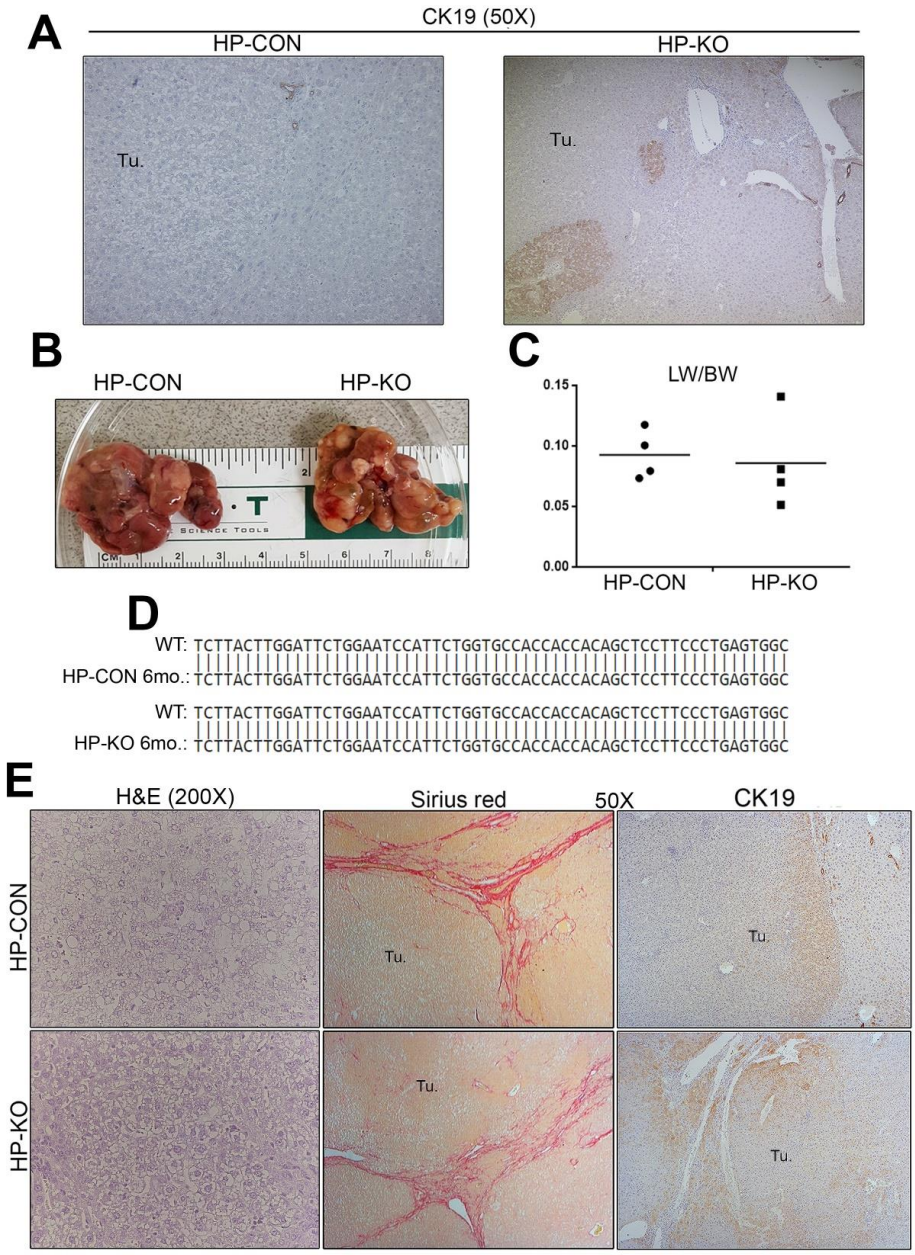

Figure 19: HP-KO have CK19-positive foci absent in HP-CON at 5 months, however HCC is comparable in HP-CON and HP-KO at 6 months after DEN/CCl4.

(A) CK19 staining is positive in biliary epithelial cells in HP-CON and HP KO, but is evident in small tumor foci within larger tumors in HP-KO at 5 months. (B) Gross images show advanced HCC in both HP-CON and HP-KO at 6 months after DEN/CCl_4. (C) Liver weight to body weight ratios are comparable at 6 months after DEN/CCl_4. (D) At 6 months, HP-CON and HP-KO have wildtype CTNNB1. (E) Representative H&E (200x), Sirius Red (50x), and CK19 (50x) suggest similar tumor composition, fibrosis, and CK19 pattern, respectively, in HP-CON and HP-KO at 6 months.

3.4.4 HP-CON and HP-KO after DEN/CCl4 show distinct temporal protein expression

Despite comparable tumor burden and histology in HP-CON and HP-KO at 5 and 6 months, we queried whether there are differences in protein expression, likely correlating with altered signaling patterns, as a result of absent Wnt secretion from hepatocytes. First, we assessed proliferation markers and relevant β-catenin activation markers via western blot (Fig.20A,C). Hypo-phosphorylated β-catenin, suggesting activation, was comparable at 5 months and significantly upregulated in HP-KO at 6 months. GS was variable, while Cyp2e1, a β-catenin target altered by CCl_4, was lower in HP-KO at 5 months, although levels in both HP-CON and HP-KO were comparably reduced at 6 months. Total levels of β-catenin were comparably reduced at 6 months compared to 5 months. Cyclin D1 was increased at 6 months compared to 5 months in both groups. PCNA remained comparably high at all times in both groups. Intriguingly, cMyc was reduced in HP-KO at both 5 and 6 months. Thus, overall hepatocyte-specific loss of Wnts appears to promote β-catenin hypo-phosphorylation and decrease cMyc levels after DEN/CCl_4.

We sought a holistic approach to assess protein levels, and performed Reverse Phase Protein Array to assess expression of over 240 proteins involved in cancer as described in Methods. Several proteins had significant differences between HP-CON and HP-KO in the 5 month or 6 month time-point, and select proteins were confirmed by western blot (Fig.20B,D). Intriguingly, at 5 months HP-KO had significantly less expression of ERK1/2, Bax, Brd4, and E-cadherin than HP-CON. By 6 months, HP-KO had increased ERK1/2 and decreased Brd4, and comparable Bax and E-cadherin. Expression of Wee1, Yap, and Cdc25 were variable, and while PKAa expression was only evident at 6 months, there was no difference between HP-CON and

HP-KO (Fig.20B,D). Taken together, this suggests HP-specific Wnts temporally regulate expression of oncogenes including ERK1/2, Bax, E-cadherin, and Brd4.

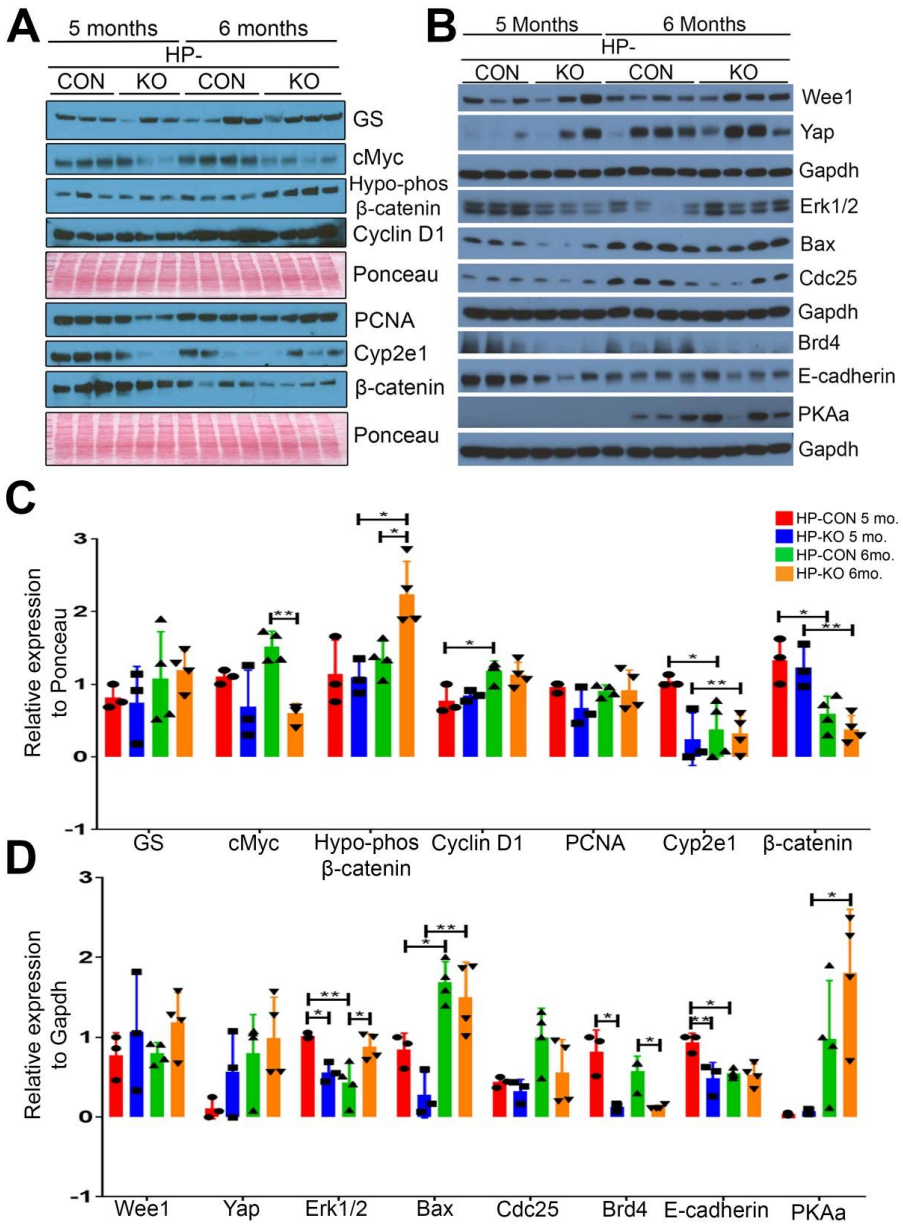

Figure 20: HP-CON and HP-KO have divergent protein expression patterns at 5 and 6 months. (A) Western blot assessing glutamine synthetase (GS), cMyc, hypo-phosphorylated β-catenin, Cyclin D1, PCNA, Cyp2e1, and total β-catenin. Ponceau shows comparable loading. (B) Western blot assessing select proteins based off RPPA analysis including Wee1, Yap, Erk1/2, Bax, Cdc25, Brd4, E-cadherin, PKAa. Gapdh shows comparable loading. (C) Densitometry of western blot from figure A highlights significant changes between HP-CON and HP-KO at 5 and 6 months. Relative expression was normalized to Ponceau. (D) Densitometry analysis of western

blot from figure B, normalizing values to Gapdh. Statistics performed with one-way ANOVA using multiple comparisons. *P<0.05, **P<0.01.

3.4.5 Comparable onset and progression of injury in response to DEN/CCl4

Lastly, we asked whether hepatocyte-Wnts contribute to DEN/CCl_4-induced injury and hence the pre-tumoral microenvironment. We subjected HP-CON and HP-KO to this insult until 3 months of age, and noted no gross hepatic differences (Fig.21A). Histology showed comparable cell death, hepatocyte ballooning, inflammation, and scarring in HP-CON and HP-KO (Fig.21B). Further analysis revealed similar fibrosis, inflammation, and proliferation via Sirius red, number of CD45+ cells, and number of Ki67-positive hepatocytes in HP-CON and HP-KO (Fig.21C). We therefore concluded removing Wntless from HP insignificantly contributes to hepatic injury during DEN/CCl_4 treatments.

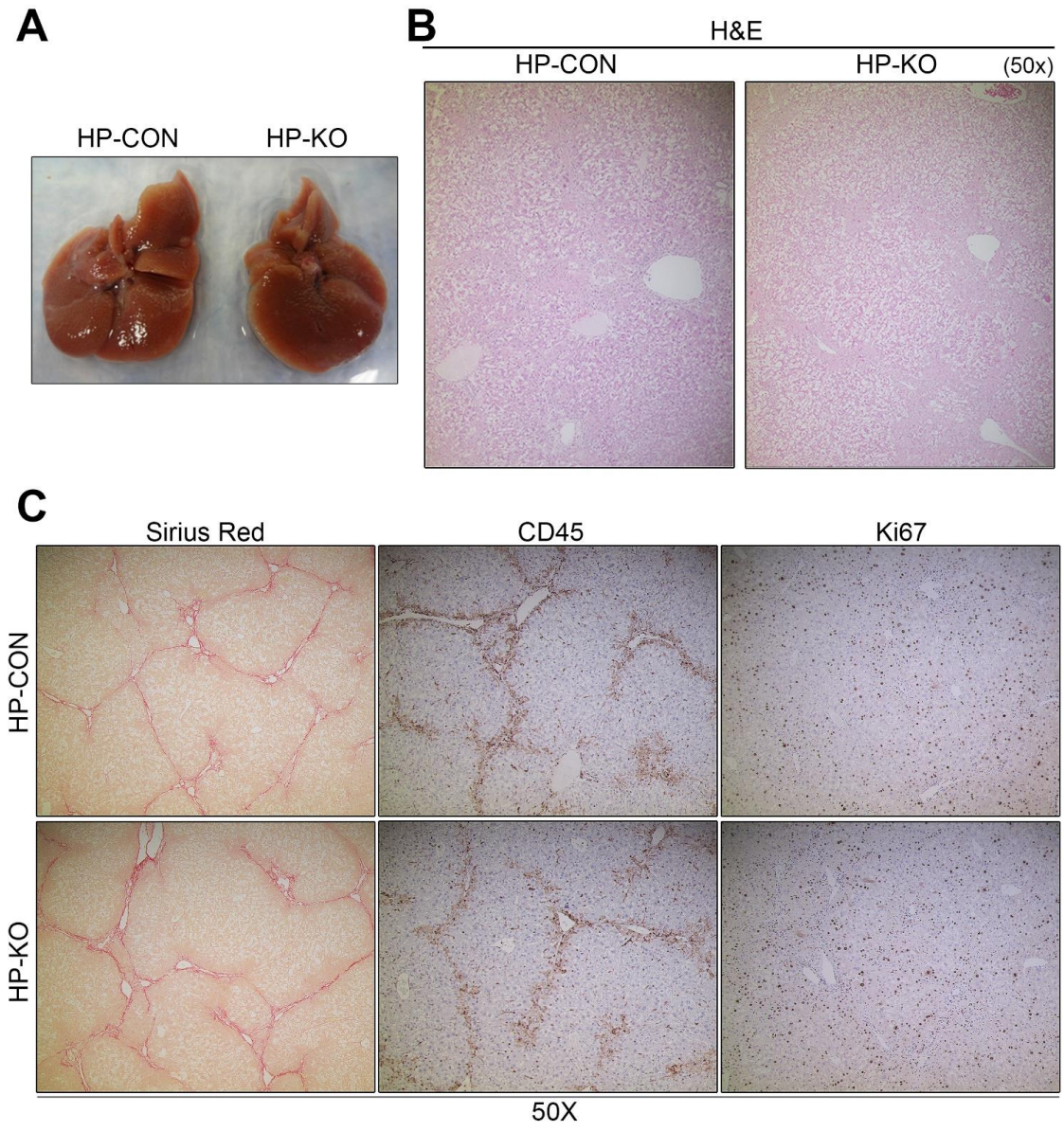

Figure 21: Comparable injury in HP-CON and HP-KO at 3 months after DEN/CCl4.
(A) Gross images of HP-CON and HP-KO livers at 3 months show similar stiffness and lack of gross tumors. (B) H&E staining shows similar histology in HP-KO and HP-CON with comparable cell death, hepatocyte ballooning, inflammation and fibrosis after 3 months of treatment with DEN/CCl4. (C) Representative images for Sirius red and immunohistochemistry for CD45 and Ki67, demonstrate comparable fibrosis, inflammation, and proliferation in HP-CON and HP-KO at 3 months after DEN/CCl4

3.5 Discussion

Activation of Wnt/β-catenin signaling in HCC is due to various mechanisms (164, 205). Overexpression of Wnt and Fzd genes have been implicated as a contributor to β-catenin activation in a subset of HCC cases (217). In fact, patients with intratumoral overexpression of Wnt and/or Fzd have more dedifferentiated tumors correlating with aggressiveness (218). Wnt upregulation has also been reported in HCC cell lines including Hep3B cells (219). To address the role of hepatocyte-derived Wnts in hepatocarcinogenesis in a relevant model, we examined injury and tumorigenesis in control mice and mice lacking Wntless in hepatocytes, which disallows secretion of all Wnts from these cells due to loss of this cargo receptor specific and essential for Wnts (13, 40, 240).

We studied the DEN/CCl_4 model of tumorigenesis, as it leads to HCC following chronic injury and fibrosis, mimicking patient progression (226). More importantly, we confirmed DEN/CCl_4-induced HCC provides evidence of β-catenin activation without mutations in Ctnnb1. Indeed, microarray data available publicly via Gene Expression Omnibus (GSE33446), confirms β-catenin target genes including CD44, Cyclin D1, EGFR, and Survivin are induced in this model whereas β-catenin targets like GS and Regucalcin, which are associated with more sustained β-catenin activation through mutations are unchanged. Further, when mRNA expression of several Wnts was assessed, Wnt1, Wnt6, Wnt10a, Wnt10b, Wnt11, and Wnt16 were upregulated at least 2-fold in comparison to control livers. While in the current study, we addressed the loss of all hepatocyte-derived Wnts, studying the relevance of individual Wnts will be interesting, especially since Wnt6 and Wnt11 can act non-canoncially, independent of β-catenin (241).

Upon challenging HP-CON and HP-KO with DEN/CCl_4, comparable tumor burden was observed at 5 months. We noted similar injury, fibrosis, inflammation, and proliferation. However, in assessing tumor differentiation, we observed the presence of small but frequent CK19-positive foci within larger CK19-negative tumors, in HP-KO. Presence of CK19 in HCC is suggested to correlate with a more dedifferentiated phenotype, overall poor prognosis and worse outcome after surgery (242-244). Finding CK19-positive foci in HP-KO was surprising, since a positive correlation between Wnt/β-catenin activation and stem markers including CK19 has been previously reported (245). However, since secretion of all Wnts is being disrupted, it is likely that the loss of non-canonical Wnts may be allowing for increased CK19 positivity. Indeed, hepatocytes and transformed hepatocytes are known to be a source of non-canonical Wnts that suppress β-catenin activity (219). Intriguingly, the increased numbers of CK19-positive foci did not lead to an overall aggressive HCC in HP-KO at 6 months and both groups of mice succumbed to excessive tumor burden, and CK19 staining was comparable at this time-point. These data suggest that the DEN/CCl_4 model is too robust leading to an aggressive disease and a model with an indolent course may be more suitable to address the overall role of hepatocyte-derived Wnts.

We also noted a reduction in cMyc in HP-KO at 5 months and 6 months. Wnt/β-Catenin activates cMyc, particularly during hepatocarcinogenesis (246). Therefore, a reduction in cMyc would likely suggest a reduction in β-catenin activity. While β-catenin target gene Cyp2e1 was reduced in HP-KO at 5 months, target gene GS and hypo-phosphorylated and total β-catenin levels were unchanged. Although at 6 months a reduced cMyc in HP-KO correlated with increased hypo-phosphorylated (and thus activated) β-catenin. cMyc can be upregulated in HCC independent of β-catenin, for example by amplification (247). The mechanism by which cMyc is

downregulated in HP-KO remains unclear and will be elucidated in the future. Overall, decreased cMyc does not seem to be altering the overall tumor biology in HP-KO since comparable tumor burden is evident in HP-KO and HP-CON. However, cMyc upregulation in HP-CON does appear to be partially Wnt/β-catenin dependent as shown previously (208, 246).

RPPA analysis further revealed altered protein expression in HP-KO versus HP-CON. While the relevance of these changes remains unclear, there are several intriguing relationships among these data. Bromodomain 4 (Brd4) is a transcription coactivator involved in many cancers. In HCC, Brd4 is overactive and its suppression correlates with cMyc suppression (248). At 5 month and 6 month timepoints, cMyc and Brd4 were both reduced in HP-KO. Whether HP-Wnts regulate cMyc through Brd4 remains a plausible mechanism to assess. E-cadherin inversely correlates with aggressive HCC, as loss leads to increased epithelial to mesenchymal transition and invasiveness (249). Reduction of E-cadherin in HP-KO at 5 months, then comparable expression to HP-CON at 6 months, supports the findings that at 5 months HP-KO tumors began to dedifferentiate, but all differences are ablated by 6 months. This likely reaffirms the model is too hepatotoxic to appreciate contributions of HP Wnts, as other pathways are able to compensate. E-cadherin can activate ERK signaling in other cancers (250), which may explain why reduced E-cadherin correlates with reduced ERK1/2 at 5 months, however further studies are required to confirm pathway activation. Finally, the role of HP-Wnts in Bax expression is unclear, despite HP-KO having reduced Bax at 5 months. Overall, we conclude HP-Wnts contribute to protein expression, which likely corresponds to signaling changes but are insignificant to the overall tumor phenotype.

Wnt signaling from hepatocytes also appears to not influence the overall pre-tumor environment. At 3 months, comparable injury, inflammation, and fibrosis was observed between

HP-CON and HP-KO. This negative data is novel and important, as we provide *in vivo* evidence that targeting hepatocyte-specific Wnts will not be an effective clinical therapy, despite literature demonstrating increased Wnts in HCC and transformed hepatocytes *in vitro*. It will be of interest to assess Wnt contributions from additional cell types, including macrophages and endothelial cells, to identify roles to injury, fibrosis, and carcinogenesis.

4.0 MACROPHAGE-SPECIFIC WNTLESS LOSS IN MICE CAN PROMOTE OR SUPPRESS HEPATIC TUMORIGENESIS IN RESPONSE TO CHRONIC INJURY AND CHEMICAL CARCINOGENESIS

Section 4.0 is a continuation from section 3.0, where we take macrophage-specific Wntless knockout mice (MP-KO) and subject them to DEN/CCl_4. We noted two distinct phenotypes, namely MP-KO had greater tumor burden than littermate controls, or MP-KO had reduced tumor burden to littermate controls. We attempt to characterize this phenotype and provide a work-in-progress mechanism, focusing on overall signaling differences, tumor immunology differences, and questioning the underlying factor responsible for the divergent phenotype. At the time of this thesis submission, the work in this section was submitted as a first-author manuscript to American Journal of Physiology and is currently under revision.

4.1 ABSTRACT

Hepatocellular carcinoma (HCC) remains an important unmet clinical need. Considering HCC occurs in fibrotic livers in 90% of cases, understanding the basis of injury progression and tumor development is therapeutically relevant. We previously reported Wnts to be upregulated in diethylnitrosamine-carbon tetrachloride (DEN/CCl4) induced model of hepatic injury, fibrosis, and tumorigenesis. In this model, we confirmed Wnts from hepatocytes to not contribute majorly

to HCC development. Here, we investigated if Wnts from macrophages are required for injury and HCC. We subjected macrophage-specific wntless knockouts (KO), unable to secrete Wnts from macrophages, and littermate controls (CON), to DEN/CCl4 for five months and assessed injury, inflammation and hepatocarcinogenesis. Exposure of MP-KO and MP-CON led to two distinct and litter-specific phenotypes. So-called Group A MP-KO had greater tumor burden than MP-CON A, while Group B MP-KO exhibited lesser HCC than MP-CON B. We therefore hypothesized that HCC occurring in Group A are phenotypically different from Group B and the macrophage-Wnts contribute disparately to tumor development based on underlying heterogeneity. Comparing MP-CON A and MP-CON B, we identified several epigenetic regulators and also signaling proteins including increased cMyc and P38 to be differentially expressed. Moreover, we identified MP-CON B to have increased M1 macrophages and infiltrating leukocytes. Elimination of Wnt secretion from macrophages thus had opposing consequences on HCC growth and development based on the molecular makeup of HCC, driven by divergent expression of epigenetic regulators, signaling and macrophage polarization. Our data suggests macrophage-Wnts can promote or suppress tumors, depending on the underlying cellular and molecular composition of HCC.

4.2 BACKGROUND

The incidence of hepatocellular carcinoma (HCC) has increased from 4.4 per 100,000 people in 2000 to 6.7 per 100,000 people in 2012 in the US. Compared to 2000, there was a 115% increase in reported HCC cases in 2012 (251). In areas of increased hepatitis infection including Eastern Asia, incidence is as high as 20 per 100,000 people. Furthermore, HCC occurs

in the context of chronic liver disease and fibrosis or cirrhosis up to 90% of the time (252). Therefore, despite advancement in understanding disease progression and mechanism, we still lack strong therapeutics to prevent and limit HCC.

Activation of Wnt signaling is known to occur in a major subset of HCC (164). While occurrence of mutations in CTNNB1 gene is one major mechanism, upregulation of Wnt signaling, via overexpression of Wnt ligands or receptors, or downregulation of Wnt antagonists, is also evident in additional subsets of HCC patients (218). However, the source of Wnts in HCC development remains unclear. Using the diethylnitrosamine and carbon tetrachloride (DEN/CCl_4) model, which causes injury and HCC, we previously confirmed tumors to harbor wildtype β-catenin (185). There was also an associated upregulation of several Wnts in this model. We provided evidence however, that hepatocyte-specific Wnts do not play a major role in injury progression, HCC development, or tumor advancement (Section 3.0) (185). However, several Wnts we identified to be upregulated after DEN/CCl_4, including Wnt10a, Wnt10b, Wnt11, and Wnt16, are present in resting and activated Kupffer cells (11). Therefore, we hypothesized that macrophages (MP) may secrete Wnts necessary for tumorigenesis, and preventing MP from secreting Wnts may impact HCC development and progression.

We subjected MP-specific Wntless knockout mice, unable to secrete all Wnts form MP (40), to DEN/CCl_4 for five months. Intriguingly we identified two distinct phenotypes that were litter-specific. Removal of MP Wnts acted as a tumor promoter or tumor suppressor. We provide evidence that these opposing roles of MP Wnts depends on underlying factors including oncogenic signaling, inflammatory milieu, and may be due to different epigenomes eventually leading to the two distinct HCC phenotypes.

4.3 METHODS

4.3.1 Animals

All animal use was performed in accordance with the Institutional Animal Care and Use Committee at the University of Pittsburgh, and animal husbandry was carried out by staff of the Division of Laboratory Animal Resources. Macrophage specific Wntless knockout mice, Lyz-$Cre^{+/-}$;$Wls^{fl/fl}$ (MP-KO) were generated and bred as described previously5. Male MP-KO (n=9) and littermate control (CON, n=9) were subjected to DEN/CCl4 as previously described (185) in section 3.2.1. Briefly, mice were given 25mg/kg DEN in saline at two weeks of age, and given twice-weekly injections of 0.5ml/kg CCl4 from 2 months to 5 months of age. Animals were monitored for morbidity. At time of harvest, livers were dissected into small sections and placed in 10% formalin for 48 hours prior to paraffin embedding, placed in O.C.T. compound to create frozen tissue sections, or flash frozen for RNA and protein analysis. Blood was extracted and serum was sent to the University of Pittsburgh Clinical Laboratory for liver injury marker testing, and liver weight and body weight were recorded.

4.3.2 Immunohistochemistry

CD45 and PCNA staining, and special stains Sirius Red and terminal deoxynucleotidyl transferase dUTP nick end labeling (TUNEL) were performed as previously described (Section 2.0) (108). For relevant antibody information, see Table 9. ImageJ was used for quantification. For Sirius Red and CD45, images were taken at 50x and for PCNA, images were taken at 100x. At least 3 fields were randomly imaged from at least 4 de-identified tissues per group were

imaged and relative intensities were measured. For TUNEL staining, positive cells were counted manually at magnification 100x from at least three images per de-identified sample, and from four samples per group. The average value for the three images was used as the final data point for statistical and graphical analyses.

4.3.3 Immunofluorescence

Liver lobes frozen in O.C.T. were used to cut 4μm sections. Sections were fixed in acetone and permeabilized with 0.1% Triton X-100. Slides were blocked in 5% serum in 0.5% BSA, and primary antibodies were incubated for one hour as per Table 9. Secondary antibodies conjugated to FITC or TRITC were used. After Dapi, coverslips were mounted with Gelvatol and slides incubated at 4° overnight. Images were taken on a Nikon Eclipse Ti microscope using NIS Elements version 4.4. For quantification, seven images per de-identified samples were taken and results presented as average. For CD68 and CD11b staining, positive cells were counted manually at 200x. For F4/80 staining, images were taken at 100x and intensity was measured with ImageJ Software.

4.3.4 Protein analysis

For Reverse phase protein array (RPPA) analysis, all samples were submitted to The University of Texas MD Anderson Cancer Center RPPA core facility. Protein lysates were prepared per the core facility instructions. For immunoblotting, protein was extracted in RIPA buffer, quantified, and 30μg was loaded onto a precast BioRad SDS gel. Gels were transferred using BioRad semi-dry transfer system. See Table 9 for antibody information. To perform cytokine array (R&D,

Mouse Cytokine Antibody Array, Panel A) three RIPA lysates per group were pooled together and used per the manufacturer's instructions. To quantify western blotting and cytokine array, ImageJ was used and mean intensities were normalized to housekeeping proteins.

Table 9: List of antibodies used in section 4.0

Protein	Company	Catalog No.	Use	Dilution
CD11b	Biolegend	101201	IF	1 to 100
CD68	Abcam	125212	IF	1 to 250
F4/80	Serotec	mca497ga	IF	1 to 500
PCNA Use with Mouse On Mouse kit (Vector Laboratories)	Santa Cruz	SC-56	IHC/WB	1 to 50/1 to 200
CD45	Santa Cruz	SC-53665	IHC	1 to 100
Cyclin D1	Thermo Fisher	RB-9041-P	WB	1 to 200
Gapdh	Proteintech	60004-1-Ig	WB	1 to 10,000
GS	Santa Cruz	SC-74430	WB	1 to 1000
Cyp2e1	Sigma Aldrich	HPA009128	WB	1 to 500
P21	Santa Cruz	SC-271532	WB	1 to 100
pRb	Cell Signaling	9308	WB	1 to 500
pAKT	Cell Signaling	13038	WB	1 to 1000
pERK	Cell Signaling	4370	WB	1 to 1000
53BP1	Cell Signaling	4937	WB	1 to 750
cMyc	Santa Cruz	SC-764	WB	1 to 200
Bax	Cell Signaling	2772	WB	1 to 750
P38 Mapk	Cell Signaling	9212	WB	1 to 1000
AR	Abcam	ab129081	WB	1 to 1000
Stat3	BD Bioscience	610189	WB	1 to 5000
Smad3	Abcam	ab40854	WB	1 to 1000
Active beta-catenin	Cell Signaling	4270	WB	1 to 1000
Beta-catenin	BD Bioscience	610154	WB	1 to 1000
Cleaved Casp3	Abcam	ab32042	WB	1 to 1000
Cleaved Caps7	Cell Signaling	9491	WB	1 to 1000

4.3.5 RNA and Qiagen qPCR array

RNA was extracted from three DEN/CCl4 treated control livers from Group A, and three from Group B using Trizol (Thermo Fisher), and after DNAse treatment (Thermo Fisher) 2µg of RNA was reverse transcribed using Superscript III (Thermo Fisher). Samples were then pooled together and Sybr Green (Thermo Fisher) was used for qPCR in the Mouse Epigenetic Chromatin Modification Enzymes PCR array (Qiagen). Ct values were normalized to several housekeeping genes within the array.

4.3.6 Statistical analysis

Graphs were generated with Microsoft Excel or Prism software. Student's T Test or One-Way ANOVA with multiple comparisons (as distinguished in figure legends) was used to calculate statistics and described appropriately in figure legends. P values less than 0.05 were considered significant.

4.4 RESULTS

4.4.1 Removing Wntless from MP results in opposing response to DEN/CCl_4

To test whether preventing Wnt secretion from MP will impact tumorigenesis, we used MP-specific Wntless knockout mice (MP-KO) (40), and subjected MP-KO and littermate controls (MP-CON) to DEN/CCl_4 until 5 months of age as previously reported (185). Four separate litters

composed of 9 MP-CON and 9 MP-KO in total were exposed to the treatment. Intriguingly, we observed a litter-specific contrasting phenotype. MP-KO exhibited greater tumor burden and liver weight to body weight ratio than MP-CON in two litters (n=4, herein referred to as Group A), and MP-KO exhibited reduced tumor burden and liver weight to body weight ratio compared to MP-CON in two litters (n=5, herein referred to as Group B) (Fig.22A,B). While serum injury markers were variable, Group A MP-CON and MP-KO had comparable injury markers ALT, AST, ALP, and Bilirubin (Fig.22C, Fig.23A). Group B MP-KO overall trended towards less injury compared to Group B CON, as MP-KO B had significantly less ALT, and insignificant reductions in AST and total Bilirubin. Direct bilirubin and ALP were comparable in Group B MP-CON and MP-KO (Fig.22C, Fig.23A).

Hematoxylin and Eosin staining was done on tissues sections to address histological differences between various groups. HCC occurring in the DEN/CCl_4 model show both inter- and intra-animal tumor heterogeneity (Fig.22D,E, Fig.23B,C). There were areas of well-differentiated HCC composed of larger hepatocytes containing glycogen (clear spaces) with normal-sized nuclei without notable pleomorphism and only few mitotic figures (Fig.22D,E: MP-CON A 3; MP-CON B 1. Fig.23B, C: MP-KO A 2; MP-KO B 2). However, both groups also showed areas of moderately-to-poorly differentiated HCC with features of high nuclear to cytoplasmic ratio, greater nuclear atypia and high mitotic index (Fig.22D,E: MP-CON A 1,2; MP-CON B 2. Fig.23B, C: MP-KO A 1,2; MP-KO B 1). Overall, there were indiscernible differences in HCC histology that could explain consistent differences in tumors between MP-KO and MP-CON in Groups A and B. However, the data did suggest that Wnts from MP may act as tumor promoters or suppressors in a contextual manner.

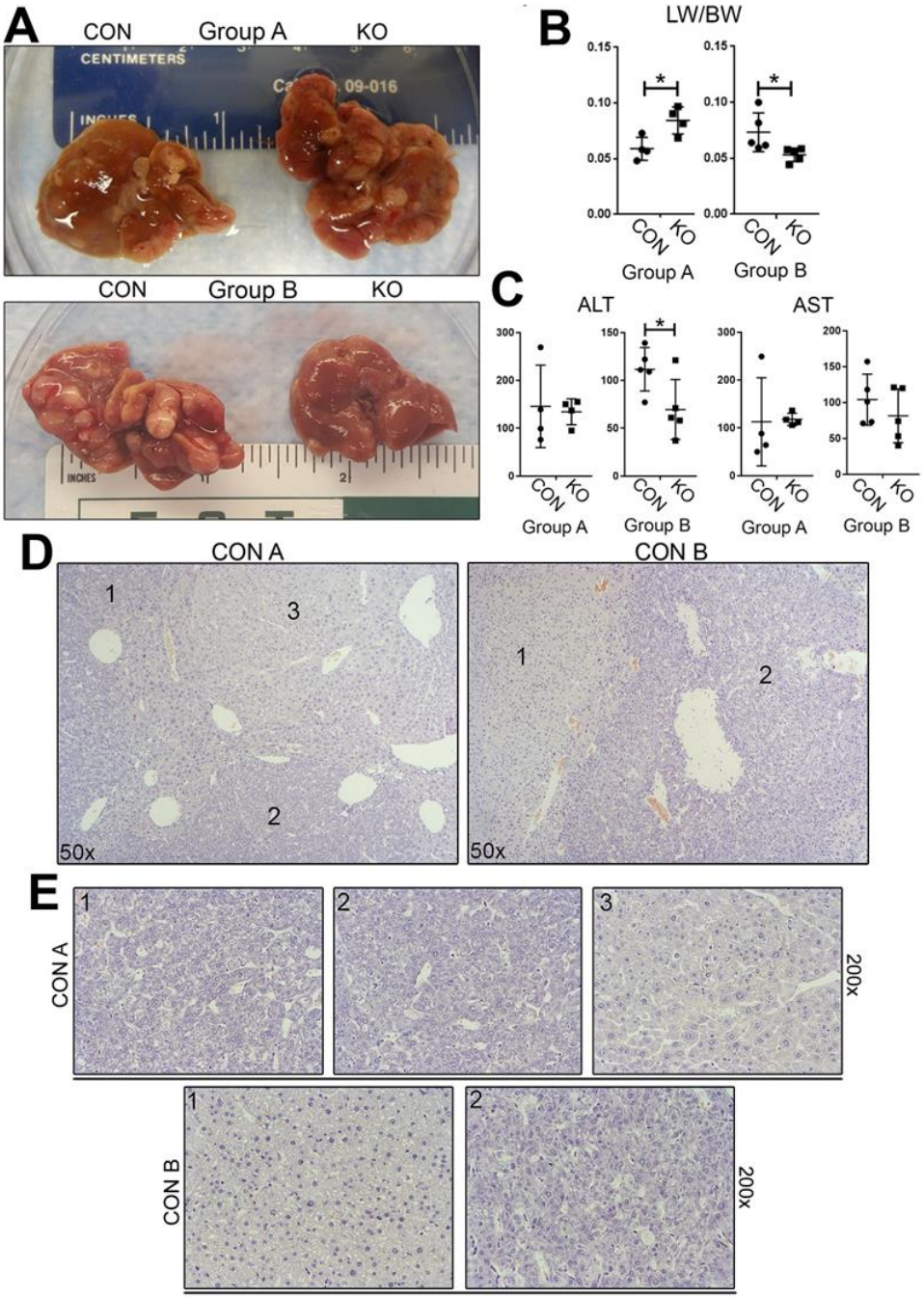

Figure 22: MP-KO have increased tumors or decreased tumors compared to littermate MP-CON.
(A) Gross images of Group A, with MP-KO having increased tumor burden, and of Group B, with MP-KO having decreased tumor burden. (B) Liver weight to body weight ratios. MP-KO are significantly increased in Group A, and significantly decreased in Group B. (C) Serum alanine aminotransferase (ALT) and serum aspartate aminotransferase (AST) are comparable in Group A, but decreased in Group B MP-KO compared to MP-CON. (D) Representative hematoxylin and eosin staining of tumors of MP-CON in Group A and Group B. Each number corresponds to a different tumor. Images at 50x. (E) H&E images of tumors taken at 200x. Each

number corresponds to the same number in D. Statistical analyses performed with Student's T Test. *P<0.05.

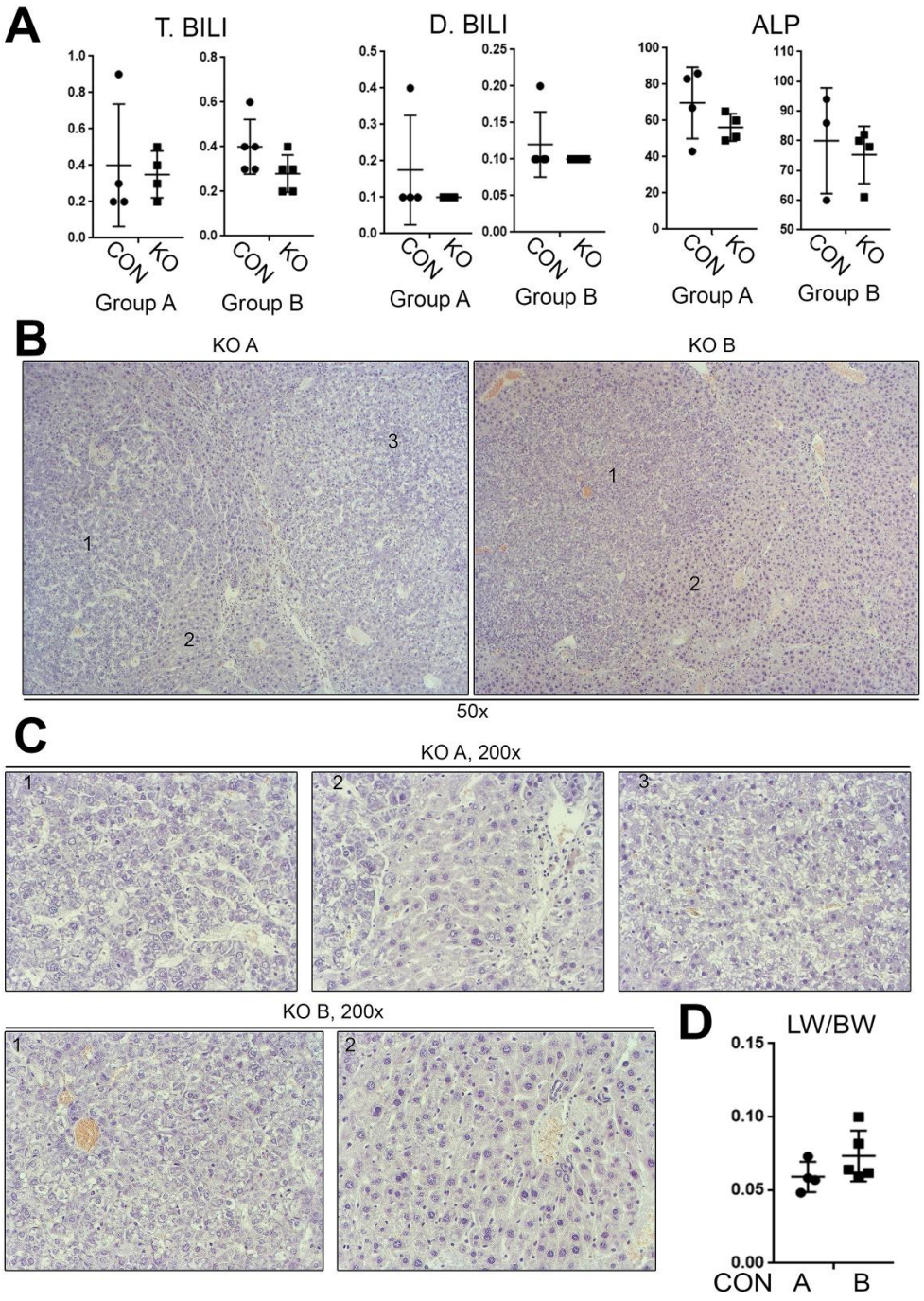

Figure 23: MP-KO and MP-CON have insignificant differences in serum bilirubin or ALP, and MP-KO display tumor heterogeneity similar to MP-CON.

(A) Serum levels of total bilirubin, direct bilirubin, and alkaline phosphatase are similar in MP-CON versus MP-KO in Group A and Group B. (B) Low magnification (50x) images of H&E

displaying different HCC subtypes. Each number corresponds to a dysplastic or tumor nodule. (C) High magnification (200x) images of tumors labeled in B. Statistics performed using Student's T Test. *P<0.05, **P<0.01.

4.4.2 Despite comparable fibrosis and cell death, MP-CON B has increased CD45-positivity while MP-CON A has increased nuclear PCNA positivity

As eliminating Wnt secretion from MP had different effects on Group A versus Group B, we predicted controls in Group A would have phenotypically different tumors than controls in Group B. Therefore, we focused on controls first and assessed staining for various injury phenotypes. Sirius red staining was comparable in MP-CON A and MP-CON B, suggesting similar fibrosis (Fig.24A). Next, we stained for CD45, marker for immune cells, and noted increased levels in MP-CON B, approaching statistical significance (Fig.24A), possibly suggesting increased leukocyte infiltration in MP-CON B. Hepatocyte cell death assessed via TUNEL staining was comparable in MP-CON A and MP-CON B (Fig.24B). Intriguingly, despite heterogeneity in PCNA staining patterns, nuclear PCNA-positivity was quantified and significantly upregulated in MP-CON A compared to MP-CON B (Fig.24B).

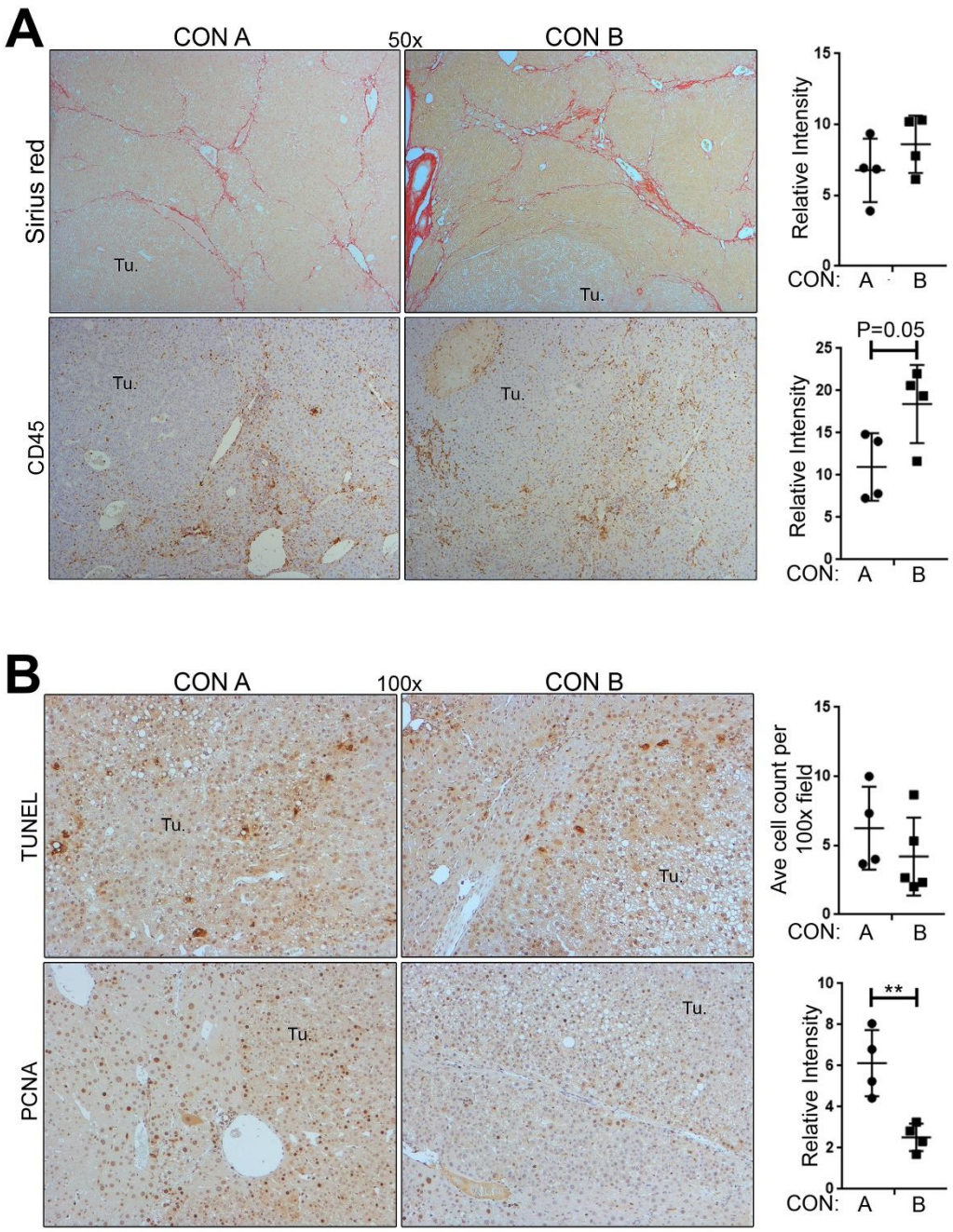

Figure 24: MP-CON A and MP-CON B have comparable fibrosis and cell death, but MP-CON B has more CD45-positivity and MP-CON A has increased nuclear PCNA intensity.

(A) Representative images of Sirius red and CD45 immunohistochemistry, taken at 50x. Quantification via ImageJ suggests similar Sirius red levels, and increased CD45 in MP-CON B. (B) 100x images of TUNEL and PCNA staining. Total number of TUNEL-positive cells were counted and numbers in MP-CON A and MP-CON B were comparable. For PCNA, nuclear intensity was measured and MP-CON A displayed increased levels. For all quantification, three

images per de-identified sample were taken and data presented as average. Statistics performed using Student's T Test. *P<0.05, **P<0.01.

4.4.3 Differential protein expression is observed in MP-CON A versus MP-CON B

Next, we questioned whether differences in protein expression, likely leading to differential signaling, could be identified between Group A and Group B CON. We performed Reverse Phase Protein Array (RPPA), assessing over 240 proteins involved in cancer to identify relative protein expression levels. Select proteins with statistically significant differences, and other HCC-relevant proteins not included in the RPPA, were validated via western blot (Fig.25A,B). While some sample-to-sample variation was present, Group A MP-CON had increased androgen receptor and cleaved Caspase 3, and consistent upregulation of cMyc and P38 MAPK. Group B MP-CON had significant increase in glutamine synthetase, although active- and total-β-catenin levels were comparable in both groups, and an insignificant increase in cleaved Caspase 7. Taken together, contrast in protein expression including cMyc and P38 MAPK suggests HCC in Group A MP-CON and Group B MP-CON utilize differential molecular signaling.

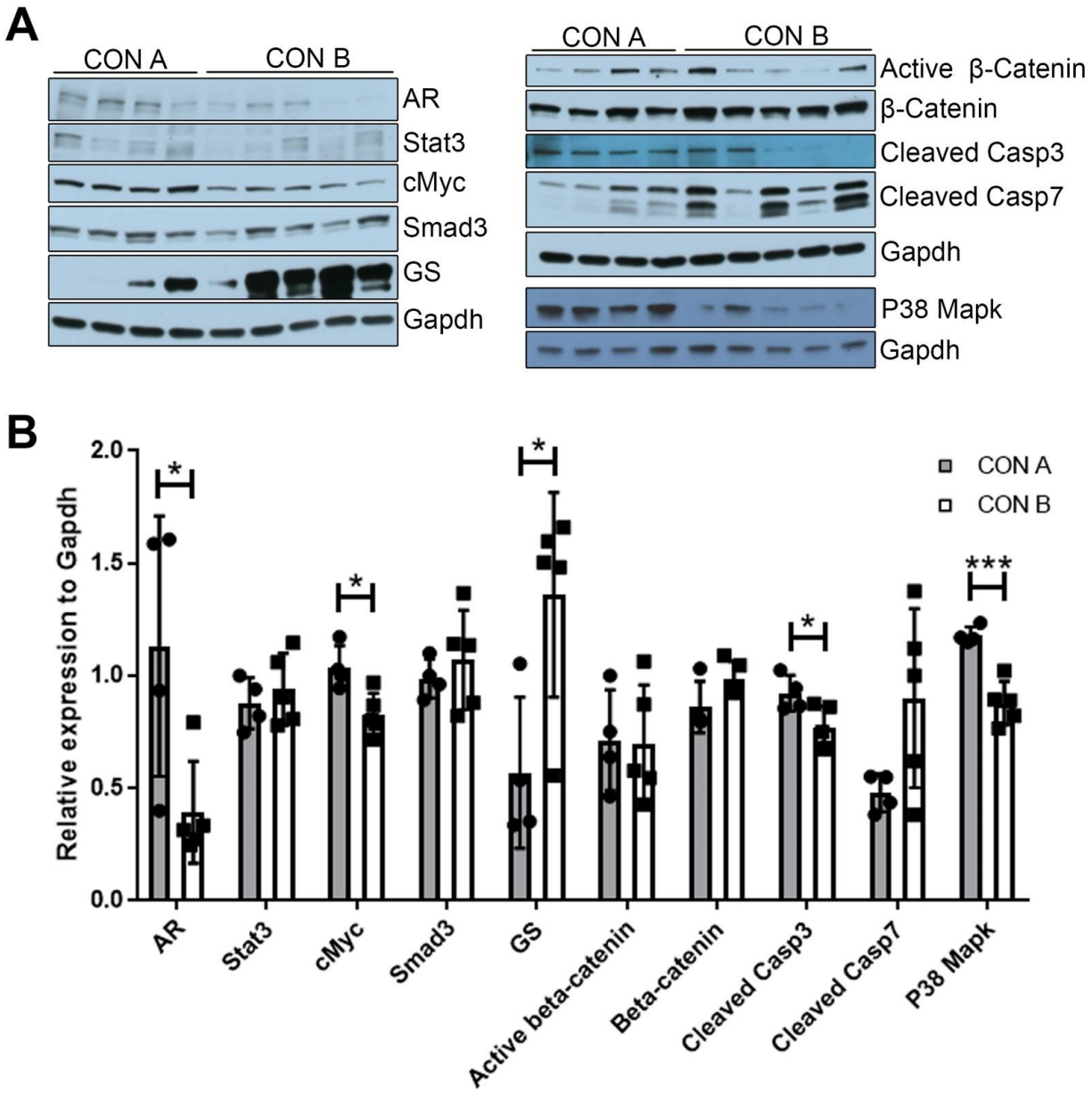

Figure 25: MP-CON A and MP-CON B have differences in protein expression.

(A) Western blot assessing proteins based on RPPA analysis and independent investigation. (B) Densitometric analysis suggests MP-CON A has increased androgen receptor (AR), cMyc, cleaved caspase 3, and P38 Mapk, while MP-CON B has increased glutamine synthetase (GS). Statistics performed using Student's T Test. *P<0.05, **P<0.01, ***P<0.005.

4.4.4 MP-CON B have increased CD68 and CD11b single-positive MP and pro-inflammatory cytokines, despite comparable MP numbers to MP-CON A

Next, we assessed how the removal of MP Wnt secretion impacts MP phenotype, as several reports have suggested activated MP to secrete Wnts including during pathogenesis of chronic liver disease (107, 253). In a resting liver, majority of Kupffer cells are CD68+CD11b-, as CD11b+ monocytes typically enter the liver from circulation before differentiating into MP. While, various treatments can lead to increase in CD68+CD11b+ and/or CD68-CD11b+ macrophages (254), the significance of such alterations is incompletely understood. To elucidate MP phenotype in our models, we performed co-immunofluorescence of CD68 and CD11b (Fig.26A,B). We observed a large portion of double positive cells, although Group B MP-CON had more CD68-CD11b+, and CD68+CD11b- single positive cells than Group A CON, despite similar numbers of total positive cells. F4/80 immunofluorescence confirmed Group A MP-CON and Group B MP-CON have comparable numbers of macrophages (Fig.26C,D).

CD68-CD11b+ cells produce proinflammatory cytokines to a greater extent than CD68+CD11b- cells (254). Less is known about the CD68+CD11b+ fraction, as this only represents 6% of Kupffer cells at baseline (254). Considering proinflammatory cytokines lead to recruitment of leukocytes (255) we performed a protein-based cytokine array to further elucidate differences in the microenvironment in Group A and Group B CON. Of 40 cytokines, 29 were noticeably expressed in whole-liver lysates and four were expressed at least 1.5-fold higher in Group B MP-CON compared to Group A MP-CON (Fig.27A). These four, IL1α, IL1β, IL16, and CCL2, all suggest an increased M1 proinflammatory phenotype (256, 257) in Group B MP-CON compared to Group A. Intriguingly, M2 markers IL4, IL13 (258), IL1Ra, and IL10 (259), were either unchanged or absent from both groups. Our data suggests that Group A MP-CON

have a different macrophage phenotype than Group B CON, and Group B MP-CON likely have increased M1 macrophages. Despite a more M1 phenotype of MP in Group B MP-CON when compared to Group A CON, there were insignificant differences in overall tumor burden between the two groups (Fig.23D). This suggests MP polarity to not be playing an exclusive role in contributing to the overall extent of HCC and other factors may also be instrumental.

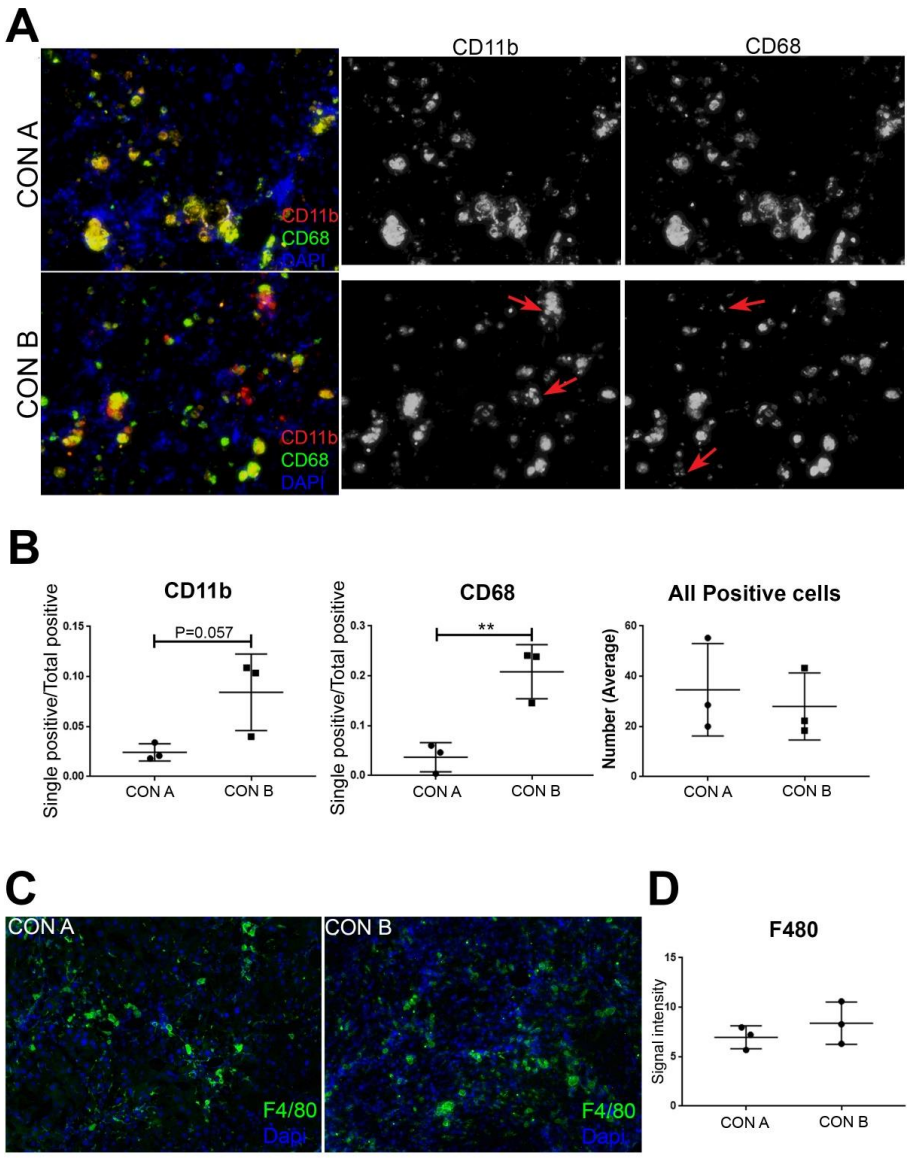

Figure 26: Despite similar number of macrophages in both groups, MP-CON B has more CD68 and CD11b single-positive macrophages.

(A) Double immunofluorescence of CD11b (red), CD68 (green), and Dapi (blue). Red arrows point to single-positive (CD11b or CD68) cells. (B) Quantification of total number of single positive (CD68-CD11b+ or CD68+CD11b-) or total number of all positive (single positive or double positive) cells. CD11b and CD68 were calculated by counting the number of single positive cells and dividing it by the number of total positive (double and single positive) cells. For each sample, seven images at 200x were taken and counted, and the average of seven images was used as a single data point. (C) F4/80 (green) immunofluorescence of MP-CON A and MP-CON B. (D) Quantification of F4/80 intensity is comparable in MP-CON A and MP-CON B. Intensity was measured using ImageJ, and each data point is the average of seven images at 100x. Statistics performed using Student's T Test. *P<0.05, **P<0.01.

4.4.5 MP-CON A upregulates transcripts of several histone and chromatin modifying enzymes compared to MP-CON B

We hypothesized the opposing phenotypes leading to differences in tumor burden between Group A versus Group B resulted from different upstream oncogenic events. While chemically-induced oncogenic events are random, we predicted one underlying event was responsible for Group A and Group B. Chappell et al. assessed tumors from DEN/CCl_4-treated mice and found no mutations in oncogenic hotspots including Ctnnb1, H-ras, and Hnf1α, all known to be mutated after chemical carcinogenesis (227). Further, they identified epigenetic changes after DEN/CCl_4 including alterations in DNA and histone methylation, to play a role in tumorigenesis. Therefore, we asked whether Group A MP-CON and Group B MP-CON have different epigenetic signatures, and performed an mRNA-based array to assess expression of 84 different genes involved in chromatin or histone modification. Of 84 genes, 26 were >2-fold increased in Group A CON, and one was >2-fold increased in Group B MP-CON (Fig.27B). Moreover, 19/26 genes increased in Group A MP-CON activate transcription (indicated in green), while 5/26 repress transcription (indicated in red), and 2/26 are context-dependent (indicated in gray). A deeper analysis revealed that a majority of these activating marks included histone phosphorylation, DNA and histone methylation, and histone acetylation (Fig.27C). While future studies are required to confirm if these changes translate to altered epigenetic status, and to elucidate specific oncogenes that may be impacted, our data suggests that Group A MP-CON has increased transcript levels of several histone and chromatin modifiers compared to Group B CON. We predict these changes to lead to differing epigenomes resulting in disparate tumor burden in Group A versus Group B.

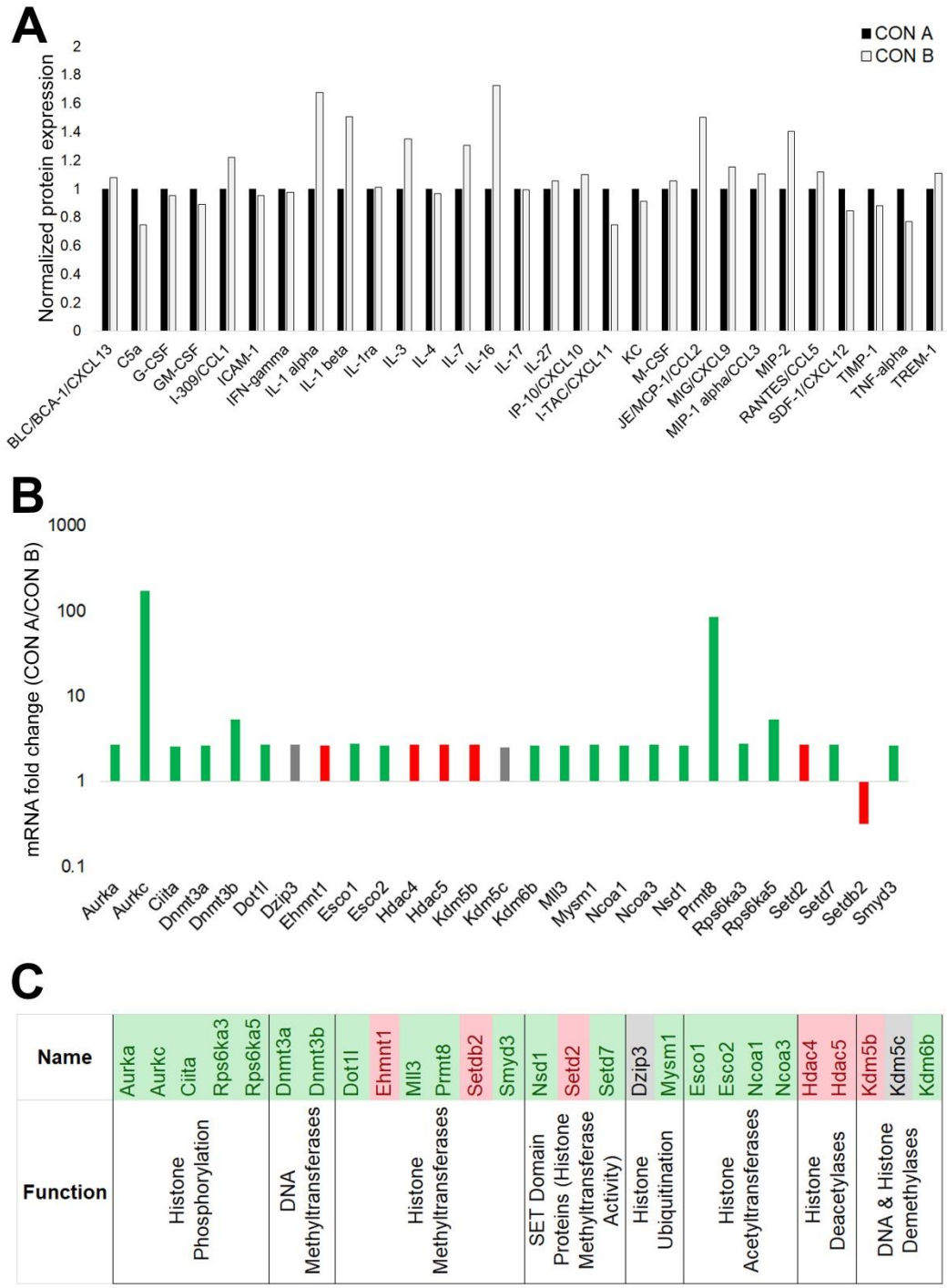

Figure 27: MP-CON B has increased levels of pro-inflammatory cytokines, while MP-CON A has increased transcript levels of several histone and chromatin modifying enzymes.

(A) Protein-based cytokine array using whole-liver lysates identified IL1α, IL1β, IL16, and CCL2 to be at least 1.5-fold increased in MP-CON B versus MP-CON A. Values are normalized to housekeeping genes per the array instructions. (B) Of 84 DNA modification enzymes, 26 were upregulated via mRNA in MP-CON A, and one was upregulated in MP-CON B. Green genes are involved in modifications that activate transcription, red genes influence modifications that

repress transcription, and gray genes are context-dependent. Values were normalized to housekeeping genes per array instructions, and values are presented as relative fold change of MP-CON A over fold change of MP-CON B. (C) List of differentially regulated genes per function.

4.4.6 Removing MP Wls further influences protein expression in Group A and Group B

To determine how preventing MP Wnt secretion impacts Group A and Group B differently, we assessed whole-liver lysates for differences in protein expression. We began by validating proliferation markers, β-catenin target genes, and other cancer relevant markers (Fig.28A,C). In Group A, MP-KO had significantly more PCNA than CON, although Cyclin D1 was comparable. Further, MP-KO A expressed higher levels of GS and Cyp2e1, suggesting increased β-catenin activity. While P21 was trending upward, phosphorylated Rb was significantly upregulated in MP-KO A, while phosphorylated AKT and ERK were comparable to MP-CON A. Next, we assessed our RPPA data, and validated select proteins that appeared to be differentially expressed in Group A MP-CON versus MP-KO. Intriguingly, MP-KO A had greater 53BP1 and Bax, but lower cMyc expression than MP-CON A (Fig.28B,C).

In Group B, MP-CON and MP-KO had comparable PCNA and Cyclin D1, however MP-KO B had increased GS and Cyp2e1, similar to the trend observed in Group A (Fig.28A,C). Moreover, Group B MP-KO had a significant reduction in P21, while phosphorylated Rb, AKT, and ERK were comparable. After analyzing our RPPA data, we validated cMyc and P38 MAPK. Although P38 MAPK levels were comparable, MP-KO B had significantly increased cMyc compared to controls (Fig.28B,C). Taken together, this data overall suggests that removing MP-specific Wnts contributes to protein expression changes after DEN/CCl_4 with divergent expression patterns in Group A and Group B.

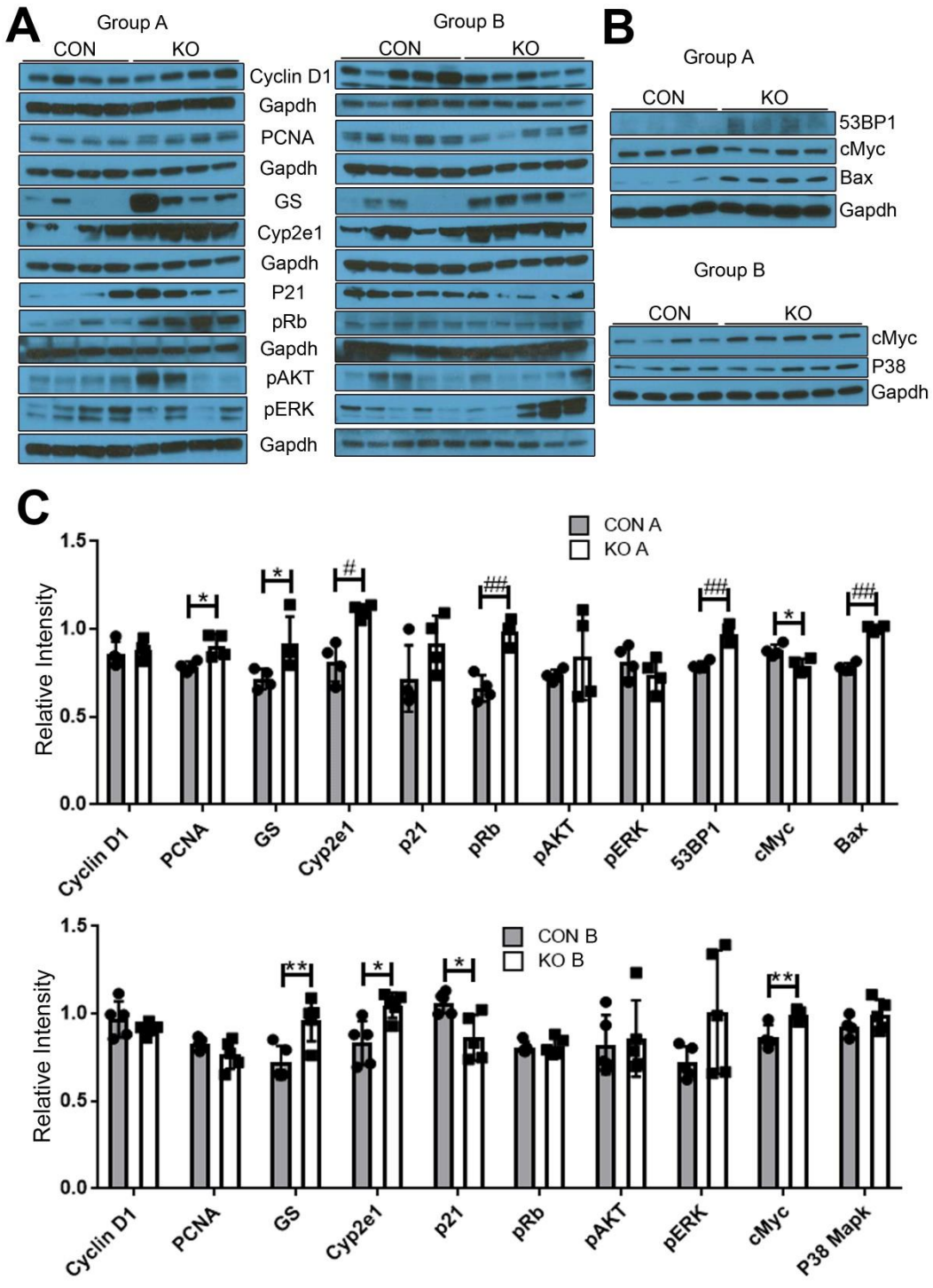

Figure 28: MP-KO influences protein expression differently in Group A and Group B.

(A) Western blot assessing proteins involved in proliferation, β-catenin signaling, and oncogenesis. (B) Western blot assessing additional proteins deemed to have significant differences in MP-CON versus MP-KO via RPPA analysis. (C) Densitometric analysis of western blot from A reveals MP-KO A has increased PCNA, GS, Cyp2e1, phospho-retinoblastoma protein (pRb), 53BP1, and Bax, and decreased cMyc compared to MP-CON A.

Further, MP-KO B has increased GS, Cyp2e1, cMyc, and decreased p21 compared to MP-CON B. Statistics performed using Student's T Test. *P<0.05, **P<0.01, #P<0.005, ##P<0.001.

4.4.7 Removing MP Wls does not majorly impact fibrosis, leukocyte or MP count, or cell death, but does influence PCNA positivity and MP polarization

We queried whether removal of MP Wls impacts fibrosis, leukocyte count, or cell death and proliferation. Sirius red staining and TUNEL staining were comparable in all groups (Fig.29A, Fig.30A,B). While no statistically significant differences in CD45-positivity were observed, MP-KO B trended lower compared to MP-CON B, and MP-KO A had a larger spread than MP-CON A. Interestingly, MP-KO A had reduced PCNA compared to MP-CON A, while MP-CON B and MP-KO B were comparable.

Lastly, we assessed how removing MP Wnts influences the immunological landscape after DEN/CCl_4. We began by assessing CD68 and CD11b co-immunofluorescence, and F4/80 fluorescence. Total number of CD68 and/or CD11b positive cells were comparable between MP-CON and MP-KO from Group A and Group B, and relative F4/80 signal intensity was also comparable (Fig.29B, Fig.30C), suggesting overall similar number of macrophages. In Group A, we noted a large spread in MP-KO when assessing number of CD68+CD11b- or CD68-CD11b+ single positive cells. Intriguingly, Group B MP-KO had fewer single positive cells than Group B MP-CON (Fig.29B, Fig.30C). We predicted preventing MP-Wnt secretion from both groups therefore partially impacted MP phenotype, so we performed the cytokine array to compare MP-CON and MP-KO. In Group A, M1 markers IL16 and CCL2 were increased in MP-KO at least 1.5-fold, and M1 marker and chemokine CXCL9 (260) was reduced in MP-KO by 1.9-fold (Fig.29C). In Group B, MP-KO had reduced expression of several markers, with 1.57-2.15-fold reduction in IL1α, IL1β, IL16, IL17, IL27, and MIP2, compared to MP-CON (Fig.29C). This

data suggests MP from Group B MP-KO have reduced activation compared to CON. This suggests that differences in MP polarization between the Group A MP-KO and MP-CON as well as Group B MP-KO and MP-CON may be contributing to overall differences in the HCC burden, although further studies will be required.

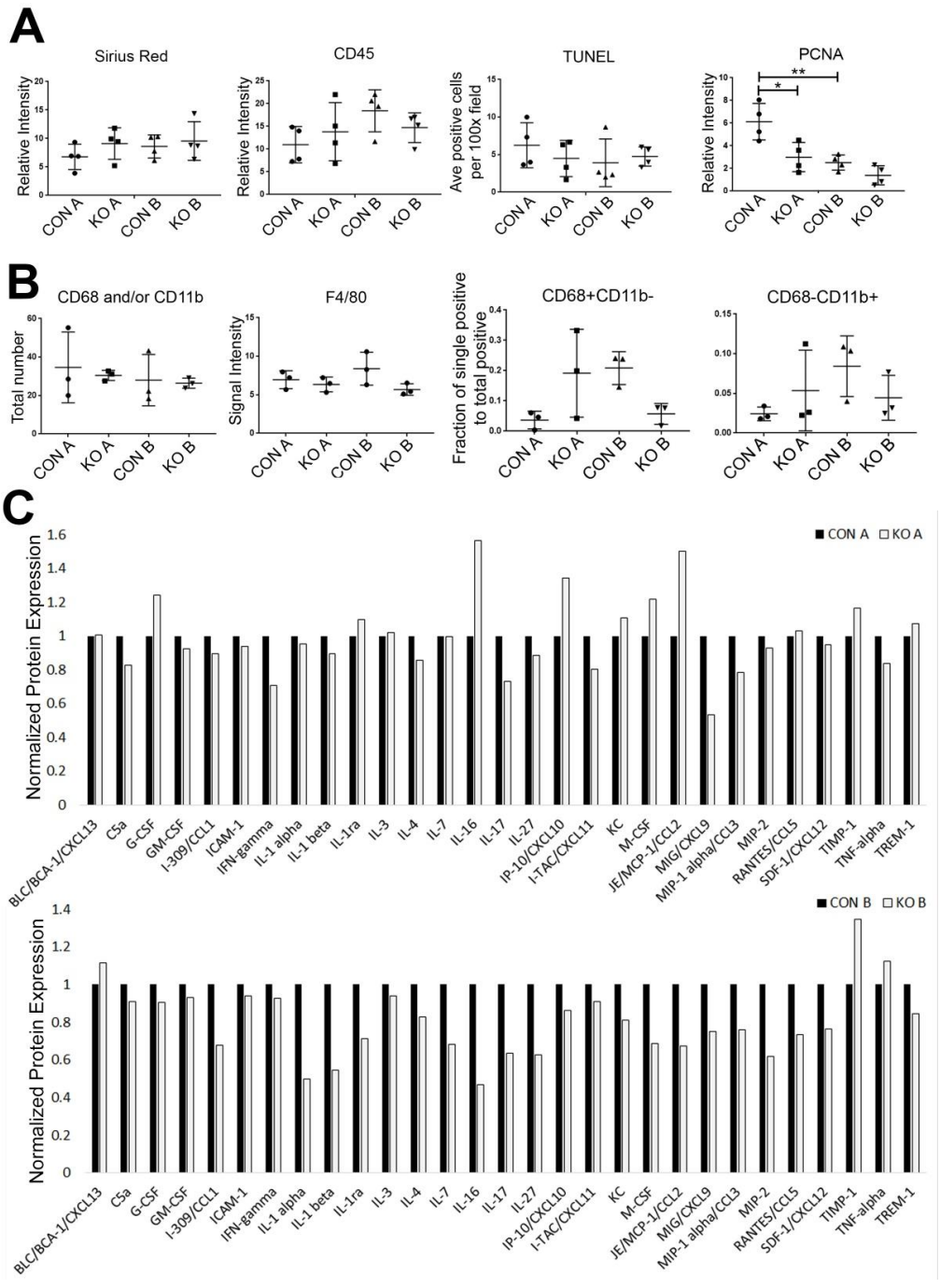

Figure 29: Removing macrophage-Wntless influences PCNA-positivity and immunological milieu.
(A) Quantification from immunohistochemistry of Sirius red, CD45, TUNEL, and PCNA from Figure 31. MP-KO A has significantly less PCNA intensity than MP-CON A, while no other changes were statistically significant. (B) Quantification of immunofluorescent staining reveals

comparable number of CD68 and/or CD11b-positive cells and F4/80 intensity, suggesting comparable macrophage levels between all groups. MP-KO A had variable levels of CD68 or CD11b single positive cells, while MP-KO B had decreased single-positive cells compared to MP-CON B, although this was insignificant via one-way ANOVA. (C) Results from cytokine array. In Group A, MP-KO A had increased IL16, CCL2, and decreased CXCL9 at least 1.5-fold. In Group B, MP-KO B had decreased IL1α, IL1β, IL16, IL17, IL27, and MIP2 at least 1.5-fold compared to MP-CON B. Statistics performed using one-way ANOVA. *P<0.05, **P<0.01.

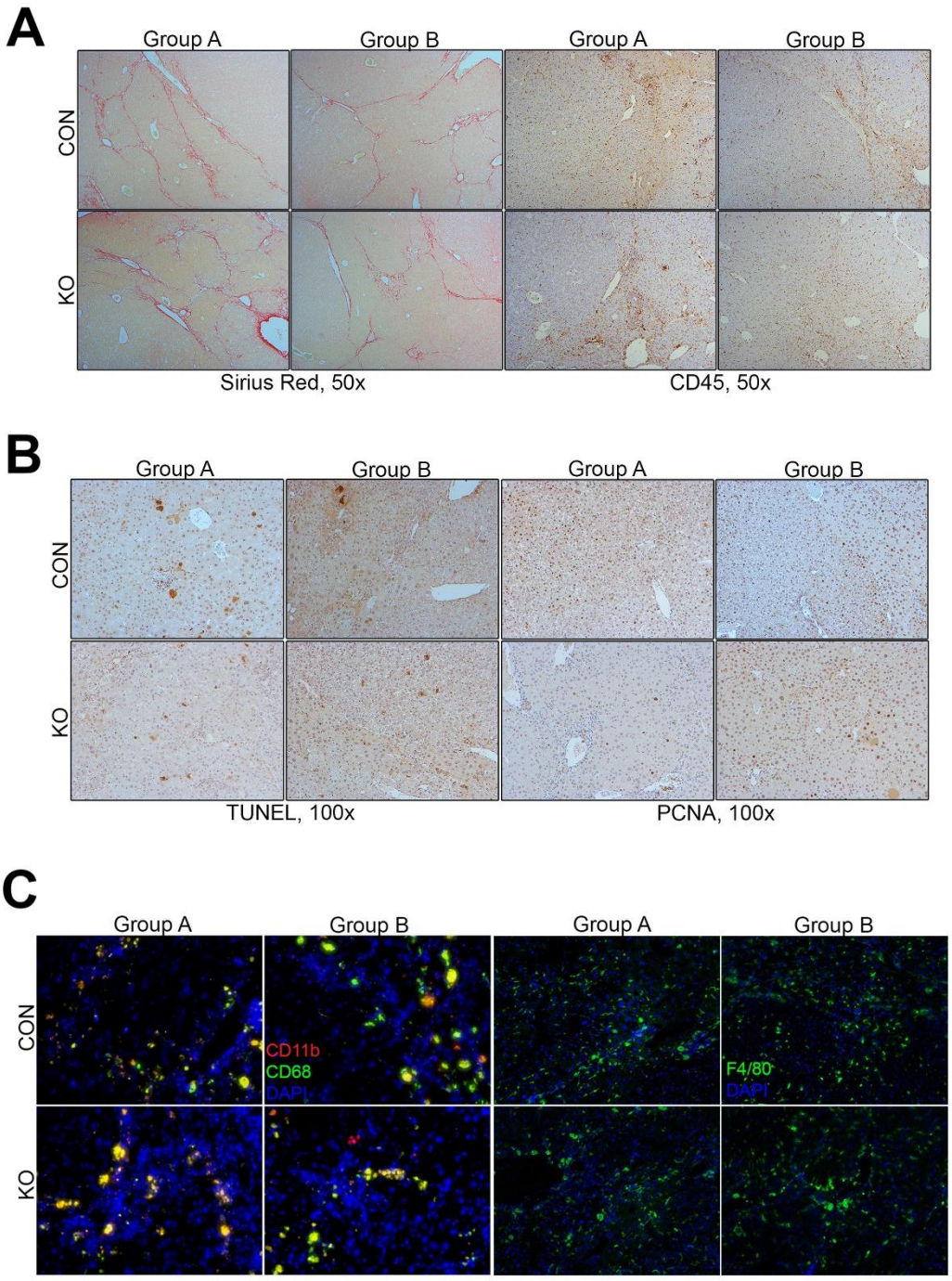

Figure 30: Immunohistochemical and immunofluorescent images of MP-CON and MP-KO from Group A and Group B as quantified in Figure 29.

(A) Images of Sirius red and CD45 staining of MP-CON and MP-KO from both groups, 50x. (B) Images from all groups of TUNEL and PCNA, taken at 100x. (C) 200x IF images of CD11b (red) and CD68 (green) co-stain (left), and of 100x images of F4/80 (green, right) stain.

4.5 DISCUSSION

Previously we have shown that loss of Wnt secretion from hepatocytes has overall minor impact on hepatic injury progression and carcinogenesis (185). We verified that DEN/CCl_4 model of hepatic injury, fibrosis, and cancer led to HCC harboring wildtype-β-catenin, but showed overexpression of several Wnts in whole liver lysates. Knowing that multiple cell types within a liver express Wnts (11), and showing Wnts from hepatocytes are dispensable for tumorigenesis, we next queried MP for their role in Wnt secretion in this model of hepatic injury-driven HCC. Using MP-specific Wntless knockout mice, unable to secrete Wnts from all myeloid cells, at 5 months of age after DEN/CCl_4 we observed two striking and opposing phenotypes that were litter-specific. In two separate litters (n=4), MP-KO had significantly more tumor burden than CON, termed Group A. In additional two litters (n=5), MP-KO had significantly reduced tumor burden, termed Group B. We therefore hypothesized Group A and Group B have different HCC subtypes, and may lead to phenotypically distinct tumors.

Focusing on MP-CON from Group A and Group B, our RPPA and independent analyses identified differences in protein expression. MP-CON A had significantly more androgen receptor, cleaved caspase 3, P38 MAPK, and cMyc than MP-CON B. Intriguingly, P38 MAPK can activate caspase 3 in hepatoma cell lines *in vitro* (261). However, caspase 3 activation does not always correlate with apoptosis in HCC (262), which is likely the case as our TUNEL staining was comparable in MP-CON A and MP-CON B, suggesting caspase 3 is playing non-apoptosis related roles or tumors are evading apoptosis through adaptive mechanisms. P38 MAPK can also activate androgen receptor, which in turn can activate cMyc in other systems including prostate cancer (263, 264). These relationships may suggest overexpression of P38 MAPK is a central oncogenic event occurring in Group A that does not occur to the same extent

in Group B, although further studies are required to validate this significance. Remarkably, MP-CON B had significantly more glutamine synthetase than MP-CON A, despite no increase in activated or total β-catenin levels. Several factors contribute to GS levels in HCC, including driver oncogenes, immunologic background and source of glutamine (265). Mitochondrial enzyme glutaminase can synthesize glutamine, and studies have identified roles for Myc in regulating expression of both GS and glutaminase. Intriguingly, one study suggests Myc-driven tumors suppress GS and upregulate glutaminase, which may explain increased Myc and lower GS levels found in MP-CON A (265). Our IHC analysis revealed increased PCNA in MP-CON A compared to all groups including MP-KO A and MP-CON B. However, western blot identified increased PCNA in MP-KO A compared to MP-CON A. We predict this discrepancy is because western blotting considers all nuclear and cytoplasmic PCNA, whereas our intensity threshold for IHC quantification was designed to only measure nuclear staining. Further, PCNA contributes to processes beyond proliferation, including DNA repair and apoptosis (266), suggesting the presence of significantly more PCNA in MP-CON A should be investigated further.

We also identified differences in MP phenotype and the resulting inflammation. While total numbers of MP were similar, MP-CON B had more CD68+CD11b- and CD68-CD11b+ single positive cells, compared to MP-CON A which had more double-positive cells. CD68+ MP, the resident Kupffer cells, are capable of optimal phagocytosis and are a known source of reactive oxygen species. CD11b+ MP are considered to be bone marrow-derived at baseline and known to produce cytokines. However, little is known about the CD68+CD11b+ population, which increases in frequency after hepatic injury and macrophage activation, likely resulting from CD11b+ infiltrating cells acquiring CD68-positivity (254). Both CD68 and CD11b can

exhibit M1 polarization based on expression of various markers (267, 268). Likewise, MP could exhibit both M1 and M2 polarization in injury states, such as after thioacetamide-induced cirrhosis (268). We identified MP in MP-CON B to exhibit a more M1-like phenotype compared to MP-CON A as supported by upregulation of inflammatory cytokines IL1α, IL1β, IL16, and CCL2 in MP-CON B. IL1α and IL1β are produced by activated MP, while various cell types including tumor cells produce CCL2 to attract T cells and monocytes capable of differentiating into tumor-associated MP. IL16 is produced by lymphocytes to activate monocytes to secrete proinflammatory cytokines, and is often implicated in cancer (269-274). Taken together, with the increase in CD45-positive leukocytes observed in MP-CON B compared to MP-CON A, it appears the inflammatory milieu between Groups A and B differ, with more M1 MP and leukocytes found in MP-CON B. As tumor-associated MP are typically M2, and M1 polarization suggests better prognosis in HCC patients (274), MP-CON B may have better survival in long-term studies compared to MP-CON A. We recognize, however, that several pro-inflammatory cytokines were unchanged per the array, which is likely attributed to the use of whole-liver lysates and MP polarization existing as a spectrum more so than a dichotomy (275).

We therefore propose that Group A HCC relies on upregulation of oncogenic signaling, including P38 MAPK and cMyc pathways, suggested by increases in protein expression. Removing MP Wls causes increased tumor burden likely because further pathways are upregulated, evident through increased expression in MP-KO A of GS, Cyp2e1, phosphorylated Rb, 53BP1, and Bax. Moreover, we propose Group B HCC is dependent on the pro-inflammatory and pro-tumorigenic microenvironment. M1 MP produce reactive oxygen species, which can lead to DNA damage and oncogenesis (254, 274). MP-KO B has fewer tumors because of fewer activated macrophages and recruited leukocytes, likely less oxidative damage,

and reduction in several cytokines compared to MP-CON B. The question remains, what leads to such dichotomy between the two groups? Although each animal displayed predictable heterogeneity in protein expression and overall phenotype, we predicted one single event may be common to Group A, and one to Group B. Chappell et al. sequenced tumors after DEN/CCl_4 for common oncogenic mutations, and were unable to find any. Instead, they observed several epigenetic events, including genomic DNA demethylation and a decrease in the repressive mark histone 3 lysine 9 trimethylation (227). Therefore, we posited Group A has a different epigenetic signature from Group B, and our mRNA data suggests this is an appropriate future direction to pursue. Group A upregulated transcripts of several chromatin and histone modifying enzymes, including those involved in histone phosphorylation, methylation, acetylation, and DNA methylation. In fact, Ribosomal Protein S6 Kinase A5 and A3, both transcriptionally upregulated in MP-CON A, can activate P38 MAPK during stress (276). Our overall hypothesis is illustrated in Figure 31.

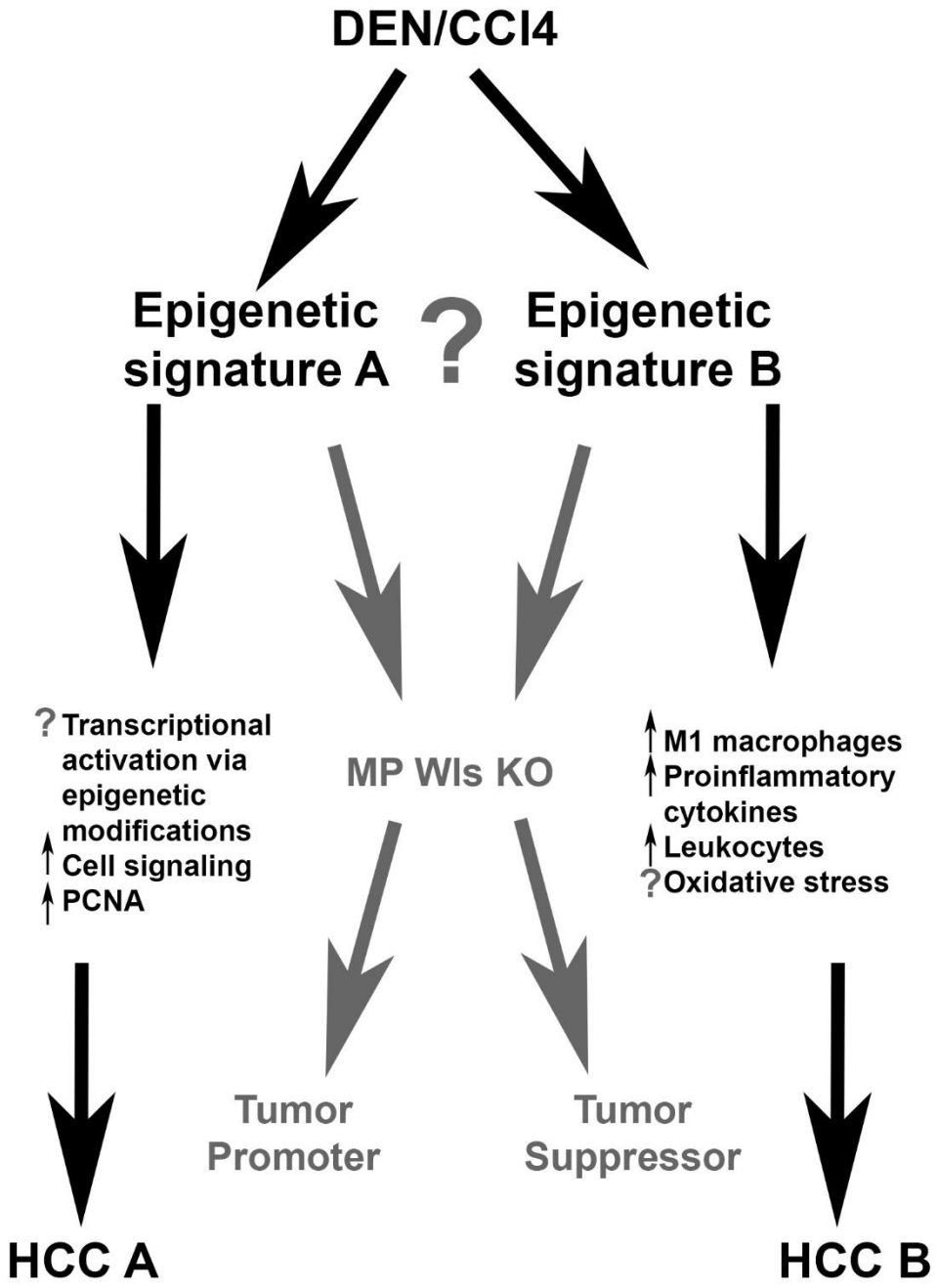

Figure 31: Overall hypothesis and summary of bimodal phenotype of MP-CON and MP-KO after DEN/CCl4.

We predict two different oncogenic events, likely epigenetic modifications, occur after DEN/CCl_4 to lead to Group A and Group B. In MP-CON A, we observed increased protein expression of several notable oncogenes compared to MP-CON B including cMyc, suggesting alterations in signaling, leading to HCC A. When macrophages cannot secrete Wnts, this promotes tumor growth further. In MP-CON B, we observed increased M1 macrophages and

CD45-positive leukocytes, potentially suggesting a tumor-promotive inflammatory milieu, leading to HCC B. When macrophages are unable to secrete Wnts, this acts as tumor suppressive. Identifying the epigenetic events responsible for Group A versus Group B, and identifying the mechanism by which macrophage Wnts contribute to HCC differentially, will be of interest for future studies.

Because the entire MP-KO in a litter conformed to the same phenotype of either less or more tumors than their MP-CON littermates, we speculate the divergent epigenetic status results from differences in breeding pairs. The role of DNA modifications in the Cre-recombinase system is unclear, and the epigenome of pups from a mother with Cre and father with a floxed gene may differ from the reverse breeding scenario. Indeed, many foreign DNA sequences inserted into mice become heavily methylated dependent on the breeder strain(277). While the animals used in this study are primarily C57BL/6, the floxed Wntless animals were originally in a 129 background. It is possible different litters retain a different fraction of 129 to C57BL/6, explaining why our phenotype is litter-specific. Recent studies have even identified different responses to a single CCl_4 dose in C57/BL6 N versus J mice (278). Furthermore, the liver is a notoriously sexual dimorphic organ. Addition of foreign DNA, as in a transgenic animal, may alter epigenetic statuses of surrounding genes to different extents in males and females (279). Therefore, if the mother carried the Cre Recombinase and the father carried the floxed Wntless, the epigenome of resulting pups may differ from breeders of the reverse genotype. Hence, it may be advantageous for investigators using DEN/CCl_4 method of hepatocarcinogenesis on genetically manipulated animals to be mindful of the breeders. In addition to the novel observation that DEN/CCl_4 can produce phenotypically distinct HCC subsets, we provide evidence that macrophage-specific Wnts can be tumor promoting or tumor suppressing, likely depending on the signaling and immunological milieu of the cancer.

5.0 ENDOTHELIAL WNTS REGULATE Β-CATENIN SIGNALING IN MURINE LIVER ZONATION AND REGENERATION

In section 5 we focus on the cellular source, identity, and initiating factors of Wnts required for liver regeneration after partial hepatectomy. This work is an extension of previously published data from our lab (40, 89), described below. Our work focusing on endothelial cells was modified for this dissertation from a manuscript recently accepted in Hepatology Communications, and our work focusing on hepatic stellate cells is still ongoing, but incorporates baseline characterization data from a previous post-doc, Dr. Rong Zhang. Lastly, data assessing endothelial cell separation and mRNA expression of Wnts after partial hepatectomy, described in section 5.4.6, was previously reported in Dr. Jing Yang's thesis (280) and is currently part of our Hepatology Communications manuscript. As Hepatology Communications is an open access journal, as first-author, written permission for re-use in this dissertation was not required.

5.1 ABSTRACT

We have previously shown that hepatocyte-specific β-catenin regulates liver regeneration (LR) after partial hepatectomy (PH), and hepatic zonation at baseline, both under the control of

canonical Wnt signaling. This is true at early timepoints up to 40–72 hours. Using cell-specific Wntless (Wls) knockout mouse models, which lack Wls and prevent Wnt secretion, we have previously determined epithelial cells are not the source of these Wnts. However, macrophage-specific Wls knockouts (MP-KO) have a marginal regeneration defect at 40 hours and displayed normal hepatic zonation. Removing Wls from all endothelial cells was embryonic lethal, therefore in this study we generated a liver-specific endothelial cell knockout model (EC-KO) and a hepatic stellate cell-specific knockout model (HSC-KO). Intriguingly, EC-KO demonstrate a marked reduction in hepatic zonation at baseline, and were protected from acetaminophen-induced liver toxicity. After PH, EC-KO display less proliferation than littermate controls until 72 hours, overall emphasizing the role of endothelial cell-specific Wnts in liver regeneration. We also noted no difference in zonation or regeneration in HSC-KO, and confirmed MP-KO do not secrete Wnts prior to 40 hours after PH, suggesting they are not the primary contributor of Wnts. We also questioned which Wnts are responsible for β-catenin activation, and identified Wnt2 and Wnt9b to be highly upregulated in endothelial cells after PH. Finally, we tested whether shear stress, evident immediately after PH due to increased portal pressure, can initiate Wnt production *in vitro*. We noted an increase in Wnt2 and Wnt9b mRNA in two separate endothelial cell types including primary liver endothelial cells. Our data suggests endothelial cells secrete Wnt2 and Wnt9b, initiated in part by shear stress early after PH, to temporally regulate hepatocyte-specific β-catenin activation and liver regeneration.

5.2 BACKGROUND

5.2.1 Introduction to liver zonation

The liver is composed of thousands of liver lobules, consisting of a central vein (CV) surrounded by six portal triads in a hexagonal shape. The portal triad, made of the hepatic artery (HA), portal vein (PV), and bile duct, bring oxygenated blood (via PV) and deoxygenated blood (via HA) into the liver (281). Blood travels through hepatic sinusoids and exits through the CV (Fig.32A, B).

Hepatocytes have heterogeneous functions and protein expression based on their location along the liver lobule, being defined as periportal (PP) near PV, midzonal (MZ), or pericentral (PC) near CV. Unsurprisingly, this is regulated in part by the oxygen gradient. For example, expression of hypoxia-inducible transcription factors are present in hepatocytes in the PC zone, where oxygen tension is low (282). Further, gluconeogenesis and urea synthesis are two processes requiring oxygen, and occur in the PP area where oxygenated blood is present (283). In addition to the oxygen gradient, morphogen gradients including Wnt, hedgehog, and HGF also result in differential hepatocyte signaling along the lobule (281). It is believed this compartmentalization, termed “zonation”, results from the liver’s requirement to perform often opposing functions simultaneously (284) (Fig.32B).

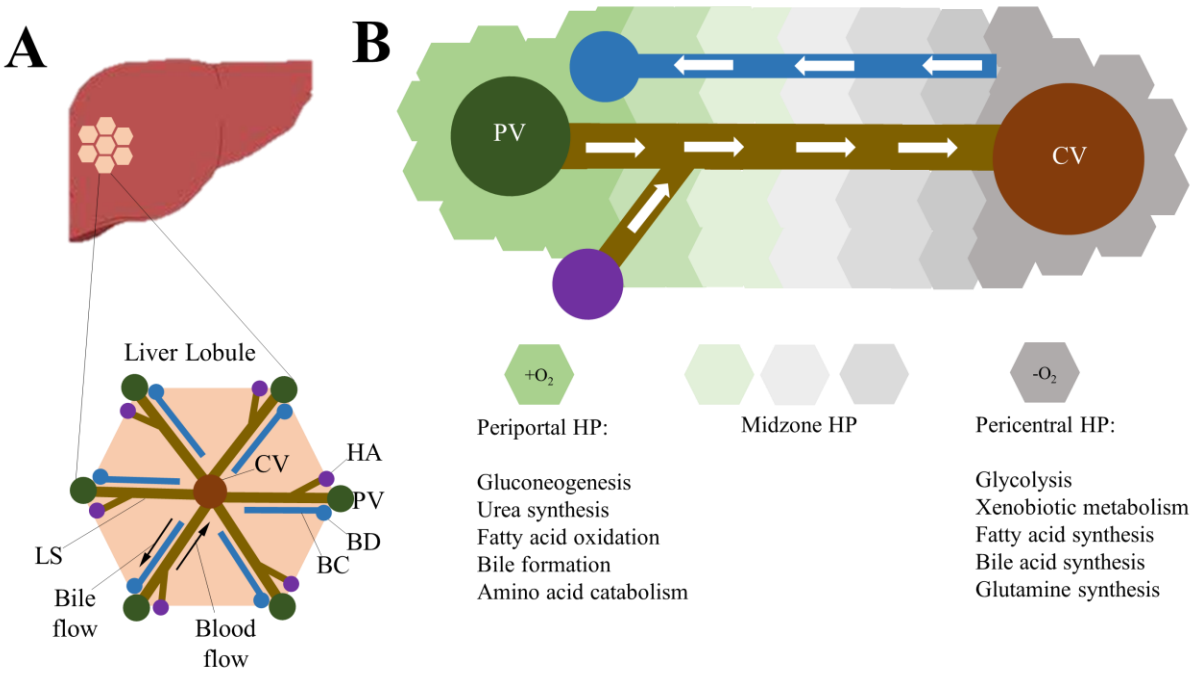

Figure 32: The liver is composed of zonated lobules.

(A) The liver has thousands of lobules, consisting of one central vein surrounded by six portal veins, hepatic arteries, and bile ducts, known as the portal triad. The central vein is connected to the portal vein and hepatic artery through liver sinusoids. Blood flows from the portal vein and hepatic artery to the central vein. Bile flows into the bile duct from the bile canaliculi. (B) Schematic highlighting different zones of the liver. Hepatocytes near the portal vein are exposed to oxygen and perform functions including gluconeogenesis and urea synthesis, whereas hepatocytes near the central vein are not exposed to oxygen and perform functions including glycolysis and xenobiotic metabolism. The midzone consists of intermediate hepatocytes. LS, liver sinusoid; CV, central vein; HA, hepatic artery; PV, portal vein; BD, bile duct; BC, bile canaliculi; HP, hepatocyte.

5.2.1.1 β-Catenin and liver zonation

β-Catenin is considered a master regulator of zonation. Although β-catenin is expressed throughout the liver at hepatocyte membranes, signal transduction predominantly occurs in the PC area and regulates PC-centric gene activity (205, 285). Target genes include PC markers involved in glutamine metabolism (GS, ornithine aminotransferase, glutamate transporter-1), xenobiotic metabolism (Cytochrome P450 Cyp2e1 and Cyp1a2), and others discussed in Table 1. APC negatively regulates β-catenin expression and is localized in the PP region (281).

Using liver-specific β-catenin knockout animals (bKO), we and others have shown loss of β-catenin in hepatocytes leads to loss of zonation (89, 163). Moreover, we have shown liver-specific Lrp5/6 knockout mice (5/6KO), which lack the Wnt co-receptor and prevent Wnt signaling while leaving β-catenin intact, phenocopy bKO (40). Similarly, mice deficient in the Wnt agonist Rspo3, lack hepatic zonation that is rescued by expression of Rspo1 (286). This suggests hepatic zonation is under the control of Wnt-dependent β-catenin activation. In an attempt to characterize the cellular source of Wnts, we generated a HP/BEC-specific Wntless knockout mouse (HP-KO) and a macrophage (MP)-specific Wntless knockout mouse (MP-KO), preventing Wnt secretion from either cell type, and noted no defects in hepatic zonation (40). Recent reports identify endothelial cells as the major Wnt-producing cells required for hepatic zonation and identified Wnt2 and Wnt9b to be highly expressed in these cells (20, 287).

5.2.2 Introduction to liver regeneration

There are over 500 million people worldwide suffering from liver disease (288). Mortality rates vary, with 7.3 in 100,000 patients in the US and 57.3 in 100,000 patients in Middle Eastern countries (289), making this a global concern. For many liver diseases, transplants or surgical resections are the only effective treatment (290, 291). A shortage of donor organs, poor regenerative capability, and high probability of recurrence makes these unlikely options for most patients, demonstrating the need for promising alternatives. The liver is unique in its capacity to regenerate after substantial loss, as evident through partial hepatectomy (PH) studies. In rodents, specific lobes are removed during PH which account for two-thirds of the liver, and the intact lobes grow to the full liver mass prior to surgery. Similar results are seen after surgical resection in larger mammals including humans (292), although the mouse is an appropriate model to study

regeneration kinetics as it is well characterized that peak proliferation occurs around 40 hours post-PH (293). Uncovering the mechanisms that initiate and propagate liver regeneration is an important step in developing alternatives to liver transplants, as the detailed mechanisms that coordinate hepatocyte repopulation are not well understood. In fact, impaired regeneration is the major cause of liver failure and liver-related death (294).

Several primary and auxiliary mitogens have been identified to play significant roles during LR post-PH. Growth factors including hepatocyte growth factor (HGF), interleukin 6 (IL6), and others are produced by nonparenchymal cells to induce HP proliferation early after PH. Noncoding RNAs, platelets, hypoxia, microbiome, immune cells, and other factors contribute to complete LR (295). Strikingly, the removal of one component may delay LR, however the liver employs compensatory mechanisms to complete regeneration, highlighting the redundancy available in maintaining hepatic homeostasis. In fact, the only known report of a complete lack of regeneration and subsequent animal death post-PH involves the concomitant inhibition of the HGF receptor Met and epidermal growth factor receptor (EGFR), while inhibiting Met or EGFR alone was not sufficient to prevent LR (296).

5.2.2.1 Wnt/β-catenin in liver regeneration

The importance of Wnt/β-catenin signaling in liver regeneration (LR) is undisputed (295). In 2001, Monga et. al demonstrated β-catenin is increased 5 minutes after partial hepatectomy (PH) in rats, resulting from a decrease in β-catenin degradation (297). A follow up study treated rats with β-catenin targeted antisense morpholinos, resulting in impaired proliferation after PH at 24 hours and 7 days, and liver weight/body weight ratios (LW/BW) were lower than controls at both timepoints (298). Additionally, bKO exhibit significantly decreased LW/BW as early as 15 days after birth, and the same trend is observed throughout the lifespan. After PH, proliferation in

bKO was compromised and Cyclin D1 levels were decreased at 40 hours, although LR rebounded after three days (89). Moreover, liver-specific transgenic mice (bTG) were generated with mutated β-catenin (serine 45 mutated to aspartic acid) under an Albumin promoter, which prevents β-catenin degradation. These mice had higher liver LW/BW than controls at 15 days and one month, but differences were absent at two months. After PH, bTG exhibited increases in mitotic cell count, PCNA-positivity, and Cyclin D1 expression at 40 hours, although control mice were eventually comparable (299), suggesting increased β-catenin activation creates a regeneration advantage at early timepoints. Furthermore, bTG mice led to the identification of Epidermal Growth Factor Receptor (EGFR) as a novel β-catenin target gene. EGFR is required for optimal liver regeneration after partial hepatectomy, as EGFR inhibition leads to increased mortality and delayed hepatocyte proliferation (31, 300).

More recently, we confirmed the importance of Wnt-dependent β-catenin signaling. 5/6KO, lacking the Wnt receptors LRP5/6, phenocopied bKO; LW/BW were decreased at baseline, and LR was impaired at 40 and 72 hours after PH (40). Taken together, these data suggest Wnt/β-catenin plays a pivotal role in LR during the first 40-72 hours.

Our lab has also published that these Wnts do not originate from hepatocytes (HP) or biliary epithelial cells (BEC). Subjecting HP-KO to PH had no effect on LR, suggesting liver epithelial cells are not the source of Wnts. Next we performed PH on MP-KO and noted a marginal decrease in regeneration at 40 hours, to a lesser magnitude than bKO or 5/6KO (40), suggesting MP are a source of Wnts during LR, but likely not the primary source.

Any additional Wnt sources, identities, and initiation mechanisms during LR are not fully understood. One report used *in vitro* Wnt2 knockout and rescue experiments to determine Wnt2 is secreted by liver sinusoidal endothelial cells (LSECs) and acts in an autocrine manner to

stimulate LSEC proliferation and angiogenesis (301). Another group added LSECs transfected with Wnt2 and HGF into a mouse that had LSECs deficient for Wnt2 and HGF, and liver mass was restored after PH compared to mice that did not receive the transfected LSECs, suggesting LSECs secrete Wnt2 and HGF which together contribute to hepatocyte proliferation in a paracrine manner (19), although the role of Wnt2 alone was not assessed. The lack of consensus of the function of Wnt2, and the little known about other Wnts, suggests more needs to be done to fully understand the role of Wnt in LR (Fig.33).

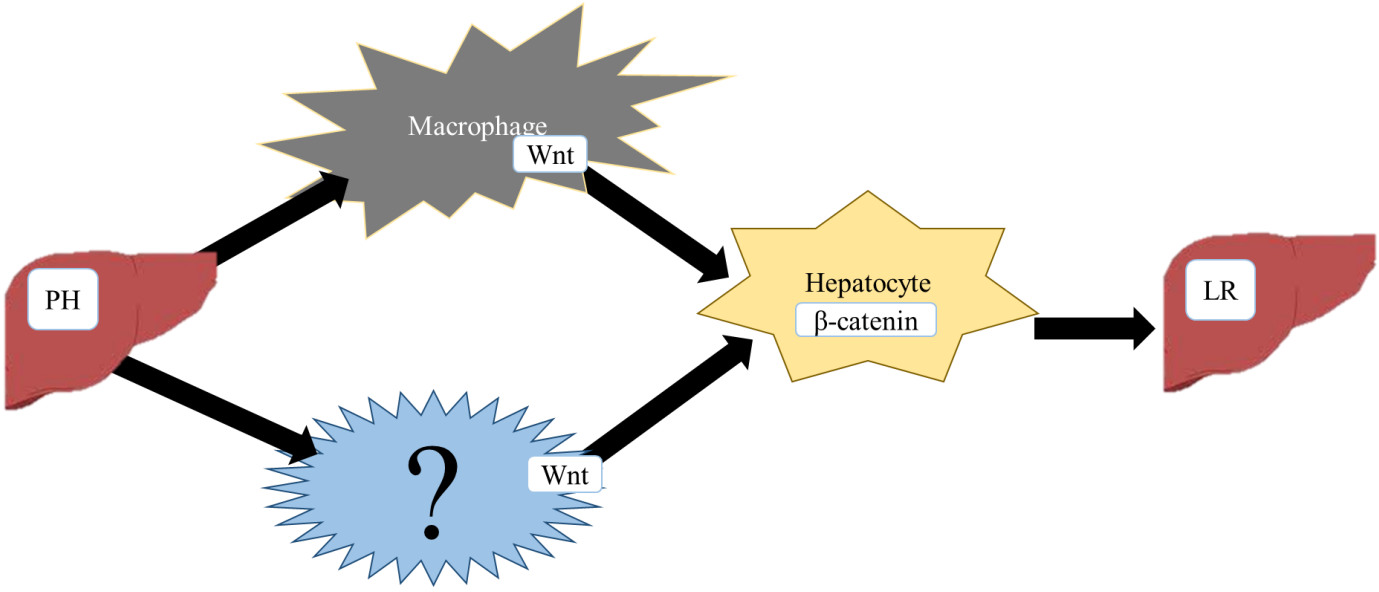

Figure 33: Schema of current understanding of Wnt/β-catenin kinetics after PH.

5.2.2.2 Shear stress and liver regeneration

Shear stress (SS) is the force acting on endothelial cells (ECs) as a result of blood flow across the endothelium, and variations in SS cause ECs to exhibit a range of responses (302, 303). Two types of SS are laminar and orbital. Laminar SS is characterized by unidirectional flow, whereas orbital SS is characterized by random speed and directional variations (304). The effect of SS on ECs has been studied for over 30 years. Early studies used novel shear loading devices to

produce fluid SS on cultured ECs (305-307), and noted increased migration, proliferation (307), and increased production of several mitogenic and vasculogenic mRNAs (305, 308), demonstrating that ECs may be activated in response to SS.

It is also known that hepatic portal venous pressure increases immediately after PH (309), causing portal hypertension due to blood flow becoming constricted to one third of the original liver. This predictably causes SS in the liver sinusoids, and several models suggest SS induces LR after PH. For example, when rats underwent a portal vein branch ligation (PVL) where the left portal venous branch that supplies two thirds of the liver is ligated, portal hypertension is increased similarly to what is seen after PH. PH and PVL samples both had increased hepatocyte proliferation compared to sham, and were comparable to each other (308, 310). These data suggest SS may initiate or otherwise contribute to the early stages of LR.

A recent study queried liver progenitor cells (LPCs), as it is posited LPCs differentiate into HP when HP proliferation is blocked, such as in the PH/2-N-acetylaminoflourene (2-AAF) model. Hypothesizing LPCs may be influenced by SS after PH/2-AAF, Nishii et al. established *in vitro* 3-dimensional LPC cultures and subjected them to SS comparable to physiological levels observed after PH. Intriguingly, after SS, LPCs increased transcript levels of Wnt1 and several immediate early genes upregulated during LR including cFos (311). While this is not applicable to the PH model as LPCs do not contribute to HP proliferation, this is the only known study suggesting a link between Wnt expression and SS. We sought to identify a further link, and hypothesized SS may induce Wnt secretion from nonparenchymal cells after PH.

5.3 METHODS

5.3.1 Mice and breeding

All animal husbandry and experimental procedures, including animal housing and diet were performed under the guidelines and approval of the National Institutes of Health and the Institutional Animal Care and Use Committee at the University of Pittsburgh. Mice were fed regular chow in standard caging and kept under 12 hour light-dark cycle with no enrichment. Lyve1-cre mice were purchased from Jackson Laboratories (312) and bred with Wntless $(Wls)^{flox/flox}$ mice (40, 240). Lyve1-$cre^{+/-}$;$Wls^{flox/flox}$ are referred hereon as EC-KO. Mice with Lyve1-$cre^{-/-}$;$Wls^{flox/flox}$ or Lyve1-$cre^{+/-}$;$Wls^{-/-}$ genotypes were used as littermate controls (EC-CON). Lyve1-cre mice were also bred to ROSA26-$Stop^{flox/flox}$-EYFP mice to label cells effectively targeted by Lyve1-cre (313). To generate hepatic stellate cell-specific Wntless knockout mice (referred to as HSC-KO), $Wls^{flox/flox}$ mice were bred with Lecithin retinol acyltransferase (Lrat)-Cre mice provided by Dr. Robert Schwabe (314). Mice with Lrat-$cre^{-/-}$;$Wls^{flox/flox}$ or Lrat-$cre^{+/-}$;$Wls^{-/-}$ genotypes were used as littermate controls (HSC-CON). MP-CON and MP-KO were generated as described elsewhere (40) and in section 4.3.1.

5.3.2 Partial hepatectomy, liver perfusion, endothelial cell separation

Two-month old male and female EC-KO and EC-CON were subjected to PH as described elsewhere (315). At 0 (n=2 male, n=3 female), 24h (n=2 male, n=2 female), 40h (n=3 male, n=2 female), or 72h (n=3 male, n=2 female), mice were euthanized via isoflurane inhalation and cervical dislocation. HSC-CON and HSC-KO (n=6-7 for 0h, n=2 for 24h, 40h,

and 72h) and MP-CON and MP-KO (n=2 for 6h, n=4-5 for 24h and 40h) were subjected to PH similarly. Livers were harvested and lobes were flash frozen or paraffin embedded for further analysis.

For liver perfusion prior to cell separation, two-month old C57BL/6 male mice were anesthetized with Nembutal and an incision was made to open the peritoneum. A 24-gauge catheter was inserted into the inferior vena cava and another in the portal vein. The inferior vena cava below the heart was clamped. Through the portal vein catheter, the liver was washed with 100 ml calcium (-) magnesium (-) HBSS with 50mM HEPES (Gibco) and 25mM EGTA at 2-3ml/min. Next the liver was digested with 0.3 mg/g collagenase type IV (Sigma) and 50mM HEPES in HBSS with calcium. Upon digestion, liver was removed and dispersed in 30ml HBSS. Dispersed cells were filtered by mesh (100μm) and centrifuged at 50g for 5min twice to isolate hepatocytes. Then supernatant is spun down at 1500 rpm for 10min to get non-parenchymal cells (NPCs).

For cell separation studies, 2-month old male C57BL/6 mice (Jackson Laboratories) (n=2) were used for two-step liver perfusion, 12h after PH and parenchymal and non-parenchymal cell fractions were separated. Magnetic bead separation was used to isolate EC and macrophages. Cell from 2 livers were pooled together for analysis. NPC fraction was incubated with anti-mouse biotin-F4/80 antibody (Biolegend) at 1:10 for 30 min on ice. Cells were washed and incubated with streptavidin-microbeads (Miltenyi Biotech) at 1:10 for 20 min on ice. Samples were passed through LS columns (Miltenyi Biotech) to obtain F4/80-positive cells. F4/80-negative fraction was processed further and incubated with anti-mouse biotin-CD31 antibody (Biolegend) at 1:20 for 30 min on ice. They were washed once and incubated with streptavidin-microbeads at 1:20 for 20 min on ice. Then LD-columns (Miltenyi Biotech) were

used to obtain CD31-positive cells (ECs). CD31-positive fractions were then processed for RNA analysis.

5.3.3 Acetaminophen toxicity studies

Ten-week old EC-CON (n=3) and EC-KO (n=5), all males were fasted overnight and injected intraperitoneally with 450mg/kg acetaminophen in 0.9% saline. Animals were sacrificed 24h post-injection as described above. Blood was drawn through the inferior vena cava and serum submitted to the University of Pittsburgh Medical Center Clinical Chemistry laboratory, which is part of Pittsburgh Liver Research Center, for alanine aminotransferases (ALT) and aspartate aminotransferase (AST) testing.

5.3.4 Immunofluorescence

Liver sections were fixed in 2% PFA for 2 hours, then 30% sucrose in PBS overnight. For immunofluorescence (IF), sections were frozen in OCT compound and cut in 5μm sections. Samples were permeabilized with 0.1% Triton and blocked in 2% serum in PBST. Primary antibodies (information in Table 10) were incubated overnight. Secondary antibodies conjugated to Alexa Fluor 555 or 488 (Life Technologies) were incubated at 1:400 in PBST for 3 hours prior to Dapi. Confocal images were taken on a Nikon A1 Spectral Confocal Microscope located at the Center for Biological Imaging at the University of Pittsburgh. Epifluorescent images were taken on a Nikon Eclipse Ti microscope using NIS Elements software.

5.3.5 Protein isolation, western blot, immunoprecipitation

Whole-cell protein lysate preparation was performed using RIPA buffer (40) and 30μg of protein was used for gel electrophoresis for Western blots (WB). Immunoprecipitation (IP) was performed using 750μg of pre-cleared protein and A/G agarose beads as described elsewhere (316). For a complete list of antibodies used see Table 10. Secondary antibodies conjugated to horse radish peroxidase were used at 1 to 10,000.

Table 10: List of antibodies used in section 5.0

Name	Company	Catalog Number	Use
GFP	Abcam	Ab13970	IF: 1 to 200
Lyve1	Abcam	Ab14917	IF: 1 to 100
EpCam	DSHB	G8.8	IF: 1 to 10 (15μg/ml)
GS	Sigma	G2781	IF: 1 to 500
GS	Santa Cruz	SC-9067	IHC: 1 to 50 WB: 1 to 1000
Cyp2e1	Sigma Aldrich	HPA009128	IHC: 1 to 500 WB: 1 to 500
Cyp1a2	Santa Cruz	SC-53241	IHC: 1 to 50* WB: 1 to 200
Active β-Catenin	Cell Signaling	4270s	WB: 1 to 750
β-Catenin	BD Biosciences	610154	WB: 1 to 1000
Actin	Millipore	MAB1501	WB: 1 to 1000
Gapdh	Proteintech	60004-1-Ig	WB: 1 to 10,000
Cyclin D1	Neomarkers	RB-9041-P	IHC: 1 to 200 WB: 1 to 200
PCNA	Santa Cruz	SC-56	IHC: 1 to 50* WB: 1 to 200
TCF4	Cell Signaling	2569s	IP: 1 to 50
TCF4	Sigma Aldrich	T5817	WB: 1 to 750
CD31	Abcam	Ab28364	IF: 1 to 50

*Use Mouse On Mouse kit (Vector Laboratories)

5.3.6 RNA isolation and qRT-PCR analysis

RNA was obtained using RNeasy Mini Kit (Qiagen) and 1-2μg was reverse transcribed using Superscript III (Invitrogen). Real-time qPCR was performed using SYBR Green on an ABI Prism 7300 sequence Detection System (Applied Biosystems) and values were normalized to GAPDH. For a list of primer sequences, see Table 11.

Table 11: List and sequence of all primers used for qRT-PCR in section 5.0.

Primer (Mouse)	Forward Sequence	Reverse Sequence
Wnt2	TCTGTCTATCTTGGGCATTCTG	TTCCTTCGCTATGTGATGTTTC
Wnt9b	GGGTGTGTGTGGTGACAATCT	GGTCCTTGCTTCCTCTCTTG
Gapdh	AACTTTGGCATTGTGGAAGG	ACACATTGGGGGTAGGAACA
Wnt2b	ACCTTCCTCTACCCTCAATCCT	TCACTCAGCCTCCTAAATCCAT
Wnt3	GTCTGCTAATGCTGGCTTGAC	TAGGAAGGGATGGGAGGTGT
Wnt4	AGAACTGGAGAAGTGTGGCTGT	AAAGGACTGTGAGAAGGCTACG
Wnt5a	GTCCTTTGAGATGGGTGGTATC	ACCTCTGGGTTAGGGAGTGTCT
Wnt5b	TGTCAGTTGTATCAGGAGCACA	GTGAAGGCAGTCTCTCGGCTA
Wnt9a	ATGGTGTGTCTGGCTCCTG	CAGTGGCTTCATTGGTAGTGCT
Wnt10a	TCCTGTTCTTCCTACTGCTGCT	ACGCACACACACCTCCATC
Wnt10b	CCACTACAGCCCAGAACCTC	GGAGAGACCCTTTCAACAACTG
Wnt11	CCCTGGAAACGAAGTGTAAATG	AGGTAGCGGGTCTTGAGGTC
Wnt16	GCTGTAACCTCCTCTGCTGTG	GTGGACATCGGTCATACTTTCA
Cyclin D1	TTTCTTTCCAGAGTCATCAAGTGT	TGACTCCAGAAGGGCTTCAA

5.3.7 Histology and immunohistochemistry

Hematoxylin and Eosin staining was performed on 4μm paraffin sections for discerning histology. Mitotic figures were identified in hepatocytes. For quantification, hepatocytes with mitotic figures were counted in 3-5 random 200x fields from 3 livers from each group at 24h, 40h and 72h. For IHC, paraffin sections were processed as described elsewhere (40, 89). A list of antibody dilutions is available in Table 10. Heat-mediated antigen retrieval was performed for IHC. Secondary antibodies conjugated to biotin were used at 1 to 400 and staining was detected

with DAB detection systems after incubation with avidin-biotin-complex (Vector). For quantification, PCNA-positive hepatocytes were counted in 3-5 random 200x fields from 3 livers from each group at 40h and 72h. For quantification of Cyclin D1-positive hepatocytes immediately bordering the central vein, we counted in both groups of mice at 24h, 40h and 72h after PH the number of Cyclin D1-positive hepatocytes lining the central vein over total hepatocytes lining that central vein and presented as a percentage. At least 5 central veins were randomly chosen for counting hepatocytes at 200x and at least 3 mice from each group and time were analyzed.

5.3.8 Cell culture and shear stress analysis

Primary murine liver sinusoidal endothelial cells (LSECs) and their culture medium Endothelial Cell Medium were purchased from Cell Biologics. Transformed Sinusoidal Endothelial Cells were a gift from Dr. Vijay Shah at the Mayo Clinic and Foundation (317) and cultured in Endothelial Cell Medium from Cell Biologics. Primary hepatocytes were isolated as described above and cultured in complete MHGM media described elsewhere (318). Raw Blue cells were obtained from InvivoGen and cultured in DMEM with 10% FBS. LSECs, and primary hepatocytes were cultured on 2% gelatin coated dishes. All cells were grown at 37°C in a humidified 5% CO_2 incubator.

Cells were cultured in 6-well plates and rotated on a cell culture incubator-appropriate orbital shaker (VWR) at 210 rotations per minute for 6 hours. RNA was then extracted using RNeasy mini kit (Qiagen). TSEC and LSEC were each cultured in triplicates and shear stress for 6h. While we performed the studies in triplicates, these were performed once each as these cells

lose differentiation rapidly upon passaging and in prolonged culture (317, 319). Raw Blue cells and primary hepatocytes were cultured in triplicates and experiments were performed twice.

5.3.9 Statistics

Data are presented as mean, standard deviation, and/or individual data points. Graphs were generated using Graphpad or Microsoft Excel. P values were calculated using Two-tailed Student's T-test or one-way ANOVA for multiple comparisons with either Tukey's post-test correction or Fisher's LSD test, and resulting P values less than 0.05 (*), less than 0.01 (**), less than 0.001 (***) or less than 0.0001 (****) were considered statistically significant.

5.4 RESULTS

5.4.1 Successful recombination of floxed alleles in hepatic sinusodial and central venous EC by Lyve1-Cre

Since Lyve1 is a known lymphatic endothelial cell marker (320), we first wanted to confirm which EC in the liver undergo recombination. Lyve1-cre mice were crossed with ROSA26-Stop$^{flox/flox}$-EYFP reporter mice. Confocal imaging showed YFP localization in sinusoidal EC as well as in EC lining central veins as highlighted by GS-expressing pericentral hepatocytes (Fig.34A). Since Lyve1 expression in adult liver has been reported in sinusoidal EC but not in EC lining central veins, we stained normal adult liver for Lyve1 (321, 322). Indeed,

Lyve1 localized to hepatic sinusoidal EC and not venous EC (Fig.34B). We also co-stained for Lyve1 and biliary marker EpCAM to distinguish portal from pericentral region (Fig.34C). Additional confirmation of Lyve1-cre driven recombination in hepatic sinusoidal and central venous EC was seen by co-localization of pan EC maker CD31 and YFP in ROSA26-Stop$^{flox/flox}$-EYFP; Lyve1+/- but not in ROSA26-Stop$^{flox/flox}$-EYFP; Lyve1-/- controls (Fig.35). Thus, while Lyve1 was only expressed in hepatic sinusoidal EC in adult liver, it did recombine reporter gene in venous EC.

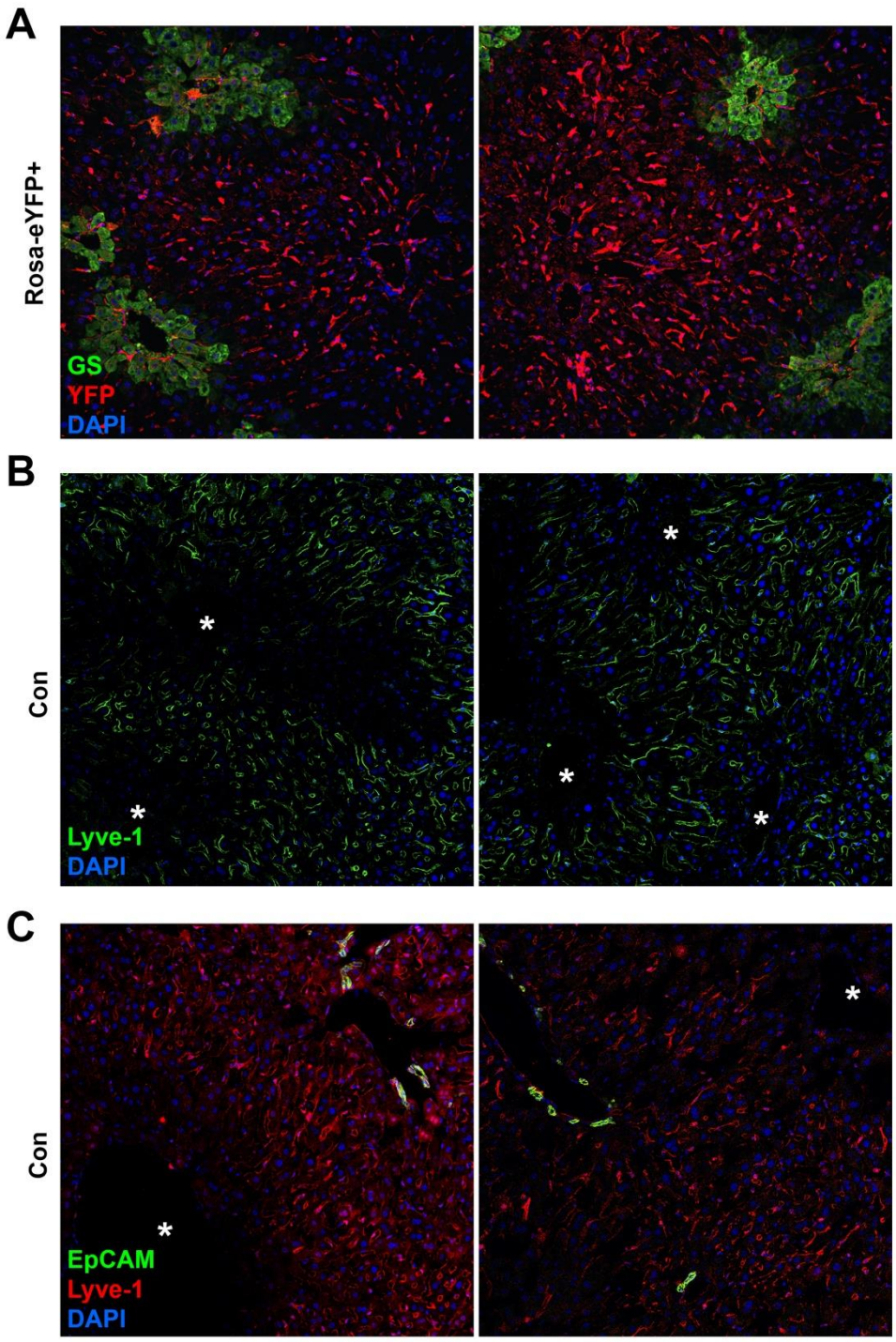

Figure 34: Lyve1-cre efficiently recombines floxed stop codon allowing expression of YFP in hepatic endothelia.

(A) Two representative confocal images show immunofluorescence (IF) staining for YFP (red), GS (green) and DAPI (blue) revealing YFP positivity in EC lining the central vein flanked by GS-positive hepatocytes in addition to sinusoidal EC in livers from ROSA26-Stop$^{flox/flox}$-EYFP; Lyve1-cre +/- mice. (B) Two representative confocal images for IF for Lyve1 and DAPI (blue) in control adult liver shows localization in predominantly hepatic sinusoidal EC but no staining in

EC lining central veins (*). (C) Two representative confocal images for IF for Lyve1 (red), EpCAM (green) and DAPI (blue) reveals predominant Lyve1 expression in sinusoidal EC in zones 1 and 2, and lack of Lyve 1 in EC lining central veins (*). EpCAM was used to outline bile ducts to help recognize periportal region.

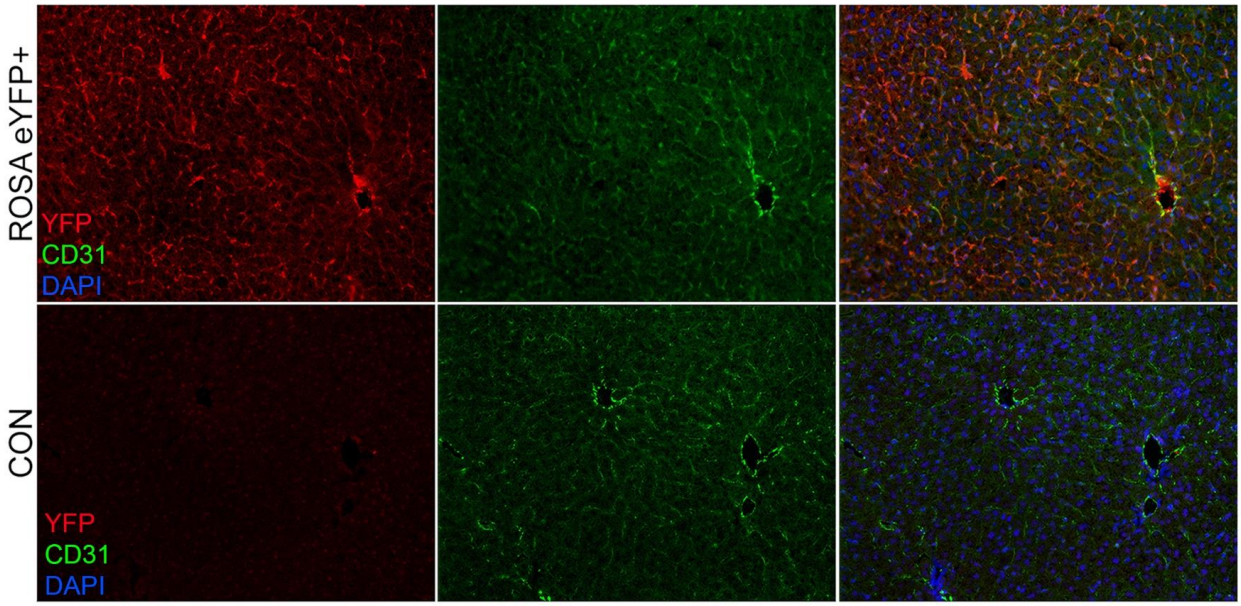

Figure 35: Confirmation of Lyve1-cre activity in sinusoidal and central venous EC in reporter mice via expression of YFP.

Immunofluorescent imaging of staining for YFP (red), CD31 (green), DAPI (blue) shows co-localization of YFP and CD31 in liver sections from ROSAeYFP+/+;Lyve1-Cre+/- but not in ROSAeYFP+/+;Lyve1-Cre-/- littermate controls (CON), shown at 100X magnification.

5.4.2 EC cell derived Wnt proteins are required for expression of pericentral β-catenin targets and metabolic zonation

To assess the role of EC Wnts in the liver, we conditionally deleted *Wls* using Lyve1-Cre through generation of EC-KO as described in the methods. Very similar to bKO and 5/6KO, we observed a significantly lower liver weight to body weight ratio (LW/BW) in EC-KO (40, 89, 240) (Fig.36A). No additional phenotype at baseline was evident grossly.

A recent study showed the central vein EC cells are the source of Wnt2 and Wnt9b essential for pericentral β-catenin activation (20). We next examined β-catenin-dependent hepatic zonation targets in the EC-KO. While total β-catenin levels were comparable in EC-CON and EC-KO, levels of hypophosphorylated-active-β-catenin were notably reduced in the EC-KO at baseline by Western blot (WB) (Fig.36B). Likewise, a profound loss of β-catenin targets including GS, Cyp2e1, and Cyp1a2 was also observed by WB and immunohistochemistry (IHC) (Fig.36B,C). To validate functionally the loss of metabolic zonation, we next administered high dose of acetaminophen (APAP) to EC-CON and EC-KO mice. Our lab and others have shown both bLKO and 5/6KO are protected from APAP-induced hepatic injury because they lack Cyp2e1 and Cyp1a2 and hence unable to convert APAP into N-acetyl-p-benzo-quinone imine (NAPQI), the metabolite critical for glutathione depletion and hepatocyte injury (40, 89, 90, 163, 323). At 24h after APAP injection, EC-CON had expectedly high serum ALT and AST levels, while EC-KO showed normal transaminases demonstrating protection (Fig.36D). Thus, Wnts from central vein EC are essential for baseline β-catenin activation and metabolic zonation.

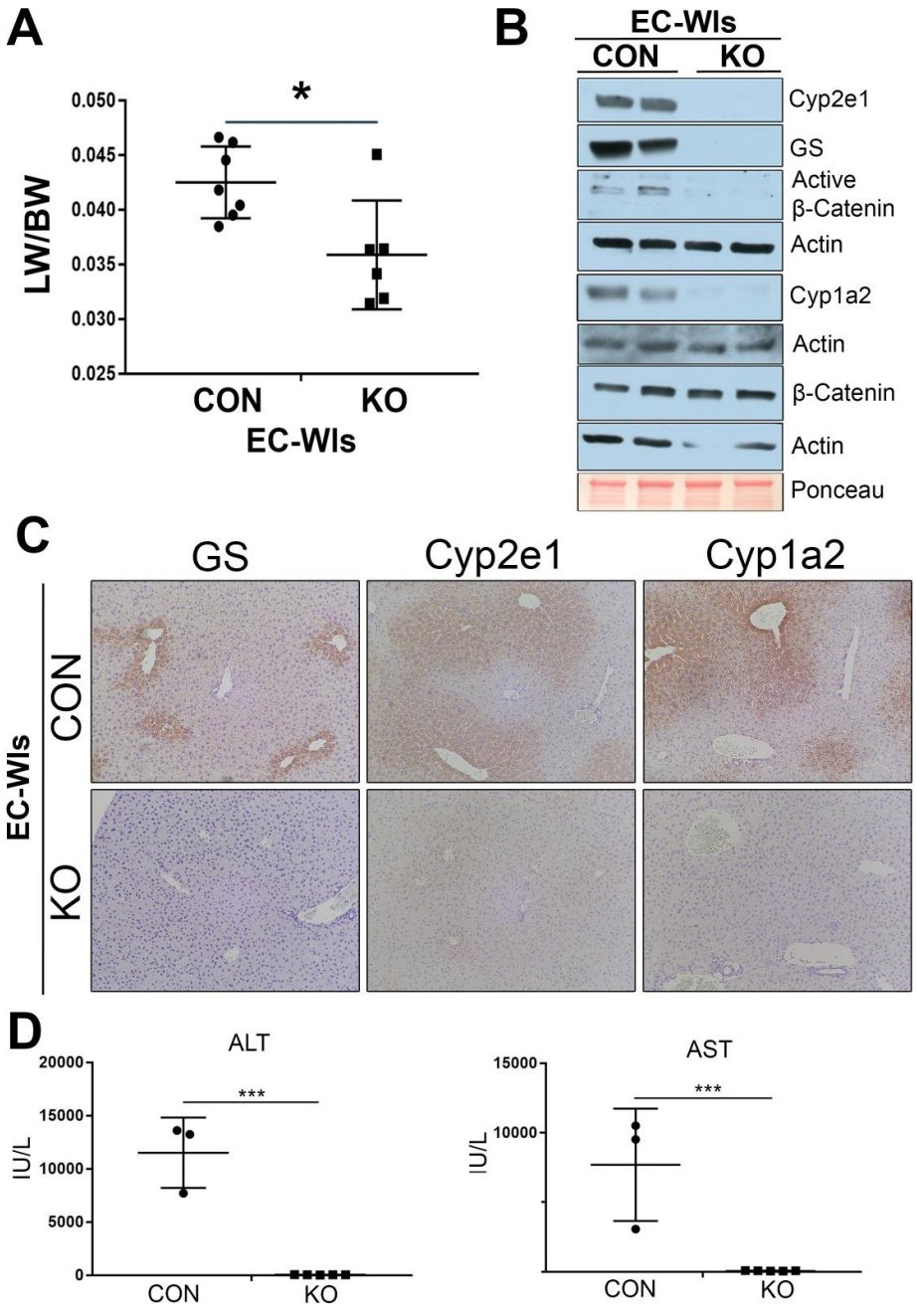

Figure 36: Characterization of EC-KO reveals low liver weights and defective metabolic zonation.
(A) EC-KO (n=6) have significantly lower LW/BW ratio at baseline as compared to littermate controls (n=7). (B) Representative WB shows noteworthy decreases in Cyp2e1, GS, Cyp1a2, and

active-β-catenin in ecWlsKO at baseline while total β-catenin is unaltered. (C) Representative IHC shows presence of GS, Cyp2e1, and Cyp1a2 in EC-CON in zone-3 hepatocytes, which is absence in EC-KO. (50X). (D) Significantly lower serum ALT and AST shows complete protection in EC-KO at 24h in response to a single intra-peritoneal injection of 450mg/kg of acetaminophen, as compared to EC-CON. (*$p<0.05$; ***$p<0.001$).

5.4.3 β-Catenin-dependent delayed LR in EC-KO after PH

EC-CON and EC-KO were next subjected to PH and regenerating livers harvested at various time-points as outlined in methods. PCNA labeling was assessed by IHC at 24h, 40h and 72h. As expected, no PCNA-positive hepatocytes were evident in both groups at 24h (Fig.37A). However, at 40h and 72h in EC-CON, several hepatocytes throughout the hepatic lobule were strongly PCNA-positive (Fig.37A,B). Intriguingly, we saw a consistent and complete lack of PCNA-positive hepatocytes in EC-KO at 40h (Fig.37A,B). At 72h, a noteworthy increase in the numbers of PCNA-positive hepatocytes was evident in EC-KO (Fig.37A).

Decrease in PCNA-positive hepatocytes in EC-KO compared to EC-CON was significant at 40h but not at 72h (Fig.38A). Hepatocyte mitotic figures as index of cell division were counted and showed significantly lower mitotic figures in EC-KO at 40h (Fig.38B). Highest hepatocyte mitosis occurred at 40h in EC-CON whereas this peak was shifted to 72h in EC-KO (Fig.38B). These observations were consistent in both sexes. WB for PCNA also confirmed its absence at 24h in both EC-CON and EC-KO (Fig.38C) while its maximal levels were seen at 40h in EC-CON with decline at 72h in both males and females (Fig.38C). PCNA was absent at 40h in EC-KO and was highest at 72h in both males and females (Fig.38C). Thus, a notable delay in LR is evident in EC-KO in response to PH, which was similar to observations in bKO and 5/6KO.

To address if delay in LR in EC-KO is due to decreased β-catenin activation, we first examined β-catenin-TCF4 interaction by immunoprecipitation (IP). A dramatic decrease in TCF4-β-catenin association was observed in EC-KO at 24h after PH as compared to EC-CON in both sexes (Fig.38D). We concurrently assessed levels and localization of cyclin-D1, a β-catenin-TCF4 target in LR. WB showed decreased cyclin-D1 in EC-KO at 24-40h in both sexes, although differences were less drastic in females likely due to higher basal cyclin-D1 (Fig.38C). At 72h, however, cyclin-D1 resurged in EC-KO and was almost comparable to EC-CON. GS, a known β-catenin target, continued to be absent all times in EC-KO indicating sustained loss of β-catenin activity (Fig.38C).

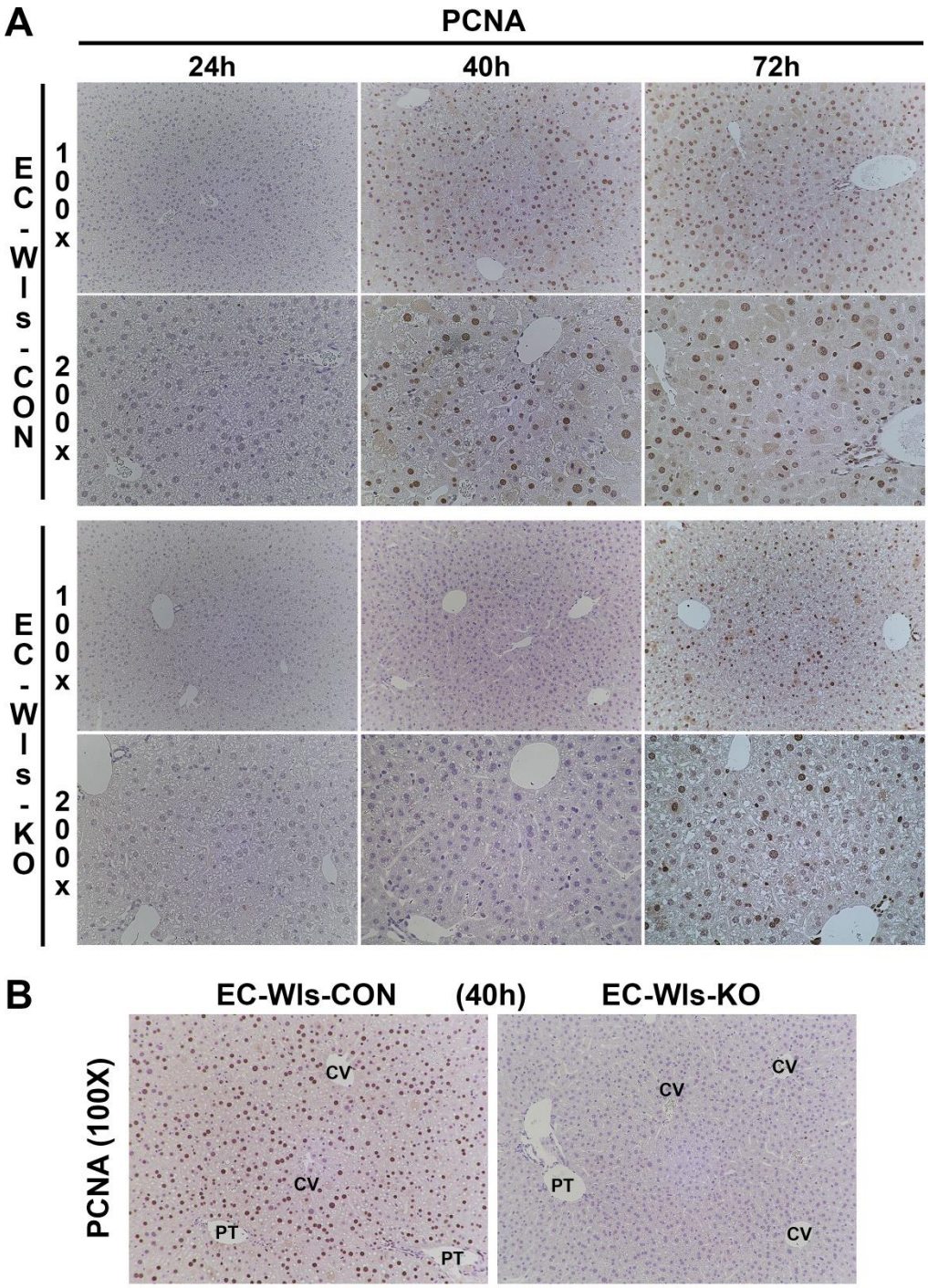

Figure 37: IHC for PCNA in regenerating livers from EC-CON and EC-KO.

(A) Representative IHC (100x and 200x) shows increased PCNA staining hepatocytes pan-zonally at 40-72h in EC-CON, whereas EC-KO show positive staining only at 72h. (B) Larger panels (100x) highlighting differences in PCNA at 40h.

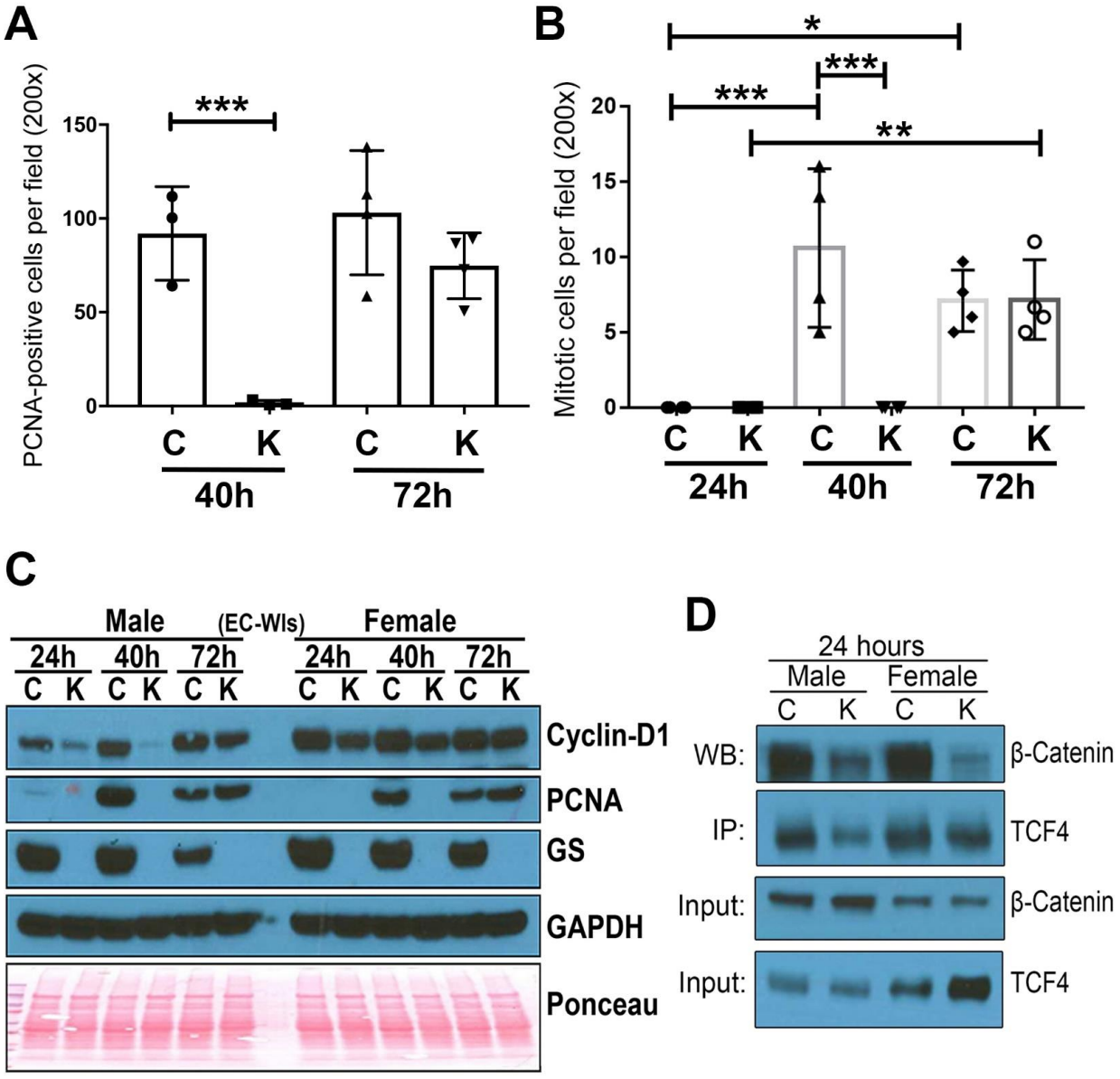

Figure 38: LR is notably delayed in the EC-KO mice as compared to controls.

(A) Quantification of PCNA IHC shows significant decreases in number of hepatocytes staining positive at 40h after PH in EC-KO as compared to controls. No differences were evident at 72h. Each symbol represents average of 5 random images at 200x magnification from one mouse. Three or more mice from each group were used for each time-point. P value was calculated by one-way ANOVA for multiple comparisons with Tukey's post-test correction. (***$p<0.001$) (B) Number of hepatocytes showing mitotic figures were counted at 24h, 40h and 72h after PH in EC-KO and EC-CON. EC-KO showed a significant decrease at 24h and 40h while these number were comparable at 72h. Each symbol represents average of 5 random images at 200x magnification from one mouse. Three or more mice from each group were used for each time-point. P value was calculated by ordinary one way ANOVA and multiple comparisons by uncorrected Fishers's LSD. (*$p<0.05$; **$p<0.01$; ***$p<0.001$) (C) Representative WB showing

levels of cyclin-D1, PCNA, and GS in EC-CON versus EC-KO from 24-72h during LR. (D) Immunoprecipitation using anti-TCF4 and probing for β-catenin shows reduced TCF4-β-catenin association in EC-KO at 24h.

5.4.4 LR begins pericentrally in EC-KO, unlike midzonal distribution in EC-CON

IHC was performed next and showed Cyclin D1 staining in the EC-KO at 24h after PH in both periportal and midzonal hepatocytes while pericentral hepatocytes were negative (Fig.39A). At 40h, Cyclin D1 localization expanded to additional hepatocytes in all zones sparing only some pericentral hepatocytes (Fig.39A). Cyclin D1-labeled hepatocytes were further increased at 72h including to a few pericentral hepatocytes (Fig.39A). EC-KO showed a prominent decrease in Cyclin D1 at 24h, but intriguingly, hepatocytes in the pericentral region showed positivity. At 40h more layers of hepatocytes surrounding central vein became Cyclin D1-positive, in stark contrast to EC-CON (Fig.39A). Cyclin D1 labeling expanded further into the midzonal hepatocytes in EC-KO at 72h. These observations were evident in both male and female mice, although decreased Cyclin D1 was less prominent in females (IHC shown for males only). To further validate this observation, we quantified Cyclin D1-positive hepatocytes bordering the central vein only as described in online methods. At all 24h, 40h and 72H, EC-KO showed significantly greater cyclin D1-positive hepatocytes along the central vein than EC-CON. (Fig.39B). Thus, there were quantitative and qualitative differences in Cyclin D1 expression between the two groups.

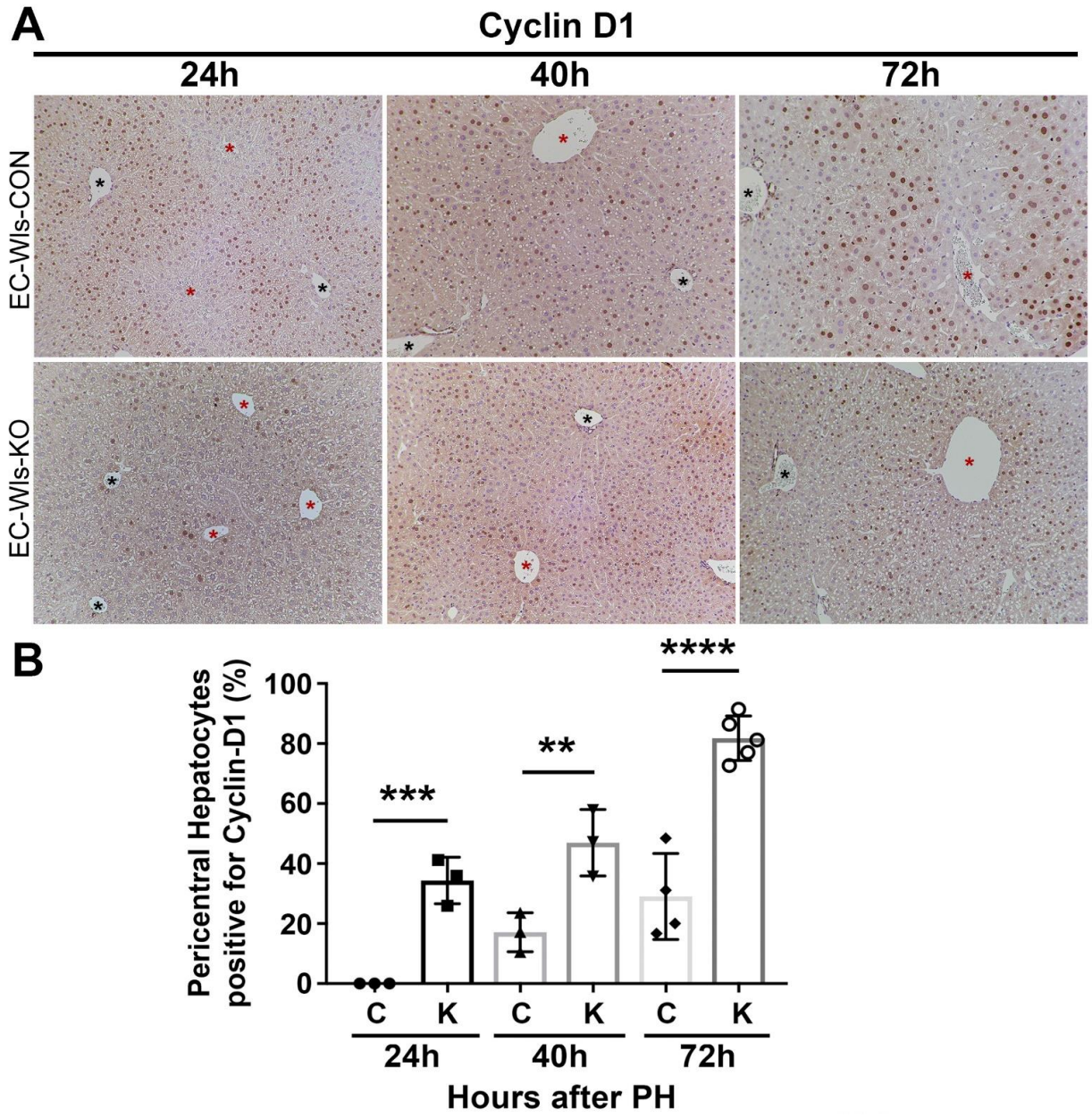

Figure 39: Quantitative and qualitative differences in hepatocyte cyclin-D1 in EC-KO versus EC-CON after PH.

(A) Representative IHC shows a gradual increase in cyclin-D1 staining during LR in periportal and midzonal hepatocytes in EC-CON from 24-40h, and almost the entire lobule sparing a few pericentral hepatocytes at 72h. Cyclin-D1 staining was apparent in few pericentral hepatocytes in EC-KO livers at 24h after PH, and gradually increased in this zone at 40h, expanding further at 72h. Black asterisk – portal triad; Red asterisk – central vein. (B) Quantification of cyclin-D1-positive versus total hepatocytes lining only central veins is represented as a percentage for both EC-CON and EC-KO at 24h, 40h and 72h post-PH. Each symbol represents the average of at least 5 200x images around central vein from one mouse. Three or more mice from each group were used for each time-point. P value was calculated by ordinary one way ANOVA and multiple comparisons by uncorrected Fishers's LSD. (**p<0.01; ***p<0.001; ****p<0.0001).

5.4.5 Hepatic stellate cells do not contribute to liver zonation or regeneration after PH

Next we questioned whether hepatic stellate cells (HSC) contribute Wnts required for LR. We crossed Wls-floxed mice with mice expressing Cre under the Lecithin retinol acyltransferase (Lrat) promoter (HSC-KO) (314). Mice exhibited no phenotype at baseline, as liver weight to body weight ratios were comparable between HSC-KO and HSC-CON (Fig.40A). Further, hepatic zonation was comparable by immunohistochemistry of GS and western blotting of GS, Cyp2e1, and Cyp1a2 (Fig.40B, C). Intriguingly we observed decreased Cyclin D1 at baseline in HSC-KO, and this trend was sustained 40 hours after PH by western blot (Fig.40B). However, this trend was not observed by immunohistochemistry, as HSC-CON and HSC-KO had comparable Cyclin D1 and PCNA positivity at 40 hours and 72 hours (Fig.40D, E). The discrepancy in Cyclin D1 may result from western blot detection of nonparenchymal cell expression. Hence, we concluded HSC likely do not contributes Wnts required for LR.

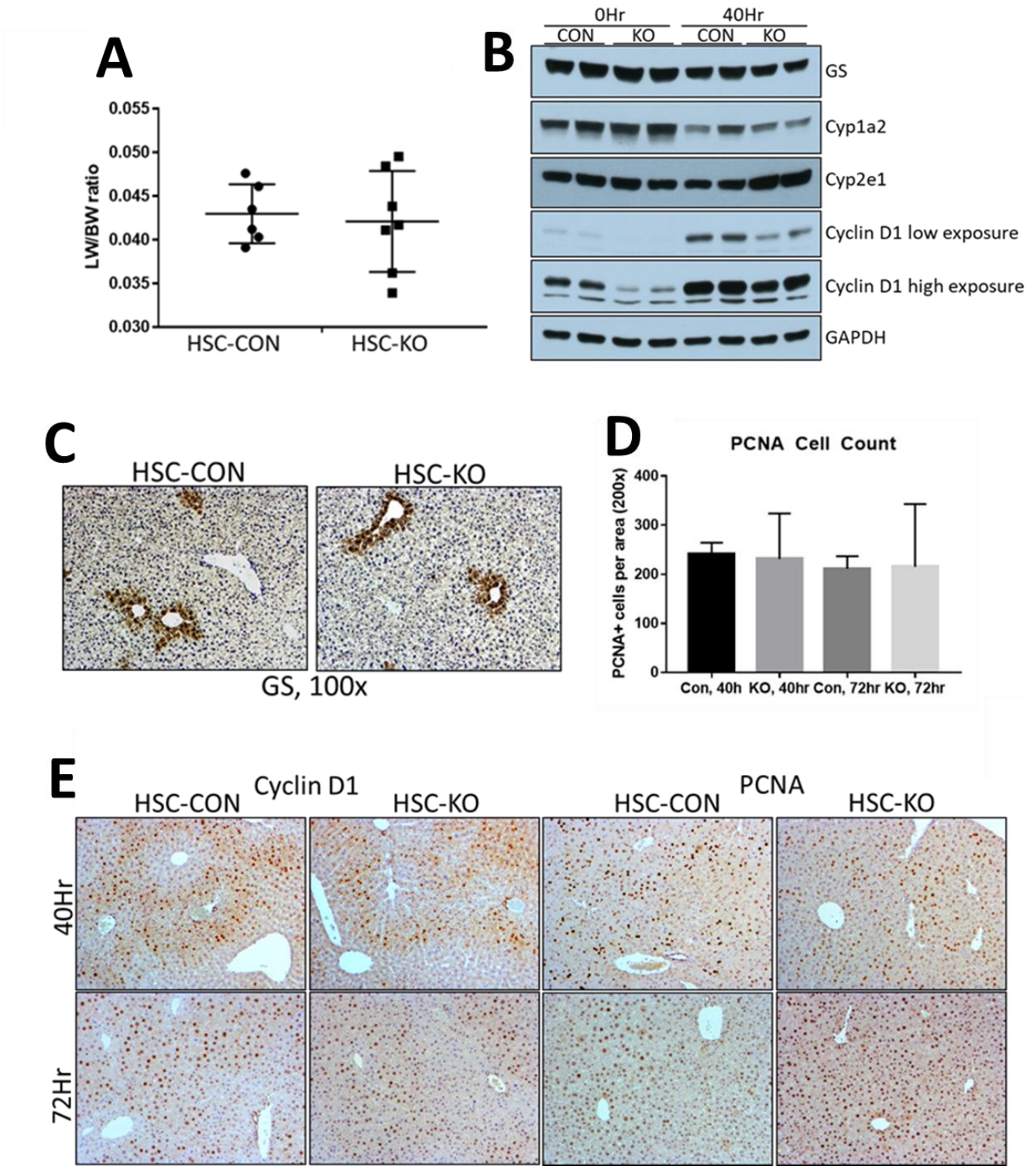

Figure 40: HSC-KO have no notable phenotype at baseline or after PH compared to HSC-CON.

(A) Liver weight to body weight ratios of male and female HSC-KO and HSC-CON are comparable. (B) Western blot analysis at baseline (0 hour) and 40 hour post PH show no deficit in zonation, however HSC-KO have reduced cyclin D1 at 0 hour and 40 hour compared to HSC-CON. (C) Representative immunohistochemistry images of glutamine synthetase show similar staining in HSC-CON and HSC-KO. (D) PCNA positivity was quantified. Three images were taken per sample and positive nuclei were counted, and the average of three images was considered. Images were taken blindly at 200x. (E) Immunohistochemistry of cyclin D1 and PCNA at 40 and 72 hours post PH show comparable staining in HSC-KO and HSC-CON. Images are taken at 100x. PCNA, proliferating cell nuclear antigen;

5.4.6 EC-KO phenocopy bKO and 5/6KO, while MP-KO and HSC-KO do not

Previous work suggested macrophages are a Wnt-secreting cell type after PH, although proliferation defects in MP-KO were marginal at 40h compared to bKO and 5/6KO (40). To confirm the primary source of Wnts are endothelial cells and not macrophages, we assessed Cyclin D1 transcription at various timepoints after PH in MP-CON and MP-KO. At 6hr and 24hr Cyclin D1 was comparable, and only at 40h was an insignificant but notable decrease in mRNA observed in MP-KO (Fig.41A). We verified this by comparing Cyclin D1 immunohistochemistry 24h after PH in bKO, 5/6KO, EC-KO, MP-KO, and HSC-KO. Expectedly, bKO and 5/6KO had reduced Cyclin D1 compared to their respective controls, and EC-KO was the only cell-specific Wntless knockout model to phenocopy this finding (Fig.41B). MP-KO and HSC-KO had comparable Cyclin D1 levels to their controls, concluding that endothelial cells, but not macrophages or stellate cells, are the primary Wnt source after PH.

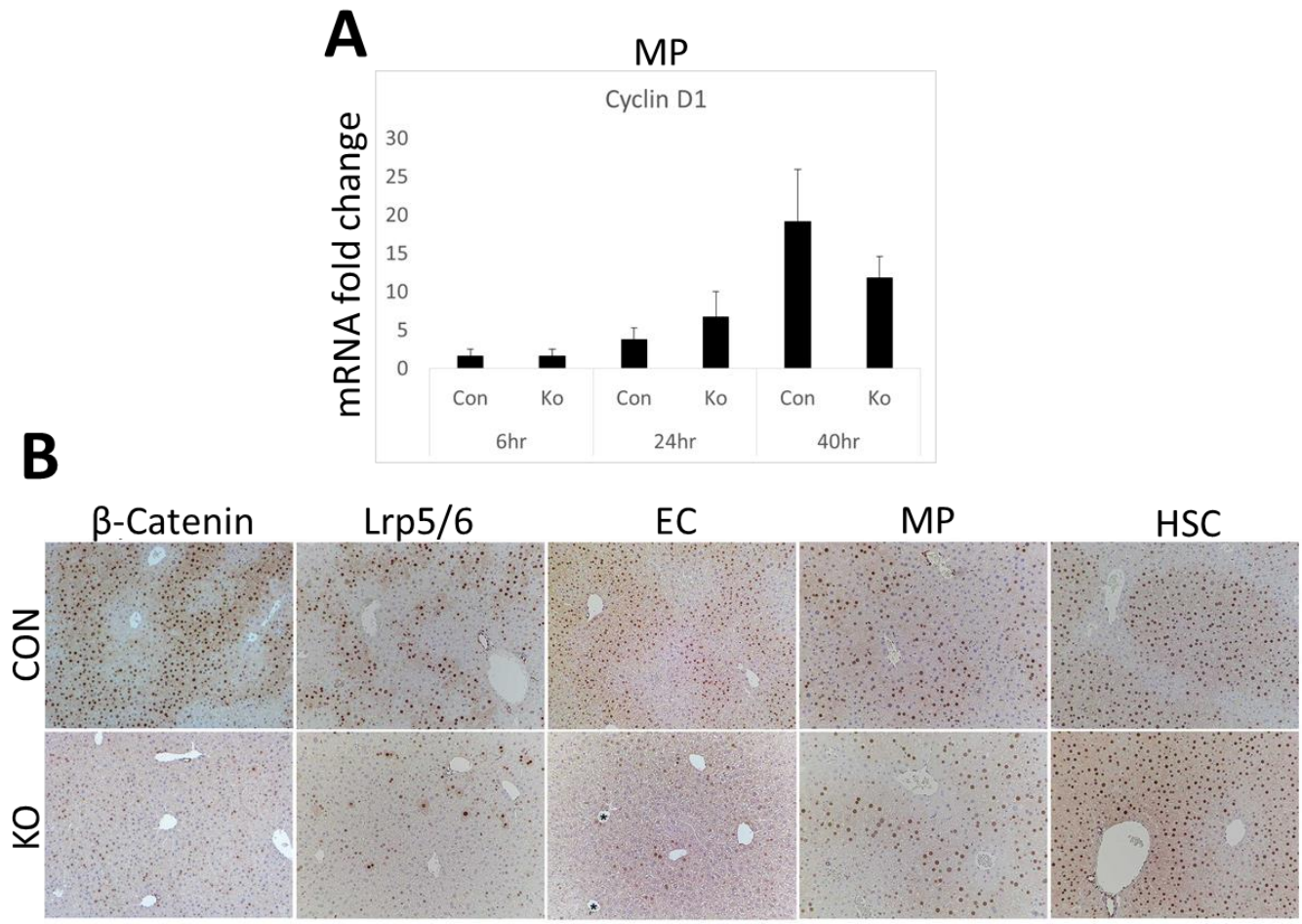

Figure 41: EC, but not MP or HSC, are the primary source of Wnts and phenocopy bKO and 5/6KO. (A) qPCR assessing Cyclin D1 expression of MP-CON and MP-KO at 6h, 24h, and 40h after PH. There is no reduction in Cyclin D1 until 40h. (B) Cyclin D1 immunohistochemistry at 24h after PH demonstrates decreased expression in bKO, 5/6KO, and EC-KO, with no deficit in MP-KO or HSC-KO.

5.4.7 Upregulation of Wnt2 and Wnt9b mRNA expression in endothelial cells hepatocytes in regenerating livers at 12h after PH

Although unpublished, the data in section 5.4.7 has been previously described in a dissertation from a previous graduate student (280). Since our current study suggests EC are the major source of Wnts during LR and HSC and MP likely are not, we focused on EC-specific Wnt

contributions. We selected 12 hours after PH to query changes in Wnt expression in EC compared to baseline.

Control mice were used to isolate hepatocytes and non-parenchymal cells by collagenase perfusion at 12h after PH, and cells were pooled from 2 mice (Fig.42A). Purity of isolated cells was confirmed by qPCR analysis for cell-specific markers. EC fraction was concluded to be pure judging by expression of Tie2 and Vegfr2, and absence of Albumin, CD68, and Lysozyme. MP fraction had marginal increase in EC-specific markers (Fig.42B), suggesting EC contamination and MP were discarded from further analysis. Analysis of hepatocyte fraction showed no appreciable changes in Wnt expression at 12h versus baseline (Fig.42C). Around 45-fold upregulation in the expression of Wnt2 and around 18-fold upregulation in the expression of Wnt9b was observed in EC at 12h after PH (Fig.42A). Lastly, at baseline, highest transcript levels of Wnt2 and Wnt9b were observed in EC, which increased significantly after PH (Fig.43B,C).

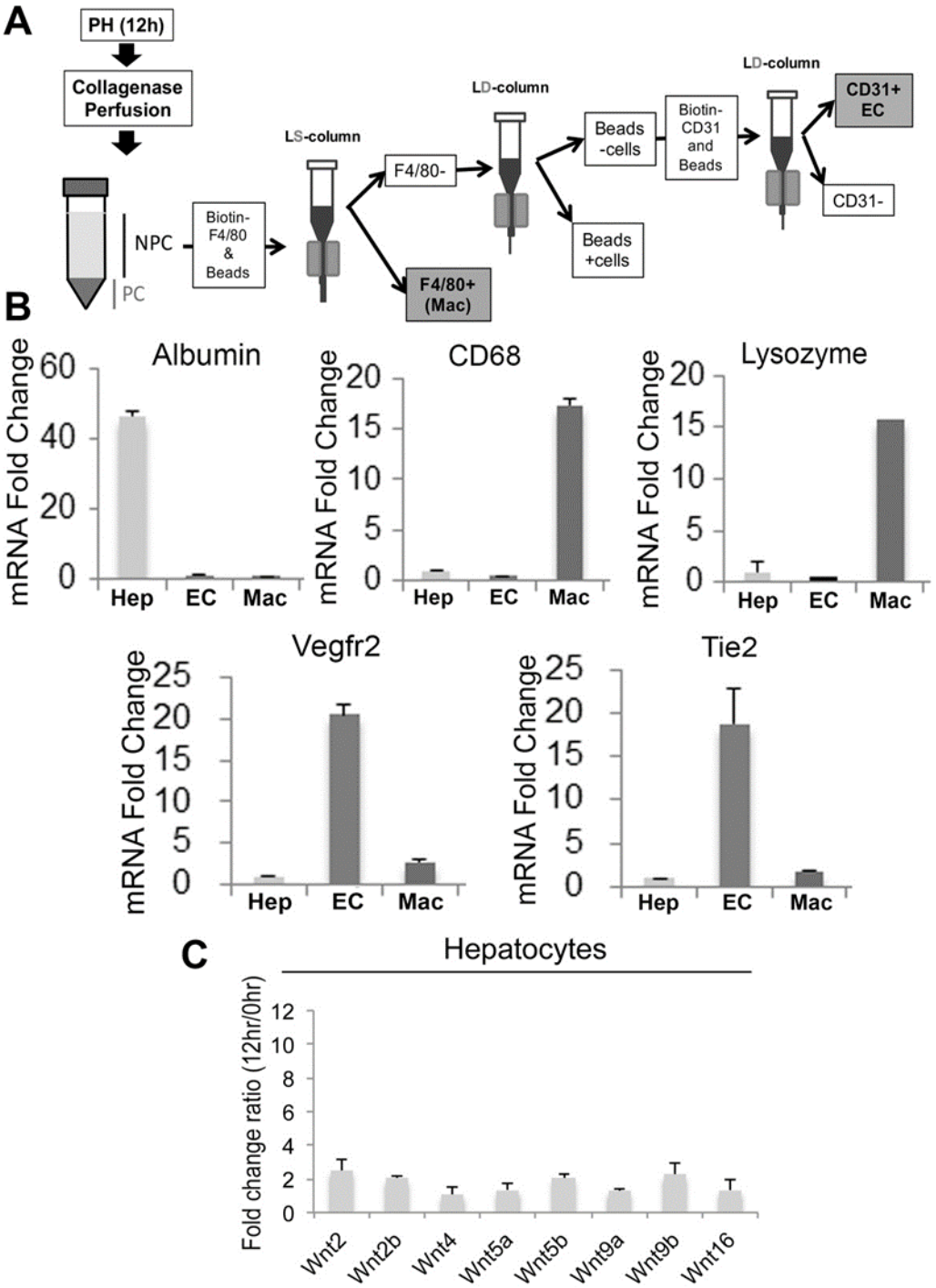

Figure 42: Cell isolation and purity validation from regenerating livers at 12h after PH.

(A) Schematic summarizing the process of cell isolation and separation at 12h after PH. Hepatocytes were obtained from parenchymal cell (PC) fraction. Non-parenchymal cell (NPC) fraction was used to separate Macrophages (Mac) and endothelial cells (EC) using magnetic columns as outlined in supplemental methods. (B) Each fraction was tested for purity using qRT-PCR for cell-specific gene expression. qRT-PCR for mouse albumin shows expression only in

hepatocytes (Hep) only, macrophage marker CD68 and Lysozyme in Mac fraction only, endothelial cell marker Vegfr2 and Tie2 in EC fraction, and small enrichment in Mac fraction, suggesting EC contamination of Mac. (C) Insignificant changes in selected Wnt genes by qRT-PCR in hepatocytes at 12h after PH when compared to their respective baseline expression.

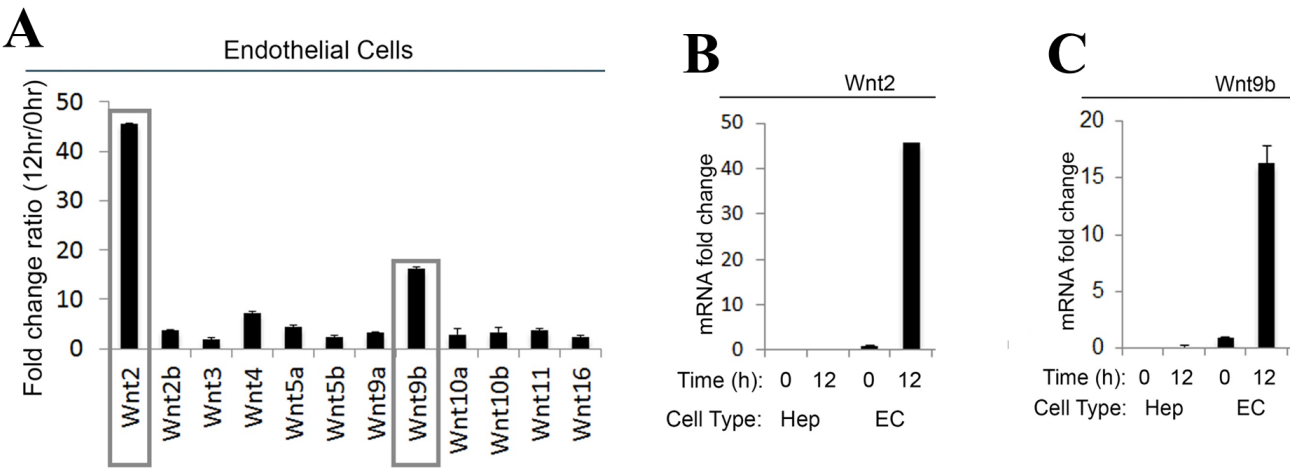

Figure 43: Upregulation of Wnt2 and Wnt9b mRNA in EC during LR.
(A) qRT-PCR analysis for selected Wnt genes in EC isolated from regenerating livers at 12h after PH. Y-axis denotes fold-change at 12h over baseline. Wnt2 mRNA increased 45-fold and Wnt9b around 15-fold. (B) Changes in Wnt2 and Wnt9b mRNA in hepatocytes (Hep) and EC. EC express highest levels of Wnt2 and Wnt9b mRNA both at baseline and after PH.

5.4.8 Shear stress can induce Wnt2 and Wnt9b transcripts in endothelial cells in vitro

Finally, to address the basis of Wnt upregulation in EC, which triggers β-catenin activation in hepatocytes thus contributing to LR, we investigated if shear stress on EC may be the major inciting mechanism. Portal pressure increase immediately after PH exerts shear stress along the sinusoids (324). There is evidence suggesting shear stress can influence EC signaling and is sufficient to induce LR (308). We cultured two liver-relevant EC, primary murine liver sinusoidal EC (LSEC) and a transformed murine liver sinusoidal EC line (TSEC) (317) and subjected them to orbital shear stress for 6h. Response of the two cells to shear stress was verified by a significant, approximate 80-fold induction of interleukin-6 (IL6) in both cells and

around 350-fold increase in endothelin-1 (ET1) in LSEC and around 200-fold increase in TSEC, two genes known to be highly shear-stress responsive (325, 326) (Fig.44A, B). In LSECs, orbital shear stress led to approximately 140-fold increase in expression of Wnt2 and 40-fold increase in Wnt9b (Fig.44C). In TSECs exposed to shear stress, Wnt2 and Wnt9b were upregulated 15- and 40-fold, respectively (Fig.44D). Primary murine hepatocytes showed no change in expression of either Wnts when subjected to orbital shear stress (Fig.44E). Raw blue macrophage cell line showed no effect of shear stress on Wnt2 expression, but did induce Wnt9b marginally (Fig.44F). Thus, hepatic sinusoidal EC are highly responsive to shear stress, which led to profound upregulation of Wnt2 and Wnt9b mRNA expression.

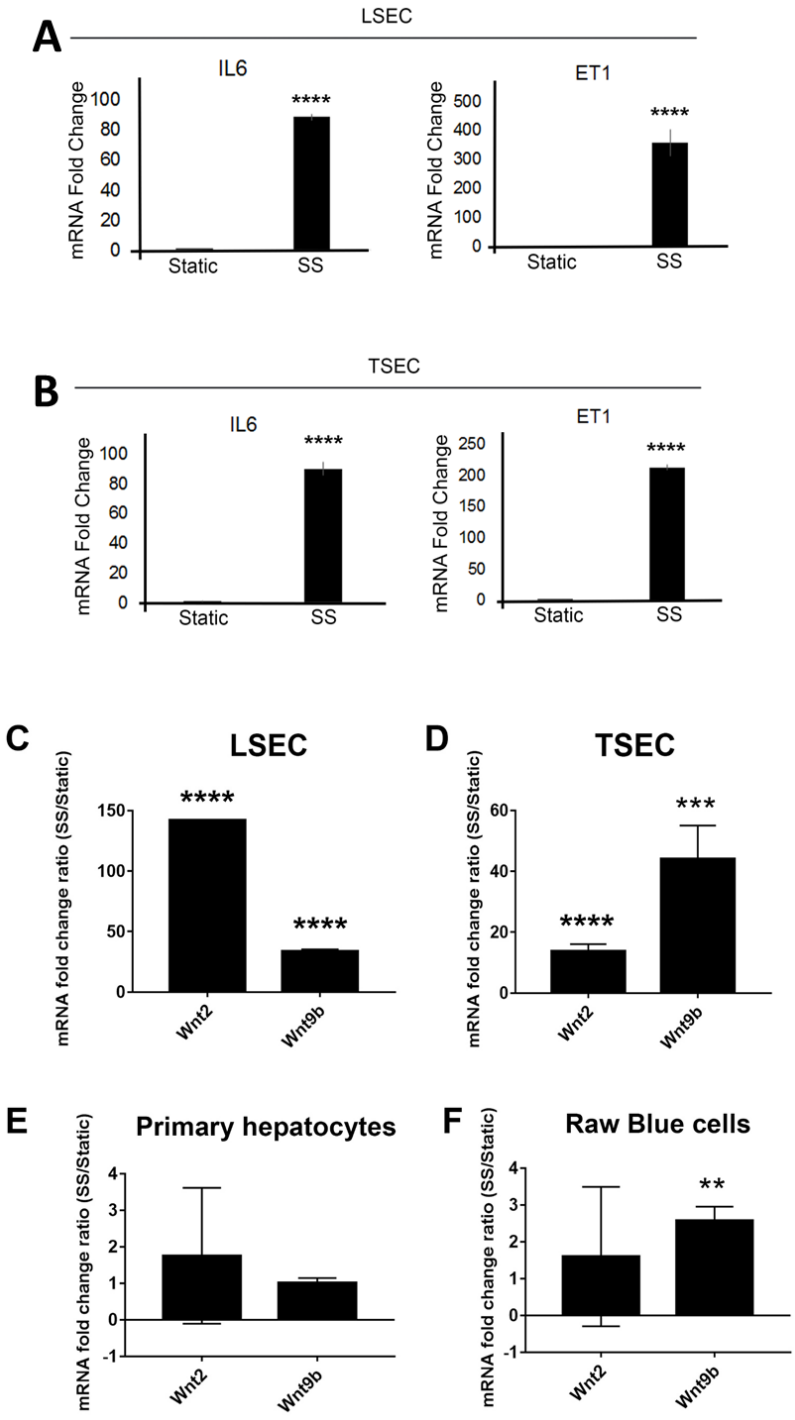

Figure 44: Effect of in vitro shear stress on hepatic endothelial cells.

(A) qRT-PCR results assessing expression of Interleukin-6 (IL6) and Endothelin-1 (ET1), following orbital shear stress generated by shaking primary liver EC (LSECs) and (B) transformed liver endothelial cell line (TSECs) at 210 rpm for 6h, which were profoundly induced. (****p<.0.001). (C) qRT-PCR on LSECs shows a significant increase in Wnt2 and

Wnt9b expression after shear stress. Y-axis denotes fold-change in mRNA expression during shear stress over static culture. (D) qRT-PCR on TSECs shows a significant increase in Wnt2 and Wnt9b expression after shear stress. Y-axis denotes fold-change in mRNA expression during shear stress over static culture. (E) No change in mRNA expression of Wnt2 and Wnt9b in primary hepatocytes exposed to shear stress. (F) No change in mRNA expression of Wnt2 but a marginal but significant increase in Wnt9b expression in Raw blue macrophage cell line subjected to 6h of orbital shear stress. (*$p<0.05$; **$p<0.01$; ***$p<0.005$; ****$p<0.001$).

5.5 DISCUSSION

The current study is a continuation of our previous work identifying hepatocyte-specific β-catenin as a major driver of hepatic zonation and LR after PH (89). Further, β-catenin in both zonation and LR is under the control of paracrine Wnt signaling (40). In the same study, we ruled out hepatocytes, cholangiocytes and macrophages as sources of Wnts in regulating pericentral β-catenin activation. However, macrophages were identified as one source of Wnts during LR, as macrophage-specific Wls knockout mice showed marginal and temporal decrease in Cyclin D1 and a resulting 20% deficit in hepatocyte proliferation at 40h.

We previously used Tie2-Cre to ablate Wls from all EC, which led to embryonic lethality, thus precluding assessment of EC contribution to β-catenin signaling in liver pathophysiology (40). We also employed PDGFi-Cre-ERT2 to generate EC-KO, which led to mosaic recombination insufficient for drawing concrete conclusions (data not shown) (327). Eventually, we employed transgenic mice expressing *Cre recombinase* under the lymphatic vessel endothelial hyaluronic acid receptor 1 (Lyve1) promoter. Lyve1 is expressed in lymphatic EC and intriguingly is also expressed in hepatic sinusoidal EC (321). Our careful fate tracing studies utilizing ROSA-YFP reporter mice also unveil Lyve1-dependent YFP expression in vascular EC in the liver including cells lining central veins, therefore enabling the removal of

Wls from most hepatic EC. This likely suggests vascular EC and sinusoidal EC may come from a common Lyve-1-positive progenitor cell, allowing for Cre activation in both cell types during embryonal development.

EC-KO mice at baseline showed lower LW/BW ratios than their controls. This observation is consistent with lack of appropriate baseline β-catenin activation in hepatocytes during early postnatal stages, which also led to lower LW/BW ratios in bKO and 5/6KO (40, 89). Indeed, our previous study has also shown β-catenin activation to be imperative in hepatocyte proliferation during early postnatal hepatic growth (328). Our study now suggests that Wnts from EC in the liver are indeed responsible for driving β-catenin activation during these early stages since livers show minimal basal proliferation after around 4-6 weeks of age.

EC-KO mice at baseline also lacked pericentral β-catenin targets like GS, Cyp2e1, and Cyp1a2 indicating disruption of metabolic zonation. This observation also phenocopied bKO and 5/6KO (40, 89, 163). Recently, EC lining the central vein have been shown to be the primary source of Wnts required for β-catenin activation in pericentral hepatocytes (20). This study also identified Wnt2 and Wnt9b to be two major Wnts responsible for this process. Since Lyve1-cre led to recombination of Wls alleles in central venous EC as well, β-catenin dependent metabolic zonation was abrogated in EC-KO. The limited movement of Wnts in general owing to their hydrophobicity secondary to palmitoylation, which is essential for their biological activity, likely restricts β-catenin activation to a few hepatocyte layers around central vein. Further, high APC expression in hepatocytes in periportal region also deters basal β-catenin activity in that region (329). The basis of constitutive Wnt2 and Wnt9b release from EC lining central veins remains unknown.

EC-KO mice, like bKO and 5/6KO also show a comparable delay in LR (40, 89, 330). This was secondary to decreased expression of known β-catenin target Cyclin D1 in hepatocytes after EC-KO were subjected to PH. This led to reduced numbers of hepatocytes entering S-phase as detected by PCNA IHC, also evident in bKO and 5/6KO during LR. However, at 72h, there was a rebound increase in both Cyclin D1 and PCNA in EC-KO, just like bKO and 5/6KO. Further analysis in EC-CON mice showed Cyclin D1 appearance in periportal and midzonal hepatocytes at 24h after PH and later expanding to all zones barring the most distal zone-3 hepatocyte layer neighboring the central vein EC. Based on these observations, and proximity to hepatocytes, sinusoidal EC are likely the major source of Wnts during LR. This was affirmed by lack of Cyclin D1 until 40h and PCNA until 72h after PH in EC-KO. Intriguingly, the location where Cyclin D1 appears in EC-KO during LR was distinct in that it was evident most prominently in pericentral hepatocytes and extended towards other zones. We are unable to address the basis of this difference but posit this is due to activation of compensatory signaling to ensure LR during continually absent β-catenin signaling. Indeed, redundancy in signaling pathways to 'guarantee' LR is well recognized (331).

Both males and females mice lacking Wls in EC showed similar defect in LR. Intriguingly, PCNA-deficiency is evident in females at 40h despite higher basal Cyclin D1 expression in EC-CON, suggesting that *de novo* Cyclin D1 expression and not the pre-existing pool is critical for initiating hepatocyte proliferation after PH. The pre-existing Cyclin D1 pool in females may be a function of estrogen since Cyclin D1 promoter has an estrogen-response element and known to control its expression (332). However, because of known pleiotropic functions of Cyclin D1 beyond proliferation such as in metabolism, it is likely that estrogen-

dependent Cyclin D1 may be performing additional functions in female livers at baseline contributing to sexual dimorphism (333).

Although convinced EC are the major source of Wnts during zonation and LR, we queried stellate cells (SC) in order to complete our assessment of liver cell populations. Our HSC-KO had no deficit in liver weight to body weight ratios or hepatic zonation at baseline. We also noted no difference in PCNA positivity at 40 hours or 72 hours. Oddly, HSC-KO displayed decreased Cyclin D1 at baseline and 40 hours by western blot, although these differences were not reconciled by immunohistochemistry (IHC), which showed comparable Cyclin D1. While we cannot conclusively state the reason for this discrepancy, one speculation is IHC is not sensitive enough to notice small differences that western blotting can identify. Alternatively, western blot accounts for all Cyclin D1 present, whereas IHC focuses on nuclear staining. However, Cyclin D1 has cytoplasmic roles regulating cell adhesion, mitosis, and migration under physiological and abnormal conditions (334, 335). Lastly, it is possible western blot accounts for nonparenchymal cell Cyclin D1 expression, while we emphasized hepatocyte-specific staining using IHC. Therefore, it would be of interest to identify whether HSC produce Wnts that regulate nonparenchymal cell proliferation after PH.

We also vetted MP-CON and MP-KO more extensively, and found no differences in Cyclin D1 expression at early timepoints including 6 and 24h. Further, by qPCR, Cyclin D1 decrease at 40h in MP-KO was statistically insignificant. To further confirm EC-KO as the only Wntless knockout animal model to phenocopy bKO and 5/6KO, we established a side-by-side comparison of Cyclin D1 via IHC at 24h to conclusively show EC-KO, bKO, and 5/6KO had similar decreases in Cyclin D1, unlike MP-KO and HSC-KO. It will be of interest to discover the mechanism by which MP-specific Wnts contribute to LR at 40h, but not before or after 40h.

The overall close resemblance of the mouse models of β-catenin activity loss in hepatocytes including bKO, 5/6KO and EC-KO underscores the existence of a Wnt-β-catenin paracrine axis composed of EC and hepatocytes in contributing to normal LR after PH. Once the cell sources of Wnts during LR were identified, we next focused on discerning their identity. Intriguingly Wnt2 and Wnt9b, the same Wnts involved in zonation, were most profoundly upregulated in both EC and macrophages at the time before β-catenin activation and Cyclin D1 expression was apparent.

In rats, nuclear translocation of β-catenin occurs almost immediately after PH (297). In mice, the kinetics of nuclear translocation is slower but is evident as 3-6h, with β-catenin-TCF4 complex formation observed at 4h persisting for 24-40h, and Cyclin D1 mRNA and protein expression increasing steadily from 12-72h (35, 40, 89, 336-338). Therefore, it is likely that there are preexisting stores of Wnt2 and Wnt9b proteins in hepatic sinusoidal EC, which get dumped towards hepatocytes for immediate β-catenin activation which however would need to be sustained for successful hepatocyte proliferation at 40h. To conclusively prove such phenomenon would require labeled Wnts and intravital imaging. Previously, genetic ablation of vascular endothelial growth factor (VEGF)-A receptor-2 (VEGFR2) in the hepatic sinusoidal EC impaired hepatocyte proliferation after PH due to diminution of EC-specific transcription factor *Id1* (19). In fact, *Id1*-deficient mice also showed defective LR initiation that was associated with decreased expression of hepatocyte growth factor (HGF) and Wnt2 in sinusoidal EC. We theorized that ongoing Wnt secretion from EC for sustained β-catenin activation in hepatocyte would be a rather dynamic process and further conjectured enhanced sinusoidal pressure secondary to increased portal pressure, and its effect on sinusoidal EC, as the regulator of Wnt expression. Indeed, portal venous pressure is induced after PH which could be

recapitulated solely by portal vein branch ligation, triggering LR seen via immediately enhanced c-fos mRNA expression (308). Subjecting two EC from liver – primary LSECs and TSECs, a profound upregulation of both Wnt2 and Wnt9b was observed along with known shear-stress responsive genes like IL6 and ET-1 (325, 326). It is important to note that for both hepatic EC cell lines, only freshly isolated and plated cells were responsive to shear stress and became rapidly resistant upon passaging and prolonged plating, likely due to their de-differentiation, which is well known (317, 319). Nonetheless, strong induction in Wnt genes was unique to EC and not hepatocytes or macrophages. Interestingly, macrophage cell line showed mild upregulation of Wnt9b by 2.5-fold following exposure to shear stress. As macrophages also line sinusoids, it is possible increased portal pressure may initiate Wnt secretion in this cell type, *albeit* to a lesser extent. Alternatively, shear stress induced production of cytokines such as IL6 or TNFα in EC, may influence Wnt expression in macrophages. While IL6 and TNFα are not direct hepatocyte mitogens (331), these may influence hepatocyte proliferation by facilitating expression of Wnt genes in non-parenchymal cells. Recently, TNFα treatment was shown to induce Wnt2 mRNA in Raw Blue cells (338). Further confirmation is needed to elucidate whether shear stress-induced mitogen production can trigger Wnt production in resident liver macrophages or EC *in vivo.*

In summary, we validate the paracrine function of Wnt-β-catenin pathway in regulating hepatic zonation and characterize the complex cell-molecule circuitry of the Wnt-β-catenin pathway during the process of LR after PH (Fig.8). We show that hepatic sinusoidal EC secrete Wnt2 and Wnt9b in response to enhanced shear stress, to act through Wnt-LRP5/6 to stabilize β-catenin, enhance its nuclear translocation and complex with TCF to contribute to normal zone 1 and zone 2 expression of Cyclin D1, which is critical for normal progression of hepatocytes into

S-phase of proliferation. Termination of Wnt/β-catenin signaling upon accomplishment of hepatocyte proliferation is at least in part achieved by Wnt5a secretion from regenerated hepatocytes (21). See Figure 45 for working summary.

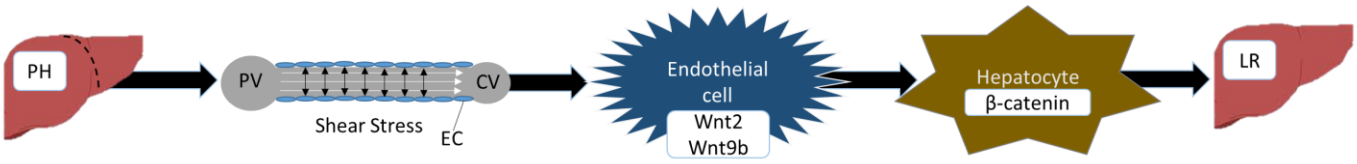

Figure 45: Schema of Wnt/beta-catenin activation after LR, induced in part by shear stress.

6.0 CONCLUDING REMARKS AND GENERAL DISCUSSION

6.1.1 Beta-catenin in hemochromatosis

6.1.1.1 Current questions and future directions

We have shown β-catenin is required for protection against hepatic iron overload in mice, in part due to its role in antioxidant production (108). There are many exciting questions that remain to be answered to further elucidate the mechanism and implications of β-catenin in iron-induced injury, and the molecular consequences that occur from loss of β-catenin in bKO. After chronic iron overload for three months, bKO had greater hepatic fibrosis, steatosis, inflammation, and oxidative stress. Further, we noted β-catenin target gene expression including GS and Cyp2e1 in bKO, mainly in areas of steatosis. This correlated with a resurgence of β-catenin expression evident by IHC. We speculated these β-catenin-positive cells were hepatocytes, but this should be confirmed. We also can confirm β-catenin reappearance is driving this ectopic GS and Cyp2e1 expression. β-Catenin was present homogenously throughout bKO+Fe livers, therefore we would expect zonation markers present at central veins, which was not the case. Yap has also been shown to upregulate GS, although a conflicting report demonstrated increased GS in Yap knockout mice (339, 340). Moreover, Yap is localized periportally, however this landscape likely changes after hepatic injury including iron overload seen in bKO, highlighting the importance of linking β-catenin resurgence to GS and Cyp2e1 expression in bKO+Fe.

Additionally, there is an opportunity to identify the source of β-catenin-positive hepatocytes. The liver stem cells, also called "oval cells", often arise when the liver must regenerate but hepatocytes and cholangiocytes are unable to proliferate (341). There is a positive correlation with the presence of ductular reaction, which was evident in bKO+Fe, and oval cell appearance in hepatic injury (151). However, if oval cells differentiate into liver epithelial cells, they will express Albumin and activate Cre, leading to loss of β-catenin. Therefore, it would be of interest to utilize a fate tracing model, such as a fluorescent reporter under the Forkhead Box L1 (FoxL1) promoter, to determine where these hepatocyte-like cells originate. FoxL1 is a bona fide hepatic progenitor marker (342). Alternatively, hepatic stellate cells may also be a source of these β-catenin-positive cells, as some data suggests if hepatocyte proliferation is blocked such as in the partial hepatectomy and 2-acetylaminofluorene model, stellate cells can transdifferentiate into progenitors and then into hepatocyte-like cells (343). Regardless of the cell source, the β-catenin-positive hepatocytes were unable to rescue the injury seen in bKO, suggesting their functionality is impaired or absent compared to bCON.

Future directions also include determining whether β-catenin is under the control of Wnt, by analyzing whether 5/6KO phenocopy bKO after iron overload. Additionally, the role of macrophages should be assessed. We noted in bKO+Fe, large iron-laden cells that are likely macrophages engulfing dead hepatocytes and excess iron. Intriguingly, in patients, activation of Kupffer cells correlated with intercellular adhesion molecule 1 (ICAM) expression on hepatocytes, and lead to heightened disease severity including increased steatosis and fibrosis (129). It will be of interest to deplete macrophages using clodronate liposomes and identify whether the phenotype is improved. We did not see a macrophage response in bCON comparable to bKO, so elucidating the mechanism of macrophage recruitment in absence of β-catenin is

important. We can consider ICAM1, and the alternatively activated pathways we noticed in bKO+Fe, including AKT, ERK, and NFkB, and their potential roles in macrophage recruitment and activation.

6.1.1.2 Clinical implications

To our knowledge, this is the first animal model to physiologically recapitulate the most severe forms of hereditary hemochromatosis. We show that hepatic injury in bKO+Fe can be protected by the administration of antioxidants which raises the opportunity of using antioxidants for patients. Antioxidants such as vitamin C would sequester free iron and prevent conversion to toxic ferric iron and thus prevent free radical production. However, vitamin C acts as a pro-oxidant in many pathological conditions (344), and in chronic iron overload, ferric iron paradoxically causes oxidation of antioxidants (345-347), preventing their efficacy as therapies.

Therefore, our model will serve to identify and test new therapeutic options targeted for the most severe cases of HH.

6.1.2 Cell-specific Wnts in HCC

6.1.2.1 Current questions and future directions

The role of the microenvironment in HCC is undisputable. We have tried to dissect the role of various relevant cellular elements in contributing to HCC development using a relevant injury and fibrosis model. We focus on Wnts from hepatocytes and macrophages in this model.

A. Role of HP Wnts during DEN/CCl_4 (Section 3.0)

At 5 months, we noted HP-KO had CK19-positive foci absent in HP-CON. Further, HP-KO had less E-cadherin expression than HP-CON at 5 months. E-cadherin inversely correlates with aggressive HCC and epithelial to mesenchymal transition (249). These findings together suggest the development of more aggressive stem-like tumors in HP-KO, however this was not evident at 6 months. In fact, HP-KO and HP-CON had comparable tumor burden including CK19-positivity and E-cadherin at this timepoint. We rationalized the DEN/CCl_4 model is too hepatotoxic to appreciate contributions of HP Wnts, however further confirmation is possible. In this current study, the development of small, aggressive foci at 5 months in HP-KO are unable to grow and flourish after an additional month of CCl_4 because the livers are continuously hit with toxins, allowing for additional oncogenic drivers and passengers to overshadow HP Wnt contributions. Therefore it will be advantageous to submit HP-CON and HP-KO to DEN/CCl_4 for 5 months, then let them "recover" for an additional month. This way, the oncogenic mutations and landscape present at 5 months can drive tumor advancement into late stages. CK19-positive foci in HP-KO may develop into full tumor nodules that undergo EMT, and we may observe more advanced tumors in HP-KO compared to HP-CON at 6 months like we initially predicted.

B. Role of MP Wnts during DEN/CCl_4 (Section 4.0)

The definitive cause of two distinct phenotypes deserves further elucidation. While MP-CON A and MP-CON B had similar tumor burden, MP-CON A had increased cMyc, P38 MAPK, AR, and others, while MP-CON B had increased GS, M1 macrophages, and leukocytes. Although we predicted these differences resulted from MP-CON A and MP-CON B having different epigenetic signatures consequentially from different breeding pairs, this should be conclusively studied. To address whether epigenetic sexual dimorphism explains these two phenotypes,

multiple cohorts from breeders of male Wntless-floxed mice and female lysozyme-Cre mice, and of the reverse, should be subjected to DEN/CCl_4. Ideally, Group A would result from one breeding scheme, and Group B would result from the other. Unbiased methylation arrays, such as LC-MS/MS (348), can then be used to assess whether general methylation differences exist in pups from different breeders. Animals with and without DEN/CCl_4 should be considered. Further, we will ask whether increased protein expression of cMyc, P38 MAPK, and others, is due to increased activated histone modifications. We can use histone-modification-specific antibodies to test the presence of specific modifications such as activating methylation marks, and perform chromatin immunoprecipitation and sequencing (ChIP-seq) to test whether the promoters of specific genes like cMyc are activated in MP-CON A versus MP-CON B. DNA methylation and histone methylation are strongly linked (349), enabling us to correlate our findings to LC-MS/MS data. We will assess tumors and adjacent non-tumor tissue, as it is possible changes in epigenetics will be observed only in tumors.

If we are unable to explain our two phenotypes via epigenetics, we predict differences in gut microbiota may lead to two different HCC types. Microbiota depletion via antibiotics protects mice against DEN/CCl_4-induced HCC (225). Further, strains including C57BL/6 mice have considerable variability in their microbial composition (350). Predictably, litters housed in the same cage may have comparable microbiomes resulting from maternal transfer and coprophagy (351).

While we show MP Wnts can suppress or promote tumorigenesis, further studies are required to fully characterize the environment that determines MP Wnts role. In particular, does the presence of overexpressed cMyc or P38 MAPK, as seen in MP-CON A, predict MP Wnts are tumor suppressive? While cMyc is “undruggable”, liver epithelial cell-specific cMyc knockout

mice are viable (352) and could be crossed with MP-KO to determine whether these double knockouts have less tumors than controls. Several P38 MAPK inhibitors exist such as SB203580 (353), and could be administered to MP-KO as well. Moreover, does more leukocyte infiltration and M1 macrophage polarization drive Group B tumors? By taking MP-CON and littermate MP-KO, subjecting them to DEN/CCl_4 while providing anti-CD47 treatment to stimulate M1 macrophage polarization (354), we can attempt to shift all animals towards a Group B phenotype and identify whether MP-KO reduces tumor burden.

6.1.2.2 Clinical implications

Several studies suggest inhibiting Wnt signaling alone or in combination will have significant therapeutic value (221, 355-357). However, these studies are performed *in vitro* or with xenograft models, and therefore do not recapitulate the tumor microenvironment or disease progression seen in patients. In our study, we used a clinically relevant chemical model to assess HP Wnt contributions and MP Wnt contributions. Our results suggest inhibiting HP-specific Wnts may not have any patient benefit, as tumors still develop and progress in their absence, albiet via distinct mechanisms. Once we delineate the specific molecular and immunological patterns that determine whether MP Wnts will contribute to or inhibit tumor growth based on epigenetic or other mechanisms, we can use this information to predict whether a patient will benefit from MP-Wnt suppression, provided a tumor biopsy is accessible.

6.1.3 Role of Wnt/beta-catenin in LR after PH

6.1.3.1 Current questions and future directions

We undisputedly show the role of endothelial cell Wnts in both hepatic zonation and Cyclin D1-dependent hepatocyte regeneration after partial hepatectomy. Future directions include confirming the mitogenic roles of Wnt2 and Wnt9b during LR and in homeostatic zonation. We are currently generating Wnt2-floxed mice and are obtaining Wnt9b-floxed mice to create cell-specific conditional knockouts. Further, using rats we can confirm *in vivo* that shear stress can induce Wnt secretion from EC using a portal vein branch ligation model which increases portal pressure while leaving the liver intact (308, 310). Lastly, we plan to further scrutinize our HSC-KO animals after PH to further confirm SC do not play a role in LR.

To continue developing a complete kinetic profile of Wnt/β-catenin signaling in LR, there are many variables to consider. The role of the Rspondin (Rspo) axis will be of importance. Rspo ligands signal through LGR receptors to augment Wnt signaling by preventing internalization of Wnt receptors (26). Loss of LGR4/5 or Rspo3 was shown to ablate β-catenin-dependent zonation at baseline, and addition of Rspo1 to increase pericentral fate (286, 358). Moreover, LGR4/5 KO showed delayed LR after PH (358). Preliminary data not shown suggests Wnt2 and Wnt9b are unable to induce β-catenin-TCF-dependent transcription *in vitro*, unless Rspo3 is present, but further studies in primary hepatocytes will be relevant. Considering current literature suggesting Rspo is required for Wnt signaling during LR, future studies can elucidate the cellular source and identity of Rspo required after PH.

The identity of Fzd receptors required during LR will also be of interest. Whole liver expresses eight of ten Fzd receptors with several of them expressed in hepatocytes (11). While Fzd7 and Fzd6 have defined roles in hepatic carcinogenesis (44, 217), to our knowledge no one has determined the receptors that interact with Wnt2 and/or Wnt9b during LR, which would greatly enhance our understanding of canonical Wnt signaling.

Another interesting question is the role of macrophage-specific Wnts during LR. As mentioned, we previously reported MP-KO have a slight regeneration deficit and hepatic zonation is unaffected. While this could suggest MP are a secondary contributor of Wnts, we speculate MP-Wnts indirectly contribute to LR through their interactions with EC. Indeed, MP depletion studies have concluded MPs are required for viable EC and to activate them during different hepatic injury models (359, 360), so it would be of interest to assess EC phenotype in MP-KO to determine if MP-Wnts are required for healthy EC.

An important unanswered question that requires further investigation is the molecular basis of regeneration in the three genotypes that lack 'physiological' β-catenin activation including bKO, 5/6KO, and EC-KO. A simplest explanation is that the liver has a common redundant mechanism that is activated when β-catenin activation via Wnts is hampered in the three genotypes based on similarly decreased Cyclin D1 at 24h-40h, lack of PCNA at 40h and increased Cyclin D1 and PCNA at 72h. Also, lack of GS-positivity in EC-KO at 72h despite resurgence of Cyclin D1 and initiation and expansion of Cyclin D1 expression at 24-72h that occurs from pericentral zone to periportal zone (as opposed to periportal to pericentral zone in control mice), suggests activation of a non-Wnt, non-β-catenin mechanism. However, the molecular basis of LR could also be distinct due to disruption of non-β-catenin signaling at different levels, in these three models. β-Catenin activation through any mechanism is precluded only in the bKO since they lack β-catenin in hepatocytes and hence redundant signaling has to be β-catenin-independent. β-Catenin activation through any Wnt is not possible in both bKO as well as 5/6KO, since the latter lack Wnt co-receptors, although β-catenin can be activated in the latter via non-Wnt-dependent mechanisms since β-catenin is still present in the hepatocytes. β-Catenin activation in hepatocytes cannot occur via Wnts from EC in either bKO, 5/6KO, or EC-

KO, but only in the latter can Wnts from non-EC sources activate β-catenin to eventually drive LR at 72h. A direct comparison of the three strains at various time points after PH is ongoing to elucidate the basis of LR in both biased and unbiased analysis. By identifying pathways that create redundancy for loss of canonical Wnt signaling during LR, we will contribute to overall knowledge of the "hepatostat" and mechanisms required for liver homeostasis.

6.1.3.2 Clinical implications

Currently the only effective treatments for most liver diseases are liver transplant or surgical resection (290, 291), which are often unrealistic due to lack of donor organs and poor regenerative capabilities of injured or transplanted livers, frequently causing hepatocyte dysfunction and "small-for-size syndrome" (361). Not surprisingly, impaired liver regeneration (LR) is the major cause of liver failure and liver-related death worldwide (294). Therefore, by understanding what initiates and propagates LR in a healthy model, we can develop alternative therapies utilizing the natural regenerative potential of the liver.

While the major goal of this study is to further understand upstream mechanisms of β-catenin signaling during LR, these and future results have therapeutic implications for liver disease patients. If we can activate β-catenin in hepatocytes after surgical resection, for example, possibly through stimulating Wnt production in endothelial cells, we could improve LR and patient survival. We can stimulate Wnt production during living donor transplants to decrease recovery time and improve regeneration, or to prevent "small-for-size syndrome". Our lab has shown thyromimetics such as T3 and GC-1 initiate hepatocyte proliferation dependent on β-catenin activation (362). Currently more physiological means are being pursued such as use of surrogate Wnt agonists (363).

APPENDIX A

LIST OF ANIMALS USED IN STUDY

Table 12: All animals used in study

Animal	Abbreviation	Description	Reference
Alb-Cre$^{+/-}$;Ctnnb1$^{fl/fl}$	bKO	Hepatocyte and cholangiocyte-specific β-catenin knockout	(89)
Lrp5$^{fl/fl}$Lrp6$^{fl/fl}$;Alb-Cre$^{+/-}$	5/6KO	Hepatocyte and cholangiocyte-specific Lrp5/6 double knockout	(40)
Wntless$^{fl/fl}$;Alb-Cre$^{+/-}$	HP-KO	Hepatocyte and cholangiocyte-specific Wntless knockout	(40)
Wntless$^{fl/fl}$;Lyz-Cre$^{+/-}$	MP-KO	Macrophage Wntless knockout	(40)
Wntless$^{fl/fl}$;Lyve1-Cre$^{+/-}$	EC-KO	Endothelial cell Wntless knockout	(312)
Wntless$^{fl/fl}$;Lrat-Cre$^{+/-}$	HSC-KO	Hepatic stellate cell Wntless knockout	(314)

APPENDIX B

PUBLICATIONS

Morgan Preziosi, Minakshi Poddar, Sucha Singh, Satdarshan P. Monga. Macrophage-specific Wnts have dual role as tumor promotor or tumor suppressor in hepatocellular carcinoma after DEN/CCl4 model of tumorigenesis, 2018. American Journal of Physiology-GI. Manuscript in revision.

Danielle Bell, Laura Molina, Junyan Tao, **Morgan Preziosi**, Tirthadipa Pradhan-Sundd, Sucha Singh, Minakshi Poddar, Sarangarajan Ranganathan, Maria Chikina, Satdarshan Monga. Hepatocyte-derived lipocalin 2 is a potential serum biomarker reflecting tumor burden in hepatoblastoma, 2018. American Journal of Pathology, Manuscript in revision.

Morgan Preziosi, Satdarshan P. Monga. Novel genetic activation screening in liver repopulation and cancer; now crispr than ever! 2018, Hepatology. Manuscript resubmitted. (editorial)

Morgan E. Preziosi, Hirohisa Okabe, Minakshi Poddar, Sucha Singh, Satdarshan P.S. Monga. Endothelial Wnts regulate β-catenin signaling in murine liver zonation and regeneration: A sequel to Wnt-Wnt situation, 2018. Hepatology Communications, Manuscript accepted.

Morgan Preziosi, Minakshi Poddar, Sucha Singh, Satdarshan P. Monga. Hepatocyte Wnts are dispensable during diethylnitrosamine and carbon tetrachloride-induced injury and hepatocellular cancer, 2018. Gene Expression, doi: 10.3727/105221618X15205148413587. [Epub ahead of print]. PubMed PMID: 29519268

Morgan E. Preziosi, Satdarshan P. Monga. Update on mechanisms of liver regeneration, 2017. Seminars for Liver Disease. 37(2):141-151. DOI: 10.1055/s-0037-1601351. PubMed PMID: 28564722 (review article)

Kari Nejak-Bowen, Akshata Moghe, Pamela Cornuet, **Morgan Preziosi**, Shanmugam Nagarajan, Satdarshan P Monga. Role and regulation of p65/β-catenin association during liver injury and regeneration: a 'complex' relationship, 2017. Gene Expression, 17(3): 219-235. DOI: 10.3727/105221617X695762. Pubmed PMID: 28474571

Morgan E. Preziosi, Sucha Singh, Erika V. Valore, Chun-Ling Jung, Minakshi Poddar, Shanguman Nagarajan, Tomas Ganz, Satdarshan P Monga. Mice lacking liver-specific β-catenin develop steatohepatitis and fibrosis after iron overload, 2017. Journal of Hepatology. 67(2): 360-369. DOI: 10.1016/j.jhep.2017.03.012. PMID: 28341391

Tamara Feliciano Alvarado, Elisabetta Puliga, **Morgan Preziosi**, Minakshi Poddar, Sucha Singh, Amadeo Columbano, Kari Nejak-Bowen, Satdarshan P. Monga. Thyroid Hormone Receptor-β Agonist Induces β-Catenin-Dependent Hepatocyte Proliferation in Mice: Implications in Hepatic Regeneration, 2016. Gene Expr. 17(1):19-34. PubMed PMID: 27226410.

Jing Yang, Antonella Cusimano, Jappmann K. Monga, **Morgan E. Preziosi**, Filippo Pullara, Guillermo Calero, Richard Lang, Terry P. Yamaguchi, Kari N. Nejak-Bowen, Satdarshan P. Monga. WNT5A Inhibits Hepatocyte Proliferation and Concludes β-Catenin Signaling in Liver Regeneration, 2015. American Journal of Pathology. 185(8). DOI: 10.1016/j.ajpath.2015.04.021

Evan Delgado, Hirohisa Okabe, **Morgan Preziosi**, Jacquelyn Olivia Russell, Tamara Feliciano Alvarado, Michael Oertel, Kari Nichole Nejak-Bowen, Yixian Zhang, Satdarshan P.S. Monga. Complete response of CTNNB1-mutated tumors to β-catenin suppression by locked nucleic antisense in mouse hepatocarcinogenesis model, 2015. Hepatology 62(2). DOI: 10.1016/j.jhep.2014.10.021

FUNDING

April 2017-May 2018: National Cancer Institute
Grant number: F31CA216994
Title: Elucidating the role of cell-specific Wnts in hepatocellular carcinoma

August 2014-August 2016: Angiopathy Training Program
Grant number: T32HL094295
Title: Role of shear stress on endothelial cell Wnt secretion and liver regeneration

BIBLIOGRAPHY

1.Clevers H. Wnt/beta-catenin signaling in development and disease. Cell 2006;127:469-480.
2.Clevers H, Nusse R. Wnt/beta-catenin signaling and disease. Cell 2012;149:1192-1205.
3.Gross JC, Chaudhary V, Bartscherer K, Boutros M. Active Wnt proteins are secreted on exosomes. Nat Cell Biol 2012;14:1036-1045.
4.Korkut C, Ataman B, Ramachandran P, Ashley J, Barria R, Gherbesi N, Budnik V. Trans-synaptic transmission of vesicular Wnt signals through Evi/Wntless. Cell 2009;139:393-404.
5.Kimelman D, Xu W. beta-catenin destruction complex: insights and questions from a structural perspective. Oncogene 2006;25:7482-7491.
6.Amit S, Hatzubai A, Birman Y, Andersen JS, Ben-Shushan E, Mann M, Ben-Neriah Y, et al. Axin-mediated CKI phosphorylation of beta-catenin at Ser 45: a molecular switch for the Wnt pathway. Genes Dev 2002;16:1066-1076.
7.Liu C, Li Y, Semenov M, Han C, Baeg GH, Tan Y, Zhang Z, et al. Control of beta-catenin phosphorylation/degradation by a dual-kinase mechanism. Cell 2002;108:837-847.
8.Aberle H, Bauer A, Stappert J, Kispert A, Kemler R. beta-catenin is a target for the ubiquitin-proteasome pathway. EMBO J 1997;16:3797-3804.
9.Miller JR, Hocking AM, Brown JD, Moon RT. Mechanism and function of signal transduction by the Wnt/beta-catenin and Wnt/Ca2+ pathways. Oncogene 1999;18:7860-7872.
10.Vincan E, Barker N. The upstream components of the Wnt signalling pathway in the dynamic EMT and MET associated with colorectal cancer progression. Clin Exp Metastasis 2008;25:657-663.
11.Zeng G, Awan F, Otruba W, Muller P, Apte U, Tan X, Gandhi C, et al. Wnt'er in liver: expression of Wnt and frizzled genes in mouse. Hepatology 2007;45:195-204.
12.Nusse R, Clevers H. Wnt/beta-Catenin Signaling, Disease, and Emerging Therapeutic Modalities. Cell 2017;169:985-999.
13.Banziger C, Soldini D, Schutt C, Zipperlen P, Hausmann G, Basler K. Wntless, a conserved membrane protein dedicated to the secretion of Wnt proteins from signaling cells. Cell 2006;125:509-522.
14.McMahon AP, Bradley A. The Wnt-1 (int-1) proto-oncogene is required for development of a large region of the mouse brain. Cell 1990;62:1073-1085.
15.Monkley SJ, Delaney SJ, Pennisi DJ, Christiansen JH, Wainwright BJ. Targeted disruption of the Wnt2 gene results in placentation defects. Development 1996;122:3343-3353.
16.Parr BA, Cornish VA, Cybulsky MI, McMahon AP. Wnt7b regulates placental development in mice. Dev Biol 2001;237:324-332.

17.Bennett CN, Longo KA, Wright WS, Suva LJ, Lane TF, Hankenson KD, MacDougald OA. Regulation of osteoblastogenesis and bone mass by Wnt10b. Proc Natl Acad Sci U S A 2005;102:3324-3329.
18.Zheng HF, Tobias JH, Duncan E, Evans DM, Eriksson J, Paternoster L, Yerges-Armstrong LM, et al. WNT16 influences bone mineral density, cortical bone thickness, bone strength, and osteoporotic fracture risk. PLoS Genet 2012;8:e1002745.
19.Ding BS, Nolan DJ, Butler JM, James D, Babazadeh AO, Rosenwaks Z, Mittal V, et al. Inductive angiocrine signals from sinusoidal endothelium are required for liver regeneration. Nature 2010;468:310-315.
20.Wang B, Zhao L, Fish M, Logan CY, Nusse R. Self-renewing diploid Axin2(+) cells fuel homeostatic renewal of the liver. Nature 2015;524:180-185.
21.Yang J, Cusimano A, Monga JK, Preziosi ME, Pullara F, Calero G, Lang R, et al. WNT5A inhibits hepatocyte proliferation and concludes beta-catenin signaling in liver regeneration. Am J Pathol 2015;185:2194-2205.
22.Okabe H, Yang J, Sylakowski K, Yovchev M, Miyagawa Y, Nagarajan S, Chikina M, et al. Wnt signaling regulates hepatobiliary repair following cholestatic liver injury in mice. Hepatology 2016;64:1652-1666.
23.Bafico A, Liu G, Yaniv A, Gazit A, Aaronson SA. Novel mechanism of Wnt signalling inhibition mediated by Dickkopf-1 interaction with LRP6/Arrow. Nat Cell Biol 2001;3:683-686.
24.Cruciat CM, Niehrs C. Secreted and transmembrane wnt inhibitors and activators. Cold Spring Harb Perspect Biol 2013;5:a015081.
25.Wang S, Krinks M, Lin K, Luyten FP, Moos M, Jr. Frzb, a secreted protein expressed in the Spemann organizer, binds and inhibits Wnt-8. Cell 1997;88:757-766.
26.Hao HX, Xie Y, Zhang Y, Charlat O, Oster E, Avello M, Lei H, et al. ZNRF3 promotes Wnt receptor turnover in an R-spondin-sensitive manner. Nature 2012;485:195-200.
27.Koo BK, Spit M, Jordens I, Low TY, Stange DE, van de Wetering M, van Es JH, et al. Tumour suppressor RNF43 is a stem-cell E3 ligase that induces endocytosis of Wnt receptors. Nature 2012;488:665-669.
28.Zebisch M, Xu Y, Krastev C, MacDonald BT, Chen M, Gilbert RJ, He X, et al. Structural and molecular basis of ZNRF3/RNF43 transmembrane ubiquitin ligase inhibition by the Wnt agonist R-spondin. Nat Commun 2013;4:2787.
29.Kakugawa S, Langton PF, Zebisch M, Howell S, Chang TH, Liu Y, Feizi T, et al. Notum deacylates Wnt proteins to suppress signalling activity. Nature 2015;519:187-192.
30.Valenta T, Hausmann G, Basler K. The many faces and functions of beta-catenin. EMBO J 2012;31:2714-2736.
31.Tan X, Apte U, Micsenyi A, Kotsagrelos E, Luo JH, Ranganathan S, Monga DK, et al. Epidermal growth factor receptor: a novel target of the Wnt/beta-catenin pathway in liver. Gastroenterology 2005;129:285-302.
32.Shtutman M, Zhurinsky J, Simcha I, Albanese C, D'Amico M, Pestell R, Ben-Ze'ev A. The cyclin D1 gene is a target of the beta-catenin/LEF-1 pathway. Proc Natl Acad Sci U S A 1999;96:5522-5527.
33.He TC, Sparks AB, Rago C, Hermeking H, Zawel L, da Costa LT, Morin PJ, et al. Identification of c-MYC as a target of the APC pathway. Science 1998;281:1509-1512.
34.Bouchard C, Thieke K, Maier A, Saffrich R, Hanley-Hyde J, Ansorge W, Reed S, et al. Direct induction of cyclin D2 by Myc contributes to cell cycle progression and sequestration of p27. EMBO J 1999;18:5321-5333.

35.Torre C, Benhamouche S, Mitchell C, Godard C, Veber P, Letourneur F, Cagnard N, et al. The transforming growth factor-alpha and cyclin D1 genes are direct targets of beta-catenin signaling in hepatocyte proliferation. J Hepatol 2011;55:86-95.
36.Nejak-Bowen KN, Zeng G, Tan X, Cieply B, Monga SP. Beta-catenin regulates vitamin C biosynthesis and cell survival in murine liver. J Biol Chem 2009;284:28115-28127.
37.Yamaguchi M. Suppressive role of regucalcin in liver cell proliferation: involvement in carcinogenesis. Cell Prolif 2013;46:243-253.
38.Hua Z, Chen J, Sun B, Zhao G, Zhang Y, Fong Y, Jia Z, et al. Specific expression of osteopontin and S100A6 in hepatocellular carcinoma. Surgery 2011;149:783-791.
39.Torre C, Perret C, Colnot S. Molecular determinants of liver zonation. Prog Mol Biol Transl Sci 2010;97:127-150.
40.Yang J, Mowry LE, Nejak-Bowen KN, Okabe H, Diegel CR, Lang RA, Williams BO, et al. beta-catenin signaling in murine liver zonation and regeneration: a Wnt-Wnt situation! Hepatology 2014;60:964-976.
41.Wilson A, Murphy MJ, Oskarsson T, Kaloulis K, Bettess MD, Oser GM, Pasche AC, et al. c-Myc controls the balance between hematopoietic stem cell self-renewal and differentiation. Genes Dev 2004;18:2747-2763.
42.Herbst A, Jurinovic V, Krebs S, Thieme SE, Blum H, Goke B, Kolligs FT. Comprehensive analysis of beta-catenin target genes in colorectal carcinoma cell lines with deregulated Wnt/beta-catenin signaling. BMC Genomics 2014;15:74.
43.Fujita T. Senescence marker protein-30 (SMP30): structure and biological function. Biochem Biophys Res Commun 1999;254:1-4.
44.Krutzfeldt J, Rosch N, Hausser J, Manoharan M, Zavolan M, Stoffel M. MicroRNA-194 is a target of transcription factor 1 (Tcf1, HNF1alpha) in adult liver and controls expression of frizzled-6. Hepatology 2012;55:98-107.
45.Burke ZD, Reed KR, Phesse TJ, Sansom OJ, Clarke AR, Tosh D. Liver zonation occurs through a beta-catenin-dependent, c-Myc-independent mechanism. Gastroenterology 2009;136:2316-2324 e2311-2313.
46.Roose J, Huls G, van Beest M, Moerer P, van der Horn K, Goldschmeding R, Logtenberg T, et al. Synergy between tumor suppressor APC and the beta-catenin-Tcf4 target Tcf1. Science 1999;285:1923-1926.
47.Filali M, Cheng N, Abbott D, Leontiev V, Engelhardt JF. Wnt-3A/beta-catenin signaling induces transcription from the LEF-1 promoter. J Biol Chem 2002;277:33398-33410.
48.Kaga S, Zhan L, Altaf E, Maulik N. Glycogen synthase kinase-3beta/beta-catenin promotes angiogenic and anti-apoptotic signaling through the induction of VEGF, Bcl-2 and survivin expression in rat ischemic preconditioned myocardium. J Mol Cell Cardiol 2006;40:138-147.
49.Hoeben A, Landuyt B, Highley MS, Wildiers H, Van Oosterom AT, De Bruijn EA. Vascular endothelial growth factor and angiogenesis. Pharmacol Rev 2004;56:549-580.
50.Moreau M, Mourah S, Dosquet C. beta-Catenin and NF-kappaB cooperate to regulate the uPA/uPAR system in cancer cells. Int J Cancer 2011;128:1280-1292.
51.Masckauchan TN, Kitajewski J. Wnt/Frizzled signaling in the vasculature: new angiogenic factors in sight. Physiology (Bethesda) 2006;21:181-188.
52.Cao G, Savani RC, Fehrenbach M, Lyons C, Zhang L, Coukos G, Delisser HM. Involvement of endothelial CD44 during in vivo angiogenesis. Am J Pathol 2006;169:325-336.
53.Guo Y, Xiao L, Sun L, Liu F. Wnt/beta-catenin signaling: a promising new target for fibrosis diseases. Physiol Res 2012;61:337-346.

54.Barker N, van Es JH, Kuipers J, Kujala P, van den Born M, Cozijnsen M, Haegebarth A, et al. Identification of stem cells in small intestine and colon by marker gene Lgr5. Nature 2007;449:1003-1007.
55.Terris B, Cavard C, Perret C. EpCAM, a new marker for cancer stem cells in hepatocellular carcinoma. J Hepatol 2010;52:280-281.
56.Lescher B, Haenig B, Kispert A. sFRP-2 is a target of the Wnt-4 signaling pathway in the developing metanephric kidney. Dev Dyn 1998;213:440-451.
57.Gonzalez-Sancho JM, Aguilera O, Garcia JM, Pendas-Franco N, Pena C, Cal S, Garcia de Herreros A, et al. The Wnt antagonist DICKKOPF-1 gene is a downstream target of beta-catenin/TCF and is downregulated in human colon cancer. Oncogene 2005;24:1098-1103.
58.Jho EH, Zhang T, Domon C, Joo CK, Freund JN, Costantini F. Wnt/beta-catenin/Tcf signaling induces the transcription of Axin2, a negative regulator of the signaling pathway. Mol Cell Biol 2002;22:1172-1183.
59.Levy L, Wei Y, Labalette C, Wu Y, Renard CA, Buendia MA, Neuveut C. Acetylation of beta-catenin by p300 regulates beta-catenin-Tcf4 interaction. Mol Cell Biol 2004;24:3404-3414.
60.Graham TA, Ferkey DM, Mao F, Kimelman D, Xu W. Tcf4 can specifically recognize beta-catenin using alternative conformations. Nat Struct Biol 2001;8:1048-1052.
61.Eichhoff OM, Weeraratna A, Zipser MC, Denat L, Widmer DS, Xu M, Kriegl L, et al. Differential LEF1 and TCF4 expression is involved in melanoma cell phenotype switching. Pigment Cell Melanoma Res 2011;24:631-642.
62.Evans PM, Chen X, Zhang W, Liu C. KLF4 interacts with beta-catenin/TCF4 and blocks p300/CBP recruitment by beta-catenin. Mol Cell Biol 2010;30:372-381.
63.Yang M, Li SN, Anjum KM, Gui LX, Zhu SS, Liu J, Chen JK, et al. A double-negative feedback loop between Wnt-beta-catenin signaling and HNF4alpha regulates epithelial-mesenchymal transition in hepatocellular carcinoma. J Cell Sci 2013;126:5692-5703.
64.Emami KH, Nguyen C, Ma H, Kim DH, Jeong KW, Eguchi M, Moon RT, et al. A small molecule inhibitor of beta-catenin/CREB-binding protein transcription [corrected]. Proc Natl Acad Sci U S A 2004;101:12682-12687.
65.Giles RH, Peters DJ, Breuning MH. Conjunction dysfunction: CBP/p300 in human disease. Trends Genet 1998;14:178-183.
66.Miyabayashi T, Teo JL, Yamamoto M, McMillan M, Nguyen C, Kahn M. Wnt/beta-catenin/CBP signaling maintains long-term murine embryonic stem cell pluripotency. Proc Natl Acad Sci U S A 2007;104:5668-5673.
67.Kaidi A, Williams AC, Paraskeva C. Interaction between beta-catenin and HIF-1 promotes cellular adaptation to hypoxia. Nat Cell Biol 2007;9:210-217.
68.Lehwald N, Tao GZ, Jang KY, Sorkin M, Knoefel WT, Sylvester KG. Wnt-beta-catenin signaling protects against hepatic ischemia and reperfusion injury in mice. Gastroenterology 2011;141:707-718, 718 e701-705.
69.Behari J. The Wnt/beta-catenin signaling pathway in liver biology and disease. Expert Rev Gastroenterol Hepatol 2010;4:745-756.
70.Monga SP, Mars WM, Pediaditakis P, Bell A, Mule K, Bowen WC, Wang X, et al. Hepatocyte growth factor induces Wnt-independent nuclear translocation of beta-catenin after Met-beta-catenin dissociation in hepatocytes. Cancer Res 2002;62:2064-2071.
71.Zeng G, Apte U, Micsenyi A, Bell A, Monga SP. Tyrosine residues 654 and 670 in beta-catenin are crucial in regulation of Met-beta-catenin interactions. Exp Cell Res 2006;312:3620-3630.

72.Apte U, Zeng G, Muller P, Tan X, Micsenyi A, Cieply B, Dai C, et al. Activation of Wnt/beta-catenin pathway during hepatocyte growth factor-induced hepatomegaly in mice. Hepatology 2006;44:992-1002.
73.Fang D, Hawke D, Zheng Y, Xia Y, Meisenhelder J, Nika H, Mills GB, et al. Phosphorylation of beta-catenin by AKT promotes beta-catenin transcriptional activity. J Biol Chem 2007;282:11221-11229.
74.Desbois-Mouthon C, Cadoret A, Blivet-Van Eggelpoel MJ, Bertrand F, Cherqui G, Perret C, Capeau J. Insulin and IGF-1 stimulate the beta-catenin pathway through two signalling cascades involving GSK-3beta inhibition and Ras activation. Oncogene 2001;20:252-259.
75.Cross DA, Alessi DR, Cohen P, Andjelkovich M, Hemmings BA. Inhibition of glycogen synthase kinase-3 by insulin mediated by protein kinase B. Nature 1995;378:785-789.
76.Robertson BW, Chellaiah MA. Osteopontin induces beta-catenin signaling through activation of Akt in prostate cancer cells. Exp Cell Res 2010;316:1-11.
77.Shashidhar S, Lorente G, Nagavarapu U, Nelson A, Kuo J, Cummins J, Nikolich K, et al. GPR56 is a GPCR that is overexpressed in gliomas and functions in tumor cell adhesion. Oncogene 2005;24:1673-1682.
78.Liu H, Hu Y, Simpson RW, Dear AE. Glucagon-like peptide-1 attenuates tumour necrosis factor-alpha-mediated induction of plasminogen [corrected] activator inhibitor-1 expression. J Endocrinol 2008;196:57-65.
79.Komiya Y, Habas R. Wnt signal transduction pathways. Organogenesis 2008;4:68-75.
80.Nishita M, Yoo SK, Nomachi A, Kani S, Sougawa N, Ohta Y, Takada S, et al. Filopodia formation mediated by receptor tyrosine kinase Ror2 is required for Wnt5a-induced cell migration. J Cell Biol 2006;175:555-562.
81.Wallingford JB, Habas R. The developmental biology of Dishevelled: an enigmatic protein governing cell fate and cell polarity. Development 2005;132:4421-4436.
82.Weiser DC, Pyati UJ, Kimelman D. Gravin regulates mesodermal cell behavior changes required for axis elongation during zebrafish gastrulation. Genes Dev 2007;21:1559-1571.
83.Westfall TA, Brimeyer R, Twedt J, Gladon J, Olberding A, Furutani-Seiki M, Slusarski DC. Wnt-5/pipetail functions in vertebrate axis formation as a negative regulator of Wnt/beta-catenin activity. J Cell Biol 2003;162:889-898.
84.Slusarski DC, Pelegri F. Calcium signaling in vertebrate embryonic patterning and morphogenesis. Dev Biol 2007;307:1-13.
85.Russell JO, Monga SP. Wnt/beta-Catenin Signaling in Liver Development, Homeostasis, and Pathobiology. Annu Rev Pathol 2018;13:351-378.
86.McLin VA, Rankin SA, Zorn AM. Repression of Wnt/beta-catenin signaling in the anterior endoderm is essential for liver and pancreas development. Development 2007;134:2207-2217.
87.Tan X, Yuan Y, Zeng G, Apte U, Thompson MD, Cieply B, Stolz DB, et al. Beta-catenin deletion in hepatoblasts disrupts hepatic morphogenesis and survival during mouse development. Hepatology 2008;47:1667-1679.
88.Cadoret A, Ovejero C, Saadi-Kheddouci S, Souil E, Fabre M, Romagnolo B, Kahn A, et al. Hepatomegaly in transgenic mice expressing an oncogenic form of beta-catenin. Cancer Res 2001;61:3245-3249.
89.Tan X, Behari J, Cieply B, Michalopoulos GK, Monga SP. Conditional deletion of beta-catenin reveals its role in liver growth and regeneration. Gastroenterology 2006;131:1561-1572.

90.Apte U, Singh S, Zeng G, Cieply B, Virji MA, Wu T, Monga SP. Beta-catenin activation promotes liver regeneration after acetaminophen-induced injury. Am J Pathol 2009;175:1056-1065.
91.Son TG, Zou Y, Jung KJ, Yu BP, Ishigami A, Maruyama N, Lee J. SMP30 deficiency causes increased oxidative stress in brain. Mech Ageing Dev 2006;127:451-457.
92.Lento W, Ito T, Zhao C, Harris JR, Huang W, Jiang C, Owzar K, et al. Loss of beta-catenin triggers oxidative stress and impairs hematopoietic regeneration. Genes Dev 2014;28:995-1004.
93.Tao GZ, Lehwald N, Jang KY, Baek J, Xu B, Omary MB, Sylvester KG. Wnt/beta-catenin signaling protects mouse liver against oxidative stress-induced apoptosis through the inhibition of forkhead transcription factor FoxO3. J Biol Chem 2013;288:17214-17224.
94.Zhang XF, Tan X, Zeng G, Misse A, Singh S, Kim Y, Klaunig JE, et al. Conditional beta-catenin loss in mice promotes chemical hepatocarcinogenesis: role of oxidative stress and platelet-derived growth factor receptor alpha/phosphoinositide 3-kinase signaling. Hepatology 2010;52:954-965.
95.Poli G. Pathogenesis of liver fibrosis: role of oxidative stress. Mol Aspects Med 2000;21:49-98.
96.Ge WS, Wang YJ, Wu JX, Fan JG, Chen YW, Zhu L. beta-catenin is overexpressed in hepatic fibrosis and blockage of Wnt/beta-catenin signaling inhibits hepatic stellate cell activation. Mol Med Rep 2014;9:2145-2151.
97.Cheng JH, She H, Han YP, Wang J, Xiong S, Asahina K, Tsukamoto H. Wnt antagonism inhibits hepatic stellate cell activation and liver fibrosis. Am J Physiol Gastrointest Liver Physiol 2008;294:G39-49.
98.Myung SJ, Yoon JH, Gwak GY, Kim W, Lee JH, Kim KM, Shin CS, et al. Wnt signaling enhances the activation and survival of human hepatic stellate cells. FEBS Lett 2007;581:2954-2958.
99.Xiong WJ, Hu LJ, Jian YC, Wang LJ, Jiang M, Li W, He Y. Wnt5a participates in hepatic stellate cell activation observed by gene expression profile and functional assays. World J Gastroenterol 2012;18:1745-1752.
100.Nejak-Bowen K, Kikuchi A, Monga SP. Beta-catenin-NF-kappaB interactions in murine hepatocytes: a complex to die for. Hepatology 2013;57:763-774.
101.Oeckinghaus A, Ghosh S. The NF-kappaB family of transcription factors and its regulation. Cold Spring Harb Perspect Biol 2009;1:a000034.
102.Go GW, Srivastava R, Hernandez-Ono A, Gang G, Smith SB, Booth CJ, Ginsberg HN, et al. The combined hyperlipidemia caused by impaired Wnt-LRP6 signaling is reversed by Wnt3a rescue. Cell Metab 2014;19:209-220.
103.Apte U, Thompson MD, Cui S, Liu B, Cieply B, Monga SP. Wnt/beta-catenin signaling mediates oval cell response in rodents. Hepatology 2008;47:288-295.
104.Hu M, Kurobe M, Jeong YJ, Fuerer C, Ghole S, Nusse R, Sylvester KG. Wnt/beta-catenin signaling in murine hepatic transit amplifying progenitor cells. Gastroenterology 2007;133:1579-1591.
105.Yang W, Yan HX, Chen L, Liu Q, He YQ, Yu LX, Zhang SH, et al. Wnt/beta-catenin signaling contributes to activation of normal and tumorigenic liver progenitor cells. Cancer Res 2008;68:4287-4295.
106.Williams JM, Oh SH, Jorgensen M, Steiger N, Darwiche H, Shupe T, Petersen BE. The role of the Wnt family of secreted proteins in rat oval "stem" cell-based liver regeneration: Wnt1 drives differentiation. Am J Pathol 2010;176:2732-2742.

107. Boulter L, Govaere O, Bird TG, Radulescu S, Ramachandran P, Pellicoro A, Ridgway RA, et al. Macrophage-derived Wnt opposes Notch signaling to specify hepatic progenitor cell fate in chronic liver disease. Nat Med 2012;18:572-579.
108. Preziosi ME, Singh S, Valore EV, Jung G, Popovic B, Poddar M, Nagarajan S, et al. Mice lacking liver-specific beta-catenin develop steatohepatitis and fibrosis after iron overload. J Hepatol 2017;67:360-369.
109. Burt MJ, George PM, Upton JD, Collett JA, Frampton CM, Chapman TM, Walmsley TA, et al. The significance of haemochromatosis gene mutations in the general population: implications for screening. Gut 1998;43:830-836.
110. Pietrangelo A. Hereditary hemochromatosis. Biochim Biophys Acta 2006;1763:700-710.
111. Pietrangelo A. Hereditary hemochromatosis: pathogenesis, diagnosis, and treatment. Gastroenterology 2010;139:393-408, 408 e391-392.
112. Witte DL, Crosby WH, Edwards CQ, Fairbanks VF, Mitros FA. Practice guideline development task force of the College of American Pathologists. Hereditary hemochromatosis. Clin Chim Acta 1996;245:139-200.
113. Siah CW, Ombiga J, Adams LA, Trinder D, Olynyk JK. Normal iron metabolism and the pathophysiology of iron overload disorders. Clin Biochem Rev 2006;27:5-16.
114. Roetto A, Papanikolaou G, Politou M, Alberti F, Girelli D, Christakis J, Loukopoulos D, et al. Mutant antimicrobial peptide hepcidin is associated with severe juvenile hemochromatosis. Nat Genet 2003;33:21-22.
115. Papanikolaou G, Samuels ME, Ludwig EH, MacDonald ML, Franchini PL, Dube MP, Andres L, et al. Mutations in HFE2 cause iron overload in chromosome 1q-linked juvenile hemochromatosis. Nat Genet 2004;36:77-82.
116. Camaschella C, Roetto A, Cali A, De Gobbi M, Garozzo G, Carella M, Majorano N, et al. The gene TFR2 is mutated in a new type of haemochromatosis mapping to 7q22. Nat Genet 2000;25:14-15.
117. Montosi G, Donovan A, Totaro A, Garuti C, Pignatti E, Cassanelli S, Trenor CC, et al. Autosomal-dominant hemochromatosis is associated with a mutation in the ferroportin (SLC11A3) gene. J Clin Invest 2001;108:619-623.
118. Feder JN, Penny DM, Irrinki A, Lee VK, Lebron JA, Watson N, Tsuchihashi Z, et al. The hemochromatosis gene product complexes with the transferrin receptor and lowers its affinity for ligand binding. Proc Natl Acad Sci U S A 1998;95:1472-1477.
119. Duck KA, Neely EB, Simpson IA, Connor JR. A role for sex and a common HFE gene variant in brain iron uptake. J Cereb Blood Flow Metab 2018;38:540-548.
120. Rossi E. Hepcidin--the iron regulatory hormone. Clin Biochem Rev 2005;26:47-49.
121. Ganz T. Hepcidin and iron regulation, 10 years later. Blood 2011;117:4425-4433.
122. Babitt JL, Huang FW, Wrighting DM, Xia Y, Sidis Y, Samad TA, Campagna JA, et al. Bone morphogenetic protein signaling by hemojuvelin regulates hepcidin expression. Nat Genet 2006;38:531-539.
123. Wallace DF, Summerville L, Lusby PE, Subramaniam VN. First phenotypic description of transferrin receptor 2 knockout mouse, and the role of hepcidin. Gut 2005;54:980-986.
124. Fleming RE, Migas MC, Holden CC, Waheed A, Britton RS, Tomatsu S, Bacon BR, et al. Transferrin receptor 2: continued expression in mouse liver in the face of iron overload and in hereditary hemochromatosis. Proc Natl Acad Sci U S A 2000;97:2214-2219.

125. Schimanski LM, Drakesmith H, Merryweather-Clarke AT, Viprakasit V, Edwards JP, Sweetland E, Bastin JM, et al. In vitro functional analysis of human ferroportin (FPN) and hemochromatosis-associated FPN mutations. Blood 2005;105:4096-4102.
126. Pietrangelo A. Hereditary hemochromatosis. Annu Rev Nutr 2006;26:251-270.
127. Pietrangelo A. The ferroportin disease. Blood Cells Mol Dis 2004;32:131-138.
128. Deugnier Y, Turlin B. Pathology of hepatic iron overload. World J Gastroenterol 2007;13:4755-4760.
129. Stal P, Broome U, Scheynius A, Befrits R, Hultcrantz R. Kupffer cell iron overload induces intercellular adhesion molecule-1 expression on hepatocytes in genetic hemochromatosis. Hepatology 1995;21:1308-1316.
130. Huang X. Iron overload and its association with cancer risk in humans: evidence for iron as a carcinogenic metal. Mutat Res 2003;533:153-171.
131. Valenti L, Fracanzani AL, Dongiovanni P, Bugianesi E, Marchesini G, Manzini P, Vanni E, et al. Iron depletion by phlebotomy improves insulin resistance in patients with nonalcoholic fatty liver disease and hyperferritinemia: evidence from a case-control study. Am J Gastroenterol 2007;102:1251-1258.
132. Bacon BR, Adams PC, Kowdley KV, Powell LW, Tavill AS, American Association for the Study of Liver D. Diagnosis and management of hemochromatosis: 2011 practice guideline by the American Association for the Study of Liver Diseases. Hepatology 2011;54:328-343.
133. Hanson EH, Imperatore G, Burke W. HFE gene and hereditary hemochromatosis: a HuGE review. Human Genome Epidemiology. Am J Epidemiol 2001;154:193-206.
134. Camaschella C. Treating iron overload. N Engl J Med 2013;368:2325-2327.
135. Yu L, Ioannou GN. Survival of liver transplant recipients with hemochromatosis in the United States. Gastroenterology 2007;133:489-495.
136. Lunova M, Goehring C, Kuscuoglu D, Mueller K, Chen Y, Walther P, Deschemin JC, et al. Hepcidin knockout mice fed with iron-rich diet develop chronic liver injury and liver fibrosis due to lysosomal iron overload. J Hepatol 2014;61:633-641.
137. Tan TC, Crawford DH, Jaskowski LA, Murphy TM, Heritage ML, Subramaniam VN, Clouston AD, et al. Altered lipid metabolism in Hfe-knockout mice promotes severe NAFLD and early fibrosis. Am J Physiol Gastrointest Liver Physiol 2011;301:G865-876.
138. Zhou XY, Tomatsu S, Fleming RE, Parkkila S, Waheed A, Jiang J, Fei Y, et al. HFE gene knockout produces mouse model of hereditary hemochromatosis. Proc Natl Acad Sci U S A 1998;95:2492-2497.
139. Fleming RE, Ahmann JR, Migas MC, Waheed A, Koeffler HP, Kawabata H, Britton RS, et al. Targeted mutagenesis of the murine transferrin receptor-2 gene produces hemochromatosis. Proc Natl Acad Sci U S A 2002;99:10653-10658.
140. Wang J, Chen G, Filebeen C, Pantopoulos K. Insights on regulation and function of the iron regulatory protein 1 (IRP1). Hemoglobin 2008;32:109-115.
141. Pantopoulos K. Function of the hemochromatosis protein HFE: Lessons from animal models. World J Gastroenterol 2008;14:6893-6901.
142. Delima RD, Chua AC, Tirnitz-Parker JE, Gan EK, Croft KD, Graham RM, Olynyk JK, et al. Disruption of hemochromatosis protein and transferrin receptor 2 causes iron-induced liver injury in mice. Hepatology 2012;56:585-593.
143. Coombs GS, Schmitt AA, Canning CA, Alok A, Low IC, Banerjee N, Kaur S, et al. Modulation of Wnt/beta-catenin signaling and proliferation by a ferrous iron chelator with

therapeutic efficacy in genetically engineered mouse models of cancer. Oncogene 2012;31:213-225.
144. Brookes MJ, Boult J, Roberts K, Cooper BT, Hotchin NA, Matthews G, Iqbal T, et al. A role for iron in Wnt signalling. Oncogene 2008;27:966-975.
145. Houglum K, Ramm GA, Crawford DH, Witztum JL, Powell LW, Chojkier M. Excess iron induces hepatic oxidative stress and transforming growth factor beta1 in genetic hemochromatosis. Hepatology 1997;26:605-610.
146. Shizukuda Y, Tripodi DJ, Rosing DR. Iron Overload or Oxidative Stress? Insight into a Mechanism of Early Cardiac Manifestations of Asymptomatic Hereditary Hemochromatosis Subjects with C282Y Homozygosity. J Cardiovasc Transl Res 2016;9:400-401.
147. Moirand R, Adams PC, Bicheler V, Brissot P, Deugnier Y. Clinical features of genetic hemochromatosis in women compared with men. Ann Intern Med 1997;127:105-110.
148. Christodoulides C, Lagathu C, Sethi JK, Vidal-Puig A. Adipogenesis and WNT signalling. Trends Endocrinol Metab 2009;20:16-24.
149. Liu ZG, Haelens A, Wuyts A, Struyf S, Pang XW, Proost P, Chen WF, et al. Isolation of a lymphocyte chemotactic factor produced by the murine thymic epithelial cell line MTEC1: identification as a 30 kDa glycosylated form of MCP-1. Eur Cytokine Netw 1996;7:381-388.
150. May LT, Shaw JE, Khanna AK, Zabriskie JB, Sehgal PB. Marked cell-type-specific differences in glycosylation of human interleukin-6. Cytokine 1991;3:204-211.
151. Williams MJ, Clouston AD, Forbes SJ. Links between hepatic fibrosis, ductular reaction, and progenitor cell expansion. Gastroenterology 2014;146:349-356.
152. Nemeth E, Tuttle MS, Powelson J, Vaughn MB, Donovan A, Ward DM, Ganz T, et al. Hepcidin regulates cellular iron efflux by binding to ferroportin and inducing its internalization. Science 2004;306:2090-2093.
153. Pigeon C, Ilyin G, Courselaud B, Leroyer P, Turlin B, Brissot P, Loreal O. A new mouse liver-specific gene, encoding a protein homologous to human antimicrobial peptide hepcidin, is overexpressed during iron overload. J Biol Chem 2001;276:7811-7819.
154. Patel BN, Dunn RJ, Jeong SY, Zhu Q, Julien JP, David S. Ceruloplasmin regulates iron levels in the CNS and prevents free radical injury. J Neurosci 2002;22:6578-6586.
155. Aisen P. Transferrin receptor 1. Int J Biochem Cell Biol 2004;36:2137-2143.
156. Toker A, Marmiroli S. Signaling specificity in the Akt pathway in biology and disease. Adv Biol Regul 2014;55:28-38.
157. Busca R, Pouyssegur J, Lenormand P. ERK1 and ERK2 Map Kinases: Specific Roles or Functional Redundancy? Front Cell Dev Biol 2016;4:53.
158. Lawrence T. The nuclear factor NF-kappaB pathway in inflammation. Cold Spring Harb Perspect Biol 2009;1:a001651.
159. Bradford JW, Baldwin AS. IKK/nuclear factor-kappaB and oncogenesis: roles in tumor-initiating cells and in the tumor microenvironment. Adv Cancer Res 2014;121:125-145.
160. Chung FL, Pan J, Choudhury S, Roy R, Hu W, Tang MS. Formation of trans-4-hydroxy-2-nonenal- and other enal-derived cyclic DNA adducts from omega-3 and omega-6 polyunsaturated fatty acids and their roles in DNA repair and human p53 gene mutation. Mutat Res 2003;531:25-36.
161. Wang XW, Hussain SP, Huo TI, Wu CG, Forgues M, Hofseth LJ, Brechot C, et al. Molecular pathogenesis of human hepatocellular carcinoma. Toxicology 2002;181-182:43-47.
162. Lu Y, Cederbaum AI. CYP2E1 and oxidative liver injury by alcohol. Free Radic Biol Med 2008;44:723-738.

163. Sekine S, Lan BY, Bedolli M, Feng S, Hebrok M. Liver-specific loss of beta-catenin blocks glutamine synthesis pathway activity and cytochrome p450 expression in mice. Hepatology 2006;43:817-825.
164. Monga SP. beta-Catenin Signaling and Roles in Liver Homeostasis, Injury, and Tumorigenesis. Gastroenterology 2015;148:1294-1310.
165. Song S, Christova T, Perusini S, Alizadeh S, Bao RY, Miller BW, Hurren R, et al. Wnt inhibitor screen reveals iron dependence of beta-catenin signaling in cancers. Cancer Res 2011;71:7628-7639.
166. Nemeth E, Rivera S, Gabayan V, Keller C, Taudorf S, Pedersen BK, Ganz T. IL-6 mediates hypoferremia of inflammation by inducing the synthesis of the iron regulatory hormone hepcidin. J Clin Invest 2004;113:1271-1276.
167. Matsusaka T, Fujikawa K, Nishio Y, Mukaida N, Matsushima K, Kishimoto T, Akira S. Transcription factors NF-IL6 and NF-kappa B synergistically activate transcription of the inflammatory cytokines, interleukin 6 and interleukin 8. Proc Natl Acad Sci U S A 1993;90:10193-10197.
168. Tontonoz P, Spiegelman BM. Fat and beyond: the diverse biology of PPARgamma. Annu Rev Biochem 2008;77:289-312.
169. Ross SE, Hemati N, Longo KA, Bennett CN, Lucas PC, Erickson RL, MacDougald OA. Inhibition of adipogenesis by Wnt signaling. Science 2000;289:950-953.
170. Guertin DA, Sabatini DM. Defining the role of mTOR in cancer. Cancer Cell 2007;12:9-22.
171. Manning BD, Cantley LC. AKT/PKB signaling: navigating downstream. Cell 2007;129:1261-1274.
172. Zhang X, Tang N, Hadden TJ, Rishi AK. Akt, FoxO and regulation of apoptosis. Biochim Biophys Acta 2011;1813:1978-1986.
173. Zhong W, Shen WF, Ning BF, Hu PF, Lin Y, Yue HY, Yin C, et al. Inhibition of extracellular signal-regulated kinase 1 by adenovirus mediated small interfering RNA attenuates hepatic fibrosis in rats. Hepatology 2009;50:1524-1536.
174. Fremin C, Ezan F, Boisselier P, Bessard A, Pages G, Pouyssegur J, Baffet G. ERK2 but not ERK1 plays a key role in hepatocyte replication: an RNAi-mediated ERK2 knockdown approach in wild-type and ERK1 null hepatocytes. Hepatology 2007;45:1035-1045.
175. Faux SP, Howden PJ. Possible role of lipid peroxidation in the induction of NF-kappa B and AP-1 in RFL-6 cells by crocidolite asbestos: evidence following protection by vitamin E. Environ Health Perspect 1997;105 Suppl 5:1127-1130.
176. Dolcet X, Llobet D, Pallares J, Matias-Guiu X. NF-kB in development and progression of human cancer. Virchows Arch 2005;446:475-482.
177. Handa P, Morgan-Stevenson V, Maliken BD, Nelson JE, Washington S, Westerman M, Yeh MM, et al. Iron overload results in hepatic oxidative stress, immune cell activation, and hepatocellular ballooning injury, leading to nonalcoholic steatohepatitis in genetically obese mice. Am J Physiol Gastrointest Liver Physiol 2016;310:G117-127.
178. Cederbaum AI. Iron and CYP2E1-dependent oxidative stress and toxicity. Alcohol 2003;30:115-120.
179. Lu Y, Wu D, Wang X, Ward SC, Cederbaum AI. Chronic alcohol-induced liver injury and oxidant stress are decreased in cytochrome P4502E1 knockout mice and restored in humanized cytochrome P4502E1 knock-in mice. Free Radic Biol Med 2010;49:1406-1416.

180. Zong H, Armoni M, Harel C, Karnieli E, Pessin JE. Cytochrome P-450 CYP2E1 knockout mice are protected against high-fat diet-induced obesity and insulin resistance. Am J Physiol Endocrinol Metab 2012;302:E532-539.
181. Loeppen S, Koehle C, Buchmann A, Schwarz M. A beta-catenin-dependent pathway regulates expression of cytochrome P450 isoforms in mouse liver tumors. Carcinogenesis 2005;26:239-248.
182. Awuah PK, Rhieu BH, Singh S, Misse A, Monga SP. beta-Catenin loss in hepatocytes promotes hepatocellular cancer after diethylnitrosamine and phenobarbital administration to mice. PLoS One 2012;7:e39771.
183. Liu B, Zhang R, Tao G, Lehwald NC, Liu B, Koh Y, Sylvester KG. Augmented Wnt signaling as a therapeutic tool to prevent ischemia/reperfusion injury in liver: Preclinical studies in a mouse model. Liver Transpl 2015;21:1533-1542.
184. Thompson MD, Wickline ED, Bowen WB, Lu A, Singh S, Misse A, Monga SP. Spontaneous repopulation of beta-catenin null livers with beta-catenin-positive hepatocytes after chronic murine liver injury. Hepatology 2011;54:1333-1343.
185. Preziosi M, Poddar M, Singh S, Monga SP. Hepatocyte Wnts are dispensable during diethylnitrosamine and carbon tetrachloride-induced injury and hepatocellular cancer. Gene Expr 2018.
186. National Cancer Institute. In; 2015.
187. Altekruse SF, McGlynn KA, Reichman ME. Hepatocellular carcinoma incidence, mortality, and survival trends in the United States from 1975 to 2005. J Clin Oncol 2009;27:1485-1491.
188. Li S, Mao M. Next generation sequencing reveals genetic landscape of hepatocellular carcinomas. Cancer Lett 2013;340:247-253.
189. Kim do Y, Han KH. Epidemiology and surveillance of hepatocellular carcinoma. Liver Cancer 2012;1:2-14.
190. Waghray A, Murali AR, Menon KN. Hepatocellular carcinoma: From diagnosis to treatment. World J Hepatol 2015;7:1020-1029.
191. Hepatocellular carcinoma - United States, 2001-2006. MMWR Morb Mortal Wkly Rep 2010;59:517-520.
192. Ma LW, W. Chua, MS. So, S. WNT/B-catenin pathway activation in hepatocellular carcinoma: a clinical perspective. Gastrointestinal Cancer: Targets and Therapy 2014;4:49-63.
193. Stravitz RT, Heuman DM, Chand N, Sterling RK, Shiffman ML, Luketic VA, Sanyal AJ, et al. Surveillance for hepatocellular carcinoma in patients with cirrhosis improves outcome. Am J Med 2008;121:119-126.
194. Schwartz M, Roayaie S, Uva P. Treatment of HCC in patients awaiting liver transplantation. Am J Transplant 2007;7:1875-1881.
195. Duffy JP, Vardanian A, Benjamin E, Watson M, Farmer DG, Ghobrial RM, Lipshutz G, et al. Liver transplantation criteria for hepatocellular carcinoma should be expanded: a 22-year experience with 467 patients at UCLA. Ann Surg 2007;246:502-509; discussion 509-511.
196. Kishi Y, Hasegawa K, Sugawara Y, Kokudo N. Hepatocellular carcinoma: current management and future development-improved outcomes with surgical resection. Int J Hepatol 2011;2011:728103.
197. Xu H, Mao Y. A brief comment on liver resection for hepatocellular carcinoma. Gastroenterol Rep (Oxf) 2013;1:184-185.
198. Llovet JM, Ricci S, Mazzaferro V, Hilgard P, Gane E, Blanc JF, de Oliveira AC, et al. Sorafenib in advanced hepatocellular carcinoma. N Engl J Med 2008;359:378-390.

199. Kudo M, Finn RS, Qin S, Han KH, Ikeda K, Piscaglia F, Baron A, et al. Lenvatinib versus sorafenib in first-line treatment of patients with unresectable hepatocellular carcinoma: a randomised phase 3 non-inferiority trial. Lancet 2018.
200. Bruix J, Qin S, Merle P, Granito A, Huang YH, Bodoky G, Pracht M, et al. Regorafenib for patients with hepatocellular carcinoma who progressed on sorafenib treatment (RESORCE): a randomised, double-blind, placebo-controlled, phase 3 trial. Lancet 2017;389:56-66.
201. Nault JC, Galle PR, Marquardt JU. The role of molecular enrichment on future therapies in hepatocellular carcinoma. J Hepatol 2018.
202. El-Khoueiry AB, Sangro B, Yau T, Crocenzi TS, Kudo M, Hsu C, Kim TY, et al. Nivolumab in patients with advanced hepatocellular carcinoma (CheckMate 040): an open-label, non-comparative, phase 1/2 dose escalation and expansion trial. Lancet 2017;389:2492-2502.
203. Kelley RK, Verslype C, Cohn AL, Yang TS, Su WC, Burris H, Braiteh F, et al. Cabozantinib in hepatocellular carcinoma: results of a phase 2 placebo-controlled randomized discontinuation study. Ann Oncol 2017;28:528-534.
204. El-Serag HB, Marrero JA, Rudolph L, Reddy KR. Diagnosis and treatment of hepatocellular carcinoma. Gastroenterology 2008;134:1752-1763.
205. Thompson MD, Monga SP. WNT/beta-catenin signaling in liver health and disease. Hepatology 2007;45:1298-1305.
206. de La Coste A, Romagnolo B, Billuart P, Renard CA, Buendia MA, Soubrane O, Fabre M, et al. Somatic mutations of the beta-catenin gene are frequent in mouse and human hepatocellular carcinomas. Proc Natl Acad Sci U S A 1998;95:8847-8851.
207. Polakis P. Wnt signaling and cancer. Genes Dev 2000;14:1837-1851.
208. Cui J, Zhou X, Liu Y, Tang Z, Romeih M. Wnt signaling in hepatocellular carcinoma: analysis of mutation and expression of beta-catenin, T-cell factor-4 and glycogen synthase kinase 3-beta genes. J Gastroenterol Hepatol 2003;18:280-287.
209. Buendia MA. Genetic alterations in hepatoblastoma and hepatocellular carcinoma: common and distinctive aspects. Med Pediatr Oncol 2002;39:530-535.
210. Polakis P. The oncogenic activation of beta-catenin. Curr Opin Genet Dev 1999;9:15-21.
211. Satoh S, Daigo Y, Furukawa Y, Kato T, Miwa N, Nishiwaki T, Kawasoe T, et al. AXIN1 mutations in hepatocellular carcinomas, and growth suppression in cancer cells by virus-mediated transfer of AXIN1. Nat Genet 2000;24:245-250.
212. Harada N, Oshima H, Katoh M, Tamai Y, Oshima M, Taketo MM. Hepatocarcinogenesis in mice with beta-catenin and Ha-ras gene mutations. Cancer Res 2004;64:48-54.
213. Tao J, Xu E, Zhao Y, Singh S, Li X, Couchy G, Chen X, et al. Modeling a human hepatocellular carcinoma subset in mice through coexpression of met and point-mutant beta-catenin. Hepatology 2016;64:1587-1605.
214. Tornesello ML, Buonaguro L, Tatangelo F, Botti G, Izzo F, Buonaguro FM. Mutations in TP53, CTNNB1 and PIK3CA genes in hepatocellular carcinoma associated with hepatitis B and hepatitis C virus infections. Genomics 2013;102:74-83.
215. Pezzuto F, Izzo F, Buonaguro L, Annunziata C, Tatangelo F, Botti G, Buonaguro FM, et al. Tumor specific mutations in TERT promoter and CTNNB1 gene in hepatitis B and hepatitis C related hepatocellular carcinoma. Oncotarget 2016;7:54253-54262.
216. Hale G, Liu X, Hu J, Xu Z, Che L, Solomon D, Tsokos C, et al. Correlation of exon 3 beta-catenin mutations with glutamine synthetase staining patterns in hepatocellular adenoma and hepatocellular carcinoma. Mod Pathol 2016;29:1370-1380.

217. Merle P, de la Monte S, Kim M, Herrmann M, Tanaka S, Von Dem Bussche A, Kew MC, et al. Functional consequences of frizzled-7 receptor overexpression in human hepatocellular carcinoma. Gastroenterology 2004;127:1110-1122.
218. Bengochea A, de Souza MM, Lefrancois L, Le Roux E, Galy O, Chemin I, Kim M, et al. Common dysregulation of Wnt/Frizzled receptor elements in human hepatocellular carcinoma. Br J Cancer 2008;99:143-150.
219. Yuzugullu H, Benhaj K, Ozturk N, Senturk S, Celik E, Toylu A, Tasdemir N, et al. Canonical Wnt signaling is antagonized by noncanonical Wnt5a in hepatocellular carcinoma cells. Mol Cancer 2009;8:90.
220. Kim M, Lee HC, Tsedensodnom O, Hartley R, Lim YS, Yu E, Merle P, et al. Functional interaction between Wnt3 and Frizzled-7 leads to activation of the Wnt/beta-catenin signaling pathway in hepatocellular carcinoma cells. J Hepatol 2008;48:780-791.
221. Hu J, Dong A, Fernandez-Ruiz V, Shan J, Kawa M, Martinez-Anso E, Prieto J, et al. Blockade of Wnt signaling inhibits angiogenesis and tumor growth in hepatocellular carcinoma. Cancer Res 2009;69:6951-6959.
222. Laurent-Puig P, Legoix P, Bluteau O, Belghiti J, Franco D, Binot F, Monges G, et al. Genetic alterations associated with hepatocellular carcinomas define distinct pathways of hepatocarcinogenesis. Gastroenterology 2001;120:1763-1773.
223. Laurent-Puig P, Zucman-Rossi J. Genetics of hepatocellular tumors. Oncogene 2006;25:3778-3786.
224. Mu X, Espanol-Suner R, Mederacke I, Affo S, Manco R, Sempoux C, Lemaigre FP, et al. Hepatocellular carcinoma originates from hepatocytes and not from the progenitor/biliary compartment. J Clin Invest 2015;125:3891-3903.
225. Dapito DH, Mencin A, Gwak GY, Pradere JP, Jang MK, Mederacke I, Caviglia JM, et al. Promotion of hepatocellular carcinoma by the intestinal microbiota and TLR4. Cancer Cell 2012;21:504-516.
226. Uehara T, Pogribny IP, Rusyn I. The DEN and CCl4 -Induced Mouse Model of Fibrosis and Inflammation-Associated Hepatocellular Carcinoma. Curr Protoc Pharmacol 2014;66:14 30 11-14 30 10.
227. Chappell G, Kutanzi K, Uehara T, Tryndyak V, Hong HH, Hoenerhoff M, Beland FA, et al. Genetic and epigenetic changes in fibrosis-associated hepatocarcinogenesis in mice. Int J Cancer 2014;134:2778-2788.
228. Zucman-Rossi J, Benhamouche S, Godard C, Boyault S, Grimber G, Balabaud C, Cunha AS, et al. Differential effects of inactivated Axin1 and activated beta-catenin mutations in human hepatocellular carcinomas. Oncogene 2007;26:774-780.
229. Wong CM, Fan ST, Ng IO. beta-Catenin mutation and overexpression in hepatocellular carcinoma: clinicopathologic and prognostic significance. Cancer 2001;92:136-145.
230. Wielenga VJ, Smits R, Korinek V, Smit L, Kielman M, Fodde R, Clevers H, et al. Expression of CD44 in Apc and Tcf mutant mice implies regulation by the WNT pathway. Am J Pathol 1999;154:515-523.
231. Ma H, Nguyen C, Lee KS, Kahn M. Differential roles for the coactivators CBP and p300 on TCF/beta-catenin-mediated survivin gene expression. Oncogene 2005;24:3619-3631.
232. Kilanczyk E, Graczyk A, Ostrowska H, Kasacka I, Lesniak W, Filipek A. S100A6 is transcriptionally regulated by beta-catenin and interacts with a novel target, lamin A/C, in colorectal cancer cells. Cell Calcium 2012;51:470-477.

233.Cheon SS, Wei Q, Gurung A, Youn A, Bright T, Poon R, Whetstone H, et al. Beta-catenin regulates wound size and mediates the effect of TGF-beta in cutaneous healing. FASEB J 2006;20:692-701.
234.Zhang X, Gaspard JP, Chung DC. Regulation of vascular endothelial growth factor by the Wnt and K-ras pathways in colonic neoplasia. Cancer Res 2001;61:6050-6054.
235.Yan D, Wiesmann M, Rohan M, Chan V, Jefferson AB, Guo L, Sakamoto D, et al. Elevated expression of axin2 and hnkd mRNA provides evidence that Wnt/beta -catenin signaling is activated in human colon tumors. Proc Natl Acad Sci U S A 2001;98:14973-14978.
236.Hovanes K, Li TW, Munguia JE, Truong T, Milovanovic T, Lawrence Marsh J, Holcombe RF, et al. Beta-catenin-sensitive isoforms of lymphoid enhancer factor-1 are selectively expressed in colon cancer. Nat Genet 2001;28:53-57.
237.Cadoret A, Ovejero C, Terris B, Souil E, Levy L, Lamers WH, Kitajewski J, et al. New targets of beta-catenin signaling in the liver are involved in the glutamine metabolism. Oncogene 2002;21:8293-8301.
238.Ovejero C, Cavard C, Perianin A, Hakvoort T, Vermeulen J, Godard C, Fabre M, et al. Identification of the leukocyte cell-derived chemotaxin 2 as a direct target gene of beta-catenin in the liver. Hepatology 2004;40:167-176.
239.Kim H, Choi GH, Na DC, Ahn EY, Kim GI, Lee JE, Cho JY, et al. Human hepatocellular carcinomas with "Stemness"-related marker expression: keratin 19 expression and a poor prognosis. Hepatology 2011;54:1707-1717.
240.Carpenter AC, Rao S, Wells JM, Campbell K, Lang RA. Generation of mice with a conditional null allele for Wntless. Genesis 2010;48:554-558.
241.Siar CH, Nagatsuka H, Han PP, Buery RR, Tsujigiwa H, Nakano K, Ng KH, et al. Differential expression of canonical and non-canonical Wnt ligands in ameloblastoma. J Oral Pathol Med 2012;41:332-339.
242.Kowalik MA, Sulas P, Ledda-Columbano GM, Giordano S, Columbano A, Perra A. Cytokeratin-19 positivity is acquired along cancer progression and does not predict cell origin in rat hepatocarcinogenesis. Oncotarget 2015;6:38749-38763.
243.Lee JI, Lee JW, Kim JM, Kim JK, Chung HJ, Kim YS. Prognosis of hepatocellular carcinoma expressing cytokeratin 19: comparison with other liver cancers. World J Gastroenterol 2012;18:4751-4757.
244.Uenishi T, Kubo S, Hirohashi K, Yamamoto T, Ogawa M, Tanaka H, Shuto T, et al. Expression of bile duct-type cytokeratin in hepatocellular carcinoma in patients with hepatitis C virus and prior hepatitis B virus infection. Cancer Lett 2002;178:107-112.
245.Yamashita T, Budhu A, Forgues M, Wang XW. Activation of hepatic stem cell marker EpCAM by Wnt-beta-catenin signaling in hepatocellular carcinoma. Cancer Res 2007;67:10831-10839.
246.Calvisi DF, Conner EA, Ladu S, Lemmer ER, Factor VM, Thorgeirsson SS. Activation of the canonical Wnt/beta-catenin pathway confers growth advantages in c-Myc/E2F1 transgenic mouse model of liver cancer. J Hepatol 2005;42:842-849.
247.Kawate S, Fukusato T, Ohwada S, Watanuki A, Morishita Y. Amplification of c-myc in hepatocellular carcinoma: correlation with clinicopathologic features, proliferative activity and p53 overexpression. Oncology 1999;57:157-163.
248.Lammel Lindemann J, Webb P. Sobetirome: the past, present and questions about the future. Expert Opin Ther Targets 2016;20:145-149.

249. Fransvea E, Angelotti U, Antonaci S, Giannelli G. Blocking transforming growth factor-beta up-regulates E-cadherin and reduces migration and invasion of hepatocellular carcinoma cells. Hepatology 2008;47:1557-1566.
250. Dong LL, Liu L, Ma CH, Li JS, Du C, Xu S, Han LH, et al. E-cadherin promotes proliferation of human ovarian cancer cells in vitro via activating MEK/ERK pathway. Acta Pharmacol Sin 2012;33:817-822.
251. White DL, Thrift AP, Kanwal F, Davila J, El-Serag HB. Incidence of Hepatocellular Carcinoma in All 50 United States, From 2000 Through 2012. Gastroenterology 2017;152:812-820 e815.
252. Mittal S, El-Serag HB. Epidemiology of hepatocellular carcinoma: consider the population. J Clin Gastroenterol 2013;47 Suppl:S2-6.
253. Cosin-Roger J, Ortiz-Masia D, Calatayud S, Hernandez C, Esplugues JV, Barrachina MD. The activation of Wnt signaling by a STAT6-dependent macrophage phenotype promotes mucosal repair in murine IBD. Mucosal Immunol 2016;9:986-998.
254. Kinoshita M, Uchida T, Sato A, Nakashima M, Nakashima H, Shono S, Habu Y, et al. Characterization of two F4/80-positive Kupffer cell subsets by their function and phenotype in mice. J Hepatol 2010;53:903-910.
255. Selzner N, Selzner M, Odermatt B, Tian Y, Van Rooijen N, Clavien PA. ICAM-1 triggers liver regeneration through leukocyte recruitment and Kupffer cell-dependent release of TNF-alpha/IL-6 in mice. Gastroenterology 2003;124:692-700.
256. Sindrilaru A, Peters T, Wieschalka S, Baican C, Baican A, Peter H, Hainzl A, et al. An unrestrained proinflammatory M1 macrophage population induced by iron impairs wound healing in humans and mice. J Clin Invest 2011;121:985-997.
257. Vasconcelos DP, Costa M, Amaral IF, Barbosa MA, Aguas AP, Barbosa JN. Modulation of the inflammatory response to chitosan through M2 macrophage polarization using pro-resolution mediators. Biomaterials 2015;37:116-123.
258. Gordon S. Alternative activation of macrophages. Nat Rev Immunol 2003;3:23-35.
259. Bouhlel MA, Derudas B, Rigamonti E, Dievart R, Brozek J, Haulon S, Zawadzki C, et al. PPARgamma activation primes human monocytes into alternative M2 macrophages with anti-inflammatory properties. Cell Metab 2007;6:137-143.
260. Wang N, Liang H, Zen K. Molecular mechanisms that influence the macrophage m1-m2 polarization balance. Front Immunol 2014;5:614.
261. Iyoda K, Sasaki Y, Horimoto M, Toyama T, Yakushijin T, Sakakibara M, Takehara T, et al. Involvement of the p38 mitogen-activated protein kinase cascade in hepatocellular carcinoma. Cancer 2003;97:3017-3026.
262. Persad R, Liu C, Wu TT, Houlihan PS, Hamilton SR, Diehl AM, Rashid A. Overexpression of caspase-3 in hepatocellular carcinomas. Mod Pathol 2004;17:861-867.
263. Khandrika L, Lieberman R, Koul S, Kumar B, Maroni P, Chandhoke R, Meacham RB, et al. Hypoxia-associated p38 mitogen-activated protein kinase-mediated androgen receptor activation and increased HIF-1alpha levels contribute to emergence of an aggressive phenotype in prostate cancer. Oncogene 2009;28:1248-1260.
264. Cottle DL, Kretzschmar K, Schweiger PJ, Quist SR, Gollnick HP, Natsuga K, Aoyagi S, et al. c-MYC-induced sebaceous gland differentiation is controlled by an androgen receptor/p53 axis. Cell Rep 2013;3:427-441.
265. Cluntun AA, Lukey MJ, Cerione RA, Locasale JW. Glutamine Metabolism in Cancer: Understanding the Heterogeneity. Trends Cancer 2017;3:169-180.

266. Venturi A, Piaz FD, Giovannini C, Gramantieri L, Chieco P, Bolondi L. Human hepatocellular carcinoma expresses specific PCNA isoforms: an in vivo and in vitro evaluation. Lab Invest 2008;88:995-1007.
267. Kroner A, Greenhalgh AD, Zarruk JG, Passos Dos Santos R, Gaestel M, David S. TNF and increased intracellular iron alter macrophage polarization to a detrimental M1 phenotype in the injured spinal cord. Neuron 2014;83:1098-1116.
268. Wijesundera KK, Izawa T, Tennakoon AH, Murakami H, Golbar HM, Katou-Ichikawa C, Tanaka M, et al. M1- and M2-macrophage polarization in rat liver cirrhosis induced by thioacetamide (TAA), focusing on Iba1 and galectin-3. Exp Mol Pathol 2014;96:382-392.
269. Harris PR, Mobley HL, Perez-Perez GI, Blaser MJ, Smith PD. Helicobacter pylori urease is a potent stimulus of mononuclear phagocyte activation and inflammatory cytokine production. Gastroenterology 1996;111:419-425.
270. Mayer-Barber KD, Andrade BB, Barber DL, Hieny S, Feng CG, Caspar P, Oland S, et al. Innate and adaptive interferons suppress IL-1alpha and IL-1beta production by distinct pulmonary myeloid subsets during Mycobacterium tuberculosis infection. Immunity 2011;35:1023-1034.
271. Ehling J, Bartneck M, Wei X, Gremse F, Fech V, Mockel D, Baeck C, et al. CCL2-dependent infiltrating macrophages promote angiogenesis in progressive liver fibrosis. Gut 2014;63:1960-1971.
272. Yoshimura T, Howard OM, Ito T, Kuwabara M, Matsukawa A, Chen K, Liu Y, et al. Monocyte chemoattractant protein-1/CCL2 produced by stromal cells promotes lung metastasis of 4T1 murine breast cancer cells. PLoS One 2013;8:e58791.
273. Tang YJ, Wang JL, Xie KG, Lan CG. Association of interleukin 16 gene polymorphisms and plasma IL16 level with osteosarcoma risk. Sci Rep 2016;6:34607.
274. Shirabe K, Mano Y, Muto J, Matono R, Motomura T, Toshima T, Takeishi K, et al. Role of tumor-associated macrophages in the progression of hepatocellular carcinoma. Surg Today 2012;42:1-7.
275. Martinez FO, Gordon S. The M1 and M2 paradigm of macrophage activation: time for reassessment. F1000Prime Rep 2014;6:13.
276. Carriere A, Ray H, Blenis J, Roux PP. The RSK factors of activating the Ras/MAPK signaling cascade. Front Biosci 2008;13:4258-4275.
277. Schumacher A, Koetsier PA, Hertz J, Doerfler W. Epigenetic and genotype-specific effects on the stability of de novo imposed methylation patterns in transgenic mice. J Biol Chem 2000;275:37915-37921.
278. McCracken JM, Chalise P, Briley SM, Dennis KL, Jiang L, Duncan FE, Pritchard MT. C57BL/6 Substrains Exhibit Different Responses to Acute Carbon Tetrachloride Exposure: Implications for Work Involving Transgenic Mice. Gene Expr 2017;17:187-205.
279. Lai CW, Chen HL, Tsai TC, Chu TW, Yang SH, Chong KY, Chen CM. Sexually Dimorphic Expression of eGFP Transgene in the Akr1A1 Locus of Mouse Liver Regulated by Sex Hormone-Related Epigenetic Remodeling. Sci Rep 2016;6:24023.
280. Yang J. WNT/BETA-CATENIN SIGNALING IN LIVER HOMEOSTASIS AND REGENERATION. D-Scholarship: University of Pittsburgh; 2014.
281. Kietzmann T. Metabolic zonation of the liver: The oxygen gradient revisited. Redox Biol 2017;11:622-630.

282. Sandau KB, Zhou J, Kietzmann T, Brune B. Regulation of the hypoxia-inducible factor 1alpha by the inflammatory mediators nitric oxide and tumor necrosis factor-alpha in contrast to desferroxamine and phenylarsine oxide. J Biol Chem 2001;276:39805-39811.
283. Kashiwagura T, Wilson DF, Erecinska M. Oxygen dependence of cellular metabolism: the effect of O2 tension on gluconeogenesis and urea synthesis in isolated rat hepatocytes. J Cell Physiol 1984;120:13-18.
284. Gebhardt R, Matz-Soja M. Liver zonation: Novel aspects of its regulation and its impact on homeostasis. World J Gastroenterol 2014;20:8491-8504.
285. Monga SP. Role of Wnt/beta-catenin signaling in liver metabolism and cancer. Int J Biochem Cell Biol 2011;43:1021-1029.
286. Rocha AS, Vidal V, Mertz M, Kendall TJ, Charlet A, Okamoto H, Schedl A. The Angiocrine Factor Rspondin3 Is a Key Determinant of Liver Zonation. Cell Rep 2015;13:1757-1764.
287. Leibing T, Geraud C, Augustin I, Boutros M, Augustin HG, Okun JG, Langhans CD, et al. Angiocrine Wnt signaling controls liver growth and metabolic maturation in mice. Hepatology 2017.
288. Global Liver Institute. In; 2014.
289. World Health Rankings. In; 2011.
290. Farges O, Malassagne B, Flejou JF, Balzan S, Sauvanet A, Belghiti J. Risk of major liver resection in patients with underlying chronic liver disease: a reappraisal. Ann Surg 1999;229:210-215.
291. Schuppan D, Afdhal NH. Liver cirrhosis. Lancet 2008;371:838-851.
292. Michalopoulos GK, DeFrances MC. Liver regeneration. Science 1997;276:60-66.
293. Mitchell C, Willenbring H. A reproducible and well-tolerated method for 2/3 partial hepatectomy in mice. Nat Protoc 2008;3:1167-1170.
294. Diehl AM, Chute J. Underlying potential: cellular and molecular determinants of adult liver repair. J Clin Invest 2013;123:1858-1860.
295. Preziosi ME, Monga SP. Update on the Mechanisms of Liver Regeneration. Semin Liver Dis 2017;37:141-151.
296. Paranjpe S, Bowen WC, Mars WM, Orr A, Haynes MM, DeFrances MC, Liu S, et al. Combined systemic elimination of MET and epidermal growth factor receptor signaling completely abolishes liver regeneration and leads to liver decompensation. Hepatology 2016;64:1711-1724.
297. Monga SP, Pediaditakis P, Mule K, Stolz DB, Michalopoulos GK. Changes in WNT/beta-catenin pathway during regulated growth in rat liver regeneration. Hepatology 2001;33:1098-1109.
298. Sodhi D, Micsenyi A, Bowen WC, Monga DK, Talavera JC, Monga SP. Morpholino oligonucleotide-triggered beta-catenin knockdown compromises normal liver regeneration. J Hepatol 2005;43:132-141.
299. Nejak-Bowen KN, Thompson MD, Singh S, Bowen WC, Jr., Dar MJ, Khillan J, Dai C, et al. Accelerated liver regeneration and hepatocarcinogenesis in mice overexpressing serine-45 mutant beta-catenin. Hepatology 2010;51:1603-1613.
300. Natarajan A, Wagner B, Sibilia M. The EGF receptor is required for efficient liver regeneration. Proc Natl Acad Sci U S A 2007;104:17081-17086.

301. Klein D, Demory A, Peyre F, Kroll J, Augustin HG, Helfrich W, Kzhyshkowska J, et al. Wnt2 acts as a cell type-specific, autocrine growth factor in rat hepatic sinusoidal endothelial cells cross-stimulating the VEGF pathway. Hepatology 2008;47:1018-1031.
302. Malek AM, Alper SL, Izumo S. Hemodynamic shear stress and its role in atherosclerosis. JAMA 1999;282:2035-2042.
303. Bodin P, Burnstock G. Evidence that release of adenosine triphosphate from endothelial cells during increased shear stress is vesicular. J Cardiovasc Pharmacol 2001;38:900-908.
304. Rochier A, Nixon A, Yamashita N, Abe R, Abe R, Madri JA, Sumpio BE. Laminar shear, but not orbital shear, has a synergistic effect with thrombin stimulation on tissue factor expression in human umbilical vein endothelial cells. J Vasc Surg 2011;54:480-488.
305. Yoshizumi M, Kurihara H, Sugiyama T, Takaku F, Yanagisawa M, Masaki T, Yazaki Y. Hemodynamic shear stress stimulates endothelin production by cultured endothelial cells. Biochem Biophys Res Commun 1989;161:859-864.
306. Frangos JA, Eskin SG, McIntire LV, Ives CL. Flow effects on prostacyclin production by cultured human endothelial cells. Science 1985;227:1477-1479.
307. Ando J, Nomura H, Kamiya A. The effect of fluid shear stress on the migration and proliferation of cultured endothelial cells. Microvasc Res 1987;33:62-70.
308. Schoen JM, Wang HH, Minuk GY, Lautt WW. Shear stress-induced nitric oxide release triggers the liver regeneration cascade. Nitric Oxide 2001;5:453-464.
309. Heikkinen E, Larmi T. Immediate effect of partial hepatectomy on portal pressure in rats. Acta Chir Scand 1968;134:367-368.
310. Wang HH, Lautt WW. Hepatocyte primary culture bioassay: a simplified tool to assess the initiation of the liver regeneration cascade. J Pharmacol Toxicol Methods 1997;38:141-150.
311. Nishii K, Brodin E, Renshaw T, Weesner R, Moran E, Soker S, Sparks JL. Shear stress upregulates regeneration-related immediate early genes in liver progenitors in 3D ECM-like microenvironments. J Cell Physiol 2018;233:4272-4281.
312. Pham TH, Baluk P, Xu Y, Grigorova I, Bankovich AJ, Pappu R, Coughlin SR, et al. Lymphatic endothelial cell sphingosine kinase activity is required for lymphocyte egress and lymphatic patterning. J Exp Med 2010;207:17-27.
313. Srinivas S, Watanabe T, Lin CS, William CM, Tanabe Y, Jessell TM, Costantini F. Cre reporter strains produced by targeted insertion of EYFP and ECFP into the ROSA26 locus. BMC Dev Biol 2001;1:4.
314. Mederacke I, Hsu CC, Troeger JS, Huebener P, Mu X, Dapito DH, Pradere JP, et al. Fate tracing reveals hepatic stellate cells as dominant contributors to liver fibrosis independent of its aetiology. Nat Commun 2013;4:2823.
315. Ye H, Holterman AX, Yoo KW, Franks RR, Costa RH. Premature expression of the winged helix transcription factor HFH-11B in regenerating mouse liver accelerates hepatocyte entry into S phase. Mol Cell Biol 1999;19:8570-8580.
316. Wickline ED, Awuah PK, Behari J, Ross M, Stolz DB, Monga SP. Hepatocyte gamma-catenin compensates for conditionally deleted beta-catenin at adherens junctions. J Hepatol 2011;55:1256-1262.
317. Huebert RC, Jagavelu K, Liebl AF, Huang BQ, Splinter PL, LaRusso NF, Urrutia RA, et al. Immortalized liver endothelial cells: a cell culture model for studies of motility and angiogenesis. Lab Invest 2010;90:1770-1781.

318. Bowen WC, Michalopoulos AW, Orr A, Ding MQ, Stolz DB, Michalopoulos GK. Development of a chemically defined medium and discovery of new mitogenic growth factors for mouse hepatocytes: mitogenic effects of FGF1/2 and PDGF. PLoS One 2014;9:e95487.
319. Hang TC, Lauffenburger DA, Griffith LG, Stolz DB. Lipids promote survival, proliferation, and maintenance of differentiation of rat liver sinusoidal endothelial cells in vitro. Am J Physiol Gastrointest Liver Physiol 2012;302:G375-388.
320. Prevo R, Banerji S, Ferguson DJ, Clasper S, Jackson DG. Mouse LYVE-1 is an endocytic receptor for hyaluronan in lymphatic endothelium. J Biol Chem 2001;276:19420-19430.
321. Mouta Carreira C, Nasser SM, di Tomaso E, Padera TP, Boucher Y, Tomarev SI, Jain RK. LYVE-1 is not restricted to the lymph vessels: expression in normal liver blood sinusoids and down-regulation in human liver cancer and cirrhosis. Cancer Res 2001;61:8079-8084.
322. Strauss O, Phillips A, Ruggiero K, Bartlett A, Dunbar PR. Immunofluorescence identifies distinct subsets of endothelial cells in the human liver. Sci Rep 2017;7:44356.
323. Raucy JL, Lasker JM, Lieber CS, Black M. Acetaminophen activation by human liver cytochromes P450IIE1 and P450IA2. Arch Biochem Biophys 1989;271:270-283.
324. Niiya T, Murakami M, Aoki T, Murai N, Shimizu Y, Kusano M. Immediate increase of portal pressure, reflecting sinusoidal shear stress, induced liver regeneration after partial hepatectomy. J Hepatobiliary Pancreat Surg 1999;6:275-280.
325. Kuchan MJ, Frangos JA. Shear stress regulates endothelin-1 release via protein kinase C and cGMP in cultured endothelial cells. Am J Physiol 1993;264:H150-156.
326. Mohtai M, Gupta MK, Donlon B, Ellison B, Cooke J, Gibbons G, Schurman DJ, et al. Expression of interleukin-6 in osteoarthritic chondrocytes and effects of fluid-induced shear on this expression in normal human chondrocytes in vitro. J Orthop Res 1996;14:67-73.
327. Claxton S, Kostourou V, Jadeja S, Chambon P, Hodivala-Dilke K, Fruttiger M. Efficient, inducible Cre-recombinase activation in vascular endothelium. Genesis 2008;46:74-80.
328. Apte U, Zeng G, Thompson MD, Muller P, Micsenyi A, Cieply B, Kaestner KH, et al. beta-Catenin is critical for early postnatal liver growth. Am J Physiol Gastrointest Liver Physiol 2007;292:G1578-1585.
329. Benhamouche S, Decaens T, Godard C, Chambrey R, Rickman DS, Moinard C, Vasseur-Cognet M, et al. Apc tumor suppressor gene is the "zonation-keeper" of mouse liver. Dev Cell 2006;10:759-770.
330. Sekine S, Gutierrez PJ, Lan BY, Feng S, Hebrok M. Liver-specific loss of beta-catenin results in delayed hepatocyte proliferation after partial hepatectomy. Hepatology 2007;45:361-368.
331. Michalopoulos GK. Hepatostat: Liver regeneration and normal liver tissue maintenance. Hepatology 2017;65:1384-1392.
332. Klein EA, Assoian RK. Transcriptional regulation of the cyclin D1 gene at a glance. J Cell Sci 2008;121:3853-3857.
333. Mullany LK, White P, Hanse EA, Nelsen CJ, Goggin MM, Mullany JE, Anttila CK, et al. Distinct proliferative and transcriptional effects of the D-type cyclins in vivo. Cell Cycle 2008;7:2215-2224.
334. Fuste NP, Fernandez-Hernandez R, Cemeli T, Mirantes C, Pedraza N, Rafel M, Torres-Rosell J, et al. Cytoplasmic cyclin D1 regulates cell invasion and metastasis through the phosphorylation of paxillin. Nat Commun 2016;7:11581.

335. Sumrejkanchanakij P, Tamamori-Adachi M, Matsunaga Y, Eto K, Ikeda MA. Role of cyclin D1 cytoplasmic sequestration in the survival of postmitotic neurons. Oncogene 2003;22:8723-8730.
336. Huang J, Schriefer AE, Cliften PF, Dietzen D, Kulkarni S, Sing S, Monga SP, et al. Postponing the Hypoglycemic Response to Partial Hepatectomy Delays Mouse Liver Regeneration. Am J Pathol 2016;186:587-599.
337. Nakamura I, Fernandez-Barrena MG, Ortiz-Ruiz MC, Almada LL, Hu C, Elsawa SF, Mills LD, et al. Activation of the transcription factor GLI1 by WNT signaling underlies the role of SULFATASE 2 as a regulator of tissue regeneration. J Biol Chem 2013;288:21389-21398.
338. Nejak-Bowen K, Moghe A, Cornuet P, Preziosi M, Nagarajan S, Monga SP. Role and regulation of p65/beta-catenin association during liver injury and regeneration: a 'complex' relationship. Gene Expr 2017.
339. Fitamant J, Kottakis F, Benhamouche S, Tian HS, Chuvin N, Parachoniak CA, Nagle JM, et al. YAP Inhibition Restores Hepatocyte Differentiation in Advanced HCC, Leading to Tumor Regression. Cell Rep 2015.
340. Cox AG, Hwang KL, Brown KK, Evason K, Beltz S, Tsomides A, O'Connor K, et al. Yap reprograms glutamine metabolism to increase nucleotide biosynthesis and enable liver growth. Nat Cell Biol 2016;18:886-896.
341. Hasuike S, Ido A, Uto H, Moriuchi A, Tahara Y, Numata M, Nagata K, et al. Hepatocyte growth factor accelerates the proliferation of hepatic oval cells and possibly promotes the differentiation in a 2-acetylaminofluorene/partial hepatectomy model in rats. J Gastroenterol Hepatol 2005;20:1753-1761.
342. Sackett SD, Li Z, Hurtt R, Gao Y, Wells RG, Brondell K, Kaestner KH, et al. Foxl1 is a marker of bipotential hepatic progenitor cells in mice. Hepatology 2009;49:920-929.
343. Kordes C, Sawitza I, Gotze S, Herebian D, Haussinger D. Hepatic stellate cells contribute to progenitor cells and liver regeneration. J Clin Invest 2014;124:5503-5515.
344. Chakraborthy A, Ramani P, Sherlin HJ, Premkumar P, Natesan A. Antioxidant and pro-oxidant activity of Vitamin C in oral environment. Indian J Dent Res 2014;25:499-504.
345. Vitamin A and iron deficiency. Nutr Rev 1989;47:119-121.
346. Herbert V. Vitamin C and iron overload. N Engl J Med 1981;304:1108.
347. Ascorbic acid and ferritin catabolism. Nutr Rev 1989;47:218-219.
348. Kurdyukov S, Bullock M. DNA Methylation Analysis: Choosing the Right Method. Biology (Basel) 2016;5.
349. Rose NR, Klose RJ. Understanding the relationship between DNA methylation and histone lysine methylation. Biochim Biophys Acta 2014;1839:1362-1372.
350. Laukens D, Brinkman BM, Raes J, De Vos M, Vandenabeele P. Heterogeneity of the gut microbiome in mice: guidelines for optimizing experimental design. FEMS Microbiol Rev 2016;40:117-132.
351. Collins J, Auchtung JM, Schaefer L, Eaton KA, Britton RA. Humanized microbiota mice as a model of recurrent Clostridium difficile disease. Microbiome 2015;3:35.
352. Sanders JA, Schorl C, Patel A, Sedivy JM, Gruppuso PA. Postnatal liver growth and regeneration are independent of c-myc in a mouse model of conditional hepatic c-myc deletion. BMC Physiol 2012;12:1.
353. Clerk A, Sugden PH. The p38-MAPK inhibitor, SB203580, inhibits cardiac stress-activated protein kinases/c-Jun N-terminal kinases (SAPKs/JNKs). FEBS Lett 1998;426:93-96.

354. Zhang M, Hutter G, Kahn SA, Azad TD, Gholamin S, Xu CY, Liu J, et al. Anti-CD47 Treatment Stimulates Phagocytosis of Glioblastoma by M1 and M2 Polarized Macrophages and Promotes M1 Polarized Macrophages In Vivo. PLoS One 2016;11:e0153550.
355. Lin HH, Feng WC, Lu LC, Shao YY, Hsu CH, Cheng AL. Inhibition of the Wnt/beta-catenin signaling pathway improves the anti-tumor effects of sorafenib against hepatocellular carcinoma. Cancer Lett 2016;381:58-66.
356. Seto K, Sakabe T, Itaba N, Azumi J, Oka H, Morimoto M, Umekita Y, et al. A Novel Small-molecule WNT Inhibitor, IC-2, Has the Potential to Suppress Liver Cancer Stem Cells. Anticancer Res 2017;37:3569-3579.
357. Ma L, Wang X, Jia T, Wei W, Chua MS, So S. Tankyrase inhibitors attenuate WNT/beta-catenin signaling and inhibit growth of hepatocellular carcinoma cells. Oncotarget 2015;6:25390-25401.
358. Planas-Paz L, Orsini V, Boulter L, Calabrese D, Pikiolek M, Nigsch F, Xie Y, et al. The RSPO-LGR4/5-ZNRF3/RNF43 module controls liver zonation and size. Nat Cell Biol 2016;18:467-479.
359. Hutchins NA, Chung CS, Borgerding JN, Ayala CA, Ayala A. Kupffer cells protect liver sinusoidal endothelial cells from Fas-dependent apoptosis in sepsis by down-regulating gp130. Am J Pathol 2013;182:742-754.
360. Schiedner G, Bloch W, Hertel S, Johnston M, Molojavyi A, Dries V, Varga G, et al. A hemodynamic response to intravenous adenovirus vector particles is caused by systemic Kupffer cell-mediated activation of endothelial cells. Hum Gene Ther 2003;14:1631-1641.
361. Abshagen K, Eipel C, Vollmar B. A critical appraisal of the hemodynamic signal driving liver regeneration. Langenbecks Arch Surg 2012;397:579-590.
362. Alvarado TF, Puliga E, Preziosi M, Poddar M, Singh S, Columbano A, Nejak-Bowen K, et al. Thyroid Hormone Receptor beta Agonist Induces beta-Catenin-Dependent Hepatocyte Proliferation in Mice: Implications in Hepatic Regeneration. Gene Expr 2016;17:19-34.
363. Janda CY, Dang LT, You C, Chang J, de Lau W, Zhong ZA, Yan KS, et al. Surrogate Wnt agonists that phenocopy canonical Wnt and beta-catenin signalling. Nature 2017;545:234-237.